Western Graduate&PostdoctoralStudies

Western University
Scholarship@Western

Electronic Thesis and Dissertation Repository

8-21-2014 12:00 AM

Comprehensive STATCOM Control For Distribution And Transmission System Applications

Shubham Gupta, *The University of Western Ontario*

Supervisor: Dr. Rajiv K. Varma, *The University of Western Ontario*
A thesis submitted in partial fulfillment of the requirements for the Master of Engineering
Science degree in Electrical and Computer Engineering
© Shubham Gupta 2014

Follow this and additional works at: https://ir.lib.uwo.ca/etd

Part of the Controls and Control Theory Commons, and the Power and Energy Commons

COMPREHENSIVE STATCOM CONTROL FOR DISTRIBUTION AND
TRANSMISSION SYSTEM APPPLICATIONS

(Thesis format: Monograph)

by

Shubham <u>Gupta</u>

Graduate Program in Electrical and Computer Engineering

A thesis submitted in partial fulfillment
of the requirements for the degree of
Master of Engineering Science

The School of Graduate and Postdoctoral Studies
The University of Western Ontario
London, Ontario, Canada

© Shubham Gupta 2014

Abstract

This thesis presents the development of a comprehensive STATCOM controller for load compensation, voltage regulation and voltage balancing in electric power distribution and transmission networks. The behavior of this controller is first validated with published results. Subsequently, the performance of this STATCOM controller is examined in a realistic Hydro One distribution feeder for accomplishing the compensation of both mildly and grossly unbalanced loads, and balancing of network voltages using PSCAD/EMTDC software. The STATCOM voltage control function is utilized for increasing the connectivity of wind plants in the same distribution feeder. The thesis further presents a frequency scanning technique for simple and rapid identification of the potential of subsynchronous resonance in induction generator based wind farms connected to series compensated lines, utilizing MATLAB software. This technique is validated by published eigenvalue analysis results. The voltage control performance of the developed comprehensive STATCOM controller is then demonstrated for different scenarios in the modified IEEE First SSR Benchmark transmission system for mitigating subsynchronous resonance in series compensated wind farms using industry grade PSCAD/EMTDC software.

Keywords

Voltage regulation, Voltage balancing, Load Compensation, STATCOM, Wind farm, SSR, Subsynchronous Resonance, Induction Generator, Frequency Scanning, Eigenvalue analysis.

Dedicated to my

Four buaji and family

Acknowledgments

<div align="right">SHUBHAM GUPTA</div>

Table of Contents

List of Tables

List of Figures

xiii

xvii

List of Abbreviations

STATCOM	:	Static Synchronous Compensator
PSCAD	:	Power System Computer Aided Design
EMTDC	:	Electro-Magnetic Transient for DC
FACTS	:	Flexible AC Transmission Systems
SVC	:	Static VAR Compensator
SSR	:	Subsynchronous Resonance
VSI	:	Voltage Sourced Inverter
SPWM	:	Sinusoidal Pulse Width Modulation
TOV	:	Temporary Overvoltage
IEEE FBM	:	IEEE First SSR Benchmark Model
IEEE SBM	:	IEEE Second SSR Benchmark Model
IG	:	Induction Generator
DFIG	:	Doubly Fed Induction Motor
PCC	:	Point of Common Coupling
PLL	:	Phase Locked Loop
SLG	:	Single Line to Ground

List of Appendices

List of Symbols

I_a	:	Condenser's armature current
I_f	:	Field excitation current
I_{SVC}	:	Current output of SVC
$I_{STATCOM}$	:	Current output of STATCOM
ω	:	Synchronous rotating speed (377 rad/sec)
θ	:	Instantaneous angle between the a-axis and d-axis
R_S	:	Inverter and transformer conduction losses
R_p	:	Power loss in the inverter switches and capacitor
L_S	:	Leakage reactance of transformer or smoothing reactor
e	:	VSI output voltage
V_S	:	Three phase voltage at PCC
V_{RMS}	:	Three phase RMS voltage at PCC
e_a, e_b, e_c	:	Phase A, B and C voltage at VSI output terminal
V_a, V_b, V_c	:	Phase A, B and C voltage to neutral at PCC
I_a, I_b, I_c	:	Phase A, B and C current output of STATCOM
e_d, e_q	:	d-q axis voltage at VSI output terminal
V_{sd}, V_{sq}	:	d-q axis parts of positive sequence voltage at PCC
V_{sdn}, V_{sqn}	:	d-q axis parts of negative sequence voltage at PCC
I_{dp}, I_{qp}	:	d-q axis part of positive sequence STATCOM current
I_{dn}, I_{qn}	:	d-q axis part of negative sequence STATCOM current
I_{dpref}, I_{qpref}	:	Reference d-q axis part of positive sequence STATCOM current
I_{dnref}, I_{qnref}	:	Reference d-q axis part of negative sequence STATCOM current
P, Q	:	Active and Reactive power output of STATCOM
P_{ref}, Q_{ref}	:	Active and Reactive power reference to STATCOM

V_{dc}	:	DC-link capacitor voltage of STATCOM
m_a, m_b, m_c	:	Modulation indices for A, B and C phase leg of Inverter
m_d, m_q	:	Modulation indices in *dq* reference frame
γ	:	Angle difference between VSI voltage vector and PCC voltage vector
I_S, I_{Load}	:	Three phase source and load current
K_{pd_p}, T_{id_p}	:	Gain and time constant of active power controller
K_{pq_p}, T_{iq_p}	:	Gain and time constant of reactive power controller
K_{pd_n}, T_{id_n}	:	Gain and time constant of negative sequence *d-axis* current controller
K_{pq_n}, T_{iq_n}	:	Gain and time constant of negative sequence *q-axis* current controller
K_{pdc}, T_{idc}	:	Gain and time constant of DC-link voltage controller
s	:	Slip of the generator
L_t	:	Leakage inductance of interconnecting transformer
R_r, X_r	:	Rotor winding resistance and leakage reactance per phase
R_{st}, X_{st}	:	Stator winding resistance and leakage reactance per phase
X_m	:	Magnetizing leakage reactance per phase
C_g	:	Capacitance of wind turbine generator terminal capacitor
R_{Line}, X_{Line}	:	Line resistance and reactance for IEEE FBM
C	:	Capacitance for series compensation in line
V_S	:	Three phase RMS voltage at wind farm terminal
w	:	Speed of wind turbine
f_{er}	:	Electrical resonant frequency
T_{emt}	:	Electromagnetic torque output of generator
T_{sh}	:	Shaft torque of turbine

Chapter 1

INTRODUCTION

Load compensation, voltage balancing and voltage regulation are some of the major problems being faced by electric power utilities across the globe. If not addressed, these issues can cause power losses in lines, mal-operation of critical loads, damage to customer equipment, and potentially power system instability. Dynamic reactive power compensation is typically required to solve the above problems. Static Synchronous Compensator (STATCOM) is a rapidly acting high power electronic dynamic reactive power compensator which is increasingly being employed worldwide for the above purposes. This chapter presents a description and literature review of each of the above problems and the different methods, including STATCOM, which are used in power industry to solve these issues. While STATCOM controllers have been developed for addressing either one or two of the above problems, the motivation for developing a new STATCOM controller for comprehensively addressing all the three problems, is presented. Finally, the outline of each of the chapters of this thesis is described.

1.1 LOAD COMPENSATION

Loads in electric power systems are both static and dynamic [1], [2]. In addition, these loads can be balanced, such as motors or unbalanced, such as single phase loads [3], [4], arc furnaces [5], or traction loads [6], [7]. The loads are typically resistive-inductive in nature. A higher inductive component results in poor power factor which causes utilities to send more current in their distribution lines to serve the same real power load. The utilities have to incur more line losses while receiving the same revenue [8]. Penal tariffs are imposed by utilities to enforce customers to regulate their power factor above utility acceptable norms, typically 0.9 [9].

The biggest problem seen in cities nowadays is public transportation. To tackle this issue, some transportation companies use state-of-the-art DC drives in the operation of metros

and subways. Due to DC drives, utilities are vulnerable to unbalanced load and poor power factor. One of these issues has been reported with Wellington's cable car in New Zealand [6].

The problem of poor power factor, voltage flicker and load unbalance is not limited to public areas but it affects the industrial sector also mainly steel industries and other metallurgical industries [6]. The latest problem has been reported in Vyksa metallurgical plant in Russia and with a steel manufacturing unit in Mississippi, USA [6]. These units use arc furnaces for their operation, which causes unbalanced load on three phase network. Due to this, voltage sensitive loads such as hospitals and surrounding utility distribution networks face problem in their regular operation [3], [6].

The development of train traffic and growth of high speed trains [7] resulted into power quality deterioration as reported by the French rail system operating between Paris and Rennes in Western France, fed from the RTE national power grid [6]. These single phase traction loads were connected with three phase power transmission and sub-transmission grid. Operation of these heavy and strongly time varying traction loads causes voltage unbalance in phases of the grid. If it had not been remedied, poor power quality would have spread throughout the grid and caused complications for other customers taking power from the same grid. Due to grid code which requires power quality at PCC (point of common coupling) within specified limits, utilities may not permit rail traffic on the lines [6].

Commercial and large industrial customers need to install devices at their locations to compensate the loads [9]. The process of load compensation involves two tasks: i) reactive power compensation to improve the power factor to unity, and ii) load balancing to eliminate the unbalance in three phase loads. As a result, even though the load is still reactive and unbalanced, the grid sees it as a balanced load with a high power factor close to unity [10], [11].

1.2 VOLTAGE UNBALANCE

This problem relates to the unbalance not in the loads but in the transmission network which feeds the loads [3]. Transmission and distribution lines supply power from the generating stations to the end loads of customers. A network unbalance may be caused by unequal inductances/impedances in each of the three phases of the lines. Lines have both self and mutual inductances. While self-inductances are generally equal in the three phases over the same length of the line, mutual inductance between the conductors depends on distance between conductors. All conductors, by the nature of design of transmission towers, cannot be placed symmetrically which results in unequal mutual inductances between the phases [12]. Generally many transmission lines have horizontal configuration due to simplified construction of the tower, which is also economical. Lines having asymmetrical conductor spacing experience different inductances in the three phases [12]. Hence, voltages become unbalanced and negative sequence voltages appear on transmission line. This can potentially lead to mal-operation of utility and customer equipment [13]. Transposition of the lines is therefore carried out to reflect equal mutual inductance between three phase conductors [8].

In New Zealand the 220 kV transmission lines are not transposed, resulting in voltage unbalance in the grid. The unbalance worsens as the load increases [13]. An Australian utility with a 500 kV transmission network has also experienced sequential tripping of generators due to excessive negative sequence voltage, causing a total blackout [14]. Unbalanced voltage has also been observed with distribution feeders [15] as it also has untransposed distribution lines and single phase lines.

Further, due to asymmetric faults on the distribution lines, voltage unbalance may occur. Because of asymmetric faults, overvoltage may occur on the healthy phases of the line while the faulted phase will have low voltage. This voltage unbalance may damage the conductor insulation and cause tripping of line from the grid, if not mitigated sooner [16].

1.3 VOLTAGE REGULATION PROBLEM

All power system equipment at generation, transmission or distribution ends require appropriate voltage magnitude to function effectively [1]. This issue of voltage regulation relates to the magnitude of voltages in three phase balanced systems, and not the unbalanced networks described in Section 1.2. Voltage regulation is of critical importance in power system. Lack of voltage control can even lead to power system instability [1], [17].

In mining, metallurgical and petro-chemical industries [18], three phase induction motors (dynamic load) are used for transportation. Induction motors are very sensitive to voltage [19]. If voltage goes low, motors consume more reactive power, which further lowers the voltage. This cyclic phenomenon potentially results in voltage collapse on the feeder line [1]. In British Columbia, due to expansion of oil pipe lines, three additional pumping stations were built. These pumping stations with high power motors created significant load change on the radial line to which they were connected, resulting in voltage instability [6].

A rolling mill is a large and unpremeditated consumer of electric power. It generates harmonics and fluctuations into the surrounding power network [6], [10]. In the event of a weak grid, large motor drives of a rolling mill can even trip out on low voltage since the startup of the mill drive can cause voltage dips of more than 10%. This may stall production and damage the plant economy as reported by Aktogay sulphide plant in Kazakhstan [6]. Lack of voltage regulation may also impede regular operation of other voltage sensitive loads such as medical services, electronic data centers etc [20], [21].

1.3.1   Voltage Control to Increase Connectivity of Wind Farms

Wind farms generate power whenever high wind flow occurs, which is typically in the night in Ontario [22], [23]. Since customer loads decrease during the nights, generation of high amounts of wind power during those hours results in the flow of excess power in the reverse direction towards the grid. This reverse power flow causes voltages to rise in the

lines beyond limits specified by the utilities [24], resulting in a restriction or curtailment of wind power that can be sent over the lines. Voltage control mechanisms are therefore installed in several utilities [23] to allow a higher connectivity of wind farms.

1.3.2   Voltage Control to Prevent Subsynchronous Resonance (SSR) in Series Compensated Wind Farms

There is growing need worldwide to increase the power transfer capacity of transmission lines to carry additional amounts of power coming from various generating sources - largely wind farms. Series compensation is employed in transmission lines to increase the stable capacity of transmission corridors without needing to construct new transmission lines at enormously high costs.

Due to the rapid growth of wind power system in the energy market, the large wind farms are being integrated with electrical networks that are series compensated [25] - [28]. Series compensation, although increases the power transfer capability of existing transmission lines, may potentially cause SSR in wind turbine generators [25], [26]. Recently, a case of subsynchronous resonance has been reported by Electric Reliability Council of Texas (ERCOT) in 2009 which occurred in a doubly-fed induction generator (DFIG) based wind farm [29]. Substantial damages to wind turbines were caused due to this event. Therefore, it is necessary to study the potential for subsynchronous resonance before planning the interconnection of wind farms to series compensated transmission lines.

Dynamic voltage control at the wind farm terminals has been shown to be an effective method of alleviating subsynchronous resonance [25]. It is therefore of paramount importance to regulate voltages appropriately over the transmission and distribution network in a power system. As stated above, all the problems of load compensation, voltage balancing and voltage regulation can be alleviated by dynamic reactive power compensation.

1.4 CONVENTIONAL REACTIVE POWER COMPENSATION METHODS

1.4.1 Synchronous Condenser

A synchronous condenser is a synchronous motor operating at no load. The synchronous condenser can supply variable reactive power for voltage regulation and power factor correction through appropriate control of field current of the motor. Figure 1.1 presents the condenser's armature current I_a with respect to field excitation current I_f.
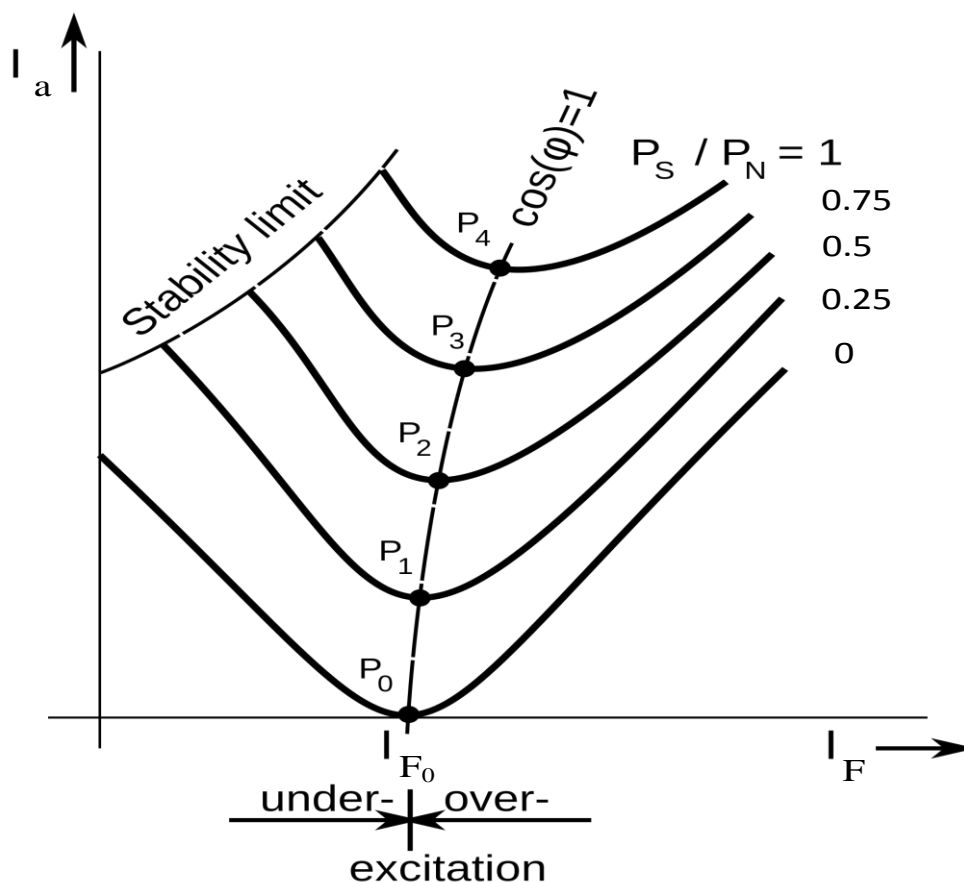
Figure 1.1 Synchronous condenser's armature current and field current relationship

This device can either work in inductive or capacitive mode depending upon field current excitation in rotor winding. With respect to different field currents, it supplies varying armature current I_a which is 90° out of phase with voltage, thereby transfering only reactive power [30].

The synchronous condenser was the very first device that provided dynamic reactive power support. Due to large inertia of the rotating mechanical part (rotor), it has slow speed of response (large time constant) and takes 300-500 ms for dynamic reactive power compensation [12]. The synchronous condenser requires no physical inductor or capacitor and does not generate harmonics. Synchronous condensers still exist and are being installed around the world.

1.4.2   Static VAR Compensator (SVC)

With the development of power electronics, Flexible AC Transmission System (FACTS) devices like SVCs have been used for dynamic reactive power compensation [1], [6], [17]. These devices are static in nature and do not have any rotating parts like synchronous condenser. Due to being static in nature and with the use of power electronic switches, SVC gives faster response than synchronous condenser.

A typical SVC is given in Figure 1.2. It consists of a capacitor connected with a mechanical switch and an inductor in series with antiparallel connected thyristor switches. The unit is connected to high voltage (HV) line with a transformer in order to lower the voltage rating of thyristor valves [1].
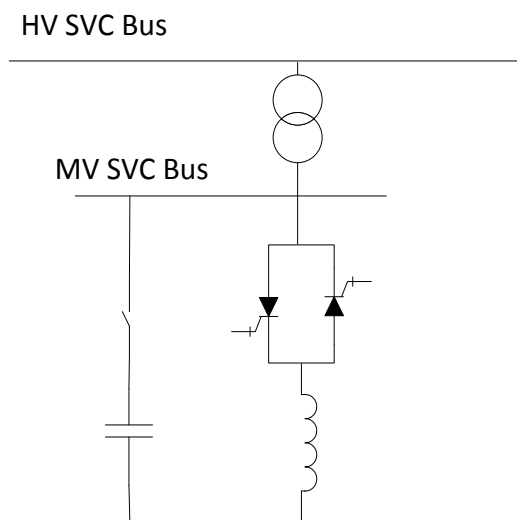
Figure 1.2 Static VAR compensator

To supply reactive power, capacitor is connected with the grid; and for dynamic support thyristors valves are operated to provide variable inductive power. Thus with combined operation SVC works as a variable capacitor or a variable inductor.

A typical *V-I* characteristic of SVC is given in Figure 1.3. It presents the reactive current I_{SVC} support by SVC for different voltages V. In capacitive and inductive operating region, SVC maintains the voltage profile at the PCC with a slope. Slope is added to SVC to make use of smaller rated SVC for large voltage fluctuation. The firing angle is controlled from $\beta = 90^0$ to 180^0. At $\beta = 180^0$, it reaches its limit on capacitive power 'Production limit', thus thyristors are blocked and only the capacitor supplies reactive power. Hence, SVC performance degrades with lower voltage. In a similar manner, thyristors are bypassed after reaching $\beta = 90°$ and SVC works on 'absorption limit' with full inductor connected in shunt [1], [17].
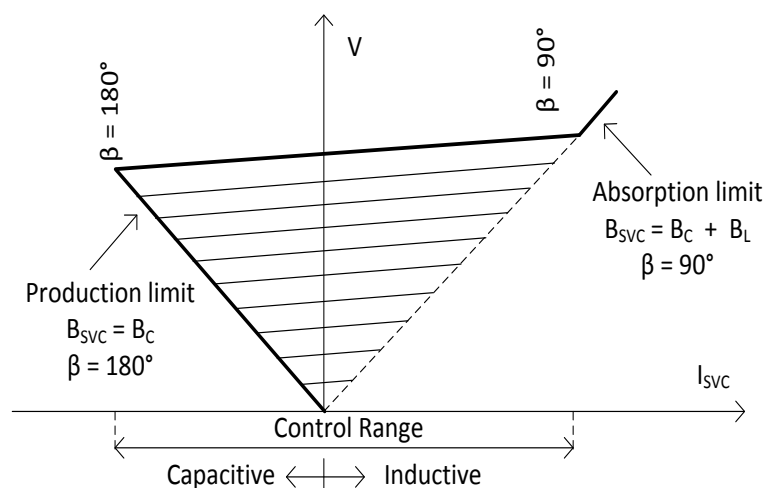
Figure 1.3 Operating characteristic of SVC

Due to switching devices, SVC generates harmonics. Thus filters need to be installed to bypass them to ground [1]. In SVC, thyristors are used as switching devices which provides only one degree of freedom. With thyristors, only their turn ON event can be controlled, but not turn-OFF. It switches OFF naturally when current becomes zero through the switch. Therefore, SVC has typical response time of 3-5 electrical cycles (50 -90 ms) [1], [3], [6]. This is faster when compared to the synchronous condenser, but SVC requires physical inductors and capacitors which require a large space and other protection strategies [1]. In

Canada, the first SVC was purchased by Hydro-Quebec in 1979 for voltage control. It was installed at Laurentides substation.

SVC has also been used with arc furnaces for load compensation and with single phase traction loads for negative sequence voltage control [3], [5], [17]. Other FACTS devices that have similar configuration to SVC are TSC, FC-TCR, MSC-TSC [1]. All these FACTS devices use thyristors and physical inductors and capacitors for reactive power compensation.

1.5 STATIC SYNCHRONOUS COMPENSATOR (STATCOM)

STATCOM is an advanced FACTS device that uses no physical inductor or capacitor for reactive power support unlike SVC. STATCOM supplies reactive power by exchanging the instantaneous reactive power among phases of the AC system.

1.5.1 Configuration

STATCOM uses IGBT, IGCT or GTO as switching devices. In these switches, both switching ON and switching OFF events can be controlled. So this gives two degrees of freedom compared to one degree of freedom given by thyristors in SVCs. This makes it faster and more effectively controllable. Figure 1.4 presents a typical STATCOM connected to a medium voltage (MV) bus. A transformer 'TR' is used to lower down the voltage from high voltage (HV) bus so that lower voltage rating switches (S_1-S_6) can be utilized. It has a capacitor at dc-link to provide the path for current [1].

Smoothing reactor / transformer is used to reduce the harmonic content in voltage. The operating time of STATCOM is 15-30 ms, which is very fast among all the FACTS devices mentioned above. Main reason for its fast response is the absence of any rotating mass and the use of IGBTs, IGCTs or GTOs as switching device. This explains the name, STATic synchronous COMpensator (STATCOM).
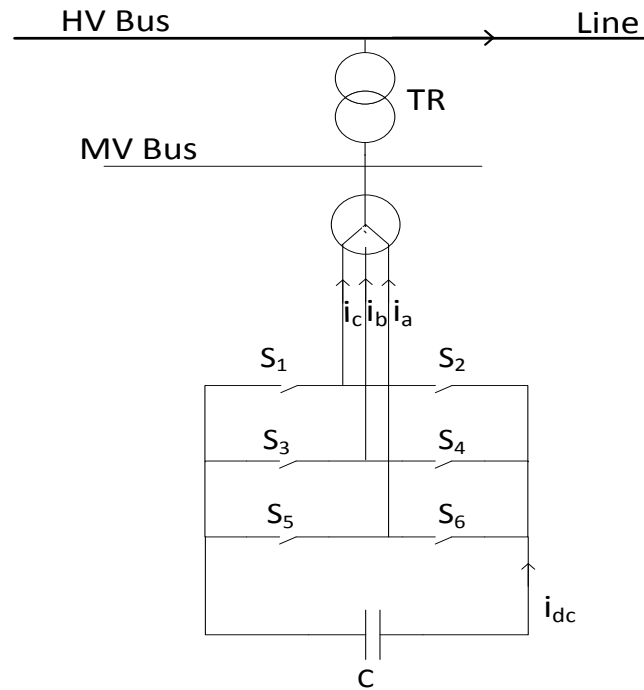
Figure 1.4 Static synchronous compensator (STATCOM)

1.5.2   Operating Characteristics

V-I characteristics of STATCOM is presented in Figure 1.5. STATCOM reactive power output does not depend on voltage at the bus. So even in case of very low bus voltage, STATCOM can work with its full capacity unlike SVC whose performance degrades with lower bus voltage (Figure 1.3). STATCOM is preferred over SVC at locations where voltage goes too low or drops down very fast, so instant control is required [1].

For unbalanced voltage control by SVCs a *3rd* harmonic filter is required. It occupies a large area. Hence it is generally avoided by utilities. Whereas, STATCOM does not have any low order filter requirements and hence is a preferred solution for mitigating unbalance. Superiority of STATCOM over SVC is presented in [5].
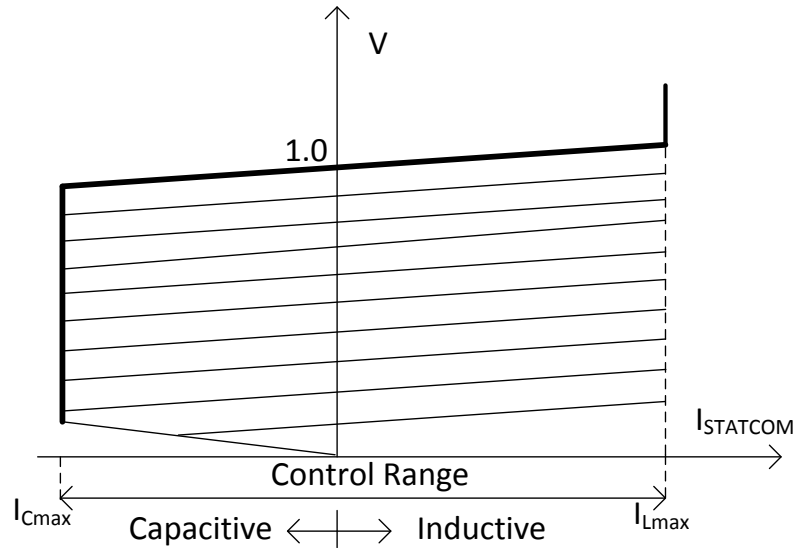
Figure 1.5 Operating characteristic of STATCOM

1.5.3   Application of STATCOM

The main application of STATCOM is to provide dynamic reactive power compensation and to regulate the voltage at the interconnecting bus within acceptable limits.

There are several jurisdictions in Canada that use STATCOM. Mining and metallurgical industries have installed STATCOM to strengthen their electrical supply [20]. Petro chemical industries use high power motors, because of which voltage goes down on the feeder [18]. To maintain the reliability of power and provide fast dynamic voltage support during balanced and unbalanced fault conditions, the utility has installed three units of 12 MVAr STATCOM in British Columbia [6].

Gold mine facilities in Ontario have used the STATCOM solution to assist their high power demand or increased load due to expansion of existing mining facility [6]. A new mining development in Ontario requires high power electrical machines fed over very long cable lengths. To assist their operation, they have used 6 units of STATCOM, each rated 4.5 MVAr for reactive power support to regulate voltage [6]. The fast response time of STATCOM ensures power performance requirement, with longevity of motors and process equipments, thus assuring fast return on investment [6].

Induction motors at mine loads are major cause of voltage collapse and poor power quality [19]. Saskatchewan has high concentration of induction motors at the mine loads [6]. With increase in load, facilities become vulnerable to equipment inefficiencies and tripping offline due to poor voltage at bus. A utility has employed two 5.5 MVAr STATCOM for dynamic VAr compensation to mitigate the network impact [6].

1.6   CONTROL STRATEGIES FOR STATCOM

STATCOM consists of a Voltage Sourced Inverter (VSI) without any DC voltage source at dc-link. There are different inverter configurations available for STATCOM such as multi-level inverter [15], modular multi-level inverter [20], six-pulse three phase inverter [1], [6], cascaded converter based STATCOM [4], cascaded H-bridge converter with star configuration [2], [31], three level neutral point clamped (NPC) inverter [32] etc. For the purpose of load compensation and voltage balancing a six-pulse inverter configuration is selected due to .

There are various modulation strategies in literature for inverters such as symmetrical multiple pulse modulation, sinusoidal pulse width modulation (SPWM), selective harmonic elimination pulse width modulation (SHEPWM) [33], [40] etc. No control over harmonics is present in symmetrical multiple pulse modulation technique. Lower order harmonics can be successfully removed with SHEPWM. However, probability of derating of converter is higher. Therefore, SPWM technique is used to keep harmonics under the limit specified by IEEE Standard 519 [34] by employing appropriate switching frequency [32].

To control the output current of STATCOM, various control strategies have been developed in literature. An average current control technique is used in [19] for load compensation. With this strategy, a compensator of higher order and bandwidth is needed to track the sinusoidal command. To reduce the complexity, $\alpha\beta$ frame control is utilized that transforms the problem of controlling a system of three half-bridge converters to controlling two equivalent subsystems [32]. Phasor based control strategies are also

proposed for STATCOM in [21], [35] and [36]. Lagrange minimization technique is suggested instead of Clark transformation (*abc* to *dq*) in [11]. Large power systems are generally analyzed in *dq* frame [37]. Also, achieving zero steady state error is simpler in *dq* reference frame control as compared to *αβ* frame control. Therefore, representation and control of STATCOM in *dq* frame is employed in [32], [38]. In this thesis, control is executed with SPWM technique in synchronous rotating (*dq*) reference frame that allows decoupled and fast control of active power and reactive power.

Being an expensive device, STATCOMs are typically installed for fast voltage regulation or power factor correction in networks where voltage excursion is large [1]. There is a trend in recent years to add more features in STATCOM to increase its versatility for various purposes and with other power sources like with petroleum industries and high speed railway [7], [18] and [39]. Following this, a co-ordination of STATCOM with other power sources is addressed in [39]. In case of unbalanced load, negative sequence current flows through compensator and introduces 2nd harmonic voltage component on DC-link. If not amended, it will cause 3rd harmonic current component on the AC side thus, deteriorating the STATCOM performance [10]. Furthermore, a severe imbalance may cause large negative sequence current on AC side forcing STATCOM to go offline and restricting its reactive power support.

To compensate the unbalanced load, different STATCOM controllers are presented in literature. A STATCOM with selective harmonic elimination technique is presented in [40]. The controller is said to be robust against parameter sensitivity, however, it is designed in stationary reference frame. A state observer based controller in same *αβ* frame is proposed in [41] for voltage regulation and load compensation. An individual phase decoupled power control of STATCOM is presented in [42] that controls power output of each phase individually. Compensation of grossly unbalanced load is also presented in [42] with four wire, three phase STATCOM. Control using SPWM technique in *dq* reference frame is executed in [10] for load compensation. The 2nd harmonic notch filter is utilized with Type I control [38] to isolate the positive sequence and negative sequence current component. The application of this filter produces a delay, hence the mathematical

modelling is carried out to get instantaneous values for feed-forward decoupling. Nevertheless, settling time of STATCOM is illustrated to be 4-5 cycles in [10].

In [2], [43], [44] in case of unbalanced voltages different techniques to limit the negative sequence current by STATCOM is discussed, however these do not discuss the mitigation of negative sequence voltage. For voltage balancing STATCOM having a Type II control [38] with SPWM has been discussed in [15], [45]. A large capacitor is suggested in [15] to reduce the ripple in DC-link capacitor voltage. To overcome this problem, an inner current control loop is cascaded with voltage balance controller in [45] to enable inverter over-current protection in a 3-phase 4-wire STATCOM. The response time with such current control loop has been reported to be 300 ms.

It is thus seen that different STATCOM controls have been proposed in literature for achieving either load compensation, voltage balancing or voltage control, individually, or in a combination of two functions. No controller seems to have been developed which can address the three issues simultaneously.

1.7 SSR WITH WIND FARM

There are two aspects of SSR: i) Self-excitation involving both induction generator effect and torsional interaction, and ii) Transient torque (also called transient SSR). Several techniques are available for the study of subsynchronous resonance in power systems. The most common techniques are: (i) Frequency scanning, (ii) Eigenvalue analysis, and (iii) Electromagnetic transient simulation [46], [47].

A commercial wind turbine can be operated in two modes: a) fixed speed, and b) variable speed [48], [49]. In the case of a fixed speed wind turbine, the generator rotates at or near a constant speed which is determined by the supply frequency of the network regardless of the wind speed. In the case of a variable speed wind turbine, maximum aerodynamic efficiency is gained by adapting different speeds of the turbine. This is achieved by keeping the tip speed ratio fairly constant [48], [49].

Most wind farms in Europe and North America use Doubly Fed Induction Generators (DFIG), and the most recent trend is to use full converter based wind turbine generators [50]-[53]. However, there are large number of wind farms across USA, India, and Australia, etc., which utilize fixed speed induction generator (IG) based wind turbines [51]-[53].

In [54] a detailed analysis of SSR in wind farm is reported, in which comprehensive eigenvalues analyses are carried out followed by electromagnetic transient simulations. Authors in [55] presented some results of frequency scanning technique to investigate the sub-synchronous control interaction in wind farm, however, only IEEE Second SSR Benchmark System is considered with Type-3 wind farm. No frequency scanning studies have been reported with the more commonly referred IEEE First SSR Benchmark system, and also for induction generator based Type 1 wind farms.

1.8 MOTIVATION AND OBJECTIVE OF THESIS

Various control strategies for load compensation, voltage regulation and voltage balancing are available in literature with different configurations of STATCOM as reported in section 1.6. However, a comprehensive STATCOM controller in synchronous rotating reference frame with a six-pulse inverter configuration for all three tasks has not been discussed in literature so far. Hence, a composite controller for achieving all the three objectives needs to be designed in dq reference frame. Based on system requirements the required controller function may be activated. The developed STATCOM controller needs to be first validated from published results and a further effort needs to be made to accomplish faster response than STATCOM controllers reported in literature.

The transmission utility of Ontario - Hydro One is facing a problem of load unbalance in its networks. Therefore, the performance of the developed controller needs to be analyzed with a realistic feeder data. Due to the penetration of wind power into the feeder, voltage at the line could go higher than the stipulated limit of Hydro One's Technical Interconnection Requirement (TIR) [24]. The effectiveness of the developed STATCOM

controller in increasing the wind farm connectivity in a realistic feeder based on both steady state voltage and Temporary Overvoltage (TOV) considerations will be demonstrated.

Frequency scanning technique is a fundamental technique for preliminary analysis of subsynchronous resonance. It is an approximate tool but has been proven as an efficient and cost effective method for analysis of subsynchronous resonance. Eigenvalue analysis and EMTP analysis give accurate results but are very time consuming. Therefore, a comprehensive frequency scanning analysis is presented to rapidly detect the potential for SSR in Type I induction generator based wind farms. The analysis is carried out considering both single-cage and double-cage induction generators. Frequency scanning analysis is performed with IEEE First and Second SSR Benchmark Systems [57], [58].

The impact of unsymmetrical faults and step change in series compensation levels on the behavior of wind farms connected to series compensated lines has not been reported before. This study has been undertaken in this thesis.

1.9 OUTLINE OF THESIS

A chapter-wise summary of this thesis is given below:

Chapter 2 explains the mathematical modelling of STATCOM controller for load compensation, voltage regulation and voltage balancing. Modifications in the controller for different configurations of coupling transformer are also explained. In addition, a controller is presented to bring down the TOV in phases of the line during asymmetrical faults.

Chapter 3 presents the validation of the proposed comprehensive STATCOM controller, explained in Chapter 2, by comparing with the results published in [10]. The selection procedure for controller parameters is also presented. Two additional studies for compensation of i) Grossly unbalanced load and ii) Network unbalance, are presented. The controller performance with different DC-link voltage levels is also demonstrated in this chapter.

Load compensation with STATCOM for a day-time heavy loading on a realistic feeder of Hydro One is presented in Chapter 4. To increase wind farm penetration with STATCOM, studies on the feeder of Hydro One are also carried out in the same. The STATCOM is used to limit over voltage at the wind farm terminal, arising due to SLG fault. The ability of STATCOM to alleviate this problem is presented in this chapter.

Chapter 5 presents the frequency scanning studies for SSR with single-cage wind farm and double cage wind farm connected with IEEE First SSR Benchmark Model and IEEE Second SSR Benchmark Model. Validation of results with eigenvalue analysis are also presented in the chapter. The effectiveness of the STATCOM is demonstrated for alleviating SSR in the series compensated transmission system. The impact of changes in compensation level, size of wind farms, location and intensity of fault and performance of comprehensive controller in case of asymmetric faults is discussed in this chapter.

Chapter 6 concludes the thesis highlighting the contributions made, and presents the future work that can be pursued as a result of this thesis.

Chapter 2

STATCOM CONTROLLER DESIGN FOR BALANCED AND UNBALANCED NETWORK

2.1 INTRODUCTION

In this chapter, a detailed modeling of STATCOM controller is presented for balanced and unbalanced electrical system. In balanced electrical system, primary STATCOM controller consists of an inner current control loop and outer control loop. Positive sequence controller design for inner current control loop is explained in synchronous rotating reference (*dq*) frame. Outer control loop for DC-link voltage control, power factor correction and voltage regulation are also discussed. Furthermore, the controller is modified to include the effect of different configurations of coupling transformer.

For STATCOM operation in unbalanced electrical system, a negative sequence controller is developed that uses Fortescue decomposition technique to obtain sequence components. Separation of positive and negative sequence components is presented without using a *2ⁿᵈ* harmonic notch filter. Subsequently, the transformation of sequence components to their respective rotating reference (*dq*) frame is described for utilization into negative sequence current control loop.

Successively, a supplementary controller is developed for load compensation, which includes power factor correction and compensation of negative sequence load current. A temporary overvoltage (TOV) regulator is also developed to regulate the overvoltage in case of asymmetric faults. A voltage balancing controller, together with voltage regulator is designed and block diagrams of complete controllers are also presented.

2.2 STATCOM CONTROL IN BALANCED NETWORK

In balanced networks, STATCOM is usually deployed for power factor correction or voltage regulation through its positive sequence controller, described below. The

STATCOM inverter is based on Type 1 control strategy that allows a decoupled control of active and reactive power flowing through STATCOM by utilizing *dq*-axis parameters [38]. In *dq* axis rotating reference frame, the three phase AC quantities become DC in nature. It is easier to apply control techniques on DC values compared to three phase AC quantities that change with time [32].

2.2.1 *abc* to *dq* Frame Transformation

The three phase electrical variables i.e. voltage, current or flux linkage can be represented by a vector. The vector representation of instantaneous three phase variables in *abc* stationary reference frame is presented in Figure 2.1 [38], [59].
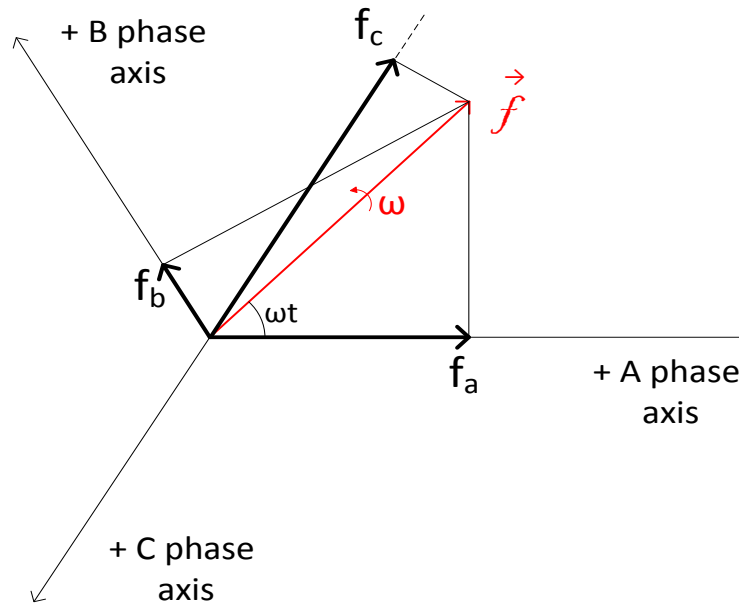
Figure 2.1 Vector representation of three phase electrical variable

Space vector $\vec{f}$ is given by

$$\vec{f}(t) = \frac{2}{3}\left(f_a(t) + f_b(t)e^{j\frac{2\pi}{3}} + f_c(t)e^{-j\frac{2\pi}{3}}\right) \tag{2.1}$$

where $f_a(t), f_b(t)$ and $f_c(t)$ are given as

$$f_a(t) = A\cos(\omega t)$$

$$f_b(t) = A \cos\left(\omega t - \frac{2\pi}{3}\right)$$

$$f_c(t) = A \cos\left(\omega t - \frac{4\pi}{3}\right) \tag{2.2}$$

where, 'A' is the amplitude of each electrical phase vector and 'ω' is the synchronous rotating speed (377 rad/sec) of space vector. The space vector rotates with speed ω with respect to stationary reference frame. These three phase variables in *abc* stationary reference frame can be transformed into two phase variables in a rotating reference frame which consists of *d*- (direct) axis and *q*- (quadrature) axis. This *dq* frame rotates with the same speed ω of space vector. Transformation is done as follows [60]:

$$\begin{bmatrix} f_d \\ f_q \end{bmatrix} = \frac{2}{3} \begin{bmatrix} \cos(\omega t) & \cos(\omega t - \frac{2\pi}{3}) & \cos(\omega t + \frac{2\pi}{3}) \\ -\sin(\omega t) & -\sin(\omega t - \frac{2\pi}{3}) & -\sin(\omega t + \frac{2\pi}{3}) \end{bmatrix} \begin{bmatrix} f_a(t) \\ f_b(t) \\ f_c(t) \end{bmatrix} \tag{2.3}$$

where, f_d and f_q are the component of space vector along *d*-axis and *q*-axis respectively.
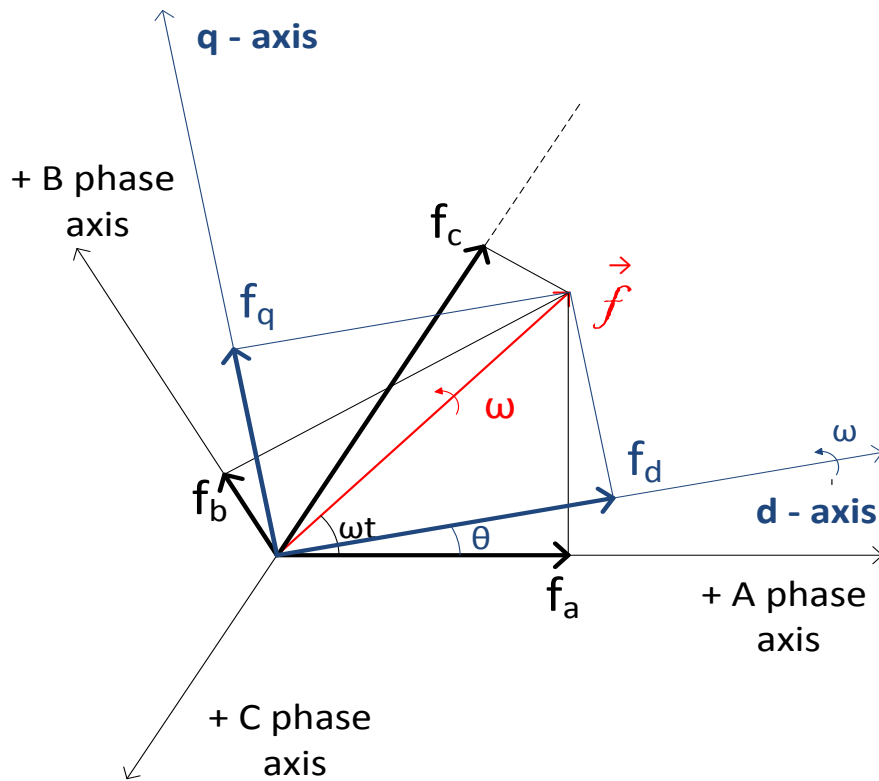
Figure 2.2 Vector representation of three phase electrical variable in stationary (*abc*) and rotating reference (*dq*) frame

Because of the transformation, f_d and f_q are DC quantities. Hence, the space vector $\vec{f}(t)$ can be expressed as

$$\vec{f}(t) = \left(f_d + jf_q \right) e^{j\omega t}$$

Figure 2.2 presents the space vector $\vec{f}(t)$ both in stationary reference frame (*abc*) and rotating reference frame (*dq*). θ is the instantaneous angle between the *a*-axis and *d*-axis. The *dq* reference frame rotates in space with speed $\omega = \frac{d\theta}{dt}$

2.2.2 Modeling of STATCOM connected to a grid
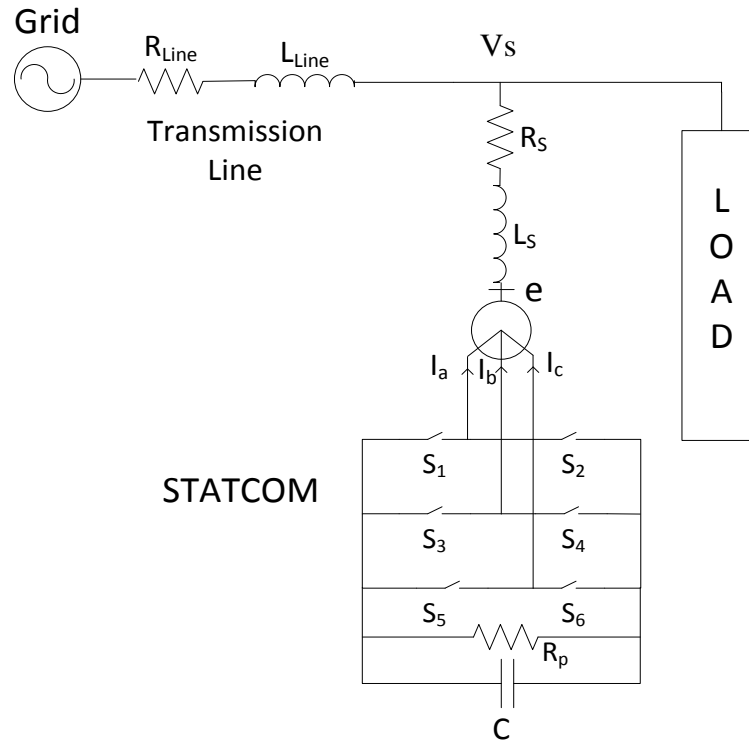
Figure 2.3 Schematic diagram of STATCOM connected to Grid

Figure 2.3 illustrates a schematic diagram of STATCOM connected to power system. The network consists of a load connected to grid through a transmission line. STATCOM, a VSI (Voltage sourced inverter) with a capacitor in DC link, is connected to provide reactive power support to load. VSI is constituted of electrical switches (S_1-S_6) such as IGBTs or GTOs and series inductance (or a transformer). In this figure, R_p represents the switching

losses in the inverter and power loss in capacitor, R_S represents inverter and transformer conduction losses and L_S is the leakage reactance of transformer or smoothing reactor or a combination of both. I_a, I_b and I_c are the phase currents flowing out of STATCOM in the Figure 2.3. PCC voltage and VSI output voltage are denoted by 'V_S' and 'e' respectively.

The output phase voltages of VSI are given by e_a, e_b and e_c . The phase voltages at the PCC are denoted as V_a, V_b and V_c . Then:

$$e_a - V_a = R_s I_a + L_s \frac{dI_a}{dt}$$

$$e_b - V_b = R_s I_b + L_s \frac{dI_b}{dt}$$

$$e_c - V_c = R_s I_c + L_s \frac{dI_c}{dt} \tag{2.4}$$

Combining all three phases:

$$p \begin{bmatrix} I_a \\ I_b \\ I_c \end{bmatrix} = \begin{bmatrix} -\dfrac{R_s}{L_s} & 0 & 0 \\ 0 & -\dfrac{R_s}{L_s} & 0 \\ 0 & 0 & -\dfrac{R_s}{L_s} \end{bmatrix} \begin{bmatrix} I_a \\ I_b \\ I_c \end{bmatrix} + \frac{1}{L_s} \begin{bmatrix} e_a - V_a \\ e_b - V_b \\ e_c - V_c \end{bmatrix} \tag{2.5}$$

where, p is operator for $\frac{d}{dt}$. Applying transformation from *abc* reference frame to synchronously rotating *dq* reference frame from (2.3) to (2.5):

$$L_s \frac{d}{dt} \begin{bmatrix} I_{dp} \\ I_{qp} \end{bmatrix} = \begin{bmatrix} -R_s & L_s \omega \\ -L_s \omega & -R_s \end{bmatrix} \begin{bmatrix} I_{dp} \\ I_{qp} \end{bmatrix} + \begin{bmatrix} e_d - V_{sd} \\ e_q - V_{sq} \end{bmatrix} \tag{2.6}$$

Subscript '*d*' and '*q*' indicate electrical quantities in *d*-axis and *q*-axis reference frame respectively.

There are two basic type of voltage source inverters [38]:
1) Inverter Type I
2) Inverter Type II

Inverter Type I is of primary interest for distribution utilities needing wider range of power control. With this type of inverter, capacitor voltage can be kept sufficiently high for independent control of I_{dp} and I_{qp} in (2.6). Inverter Type II is primarily used with transmission lines and have limited decoupled control on power flow [38]. Therefore, in this thesis control strategy of Type I inverter is utilized to meet the stated objectives.

2.2.3   Basic STATCOM Type I Controller

Figure 2.4 depicts the block diagram of basic Type I controller for STATCOM. In this figure, 'DC-link voltage regulator' is used to keep the constant capacitor voltage. 'Reference signal generator' block supplies reference current values needs to be supplied by STATCOM in *dq* frame. 'PLL' block takes PCC voltage V_S as input and generate signal 'ωt' which is synchronized with phase 'A' of the V_S. Simultaneously, STATCOM current $I_{STATCOM}$ is transformed to *dq* reference frame and is given to 'positive sequence controller' block as feedback signal. This controller generates modulating signals in *dq* frame which are transformed to stationary *abc* frame and are forwarded to designated switching leg of inverter. Equations for *abc* to *dq* block are given in (2.3). The detailed description of other blocks is discussed below.
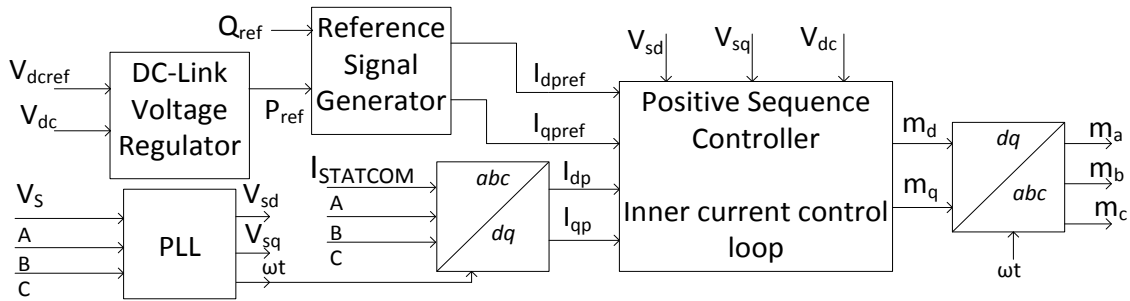
Figure 2.4 Block diagram of basic Type I controller for STATCOM

2.2.4   Phase Locked Loop (PLL) Design

Figure 2.5 presents the block diagram of PLL. A PLL comprises of a PI controller and voltage controlled oscillator (VCO). PLL is designed to synchronize the *d*- axis of rotating

reference frame with the phase A. The PCC voltage vector, therefore makes $\theta = 0°$ (Figure 2.2). Input signals to PLL are dq parts of PCC voltage. PI controller is used to obtain $V_{sq}=$ 0 and VCO outputs angle 'ωt'. The output of PLL is the angle ωt which is utilized to get dq frame transformation (2.3) of PCC voltage (V_{sd} and V_{sq}). V_{sd} attains the maximum phase voltage value as V_{sq} becomes zero.
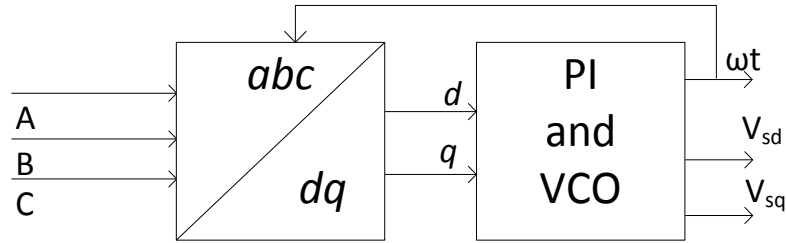
Figure 2.5 Block diagram of phase locked loop (PLL)

2.2.5   Control of Real and Reactive Power Output from VSI

VSI power output equations can be calculated in dq reference frame [38]. The real power (P) and reactive power (Q) in dq frame are expressed as:

$$P = \frac{3}{2}\left(V_{sd}I_{dp} + V_{sq}I_{qp}\right)$$

$$Q = \frac{3}{2}\left(V_{sq}I_{dp} - V_{sd}I_{qp}\right)$$

(2.7)

Since, PLL calculates $V_{sq} = 0$, (2.7) can be rewritten as

$$P = \frac{3}{2}\left(V_{sd}I_{dp}\right)$$

$$Q = \frac{3}{2}\left(-V_{sd}I_{qp}\right)$$

(2.8)

V_{sd} denotes the grid voltage which does not change significantly. Hence power output from VSI can be controlled by I_{dp} and I_{qp}. Therefore, to get reference power P_{ref} and Q_{ref}, the desired current outputs from VSI are given as

$$I_{dpref} = \frac{2}{3V_{sd}}P_{ref}$$

$$I_{qpref} = -\frac{2}{3V_{sd}}Q_{ref} \quad\quad\quad (2.9)$$

This equation explains the operation of 'Reference Signal Generator' block presented in Figure 2.4.

2.2.6 VSI Output Voltage Vector in Synchronous Rotating Reference frame

Sinusoidal pulse width modulation (SPWM) technique is utilized for generating firing pulses for electrical switches (S_1-S_6). In this scheme, VSI output voltage in Figure 2.3 is given as:

$$e_a = m_a(t)\frac{V_{dc}}{2}$$

$$e_b = m_b(t)\frac{V_{dc}}{2} \quad\quad\quad (2.10)$$

$$e_c = m_c(t)\frac{V_{dc}}{2}$$

where m_a, m_b, m_c are the modulation indices of each leg of the inverter and v_{dc} is the voltage of DC link capacitor. For dynamics and control analysis purposes, high frequency components can be omitted [32]. Also filters and controllers exhibit low pass characteristics in closed loop system. Hence, the average value of output voltage is considered instead of instantaneous value [32]. Considering only fundamental component of switching pulses:

$$m_{a_1} = k\sin(\omega t + \Upsilon)$$

$$m_{b_1} = k\sin\left(\omega t + \Upsilon - \frac{2\pi}{3}\right) \quad\quad\quad (2.11)$$

$$m_{c_1} = k\sin\left(\omega t + \Upsilon + \frac{2\pi}{3}\right)$$

where, k is a factor which relates the DC-link voltage to the amplitude of the phase voltage at the inverter AC side terminal. It should be less than 1 for linear operation of inverter

[38], [32], [61]. Y is the angle by which the VSI voltage $\vec{e}$ leads the PCC voltage. Neglecting the voltage harmonics produced by VSI, fundamental output voltage will be

$$e_{a_1} = m_{a_1}(t) \frac{V_{dc}}{2}$$

$$e_{b_1} = m_{b_1}(t) \frac{V_{dc}}{2} \tag{2.12}$$

$$e_{c_1} = m_{c_1}(t) \frac{V_{dc}}{2}$$

Applying *abc* to *dq* transformation from (2.3) to (2.12)

$$e_d = \frac{V_{dc}}{2} m_d$$

$$e_q = \frac{V_{dc}}{2} m_q \tag{2.13}$$

where m_d and m_q are modulation indices in *dq* reference frame. Hence, the VSI output voltage vector from (2.13) can be expressed as

$$\vec{e}(t) = \left(e_d + je_q\right) e^{j\omega t}$$
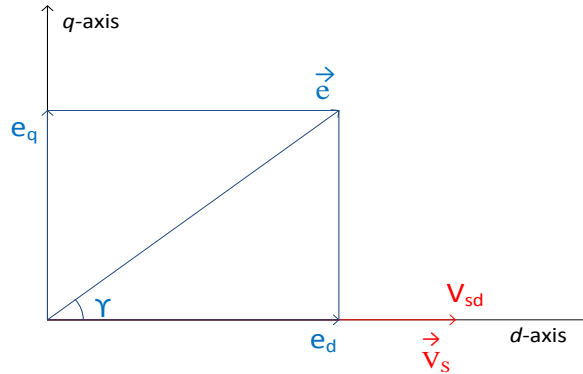
Figure 2.6 VSI output voltage vector and PCC voltage in *dq* reference frame

Figure 2.6 presents the VSI output voltage vector $\vec{e}$ in *dq* plane. $\vec{V_s}$ represents the voltage vector of PCC. The angle 'Y' and magnitude difference of $\vec{e}$ and $\vec{V_s}$ determine the active and reactive power exchange with STATCOM.

2.2.7 Inner Current Control Loop (VSI Current Control)

Substituting values of e_d and e_q from (2.13) to (2.6). The equations are given as

$$L_s \frac{dI_{dp}}{dt} = -R_s I_{dp} + L_s \omega I_{qp} + \frac{V_{dc}}{2} m_d - V_{sd}$$

$$L_s \frac{dI_{qp}}{dt} = -R_s I_{qp} - L_s \omega I_{dp} + \frac{V_{dc}}{2} m_q - V_{sq} \qquad (2.14)$$

To facilitate decoupled control of output power, the control of I_{dp} and I_{qp} should be decoupled. As per (2.14) I_{dp} and I_{qp} are state variables. Coupling is present in system due to presence of $L_s\omega$ term. To decouple I_{dp} and I_{qp} we select m_d and m_q such that

$$m_d = \frac{2}{V_{dc}} \left(u_d - L_s \omega I_{qp} + V_{sd} \right)$$

$$m_q = \frac{2}{V_{dc}} \left(u_q + L_s \omega I_{dp} + V_{sq} \right) \qquad (2.15)$$

where, u_d and u_q are control inputs, terms $L_s\omega I_{qp}$ and $L_s\omega I_{dp}$ are decoupling feed forward input and V_{sd} and V_{sq} are added as given in (2.14). Substituting m_d and m_q to (2.14), it simplifies to

$$L_s \frac{dI_{dp}}{dt} = -R_s I_{dp} + u_d$$

$$L_s \frac{dI_{qp}}{dt} = -R_s I_{qp} + u_q \qquad (2.16)$$

These equations describe two first order decoupled systems. A PI controller suffices the need of controlling I_{dp} and I_{qp} [32]. Figure 2.7 presents the block diagram of inner loop control of STATCOM which is also presented in Figure 2.4 also. In Figure 2.7 I_{dpref} is the reference current for active power and I_{dp} is the d-axis parameter of STATCOM current. The error signal is fed to PI controller which outputs u_d. The PI controller parameters (K_{pd_p} and T_{id_p}) are selected by trial and error method to meet the specific requirements. The procedure is explained in Section 3.2.2. After obtaining u_d from controller, equations 2.15 is implemented in figure for getting m_d. The similar procedure is followed for obtaining m_q [32]. The PI controller for I_{qp} control has parameters as (K_{pq_p} and T_{iq_p}). A low pass filter is employed with dq parameters of the PCC voltage to remove the higher switching harmonics present in the voltage.
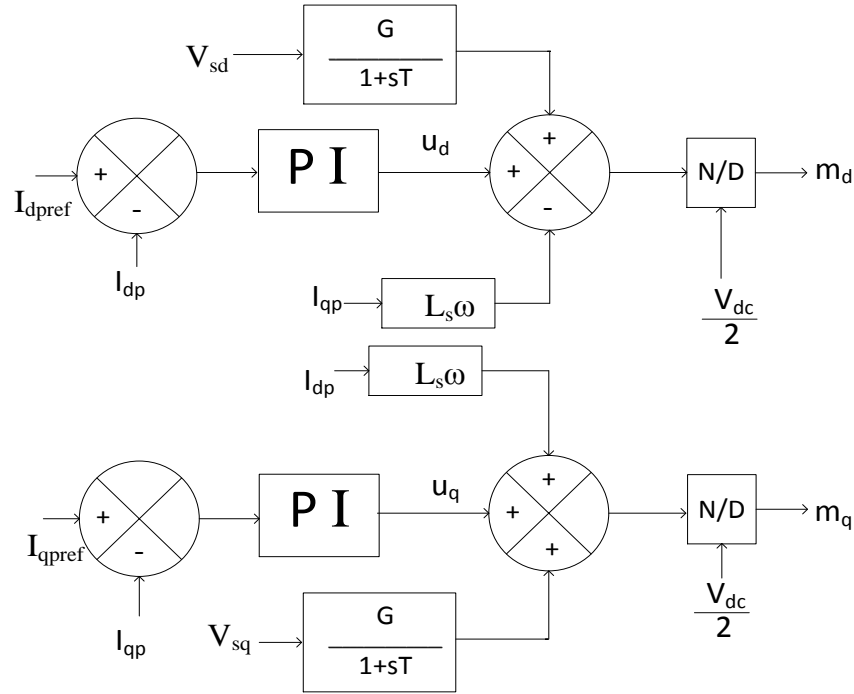
Figure 2.7 Block diagram of inner loop current controller of STATCOM

2.2.8 SPWM Technique

Modulation indices (m_a, m_b and m_c) from Figure 2.4 are the three reference signals for SPWM technique. *dq* to *abc* transformation is carried out to get three phase modulation indices. The *dq* to *abc* transformation matrix can be generated by inverting the matrix given in (2.3):

$$\begin{bmatrix} m_a(t) \\ m_b(t) \\ m_c(t) \end{bmatrix} = \begin{bmatrix} \cos(\omega t) & -\sin(\omega t) \\ \cos(\omega t - \dfrac{2\pi}{3}) & -\sin(\omega t - \dfrac{2\pi}{3}) \\ \cos(\omega t + \dfrac{2\pi}{3}) & -\sin(\omega t + \dfrac{2\pi}{3}) \end{bmatrix} \begin{bmatrix} m_d \\ m_q \end{bmatrix} \tag{2.17}$$

In SPWM technique the modulating signals are compared with the triangular wave of unit amplitude and of certain frequency called carrier wave frequency. The output is then fed to the IGBTs that generate voltage pulse, the averaged output of which is sinusoidal VSI voltage waveform. The voltage output at one phase of three phase system due to switching

is illustrated in Figure 2.8 [62]. When modulation signal is greater than triangular wave, $\frac{+V_{dc}}{2}$ appears at phase output and when it is lesser than triangular wave $\frac{-V_{dc}}{2}$ appears at the phase voltage. Taking an average over carrier wave time period, the output voltage results into a sinusoidal output.
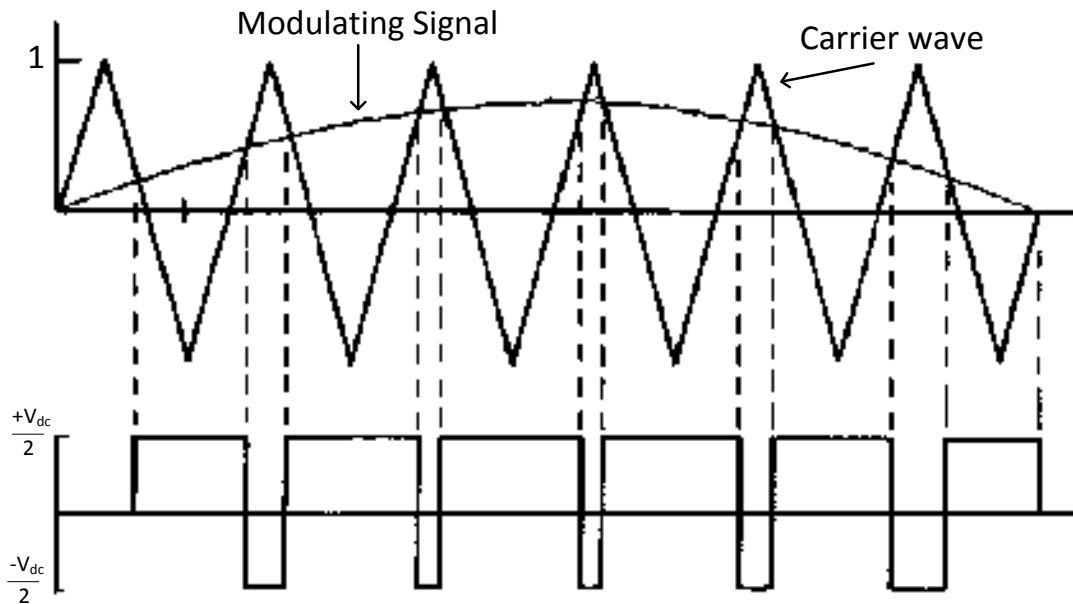
Figure 2.8 Sinusoidal pulse width modulation (SPWM) technique for VSI [62]

2.2.9   DC Link Voltage Control

In STATCOM, a capacitor is employed in DC link instead of a DC voltage source. Due to current flow through the electrical switches and the transformer, power loss occurs in STATCOM. This cause the capacitor voltage to go down. The DC link voltage needs to be maintained at a constant value for proper operation of STATCOM [32]. To keep capacitor voltage at constant value a small amount of active power needs to be drawn into the STATCOM from grid. The required power is calculated with the help of a DC link voltage controller and corresponding value of I_{dpref} is fed to the inner loop controller. The insight of 'DC link voltage controller' is presented in Figure 2.9. In this figure V_{dc} is the voltage

at the capacitor and C is the capacitance used at DC link [32]. A PI controller with parameters (K_{pdc} and T_{idc}) is utilized to get required active power reference.
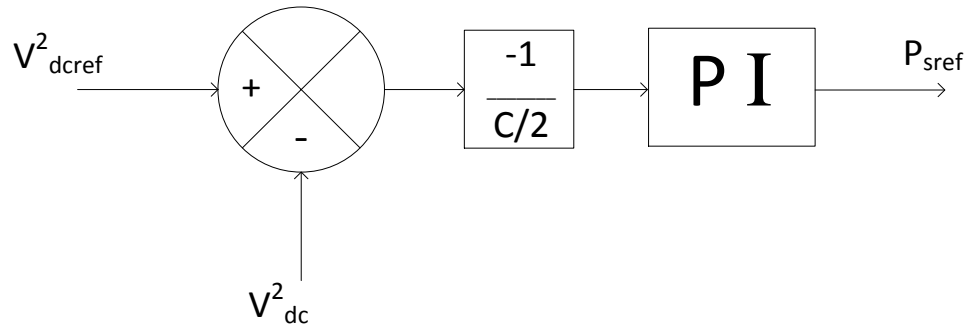
Figure 2.9 DC link voltage controller

2.2.10   Voltage Regulation and Power Factor Correction

STATCOM regulates the PCC voltage by exchanging reactive power. STATCOM reactive power as calculated in (2.8) relates to I_{qp}. For voltage regulation, a simple PI controller is used to obtain reference reactive power Q_{ref}. Block diagram of STATCOM voltage regulator is presented in Figure 2.10. It calculates the error signal by subtracting the RMS voltage V_{RMS} from reference voltage (1 pu normally).
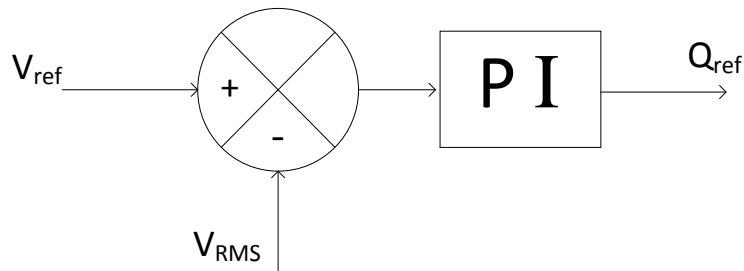
Figure 2.10 Block diagram of STATCOM voltage regulator

Generally PCC voltage is regulated at 1 pu. For power factor correction the reactive power required by load is calculated and supplied by STATCOM. Therefore, Grid does not supply reactive power to load and sees only a resistive load. This however may cause the PCC voltage to go below 1 pu. Hence, the reactive power reference Q_{ref} to STATCOM is

$$Q_{ref} = Q_{load}$$

2.2.11   Modification of Controller due to Transformer

Transformers are used to step down voltage at the inverter side, so that low voltage rating IGBTs or GTOs can be used. Figure 2.11 presents the STATCOM connection with a Y-Y transformer. ABC represents three phase connection points to PCC.
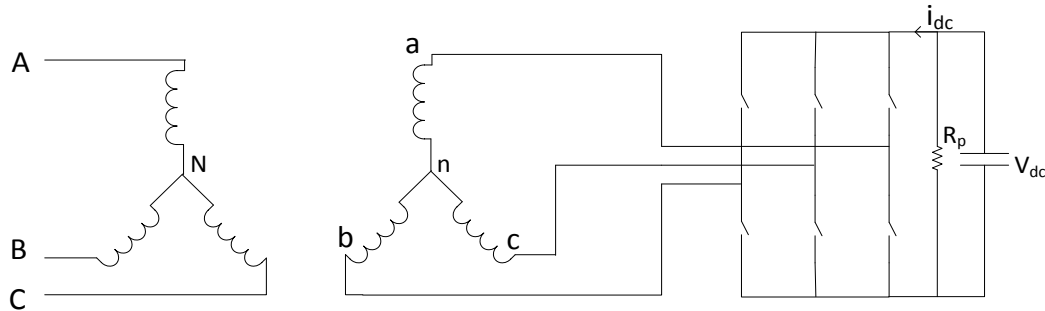
Figure 2.11 STATCOM connected to Y-Y coupling transformer

In (Y-Y) configuration, transformer's each winding is exposed to $\frac{V_{dc}}{2}$. Hence, at each phase VSI average output is considered as

$$e = m(t) \frac{V_{dc}}{2}$$ (2.18)

Where, *m* is the modulation index. Usually star-delta (Y-Δ) transformer is preferred over star-star (Y-Y) configuration as it does not allow zero sequence component to flow through the STATCOM. Figure 2.12 illustrates such a system in which secondary windings are configured as delta. In (Y-Δ) transformer, delta windings are exposed to voltage V_{dc} during switch ON. Therefore, voltage per leg on secondary side $V_{ab} = V_{dc}$
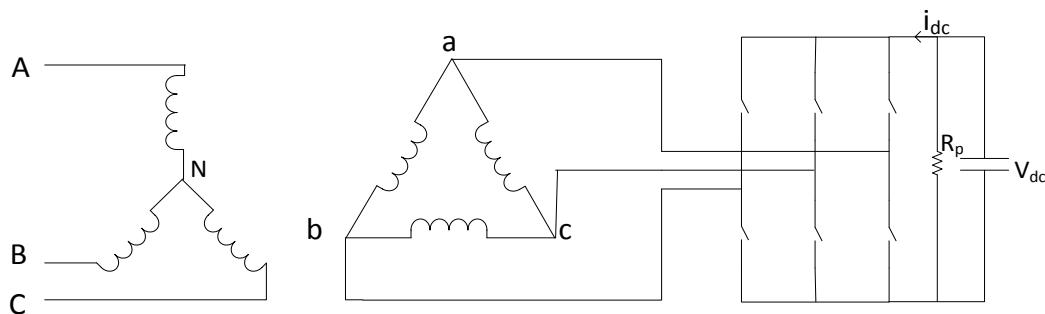
Figure 2.12 STATCOM connected to Y-Δ coupling transformer

Primary side per phase voltage, $V_{AN} = V_{ab} = V_{dc}$ (considering transformation ratio = 1)

Hence, per phase VSI average output will be modified in (2.12)

$$e = m(t)V_{dc} \tag{2.19}$$

If the transformation ratio is not unity, the STATCOM output voltage on primary side of transformer will be

$$V_{AN} = m(t)\frac{V_{l-l_p}}{\sqrt{3}V_{l-l_s}}V_{dc} \tag{2.20}$$

Where, V_{l-l_p} is primary side line to line voltage rating of transformer. V_{l-l_s} is secondary side line to line voltage rating of transformer.
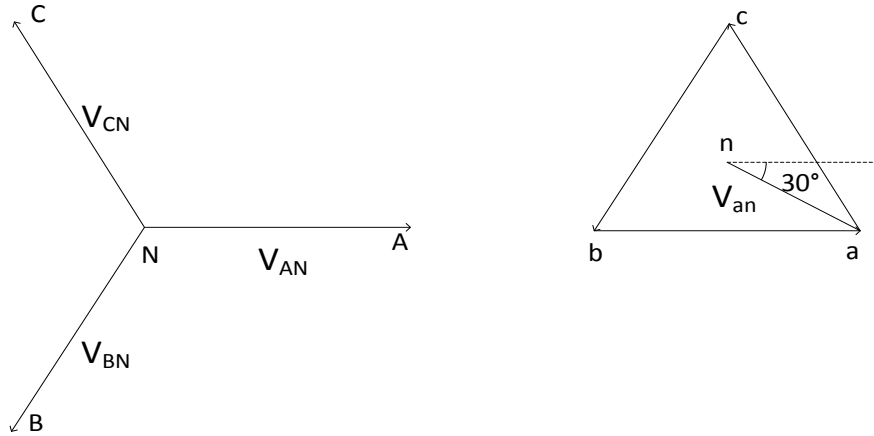
Figure 2.13 Positive sequence phasor diagram of Y-Δ transformer

Y-Δ transformer also causes a phase shift between the primary and secondary side voltage as explained in Figure 2.13 which needs to be compensated in the modulating signal generation. The positive sequence voltage at primary side (star configuration) leads the voltage at secondary side (delta configuration) by 30° [63]. So angle compensation is required in STATCOM controller for this purpose as PLL gives the angle ωt for the voltage measured at primary side of transformer. Therefore, in (2.17) angle ωt will be replaced by ωt'. Also,

$$\omega t' = \omega t - 30°$$
$$\cos(\omega t') = \cos(\omega t)\cos(30°) + \sin(\omega t)\sin(30°)$$
$$\sin(\omega t') = \sin(\omega t)\cos(30°) - \cos(\omega t)\sin(30°) \tag{2.21}$$

2.3   STATCOM CONTROL IN UNBALANCED NETWORK

For separate control of positive and negative sequence STATCOM current, *dq* parts of measured voltage and current must be computed in their respective rotating reference frame. Negative sequence components rotate in the opposite direction to corresponding positive sequence components in the vector space. Therefore, *dq* transformation of unbalanced three phase variables gives a dc signal (due to positive sequence component) and a *2nd* harmonic component (due to negative sequence component) when *dq* frame rotation direction is taken same as that of positive sequence component. The opposite will hold when *dq* frame is considered rotating in direction of negative sequence component. Therefore, a second harmonic removing notch filter is used traditionally to separate the positive and negative sequence *dq* component [10]. This filter introduces a delay in controller response as shown in Figure 2.14. To avoid *2nd* harmonic notch filter, sequence components are separated before applying *dq* transformation. To get sequence components from three phase voltage and current, Fortescue decomposition is utilized.
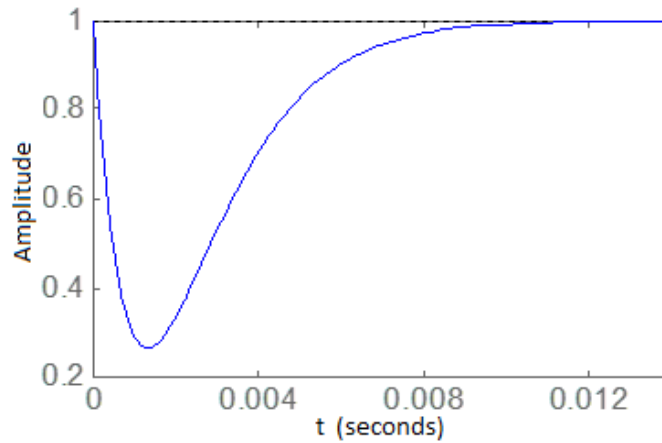
Figure 2.14 Step time response of a notch filter

2.3.1   Decomposition into Symmetrical Components

A set of N unbalanced phasors can be decomposed to a sum of N symmetrical set of balanced phasors [8]. Hence, three phase unbalanced voltage can be expressed as:

$$\begin{bmatrix} V_a \\ V_b \\ V_c \end{bmatrix} = \begin{bmatrix} V_a^0 \\ V_b^0 \\ V_c^0 \end{bmatrix} + \begin{bmatrix} V_a^+ \\ V_b^+ \\ V_c^+ \end{bmatrix} + \begin{bmatrix} V_a^- \\ V_b^- \\ V_c^- \end{bmatrix} \qquad (2.22)$$

$$\begin{bmatrix} V_a \\ V_b \\ V_c \end{bmatrix} = \begin{bmatrix} 1 & 1 & 1 \\ 1 & \alpha^2 & \alpha \\ 1 & \alpha & \alpha^2 \end{bmatrix} \begin{bmatrix} V^0 \\ V^+ \\ V^- \end{bmatrix} \tag{2.23}$$

$$[V_{abc}] = [A][V^{0+-}]$$

Where, superscripts ^{0}, $^+$ and $^-$ denote zero sequence, positive sequence and negative sequence components respectively and $\alpha = e^{j120°}$. Considering a general grid element such as line impedance:

$$\begin{bmatrix} V_a \\ V_b \\ V_c \end{bmatrix} = \begin{bmatrix} E_a \\ E_b \\ E_c \end{bmatrix} - \begin{bmatrix} Z_s & Z_m & Z_m \\ Z_m & Z_s & Z_m \\ Z_m & Z_m & Z_s \end{bmatrix} \begin{bmatrix} I_a \\ I_b \\ I_c \end{bmatrix} \tag{2.24}$$

where, Z_s is self-inductance of the phase and Z_m is mutual inductance between two phases. A transposed line is considered here.

$$[V_{abc}] = [E_{abc}] - [Z_{abc}][I_{abc}] \tag{2.25}$$

Pre multiplying by $[A]^{-1}$ on both sides:

$$[A]^{-1}[V_{abc}] = [A]^{-1}[E_{abc}] - [A]^{-1}[Z_{abc}][A][A]^{-1}[I_{abc}]$$

$$[V^{0+-}] = [E^{0+-}] - [Z^{0+-}][I^{0+-}] \tag{2.26}$$

Where, $[Z^{0+-}] = [A]^{-1}[Z_{abc}][A]$

If $[Z_{abc}]$ is symmetrical, then $[Z^{0+-}]$ will be a diagonal matrix with entries as eigenvalue of $[Z_{abc}]$. Hence, this decomposition enables us to analyze 3-ϕ network as three fully decoupled sequence networks.

2.3.2 Separation of Sequence Components Using All Pass Filter

To alleviate the problem of negative sequence voltage a separate negative sequence controller is augmented with the primary positive sequence controller. In this thesis, the concept of symmetrical components has been extended to signals as function of time [64]. Assuming transformer provides same inductance in all three phases:

$$\begin{bmatrix} f_a^+ \\ f_b^+ \\ f_c^+ \end{bmatrix} = \frac{1}{3} \begin{bmatrix} 1 & \alpha & \alpha^2 \\ \alpha^2 & 1 & \alpha \\ \alpha & \alpha^2 & 1 \end{bmatrix} \begin{bmatrix} f_a \\ f_b \\ f_c \end{bmatrix} \tag{2.27}$$

where f_a, f_b, f_c indicate phase voltage and current. Superscript $^+$ denotes the positive sequence components and $^-$ denotes the negative sequence components of electrical quantity respectively. Substituting $\alpha = -\frac{1}{2} + \frac{\sqrt{3}}{2}j$ in the (2.27):

$$\begin{bmatrix} f_a^+ \\ f_b^+ \\ f_c^+ \end{bmatrix} = \frac{1}{3} \begin{bmatrix} f_a - \frac{1}{2}(f_b + f_c) - \frac{\sqrt{3}}{2}S_{270}(f_b + f_c) \\ f_b - \frac{1}{2}(f_c + f_a) - \frac{\sqrt{3}}{2}S_{270}(f_c + f_a) \\ f_c - \frac{1}{2}(f_a + f_b) - \frac{\sqrt{3}}{2}S_{270}(f_a + f_b) \end{bmatrix} \tag{2.28}$$

Similarly, negative sequence components can be obtained as

$$\begin{bmatrix} f_a^- \\ f_b^- \\ f_c^- \end{bmatrix} = \frac{1}{3} \begin{bmatrix} f_a - \frac{1}{2}(f_b + f_c) + \frac{\sqrt{3}}{2}S_{270}(f_b + f_c) \\ f_b - \frac{1}{2}(f_c + f_a) + \frac{\sqrt{3}}{2}S_{270}(f_c + f_a) \\ f_c - \frac{1}{2}(f_a + f_b) + \frac{\sqrt{3}}{2}S_{270}(f_a + f_b) \end{bmatrix} \tag{2.29}$$

where, S_{270} indicates 270° phase shift. The phase shift is attained using an all pass filter [64].
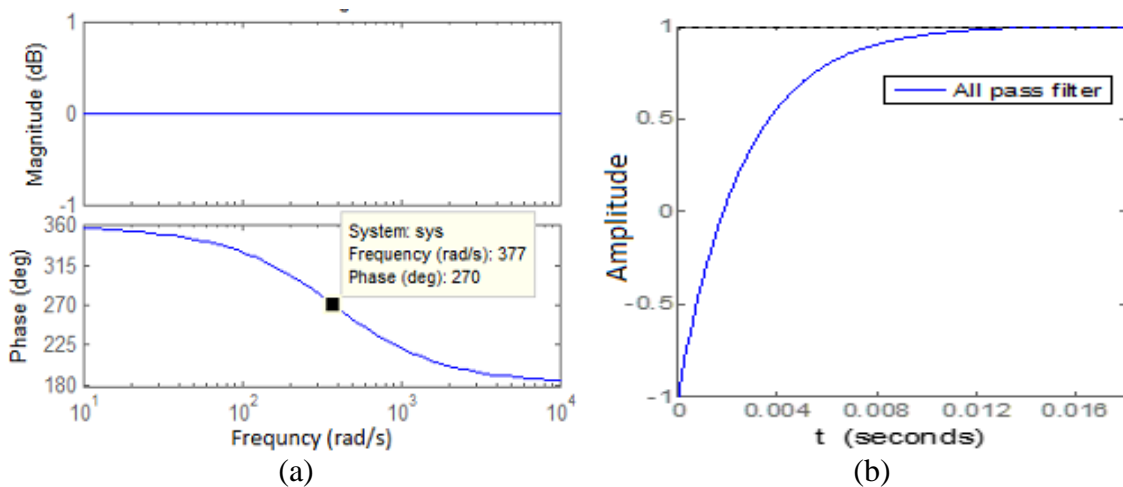
Figure 2.15 (a) Frequency response and (b) Step time response of an all pass filter

The transfer function of the filter is given by

$$S_{270} = \frac{1 - sT}{1 + sT} \tag{2.30}$$

where $T = 1/(2\pi f)$ and f is grid frequency (60 Hz). Bode plot for this filter is given in Figure 2.15 which shows phase shift of 270° at frequency of 60 Hz (377 rad/s). This filter also has a similar settling time as notch filter, given in Figure 2.14. However, this is not integrated to controller directly unlike traditional notch filter [10]. Hence, this delay does not add up completely in the controller response. *abc* to *dq* transformation is done for positive sequence and negative sequence components separately. The space phasor for positive sequence components is defined as:

$$\vec{f}_{\alpha\beta}(t) = \frac{2}{3}\left(f_a^+(t) + f_b^+(t)e^{j\frac{2\pi}{3}} + f_c^+(t)e^{-j\frac{2\pi}{3}}\right)$$

$$\vec{f}_{\alpha\beta}(t) = f_\alpha + jf_\beta$$

The positive sequence phasor rotates in stationary frame with speed ω in anticlockwise direction. The phasor is transformed in synchronously rotating reference frame which allows for simpler and easily decoupled control of currents [32], [60]. The transformation is as in (2.3):

$$f_{dp} + jf_{qp} = \vec{f}_{\alpha\beta}(t)e^{-j\omega t}$$

$$\begin{bmatrix} f_{dp} \\ f_{qp} \end{bmatrix} = \frac{2}{3}\begin{bmatrix} \cos(\omega t) & \cos(\omega t - \frac{2\pi}{3}) & \cos(\omega t + \frac{2\pi}{3}) \\ -\sin(\omega t) & -\sin(\omega t - \frac{2\pi}{3}) & -\sin(\omega t + \frac{2\pi}{3}) \end{bmatrix}\begin{bmatrix} f_a^+(t) \\ f_b^+(t) \\ f_c^+(t) \end{bmatrix} \tag{2.31}$$

abc to *dq* transformation for negative sequence components is done in a similar manner as in (2.31). However, the phasor of negative sequence components rotates in clockwise direction with speed ω in stationary frame. Therefore,

$$\vec{f}_{\alpha\beta}(t) = \frac{2}{3}\left(f_a^-(t) + f_b^-(t)e^{j\frac{2\pi}{3}} + f_c^-(t)e^{-j\frac{2\pi}{3}}\right)$$

$$\vec{f}_{\alpha\beta}(t) = f_\alpha + jf_\beta$$

The transformation in synchronously rotating reference frame is given as:

$$f_{dn} + jf_{qn} = \vec{f}_{\alpha\beta}(t)e^{-j\omega t}$$

$$\begin{bmatrix} f_{dn} \\ f_{qn} \end{bmatrix} = \frac{2}{3}\begin{bmatrix} \cos(\omega t) & \cos(\omega t + \frac{2\pi}{3}) & \cos(\omega t - \frac{2\pi}{3}) \\ \sin(\omega t) & \sin(\omega t + \frac{2\pi}{3}) & \sin(\omega t - \frac{2\pi}{3}) \end{bmatrix}\begin{bmatrix} f_a^-(t) \\ f_b^-(t) \\ f_c^-(t) \end{bmatrix} \qquad (2.32)$$

The block diagram to obtain separate *dq* components for positive and negative sequence voltage and current is presented in Figure 2.16. 'Positive sequence Block' and 'Negative sequence Block' consist of (2.28) and (2.29) respectively. The transformation to positive sequence *dq* component and negative sequence *dq* component utilizes (2.31) and (2.32) respectively.
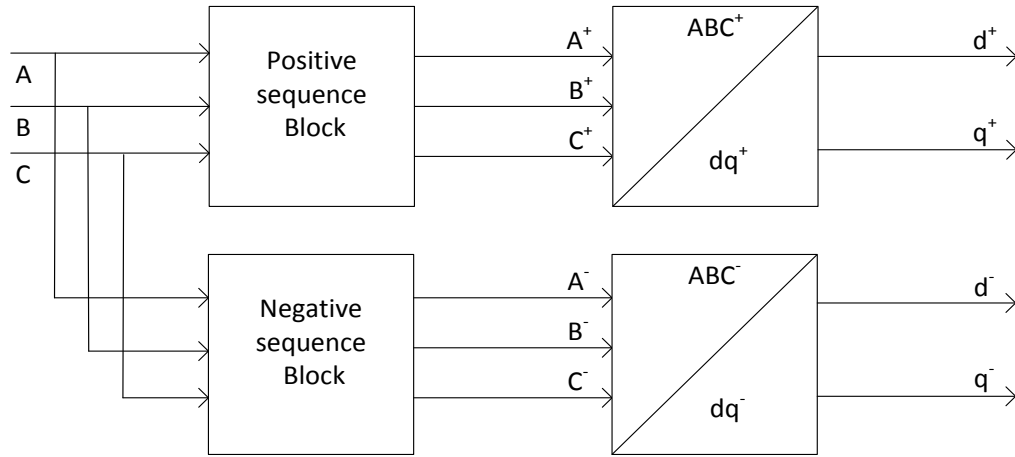
Figure 2.16 Extraction of positive and negative sequence components

2.3.3 Negative Sequence Current Control Loop

Circuit equations for negative sequence current control are same as of positive sequence current control explained in section 2.2.7. Hence, the controller design is similar as given in Figure 2.7 except that negative sequence components of voltage and currents are utilized. However, different controller gains (K_{pd_n} and K_{pq_n}) and time constants (T_{id_n} and T_{iq_n}) are used for *d*-axis and *q*-axis negative sequence current control. The outputs of the control loop are negative sequence modulation indices (m_d^- and m_q^-). During system unbalance both inner current control loops (positive sequence and negative sequence) operate simultaneously.

2.3.4   SPWM Technique for Unbalanced Control of STATCOM

To get switching instants, modulating signals from *dq* frame need to be transformed to *abc* frame. The transformation matrix for modulating signals of positive sequence current controller is same as given in (2.17)

$$
\begin{bmatrix} m_a^+(t) \\ m_b^+(t) \\ m_c^+(t) \end{bmatrix} = \begin{bmatrix} \cos(\omega t) & -\sin(\omega t) \\ \cos(\omega t - \dfrac{2\pi}{3}) & -\sin(\omega t - \dfrac{2\pi}{3}) \\ \cos(\omega t + \dfrac{2\pi}{3}) & -\sin(\omega t + \dfrac{2\pi}{3}) \end{bmatrix} \begin{bmatrix} m_d^+ \\ m_q^+ \end{bmatrix} \tag{2.33}
$$

For negative sequence components, *dq* to *abc* transformation matrix is the inverse of *abc* to *dq* transformation matrix given in (2.32):

$$
\begin{bmatrix} m_a^-(t) \\ m_b^-(t) \\ m_c^-(t) \end{bmatrix} = \begin{bmatrix} \cos(\omega t) & \sin(\omega t) \\ \cos(\omega t - \frac{2\pi}{3}) & \sin(\omega t - \frac{2\pi}{3}) \\ \cos(\omega t + \frac{2\pi}{3}) & \sin(\omega t + \frac{2\pi}{3}) \end{bmatrix} \begin{bmatrix} m_d^- \\ m_q^- \end{bmatrix} \tag{2.34}
$$

The reference signal for the SPWM technique is generated as explained in [15]:

$$
\begin{bmatrix} m_a(t) \\ m_b(t) \\ m_c(t) \end{bmatrix} = \begin{bmatrix} m_a^+(t) \\ m_b^+(t) \\ m_c^+(t) \end{bmatrix} + \begin{bmatrix} m_a^-(t) \\ m_b^-(t) \\ m_c^-(t) \end{bmatrix} \tag{2.35}
$$

The modulating signals m_a, m_b and m_c are compared with the triangular wave of unit amplitude and carrier wave frequency to generate electrical switch ON and OFF signals. The signals are fed to the IGBTs that generates the voltage pulses, whose average is sinusoidal voltage output at VSI.

2.3.5   Modification in DC Link Voltage Controller

The DC link voltage controller provides active power to keep the capacitor voltage at its reference value. It needs positive sequence active power to charge the capacitor. Due to negative sequence current through STATCOM, a *2nd* harmonic component in DC link voltage can be seen. Therefore, a notch filter is utilized before DC-link voltage controller

so that the controller does not see the *2nd* harmonic component in DC-link voltage and regulates only the average value of capacitor voltage. To reduce the magnitude of *2nd* harmonic component a larger size capacitor is suggested [15]. However, with this control strategy no *3rd* harmonic component appears at the AC-side of inverter.

2.3.6 Modification of Controller Due to Negative Sequence Voltage through Transformer

Unlike the positive sequence voltage, negative sequence voltage on star side lags 30° from negative sequence voltage on delta side (Figure 2.12). The phasor diagram for negative sequence voltage in Y-Δ transformer is given in Figure 2.17 [63]. It is clear from figure that negative sequence voltage 'V$_{AN}$' lags 30° to voltage 'V$_{ab}$'. Therefore, in negative sequence controller, in (2.17) angle ωt is replaced by ωt' such that:

$$\omega t' = \omega t + 30°$$

$$\cos(\omega t') = \cos(\omega t)\cos(30°) - \sin(\omega t)\sin(30°)$$

$$\sin(\omega t') = \sin(\omega t)\cos(30°) + \cos(\omega t)\sin(30°) \tag{2.36}$$
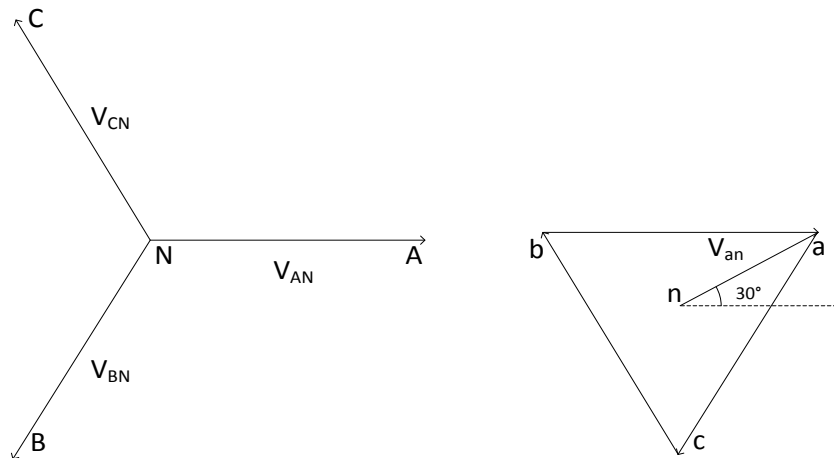
Figure 2.17 Negative sequence phasor diagram of Y-Δ transformer

2.4   COMPREHENSIVE STATCOM CONTROLLER

The steps for developing comprehensive STATCOM controller are explained in previous sections. The controller is constituted of two outer control loop, one for positive sequence and second for negative sequence parameters. Each control loop is linked with its respective sequence inner current control loop.

Positive sequence control loop can regulate voltage and correct power factor by exchanging reactive power. Negative sequence control loop is utilized to compensate the negative sequence load current and regulate the negative sequence voltage at PCC to zero. Therefore, the STATCOM can perform load compensation or voltage regulation or voltage balancing with voltage regulation.

2.4.1   Load Compensation

Figure 2.18 presents the complete STATCOM controller for load compensation. DC-link voltage regulator (Section 2.2.9) gives the active power reference 'P_{ref}'. 'Q_{ref}' is the load reactive power that needs to be compensated. *dq* components of STATCOM reference current are generated for corresponding power values as explained in Section 2.2.5. STATCOM current $I_{STATCOM}$ is transformed into positive (I_{dp} and I_{qp}) and negative (I_{dn} and I_{qn}) sequence *dq* components as explained in Section 2.3.1. The positive and negative sequence current signals are given to corresponding positive and negative sequence controllers as feedback signals. Positive sequence controller follows the reference current command and provides positive sequence modulation indices (m_d^+ and m_q^+). V_{sd} and V_{sq} are *d*- axis and *q*- axis parts of positive sequence voltage at PCC.

STATCOM supplies negative sequence current to the load so that only positive sequence current flows through the grid. To compensate for negative sequence current, first negative sequence reference current is extracted from load current I_{Load}.   The *abc* to *dq* transformation is applied from (2.32) to obtain *dq* parts (I_{dnref} and I_{qnref}) of negative sequence load current. Negative sequence controller provides negative sequence

modulation indices (m_d^- and m_q^-). In negative sequence controller, V_{sdn} and V_{sqn} are d-axis and q- axis parts of negative sequence voltage at PCC.

Positive and negative sequence modulation indices are transformed to stationary (*abc*) frame and are summed to get final modulated sine waves (m_a, m_b *and* m_c) as explained in section 2.3.4. These waves are compared to triangular wave and switching signals are fed to IGBTs.
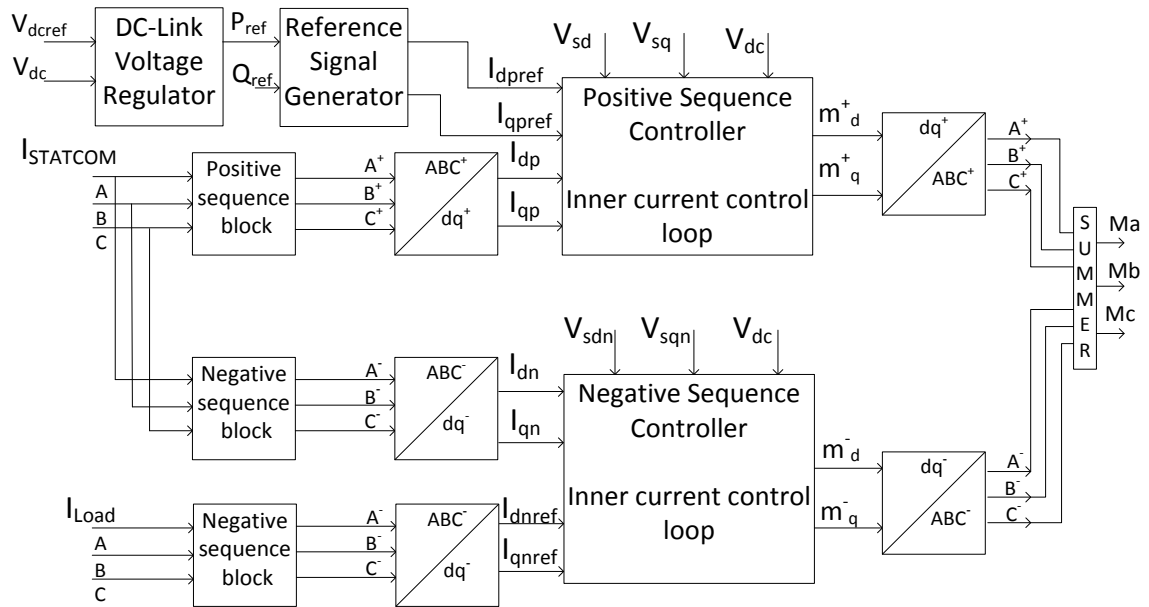
Figure 2.18 Block diagram of complete STATCOM controller for load compensation

If there is no unbalanced load in the network, STATCOM does not supply negative sequence current to load. In that case it only compensates load reactive power, thus working as power factor corrector.

2.4.2　Voltage Regulation

With the proposed controller, STATCOM can also perform voltage regulation exclusively. The controller diagram in Figure 2.19 is similar as the one presented for load compensation except in this case Q_{ref} is calculated from a voltage regulator as shown in Figure 2.10 and reference negative sequence currents (I_{dnref} and I_{qnref}) are made zero. This allows

STATCOM to regulate three phase voltage without being affected by negative sequence voltage at its terminal in asymmetric networks. Therefore, STATCOM supplies only positive sequence current to regulate the RMS voltage at PCC. If network is balanced then negative sequence modulation indices (m_d^- and m_q^-) can also be made zero to regulate PCC voltage exclusively.
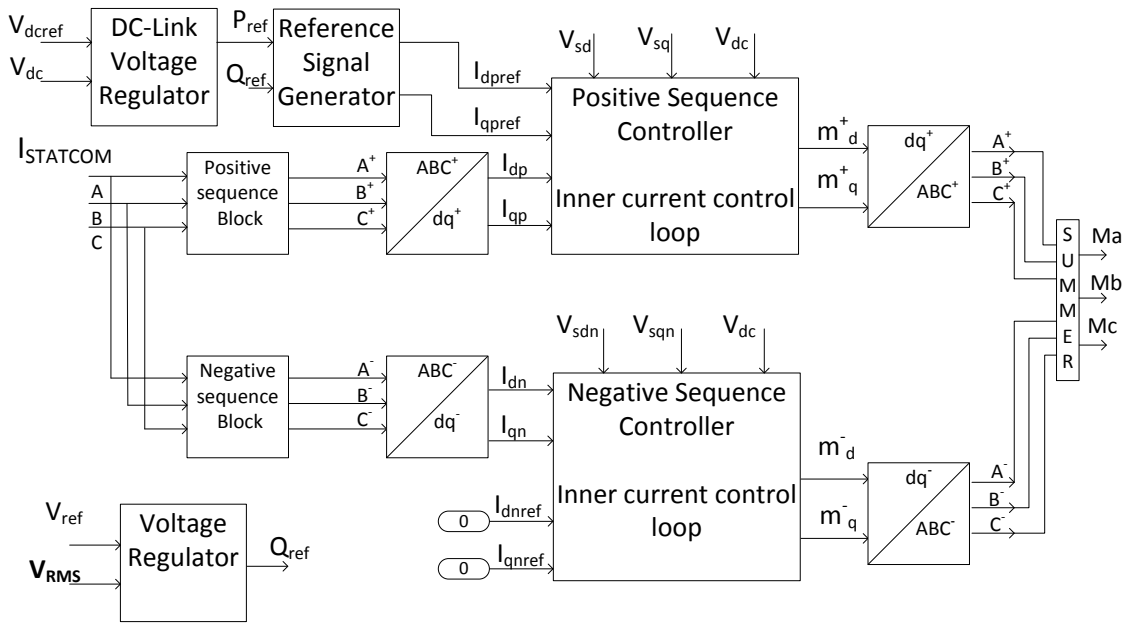
Figure 2.19 Block diagram of complete STATCOM controller for voltage regulation

2.4.3   Temporary Over-Voltage (TOV) Regulation

During asymmetric fault in the network, lines may be subjected to temporary overvoltage; which if not cured may damage the network. In such a scenario, STATCOM is expected to regulate TOV instead of three phase RMS voltage.

Figure 2.20 presents the logic for detection of TOV and its mitigation technique. For detection overvoltage, RMS voltage at three phases are measured and compared to a reference value 'Trg$_{ref}$'. For any phase voltage (RMS) less than reference value, TOV regulator is triggered ON. If fault is recovered and phase voltage is above the reference value, the TOV regulator is triggered OFF. Reference value 'Trg$_{ref}$' is decided based on TOV limit set by the utility. To mitigate TOV, maximum RMS phase voltage of PCC is

applied as feedback signal to TOV regulator. The controller compares it with a reference value V_{ref} and generate appropriate reactive power reference Q_{ref}. TOV regulator is comprised of a PI controller that gives Q_{ref} based on voltage error. The complete controller diagram is similar as of Figure 2.18 except instead of voltage regulator, TOV regulator is placed to give Q_{ref}.
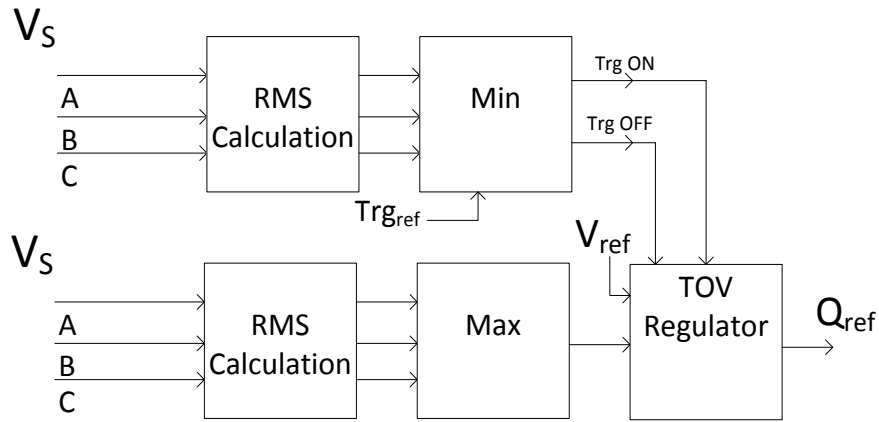
Figure 2.20 Block diagram of temporary overvoltage (TOV) regulator

2.4.4   Voltage Regulation and Voltage Balancing
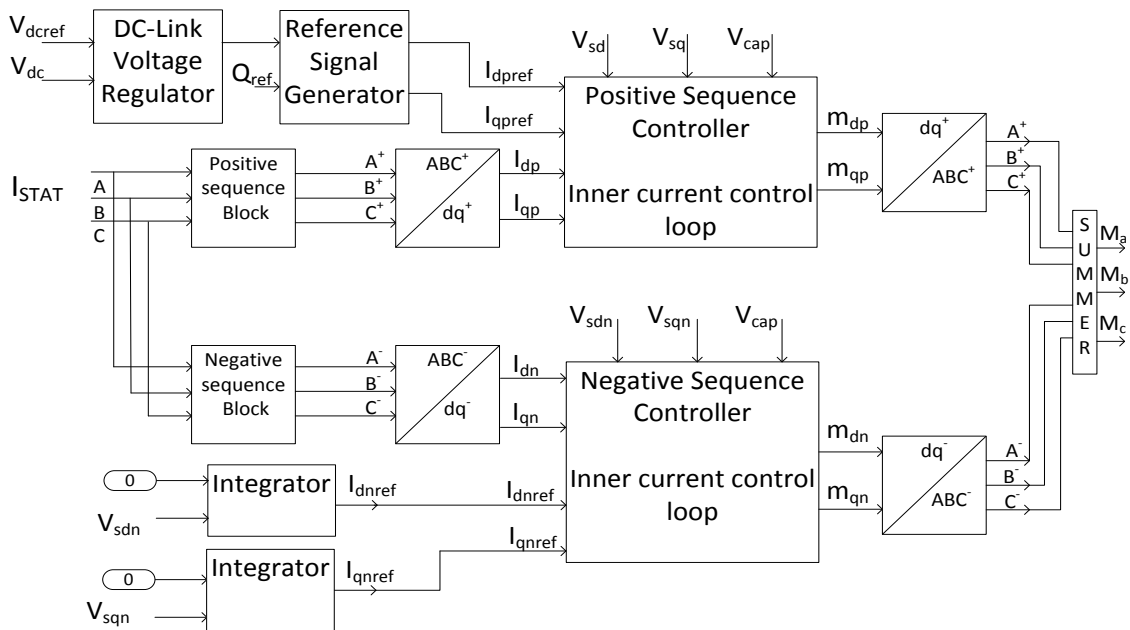
Figure 2.21 Block diagram of complete STATCOM controller for voltage regulation and voltage balancing

For voltage balancing, STATCOM compensates negative sequence voltage by supplying enough negative sequence current such that load sees a symmetric grid [15]. Figure 2.21 presents the complete controller for voltage regulation and balancing. The controller structure is similar as in Figure 2.19 except that integral controllers are used for regulating negative sequence voltage to zero. The outputs from this controller are fed to the negative sequence inner current control loop as reference negative sequence currents (I_{dnref} and I_{qnref}).

2.5 CONCLUSION

In this chapter, modelling of STATCOM and development of comprehensive STATCOM controller are discussed. A Type I inverter control strategy is employed to control voltage sourced inverter (VSI) based STATCOM because of its wide range control facility. STATCOM control for balanced network is presented that includes voltage regulation and power factor correction. Subsequently, controller is modified to compensate 30° phase shift introduced by Y-Δ transformer.

To achieve STATCOM control in unbalanced system, Fortescue decomposition is used to obtain sequence components. An all pass filter is utilized to separate the positive and negative sequence components of voltage and current which is followed by transformation of sequence components to their respective rotating (*dq*) reference frame. Thus, it eliminates the need for *2nd* harmonic notch filter and allows fast settling time of controller.

Successively, STATCOM controller is improved to augment negative sequence controller and for simultaneous operation of both sequence controllers. Furthermore, the developed comprehensive controller for load compensation, voltage regulation, TOV regulation and voltage balancing with voltage regulation is described using block diagrams.

Chapter 3

ASSESSMENT OF COMPREHENSIVE CONTROLLER FOR LOAD COMPENSATION, VOLTAGE BALANCING AND VOLTAGE REGULATION

3.1 INTRODUCTION

This chapter presents STATCOM performance for (i) Load compensation, (ii) Voltage balancing and (iii) Voltage regulation in a distribution feeder having unbalanced loads or asymmetric network. The STATCOM controllers developed in Chapter 2 are employed for different studies. At first, the performance of the developed STATCOM controller is validated with results published in [10]. Out of above three aspects of STATCOM, load compensation is considered for validation with a typical study system given in [10]. For getting desired response characteristics, the selection procedure for controller parameters is also explained.

Subsequently, the power distribution system is modified for steady state analysis and transient analysis for load compensation. The controller performance together with harmonic analysis is demonstrated with the modified system. Further studies with a gross unbalanced load are also reported to investigate the impact of the DC-link voltage on controller functioning.

A network unbalance scenario resembling untransposed transmission lines is created in study system. The STATCOM's capability for balancing steady state voltages together with voltage regulation is exhibited for the above system. Electromagnetic transient simulation studies using PSCAD/EMTDC are performed for assessment of STATCOM performance in all the application of load compensation, voltage balancing and voltage regulation.

3.2 CASE STUDY 1

The validation of developed STATCOM controller is presented in this section. Study system is taken from [10] to validate controller performance for load compensation.

3.2.1   Study System-1 Description

Figure 3.1 depicts the Study System-1 comprising a 110 kV transmission system. The transformer 'TR$_1$' steps down the voltage to 20 kV and connects the grid through a cable to a combination of balanced and unbalanced load (respectively 'Load 1' and 'Load 2'). A STATCOM is utilized at PCC with a coupling transformer 'TR$_2$' to compensate the load reactive power and negative sequence current. STATCOM consists of six electrical switches S$_{1-6}$ (IGBTs or GTOs) and a dc-link capacitor 'C'. PCC voltage is denoted by 'V_S'. System data is given in Appendix A.
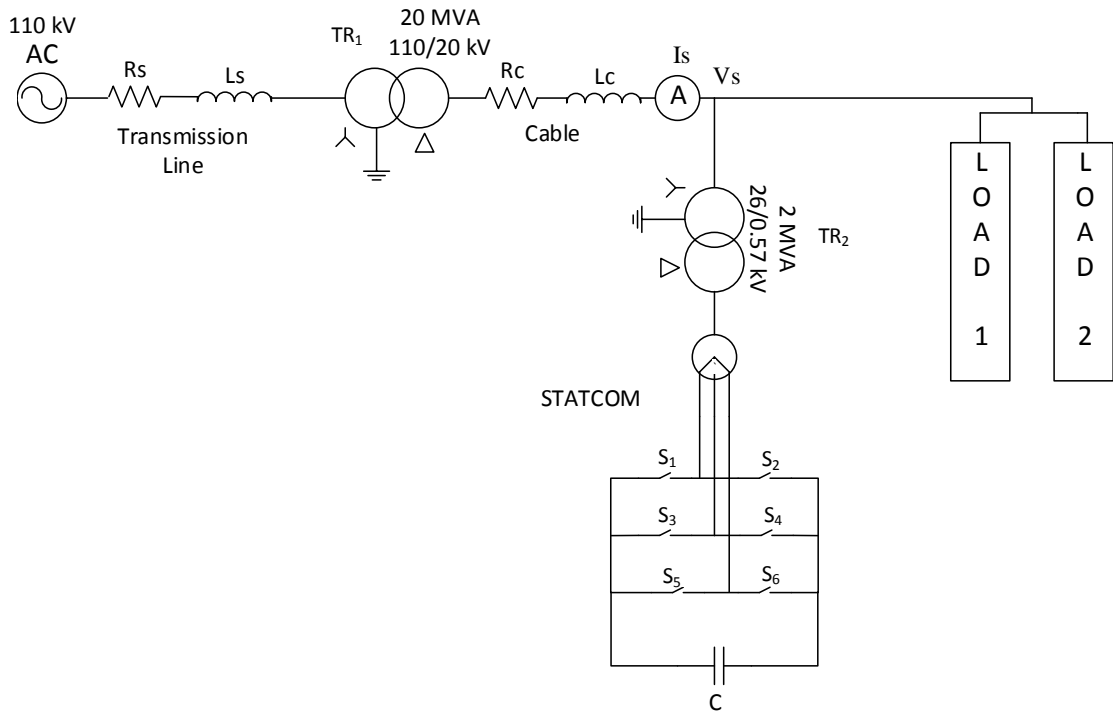
Figure 3.1 Schematic diagram of Study System-1

Figure 3.2(a) presents the simulation results with the proposed study system whereas Figure 3.2(b) depicts the results published in [10]. Figure 3.2(a) presents (i) the three phase source currents I_S, (ii) load current I_{Load}, (iii) STATCOM current $I_{STATCOM}$ and (iv) dc-link voltage V_{dc}. The same sequence of waveform is followed in Figure 3.2(b).

In Figure 3.2(a), STATCOM operation in three modes is illustrated:

1. Mode-1 floating state (inoperative) ($t = 1.85$ to 1.9 sec)

2. Mode-2 Power factor correction ($t = 1.9$ to 2.0 sec)

3. Mode-3 Load compensation ($t = 2.0$ to 2.1 sec)
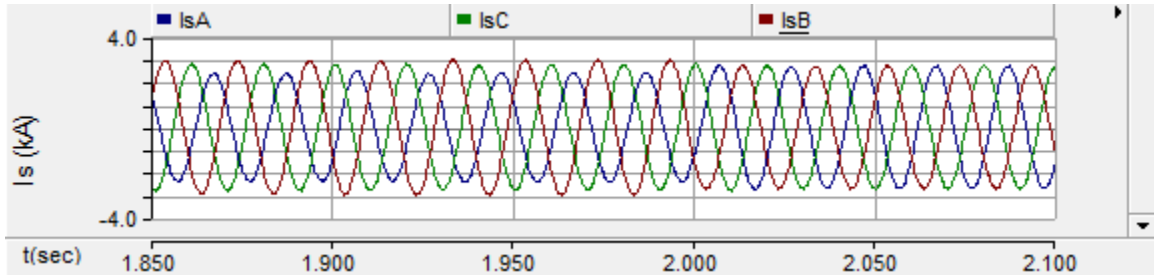
(i)
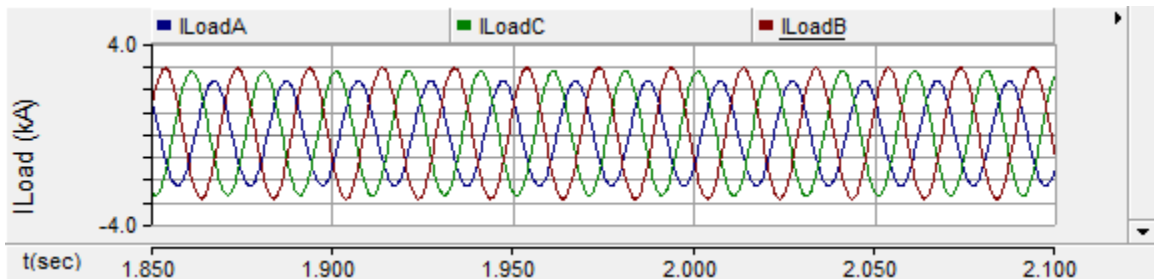
(ii)
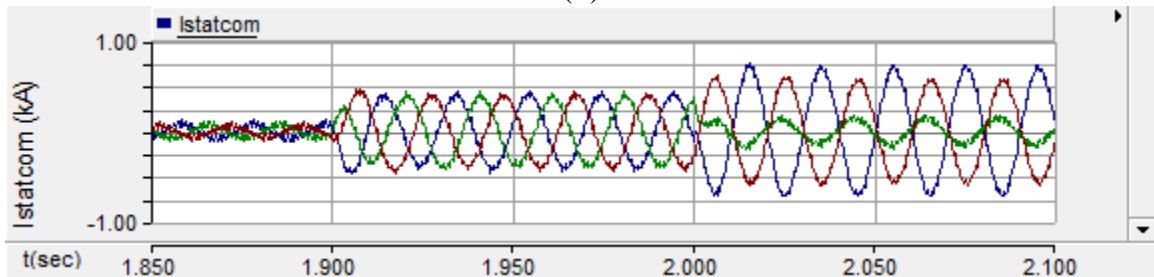
(iii)
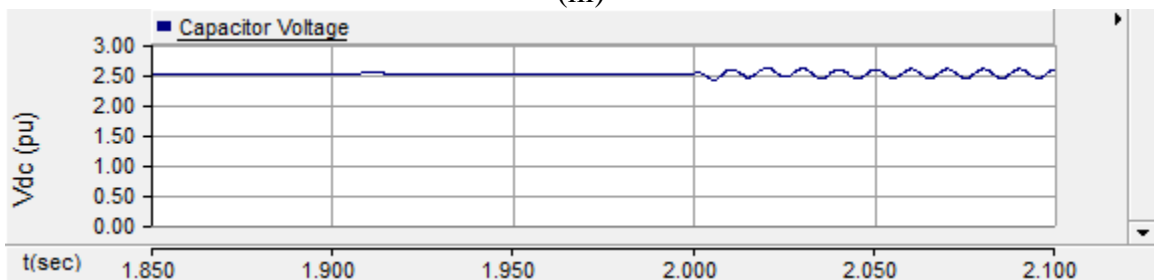
(iv)

(a) (i) Source current, (ii) Load current, (iii) STATCOM current and
(iv) DC-link voltage
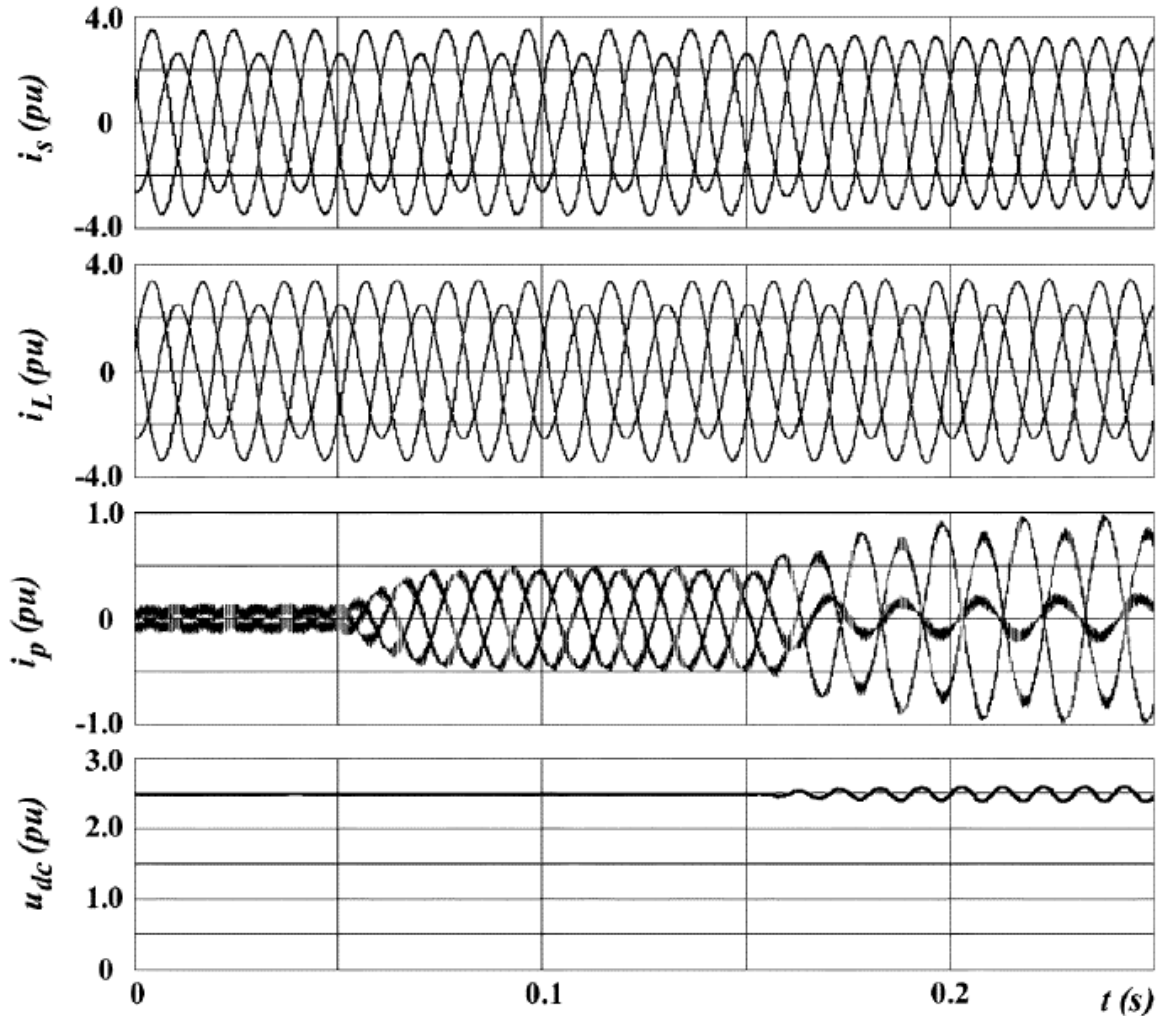
(b) Source side, load side and STATCOM three phase current and DC-link voltage [10]

Figure 3.2 (a) Simulation and (b) published results for compensation of unbalanced load for Study System-1

In floating state, STATCOM does not exchange any reactive power with grid whereas in Mode-2 it corrects the load power factor by providing reactive power. In Mode-3, it compensates the load reactive power and negative sequence load current.

Before $t = 1.9$ sec, STATCOM operates in floating state. At $t = 1.9$ sec, STATCOM starts power factor correction and current starts to flow through STATCOM as shown in Figure 3.2(a) (iii). Because of the unbalanced load, load current and consequently source current also become asymmetric [10]. At $t = 2.0$ sec, negative sequence controller of STATCOM starts compensating the negative sequence load current. As a result, source side current

becomes symmetric even when the load current is asymmetric as seen in Figures 3.2(a) (i) and (ii). STATCOM now supplies unbalanced current for load compensation and hence, $I_{STATCOM}$ becomes asymmetric.

Because of negative sequence current flow through STATCOM, V_{dc} has 2nd harmonic component in voltage as seen in Figure 3.2(a) (iv) [10]. To lessen the ripples a large size capacitor is suggested in [15]. The simulated results are similar to the published results in Figure 3.2(b), and thus validate the design of controller.

Load power factor for the same study system is presented in Figure 3.3. Before $t = 1.9$ sec, the power factor is 0.99 which increases to unity after STATCOM transitions to mode-2 for power factor correction. Nonetheless, 2nd harmonic components in power factor are still observed. After $t = 2.0$ sec, STATCOM starts compensating negative sequence currents and hence, power factor becomes unity. No 2nd harmonic components are observed during this period.
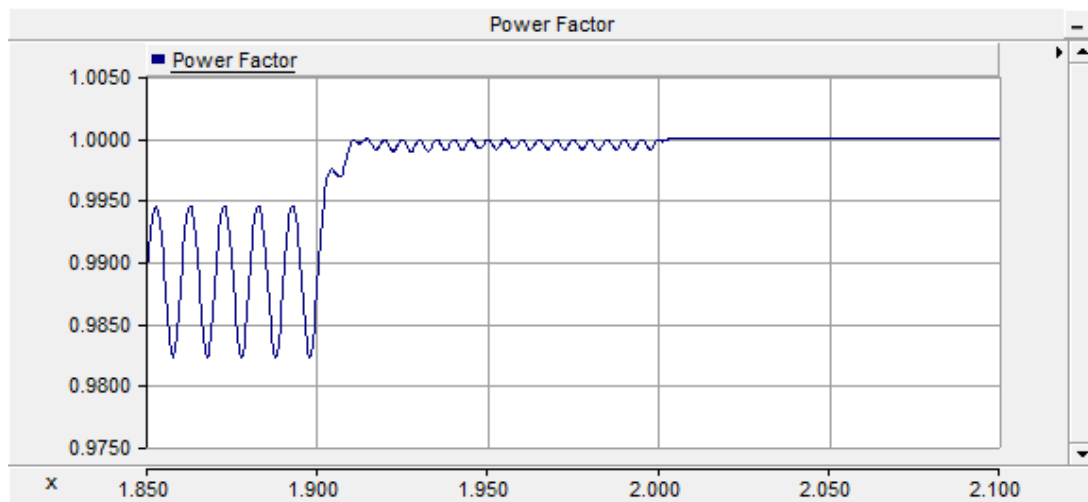
Figure 3.3 Power factor during load compensation for study system-1

Figure 3.4 presents the pu values of STATCOM current in dq reference frame for the same study. Figure 3.4(a) depicts the simulation results with proposed study system and Figure 3.4(b) depicts the results published in [10]. Figure 3.4(a) presents (i) the positive sequence q axis component of STATCOM current I_{qp} . Figures 3.4(a) (ii) and (iii) present the negative sequence d and q axis parts of STATCOM current I_{dn} and I_{qn} respectively. The same sequence is followed in Figure 3.4(b).

As discussed in Chapter 2, I_{qp} represents reactive power (positive sequence) flow through the STATCOM. The STATCOM is in mode-1 before $t = 1.9$ sec, therefore, I_{qp} is zero. As STATCOM enters into mode-2, I_{qp} reaches its reference value (Load reactive power) in less than a cycle. During this time, the negative sequence controller is inactive. Therefore I_{dn} and I_{qn} have zero steady state values. The transients at time $t = 1.9$ sec are attributed to incomplete decoupling of positive and negative sequence currents [10]. At time $t = 2.0$ sec, the STATCOM transitions to mode-3, thus compensates load negative sequence currents (I_{dpref} and I_{qpref}) in less than 2 cycles. The transients at this time are also caused by incomplete decoupling of positive and negative sequence currents.
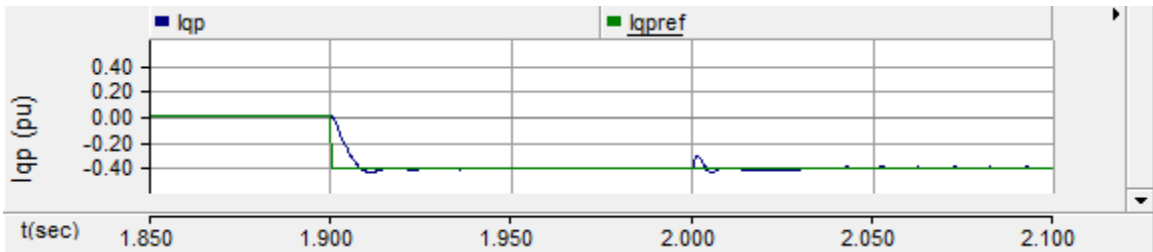
(i)
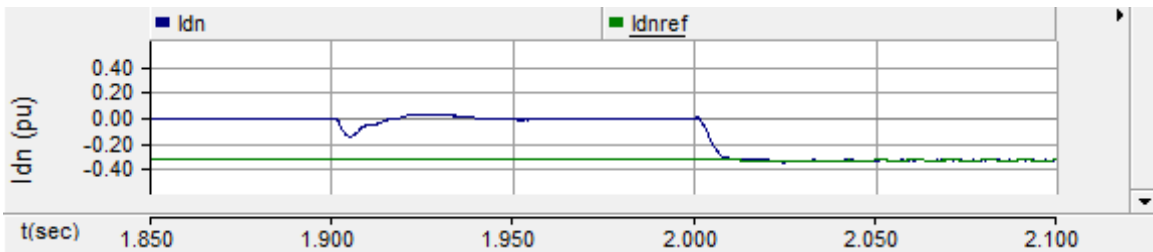
(ii)
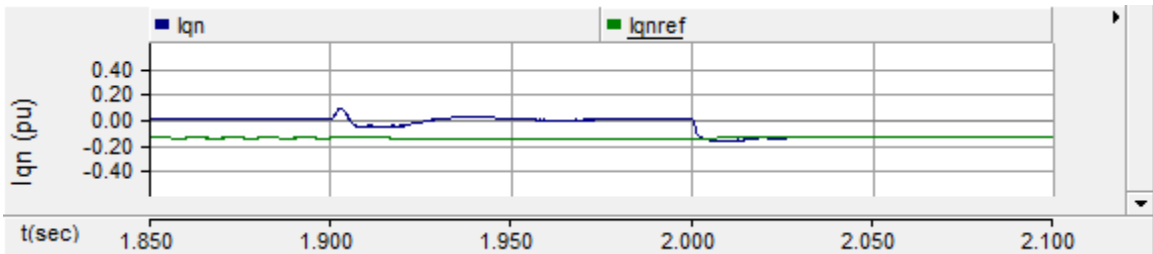
(iii)

(a) (i) Positive sequence q axis STATCOM current, (ii) and (iii) negative sequence d and q axis STATCOM current
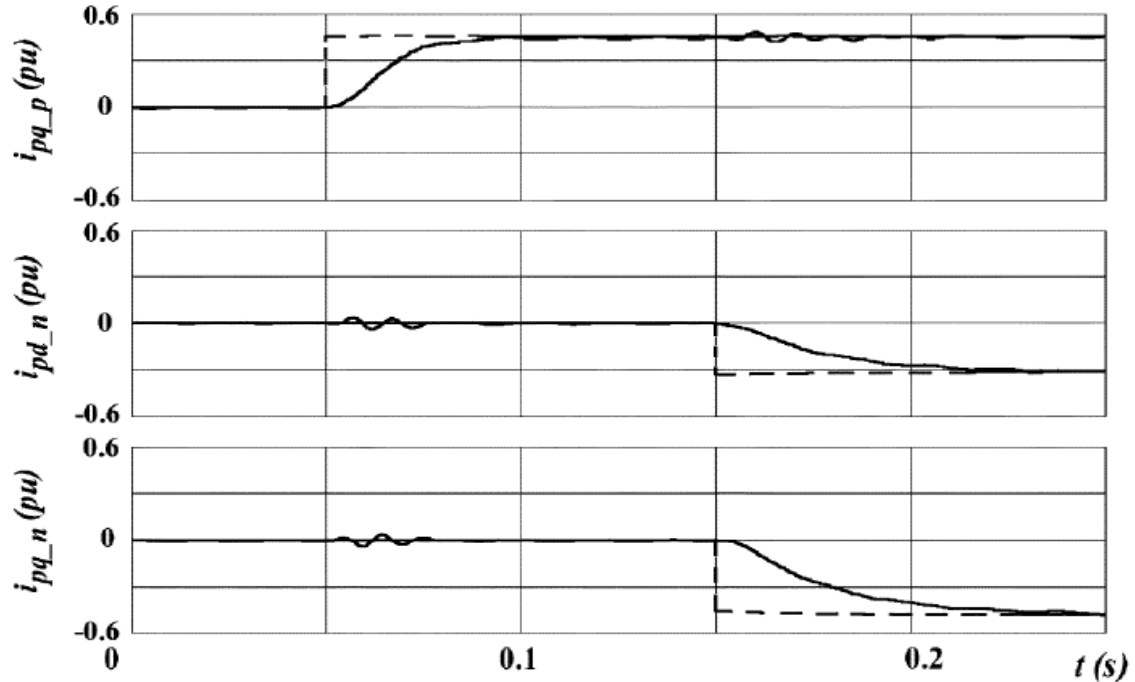
(b) *q* axis part for positive sequence and *d* and *q* axis parts negative sequence STATCOM current

Figure 3.4 Positive and negative sequence currents in *dq* reference frame in (a) simulation and (b) published [10] results for load compensation for Study System-1

Figure 3.4(b) illustrates response of controller proposed in [10]. The change of sign of I_{qp} in Figure 3.4(a) and Figure 3.4(b) is because of different convention of power flow used in this thesis. The magnitude difference in negative sequence current is due to Y-Δ transformer. As in this simulation, voltage and currents are measured at high voltage side (Y) of transformer and in [10] the measurements are done at low voltage side (Δ) of transformer.

On comparison of Figures 3.4(a) and (b), at time $t = 1.9$ sec, I_{qp} reaches its reference value in less than a cycle in Figure 3.4(a) (i) while it takes more than 2 cycles for the same in Figure 3.4(b). Also, in Figures 3.4(a) (ii and iii) at time $t = 2.0$ sec, I_{dn} and I_{qn} track their reference values in 2 cycles, whereas a settling time of 4 cycles is illustrated in Figure 3.4(b).

Therefore, a faster response of STATCOM is exhibited by proposed controller. This is attributed to the use of an all pass filter, explained in Section 2.3.1 with that instant separation of positive and negative sequence components is possible.

3.2.2   Selection of Controller Parameters

Controller parameter design is important for suitable STATCOM response [1]. The response should have a fast rise time, a very small settling time (within 2% of reference value) and an overshoot no more than 15%. A PI controller is used to control active and reactive power output of STATCOM. The controller parameters of positive sequence inner current control loop are denoted by (K_{pd_p} and T_{id_p}) and (K_{pq_p} and T_{iq_p}) respectively and are described in section 2.2.7. Also, for negative sequence controller, the PI controller parameters, respectively, are (K_{pd_n} and T_{id_n}) and (K_{pq_n} and T_{iq_n}). A PI controller (K_{pdc} and $T_{idc)}$ is also used to control the DC link voltage.

3.2.2.1   Selection of reactive power controller gain (K_{pq_p})

Figure 3.5 illustrates positive sequence component of STATCOM current for different values of gain K_{pq_p} keeping T_{iq_p} constant for load compensation with Study System-1. Figure 3.5(a) presents the positive sequence *d* and *q* axis parameters of STATCOM current (I_{dp} and I_{qp} respectively). When K_{pq_p} is taken as 0.08, a very large overshoot (60%) is seen in the response of I_{qp} after time *t* = 1.9 sec at the event of power factor correction. Also, it increases the settling time. Figure 3.5(b) presents the response when K_{pq_p} is increased to 10 times the previous value. Overshoot for the value of I_{qp} is reduced to 45% but still it is not within stated range.

Figure 3.5(c) depicts the response with K_{pq_p} = 80. At time *t* = 1.9 sec, I_{qp} responds with desired characteristics, but the settling time for active power control (I_{dp} control) is increased to 3 cycles compare to the response presented in Figures 3.5(a) and (b). With more increment in gain (K_{pq_p} = 800), sustained oscillation in active power reference can be seen in Figures 3.5(d). Considering all these responses, controller is tuned to a value of K_{pq_p} = 8 and corresponding response is given in Figure 3.4(a) (i).

(a) $K_{pq\_p} = 0.08$

(b) $K_{pq\_p} = 0.8$

(c) $K_{pq\_p} = 80$

(d) $K_{pq\_p} = 800$
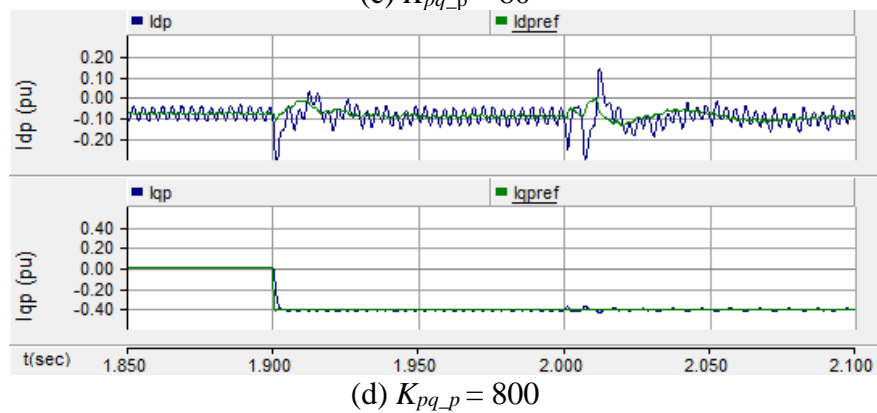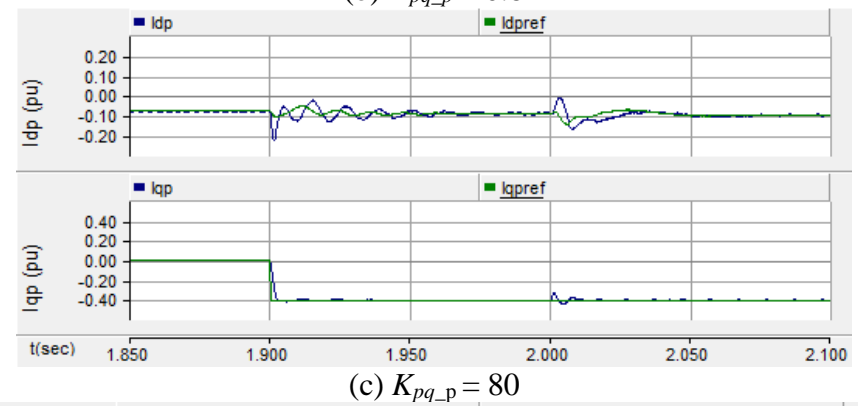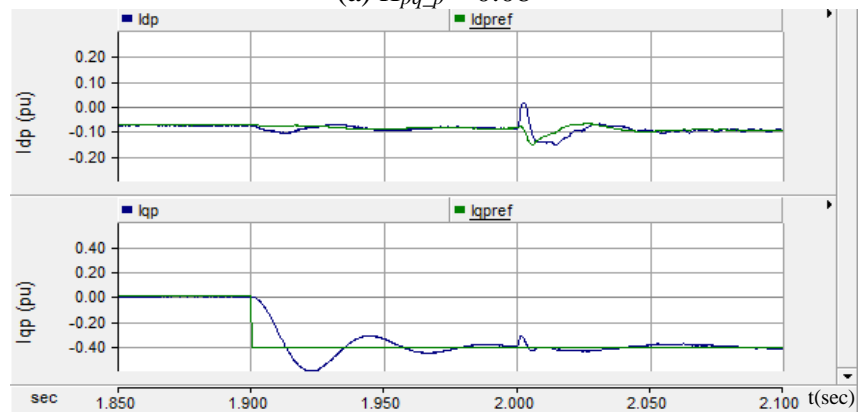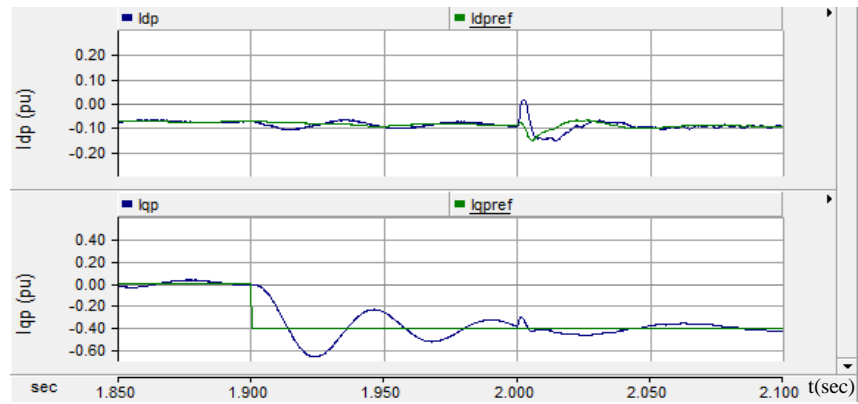
Figure 3.5 Positive sequence current (in *dq* frame) for different gain (K_{pq_p}) values

3.2.2.2   **Selection of reactive power controller time constant (T_{iq_p})**

Figure 3.6 illustrates positive sequence component of STATCOM current for different values of time constant T_{iq_p}, keeping gain K_{pq_p} constant for load compensation study.

(a) $T_{iq\_p} = 5e\text{-}05$

(b) $T_{iq\_p} = 1e\text{-}04$

(c) $T_{iq\_p} = 4e\text{-}04$

Figure 3.6 Positive sequence current (in *dq* frame) for different time constant (T_{iq_p})

Figure 3.6(a) presents the positive sequence d and q axis parts of STATCOM current (I_{dp} and I_{qp} respectively) for time constant T_{iq_p} = 5e-05. At time t =1.9 sec, for power factor correction, a large overshoot is seen in the response of i_{qp}. With twice the value of previous time constant, response is presented in Figure 3.6(b). In this case, overshoot is reduced but not sufficiently. As time constant increases in Figure 3.6(a) and (b), overshoot in response of I_{qp} reduces although rise time increase. With T_{iq_p} = 4e-04, the response of the controller is presented in Figure 3.6(c). Not much change is observed in the response of I_{dp} controller for all three cases. However, settling time increases to 2 cycles without an overshoot after t = 1.9 sec. Considering all the factors, T_{iq_p} is taken such that settling time can be reduced to half cycle for power factor correction with overshoot in acceptable limit. The value is found to be T_{iq_p} = 2e-04. The response is given in Figure 3.4(a) (i) for this value.

The same strategy is applied for finding controller parameters for DC-link voltage regulator, active power controller and negative sequence current controller. The values of controller parameters for each control are given in Appendix A.

3.3 CASE STUDY 2

The study system in [10] resembles a European radial network which operates at frequency of 50 Hz. To have a North American look alike system and for furthermore studies, system is modified in this section. For studies in section 3.2, positive and negative sequence controllers do not operate together instantly [10]. But in this section, a simultaneous operation of both controllers is presented as load becomes unbalanced.

3.3.1   Study System-2 Description

Figure 3.7 depicts the Study System-2 for steady state studies and load compensation studies in this section. System is identical as described in section 3.2.1, except the operating frequency is made 60 Hz (as in North America). Also the unbalanced load (Load 2) is connected with a mechanical switch 'SW' instead of being connected permanently. This is done to assess the instant operation of positive and negative sequence controllers. The

controller of STATCOM has also been modified for the study and the design procedure is same as discussed in section 3.2.2. The details of STATCOM are given in Appendix A.
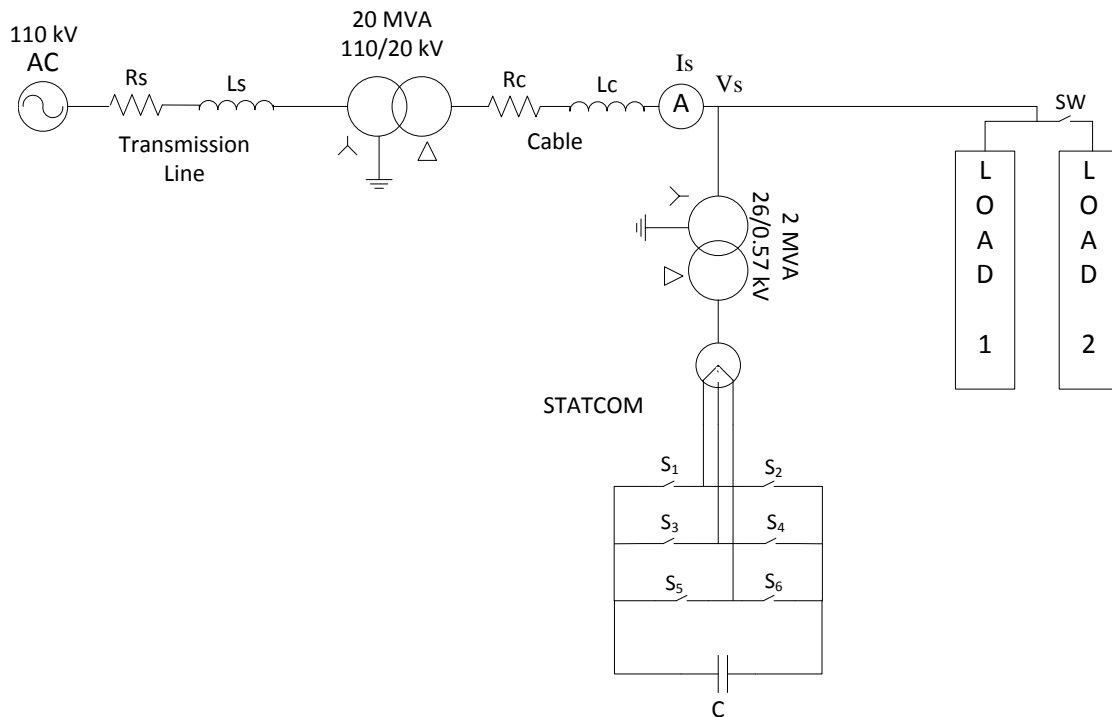
Figure 3.7 Schematic diagram of Study System-2

3.3.2   Steady State Operation

In this study only balanced load is connected to system. The switch 'SW' is kept open. All positive and negative sequence controllers of STATCOM are made active for this study. Figure 3.8 illustrates STATCOM operation in steady state. Figure 3.8(a) depicts voltage at PCC V_S , Figure 3.8(b) depicts RMS voltage at PCC V_{RMS} and Figure 3.8(c) presents three phase source current. STATCOM operates in three zones

1. Zone 1 (floating state, before $t = 2.3$ sec)
2. Zone 2 (maximum capacitive, 2.3 sec $< t < 2.4$ sec)
3. Zone 3 (maximum inductive , after $t = 2.4$ sec)
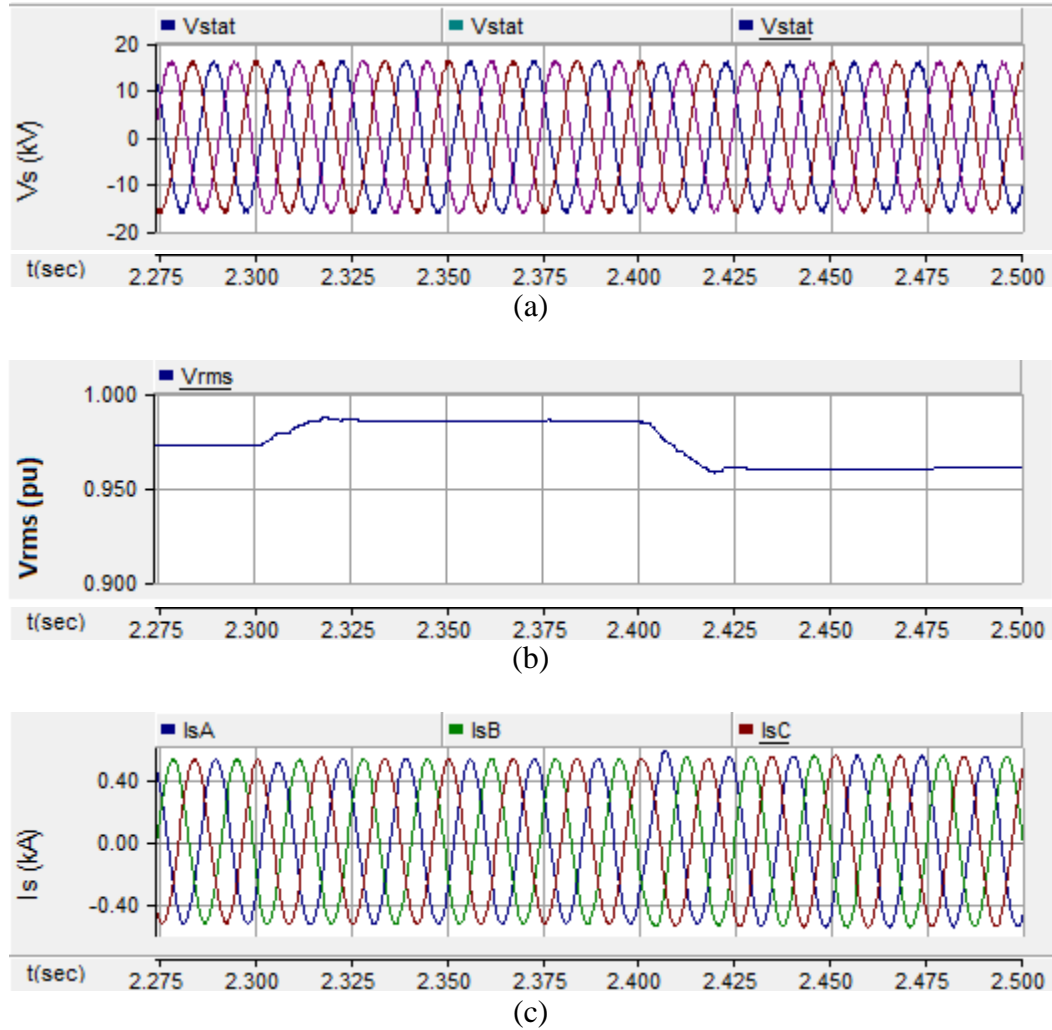
Figure 3.8 (a) PCC Voltage, (b) RMS voltage and (c) source current for steady state operation with Study System-2

At time $t = 2.3$ sec, STATCOM is given a command to supply its rated 2 MVAr capacitive power. At time $t = 2.4$ sec, it is commanded to operate at rated 2 MVAr inductive power. Therefore, it transitions from one limit (rated capacitive) to another limit (rated inductive) at time $t = 2.4$ sec.

When STATCOM is in zone 1, V_{RMS} is 0.98 pu. PCC voltage V_S and source currents I_S are balanced and a slight increase in RMS voltage is seen due to reactive power flow from STATCOM to PCC at $t = 2.3$ sec. After $t = 2.4$ sec, due to operation in inductive range, V_{RMS} drops to 0.96 pu. The PCC voltage and source current are balanced because there is no asymmetry in the system.
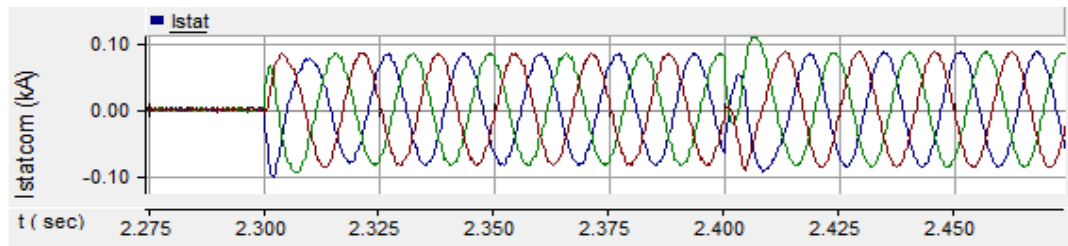
(a)
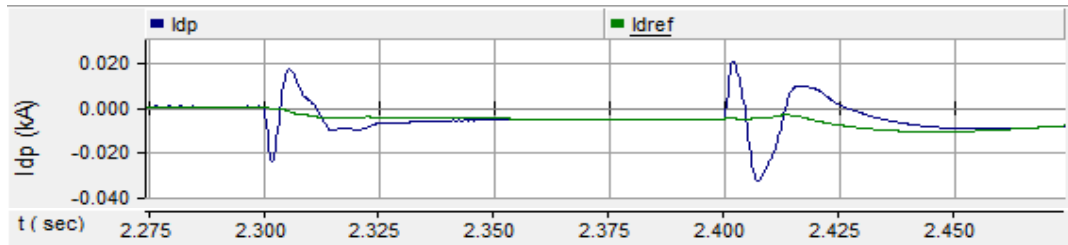
(b)
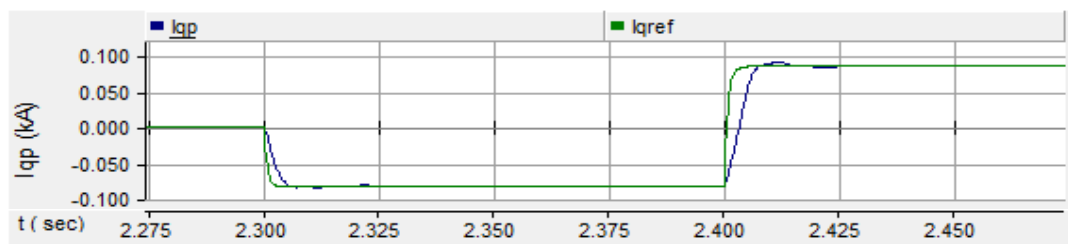
(c)
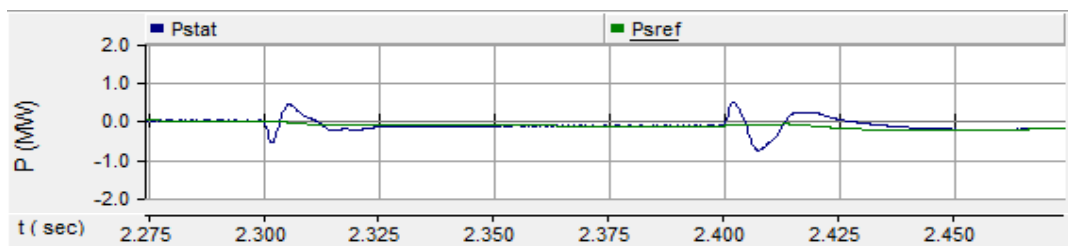
(d)
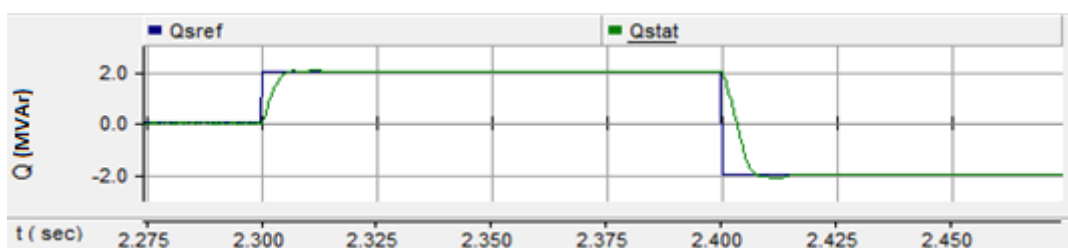
(e)

Figure 3.9 (a) STATCOM current (b) and (c) positive sequence component of current in *dq* frame, (d) and (e) active and reactive power output for steady state operation with Study System-2

Figure 3.9 presents the detailed performance of STATCOM controller for steady state operation. Figure 3.9(a) depicts the current through device ($I_{STATCOM}$), Figures 3.9(b) and (c) depict the *dq* parts of positive sequence current of STATCOM respectively. Figures 3.9(d) and (e) present the active and the reactive power outputs of STATCOM respectively.

In zone 1 STATCOM is in floating state, therefore, before t = 2.3 sec, $I_{STATCOM}$ is zero (Figure 3.9(a)). At t = 2.3 sec, STATCOM enters in zone 2, and starts supplying rated capacitive power. In Figures 3.9(b) and (d) the active power component of $I_{STATCOM}$ and active power flow itself is very small as STATCOM only needs active power to supply its losses. From Figures 3.9(c) and (e), I_{qp} tracks it reference value in half cycle. This is an acceptable response time of a STATCOM [1].

At t = 2.4 sec, STATCOM makes a transition from its maximum capacitive limit to maximum inductive limit. Therefore, in Figure 3.9(a) $I_{STATCOM}$ changes its phase 180° while keeping the magnitude constant with an intermediate transient. A little transient, due to incomplete decoupling, in response of I_{dp} is seen in Figure 3.9(b) [32]. However, the active power flow is still very small as seen in Figure 3.9(d). It is evident from Figure 3.9(e), the reactive power changes from 2 MVAr capacitive to inductive within half cycle and the similar response is indicated in Figure 3.9(c).

Negative sequence component of STATCOM current in *dq* frame is presented in Figure 3.10. Figure 3.10(a) presents the *d*-axis parts of negative sequence component of STATCOM current I_{dn} and of load current I_{dnref}. Figure 3.10(b) illustrates *q*-axis parts of negative sequence component of STATCOM current I_{qn} and of load current I_{qnref}. Since only balanced load is connected, reference values (I_{dnref} and I_{qnref}) are zero. At time t = 2.3 sec, and t = 2.4 sec, transients appear which die out in steady state as negative sequence controllers are fully decoupled in steady state [10]. Thus, STATCOM supplies no negative sequence current in steady state.
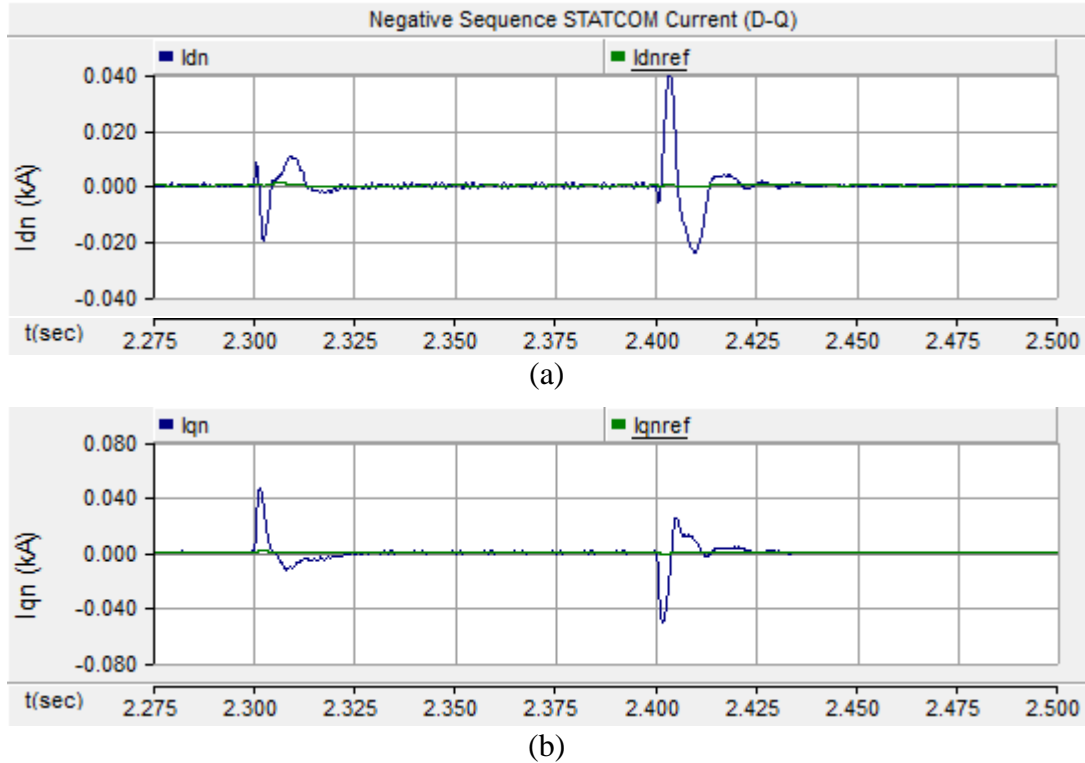
Figure 3.10 (a) *d*-axis and (b) *q*-axis parts of negative sequence component of
STATCOM current for steady state operation with Study System-2

3.3.3 Transient Operation with Unbalanced Load

In this case an unbalanced load 'Load 2', as shown in Figure 3.7, is switched ON at time
$t = 2.0$ sec. When STATCOM is not active, the response of the system in presented in
Figure 3.11. Switching of unbalanced load causes mild unbalance in system. Figure 3.11
depicts (a) the PCC voltage V_S, (b) the load power factor and (c) the source current 'I_S'.
At $t = 2.0$ sec, the unbalanced load is connected with the network. Therefore source current
becomes asymmetric after $t = 2.0$ sec in Figure 3.11(c). In power factor, 2nd harmonic
oscillations can also be seen after $t = 2.0$ sec.

In Figure 3.12, the response of system is presented with STATCOM. STATCOM is used
to compensate the load such that unbalanced current comes from STATCOM and grid is
loaded only with positive sequence currents. The parameters are presented in similar format
as in Figure 3.11.

Before $t = 1.9$ sec, STATCOM is in floating state with all controllers active. At time $t = 1.9$, STATCOM is commanded for power factor correction with balanced load connected. It is apparent from Figure 3.12(b) that STATCOM compensates the reactive power in less than a cycle, making the load power factor unity. PCC voltage and source current remain balanced.

At $t = 2.0$, unbalanced load is switched on, the STATCOM starts load compensation instantly, making source current balanced as shown in Figure 3.12(c) compared to unbalanced current I_S in Figure 3.11(c). No steady state oscillations in power factor are observed with STATCOM in Figure 3.12(b).

(a)

(b)

(c)
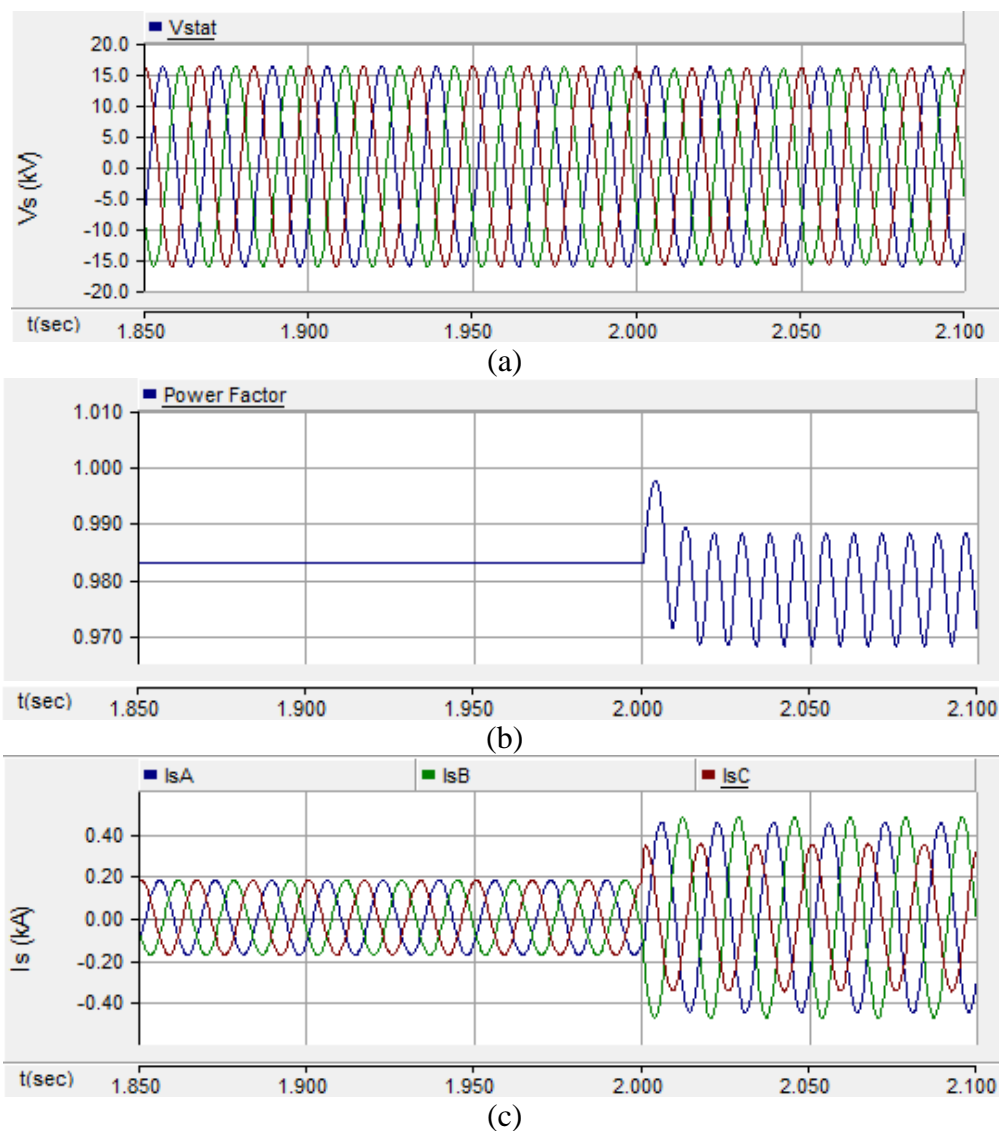
Figure 3.11 (a) PCC Voltage, (b) power factor and (c) source current for Study System-2 without STATCOM
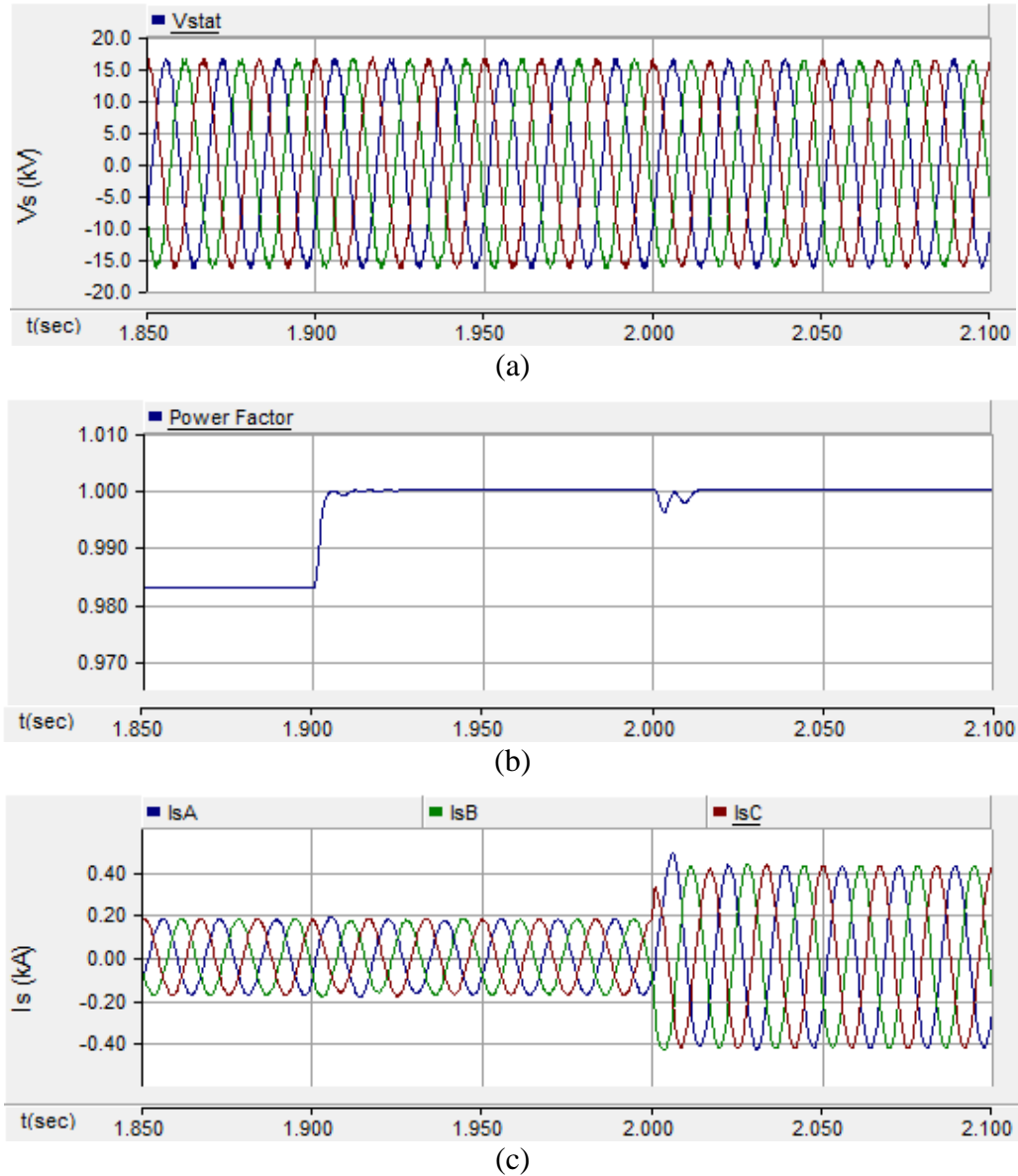
Figure 3.12 (a) PCC Voltage, (b) power factor and (c) source current for load compensation study for Study System-2 with STATCOM

The performance of STATCOM controller for the unbalanced load compensation with Study Sytem-2 is presented in Figure 3.13. Figure 3.13(a) depicts the current through device $I_{STATCOM}$, Figures 3.13(b) and (c) depict the q-axis part of positive sequence current of STATCOM and reactive power output Q respectively. Figures 3.13(d) and (e) depict the d-axis part of positive sequence current of STATCOM and active power output respectively. Figure 3.13(f) depicts the dc-link capacitor voltage of STATCOM.
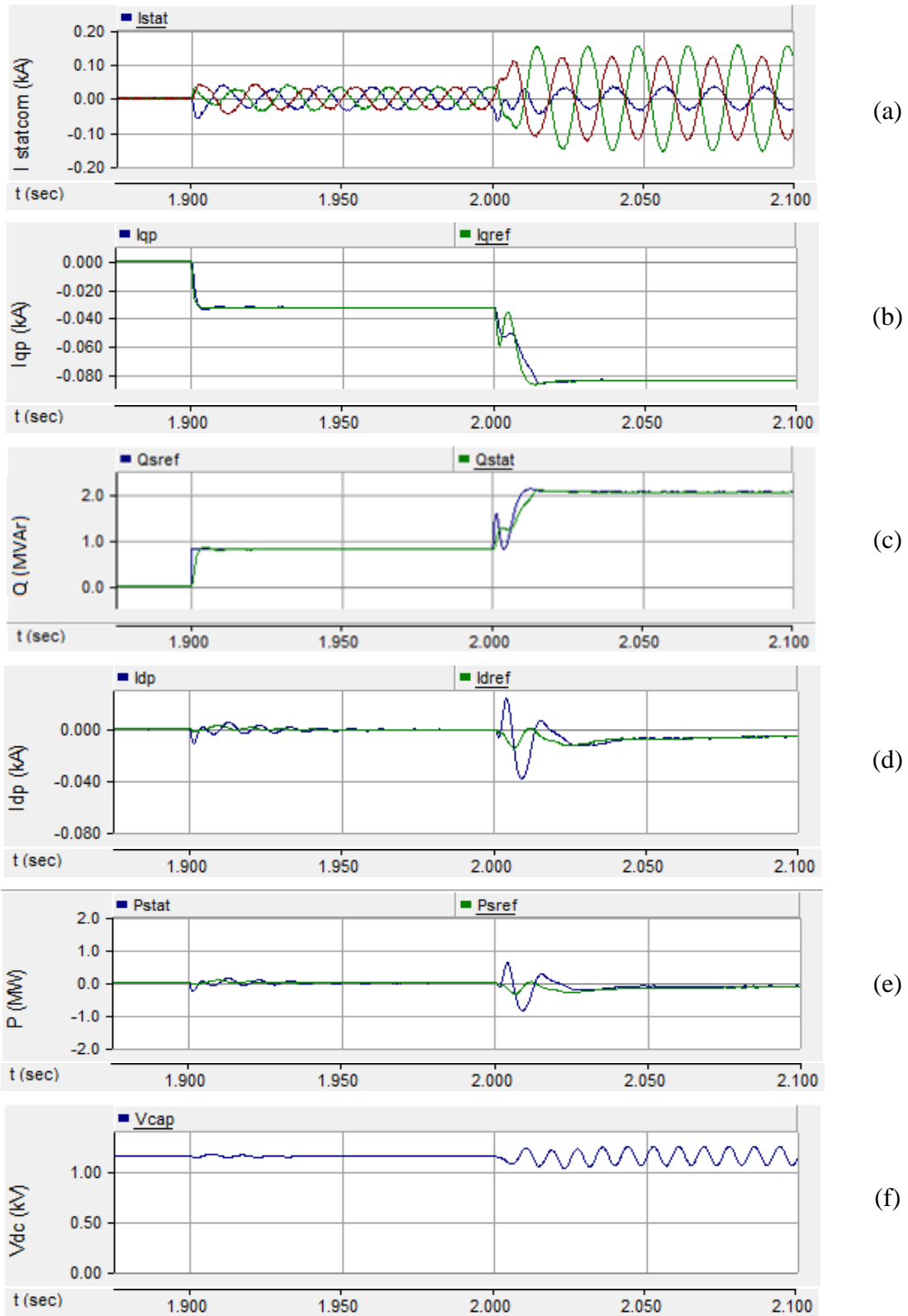
Figure 3.13 (a) STATCOM current, (b) *q*-axis part of current, (c) reactive power output in *dq* frame, (d) *d*-axis part of current, (e) active power output in *dq* frame and (f) DC-link voltage for load compensation for Study System -2

Before $t = 1.9$ sec, STATCOM is in floating state. Therefore, $I_{STATCOM}$ is zero (Figure 3.13(a). At t = 1.9 sec, STATCOM starts reactive power compensation. It is observed in Figures 3.13(b) and (c), that I_{qp} and reactive power Q tracks its reference value in less than a cycle making power factor unity. Figures 3.13(d) and (e) indicate a little active power flow into the STATCOM to supply losses. The DC-link voltage remains constant at its reference value of 1.155 kV.

At $t = 2.0$ sec, STATCOM starts supplying negative sequence current to load. Therefore, $I_{STATCOM}$ becomes asymmetric as shown in Figure 3.13(a). Additional load draws more reactive power, therefore STATCOM increases its reactive power output to compensate the load reactive power as shown in Figures 3.13(b) and (c). Because of unbalanced current through STATCOM the losses in the device increase, giving rise to active power input as observed in Figures 3.13(d) and (e). Negative sequence current flowing through STATCOM causes 2nd harmonic voltage at the dc-link. Therefore, 2nd harmonic oscillation can be seen in Figure 3.13(f). However, average dc-link voltage is still 1.155kV.

Figure 3.14(a) presents the d-axis part of negative sequence component of STATCOM current I_{dn} and of load current I_{dnref}. Figure 3.14(b) presents the q-axis part of negative sequence component of STATCOM current I_{qn} and of load current I_{qnref}. Before $t = 2.0$ sec, there is no asymmetry in network, therefore, no negative sequence current flows through STATCOM in steady state.

After $t = 2.0$ sec, with the introduction of unbalanced load, I_{dnref} and I_{qnref} attain non-zero value. I_{dn} and I_{qn} track their reference values in less than 2 cycles as illustrated in Figure 3.14. The undershoot in I_{dnref} at time $t = 2.0$ sec, is due to response of all pass filter. For high frequency components, all pass filter provides a phase shift of 180° (Figure 2.15). Hence, to reduce the undershoot a low pass filter is recommended after the extraction of dq-axis components of sequence currents [64].
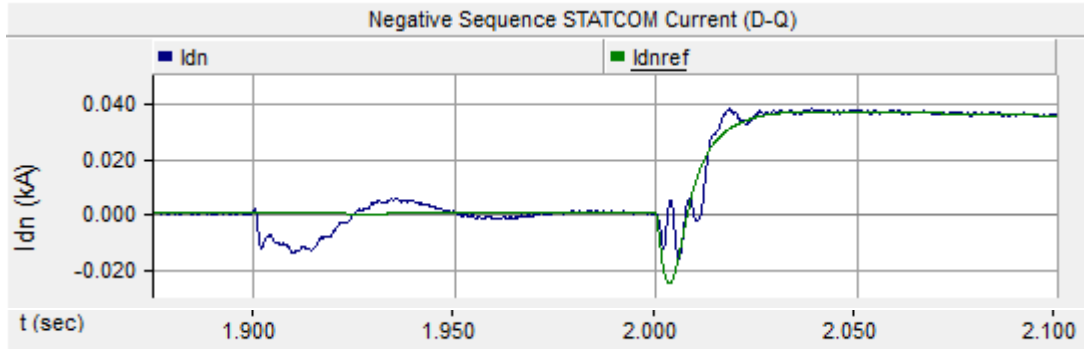
(a)
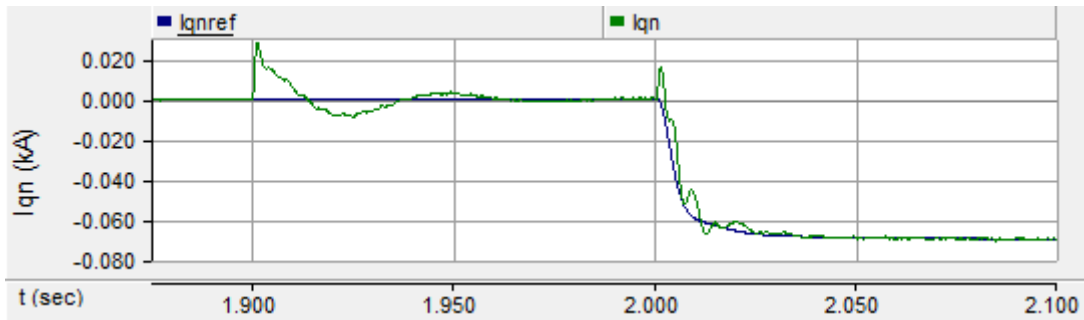
(b)

Figure 3.14 (a) *d*-axis and (b) *q*-axis parts of negative sequence component of
STATCOM current for load compensation for Study System -2

Table 3.1 gives THD for PCC voltage and STATCOM current. THD comes out fairly
below the limit of 5% in each case as specified in IEEE std 519 [34]. 3rd harmonic content
is analyzed in STATCOM current. The maximum content is 1.7% in phase 'A' which is
also below 4% limit specified in [34]. Hence, STATCOM successfully operates with
SPWM technique without generating undesirable magnitude of harmonics.

Table 3.1 Harmonic analysis with STATCOM operation for load compensation

Harmonic analysis	Phase A (%)	Phase B (%)	Phase C (%)
THD of PCC Voltage	0.04	0.03	0.03
THD of STATCOM current	1.9	0.2	0.4
3rd harmonic content in STATCOM current	1.7	0.12	0.32

3.4 CASE STUDY 3

In this case study, the STATCOM controller performance is investigated with a gross unbalanced load. The impact of DC-link voltage on its performance is also presented. To investigate it, the Study System-2 is modified to have a Δ configured load.

3.4.1   Study System-3 Description

Figure 3.15 depicts the Study System-3 having a gross unbalanced load. The system is similar to study system given in Section 3.3.1 except that instead of two loads, a balanced delta connected load 'Load 1' is considered which has a mechanical switch 'SW' in one of its branch. The switch allows the condition of gross unbalanced load to be created such that only 2 branches of load are connected and one branch is isolated from the network. The same STATCOM controller given in section 3.3.1 is used. The 'Load 1' data is given in Appendix A.

3.4.2   Gross Unbalance in Load
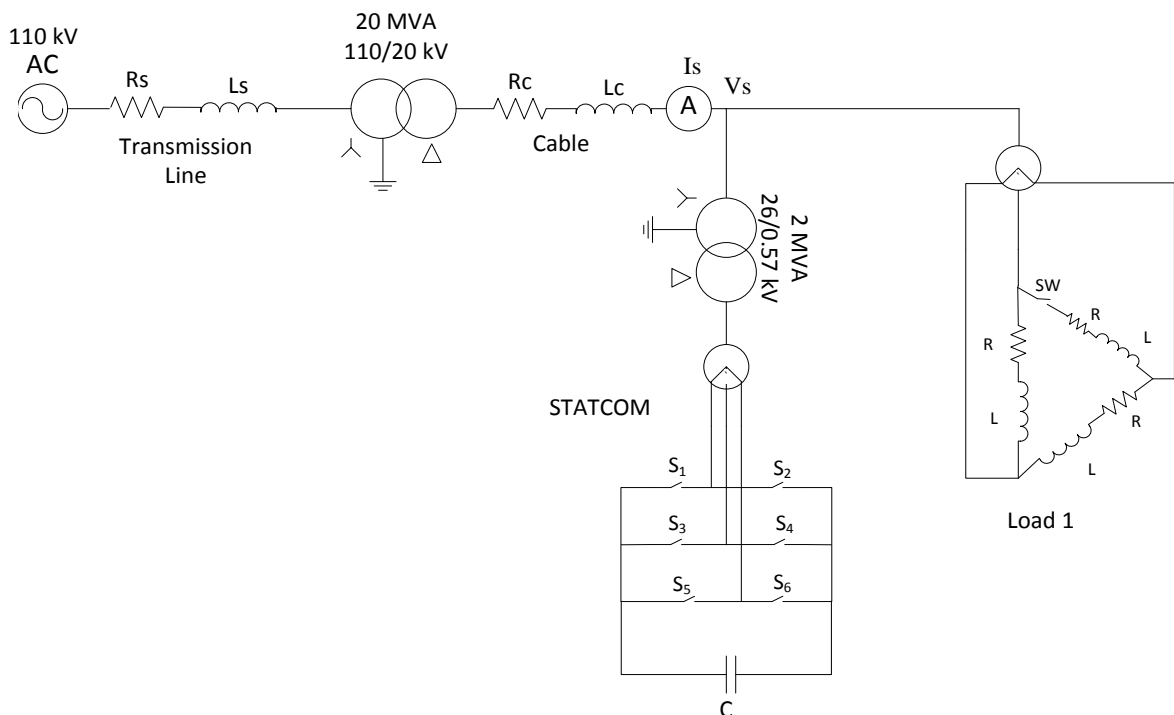
Figure 3.15 Schematic diagram of Study System-3

Before t = 2.1 sec, switch 'SW' is in closed position and system is balanced. At time t = 2.1 sec, switch is opened to allow gross unbalanced load connection. This causes a severe

imbalance in system. Figure 3.16 presents the response of the system to this imbalance in the absence of STATCOM. Figure 3.16 depicts (a) the PCC voltage V_S , (b) the power factor of load and (c) the source current I_S from the grid. Due to the isolation of one branch, the source current in one phase becomes zero as shown in Figure 3.16(c). Also power factor oscillates with a large magnitude in Figure 3.16(b). This kind of imbalance can affect voltage significantly. It can be seen in Figure 3.16(a) that phase B (green) voltage becomes lower than other phase voltages.
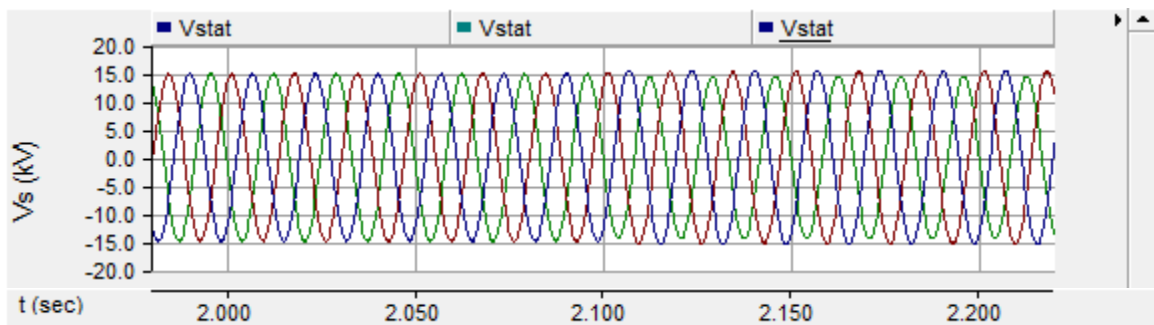
(a)
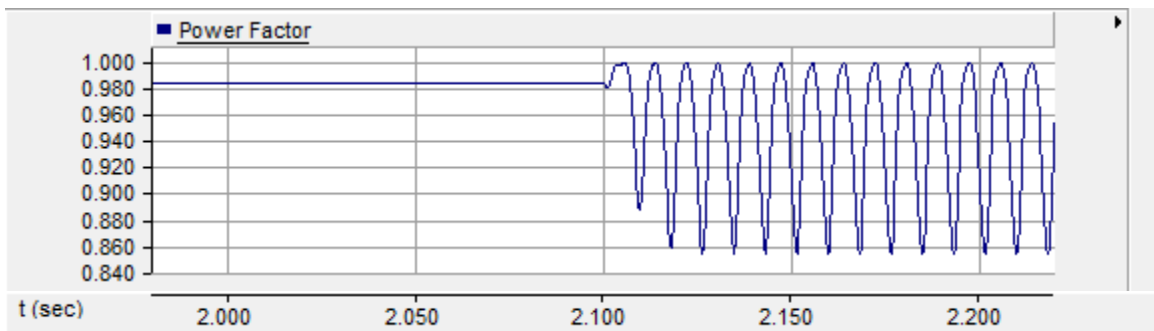
(b)
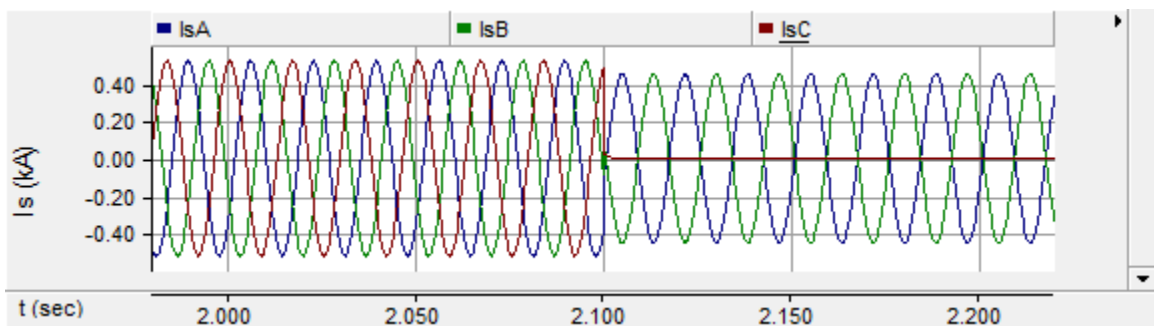
(c)

Figure 3.16 (a) PCC Voltage, (b) power factor and (c) source current for study with gross unbalanced load without STATCOM
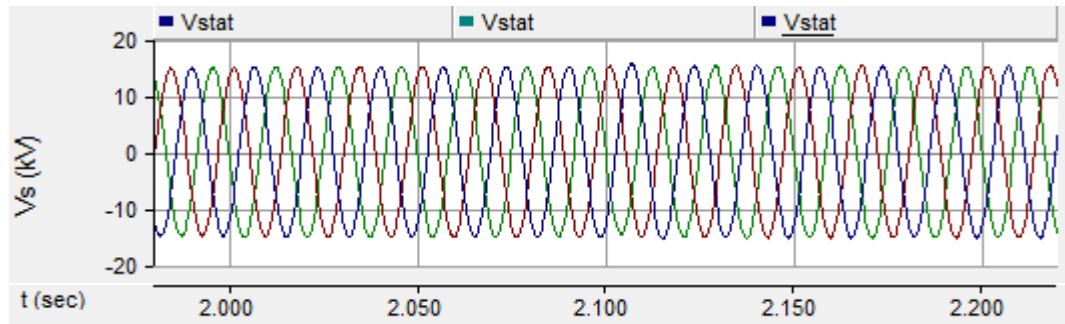
(a)
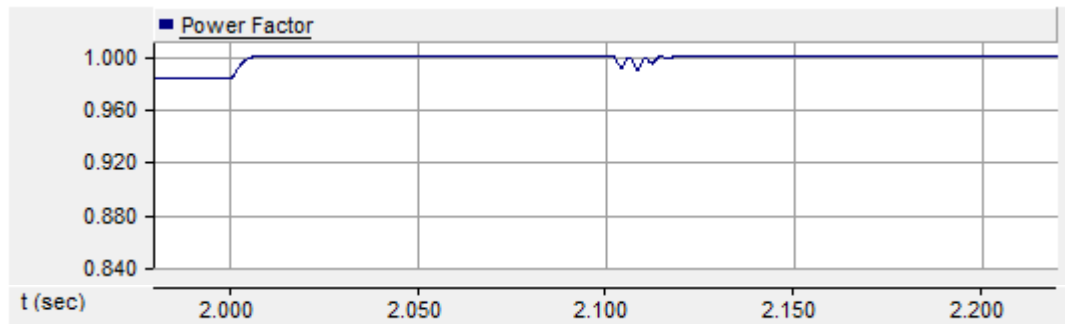
(b)
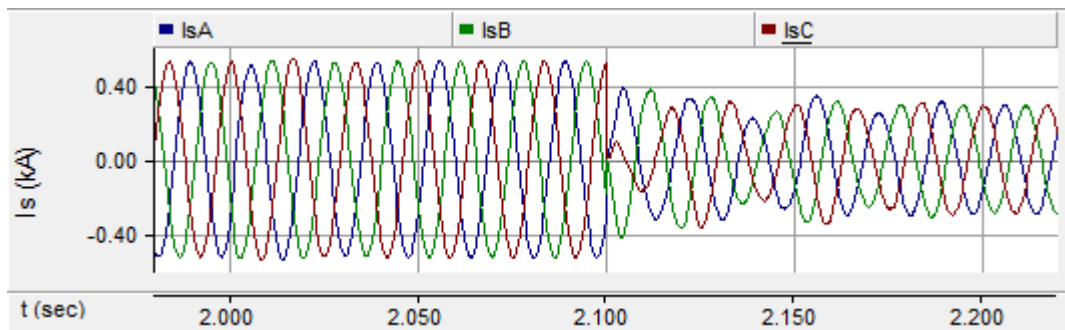
(c)

Figure 3.17 (a) PCC Voltage, (b) power factor and (c) source current for study with gross unbalanced load with STATCOM

Response of the system with STATCOM is presented in Figure 3.17, which presents the parameters in same sequence as illustrated in Figure 3.16. Before $t = 2.0$ sec, STATCOM operates in floating state with all controllers active. At $t = 2.0$ sec, it is commanded for reactive power compensation. Therefore, it improves power factor to unity as seen in Figure 3.17(b). Source current and voltage are symmetric at this time. At time $t = 2.1$ sec, gross unbalance occurs in the load and STATCOM instantly tries to compensate the negative sequence currents. As seen in Figure 3.17(c), it rebalances the three phase current, although the time taken is about 4 cycles. This response time is more than the typical

response of STATCOM. The power factor remains unity after occurrence of imbalance (Figure 3.17(b)) and voltage V_S becomes balanced after STATCOM operation.

(a)

(b)

(c)

(d)
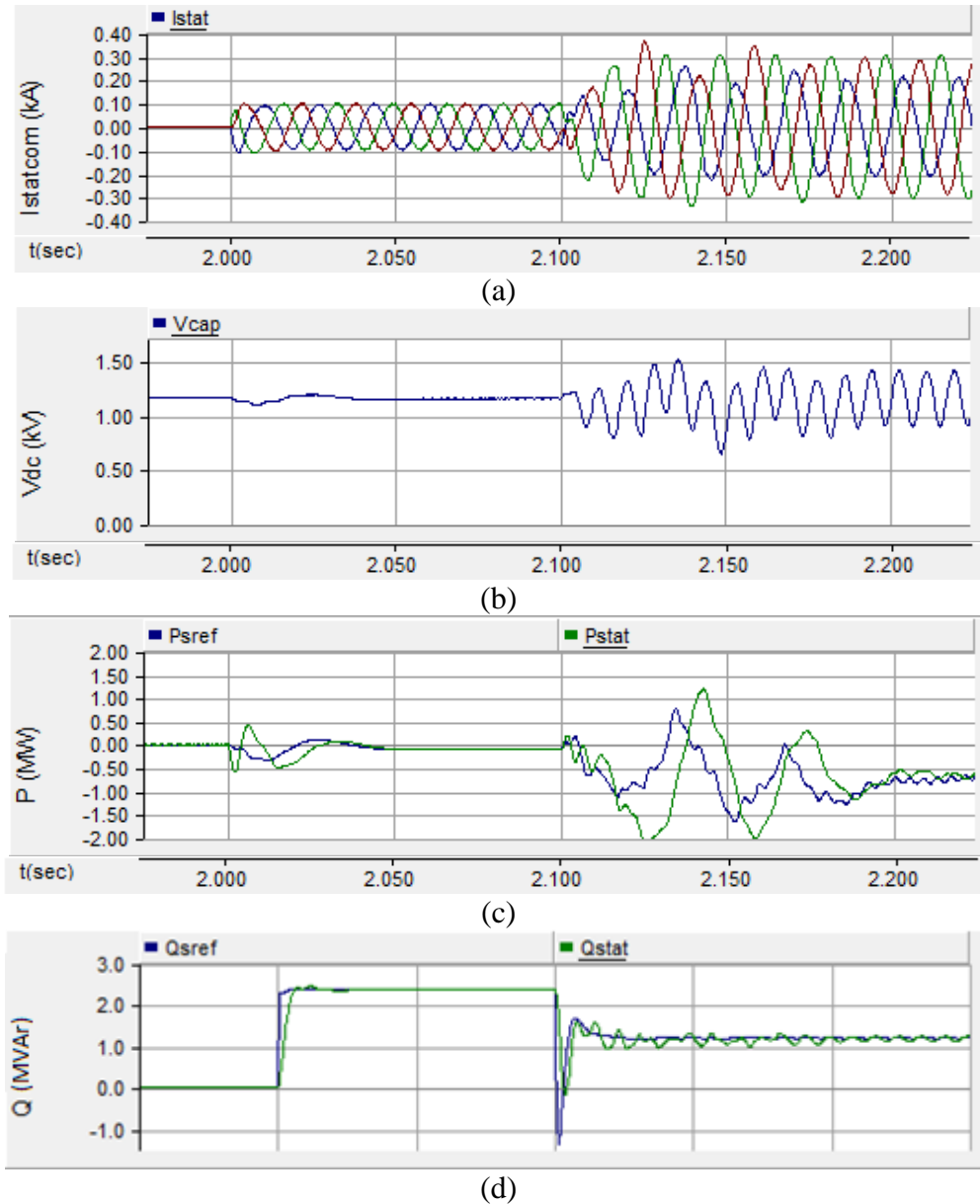
Figure 3.18 (a) STATCOM current, (b) capacitor voltage, (c) and (d) active and reactive power output, respectively for gross unbalanced load with STATCOM

The controller performance is shown in Figure 3.18. Figure 3.18(a) illustrates the current through device $I_{STATCOM}$, Figure 3.18(b) presents capacitor voltage V_{dc} and Figures 3.18(c) and (d) present the active and the reactive power flow out of STATCOM, respectively. In Figure 3.18(a), three phase current starts flowing after $t = 2.0$ sec for reactive power

compensation. It starts load compensation just after inception of imbalance at $t = 2.1$ sec. Thus, STATCOM current becomes asymmetric. Because of the imbalance, capacitor voltage in Figure 3.18(b) oscillates with large magnitude and goes below 1 kV sometimes. This is the main reason behind the deterioration in controller response that it takes 4 cycles instead of 2 cycles to compensate load unbalance. In Figure 3.18(c) after $t = 2.1$ sec, fluctuations in active power flow can be seen. The active power into the STATCOM increases in Figure 3.18(c) which shows that with unbalance case, losses in the device increases. Hence, it is important to keep track of the active power flow and rating of STATCOM while supplying negative sequence currents to load. The reactive power output reduces to 1.2 MW from 2.4 MW in Figure 3.18(d) because only 2 branches are operational of load.

(a)

(b)
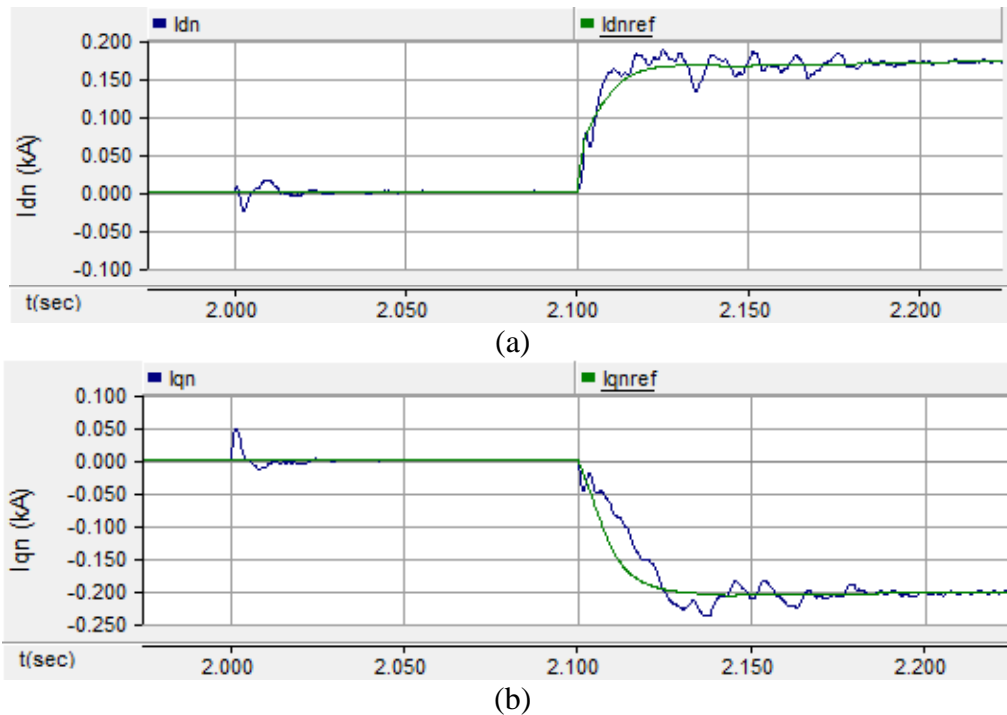
Figure 3.19 (a) *d*-axis and (b) *q*-axis parts of negative sequence component of STATCOM current for gross unbalanced load

Figures 3.19(a) and (b) depict the *d*-axis and *q*-axis parts for negative sequence component of STATCOM current respectively. After the occurrence of gross unbalance, I_{dn} and I_{qn} track theirs reference values but due to low capacitor voltage, the settling time increases to 4 cycles.

3.4.3 Impact of DC-link Capacitor Voltage

The DC link voltage plays an important role in the STATCOM operation as explained in Chapter 2. If a higher capacitor voltage is selected, the cost of the device increases and more active power is required to charge up the device. It must be fairly large enough for linear operation of VSI under the worst case operation. If it attains a value below a threshold, SPWM technique response will not be linear and there will be an excursion from estimated response [32]. Hence, for gross unbalanced load studies, capacitor reference voltage is increased from 1.155 kV to 1.4 kV. The corresponding response is given in Figure 3.20 – Figure 3.22.

(a)

(b)

(c)
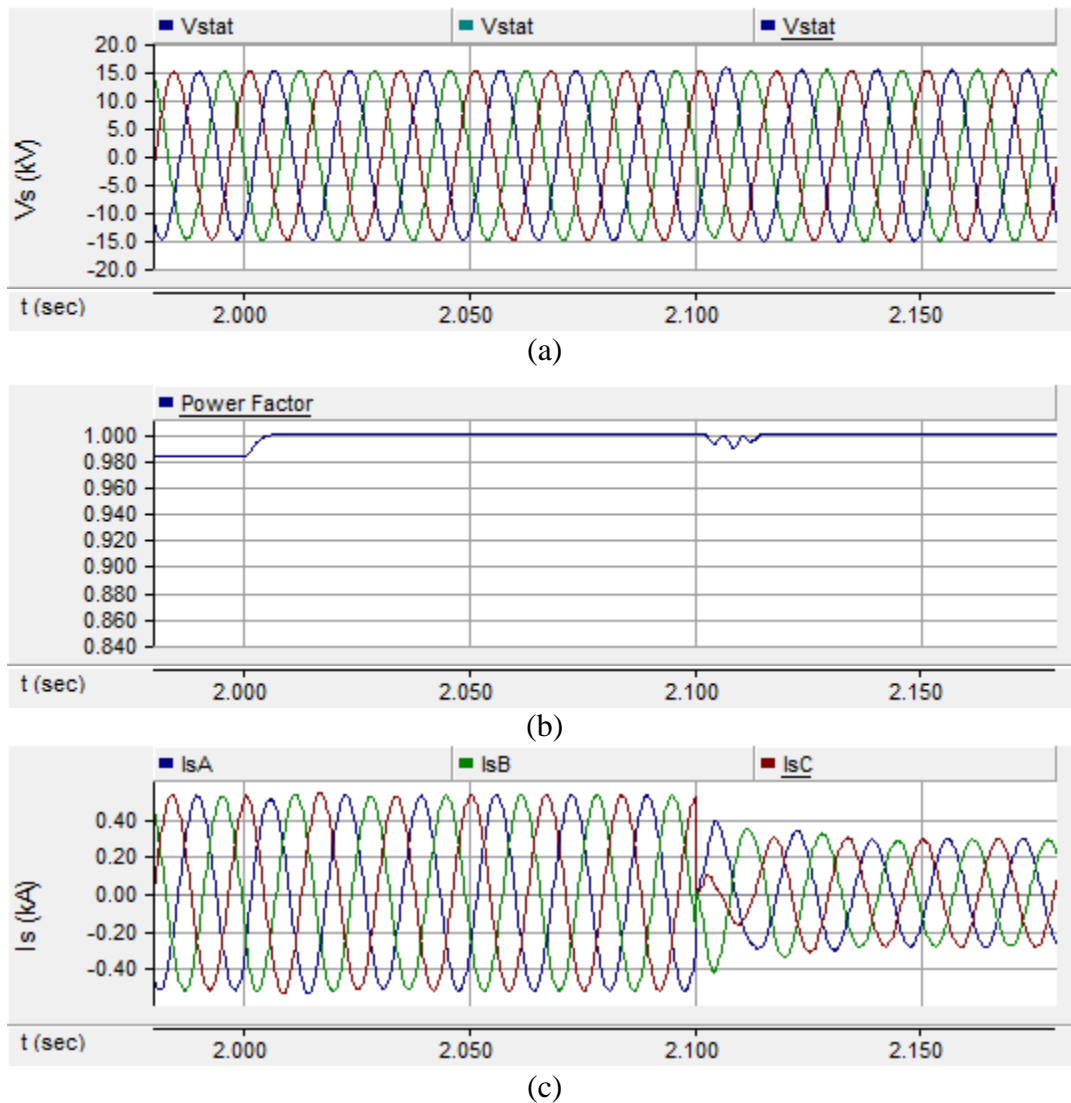
Figure 3.20 (a) PCC Voltage, (b) power factor and (c) source current for gross unbalanced load with $V_{dc} = 1.4$ kV

Figure 3.20 presents the parameters in same sequence as in Figure 3.17. The response of STATCOM is similar to response in Figure 3.17 before $t = 2.1$ sec. It is apparent by comparing Figure 3.17(c) and Figure 3.20(c) that in the latter case, STATCOM has a response (settling time of 2 cycles) which is expected from the controller.
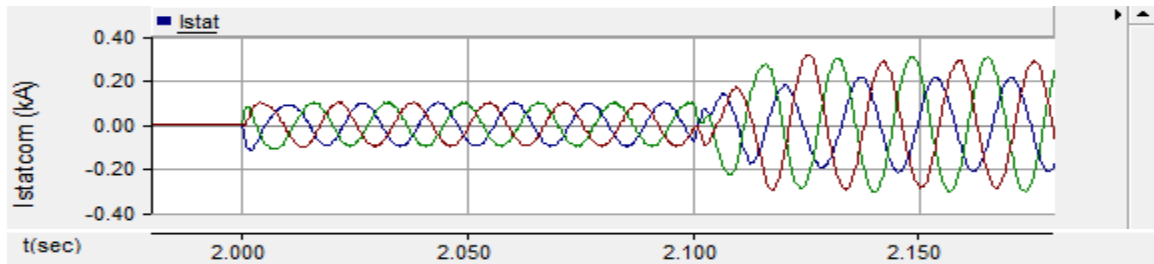
(a)
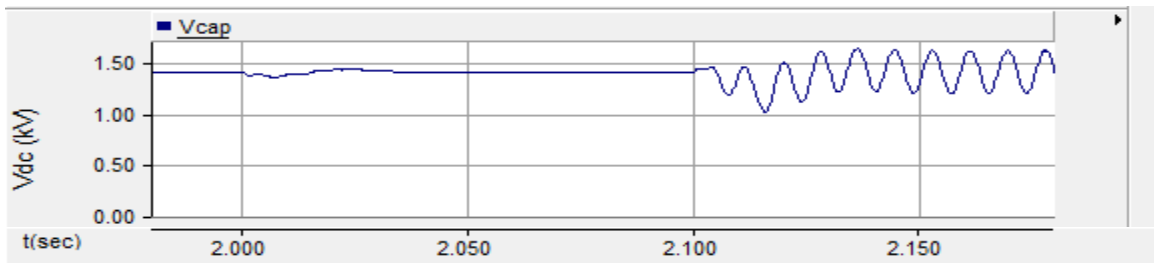
(b)
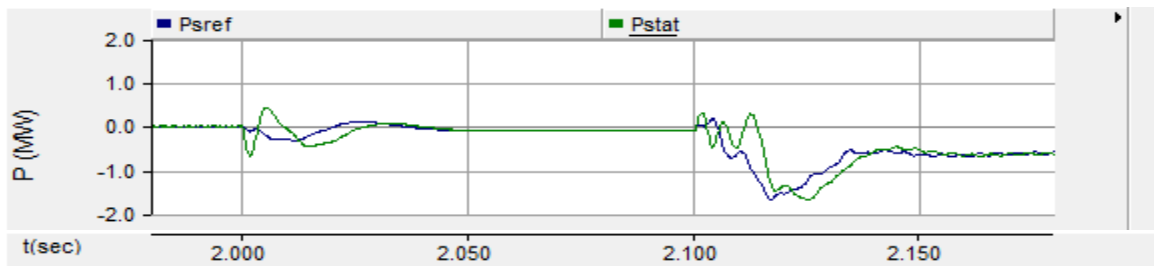
(c)
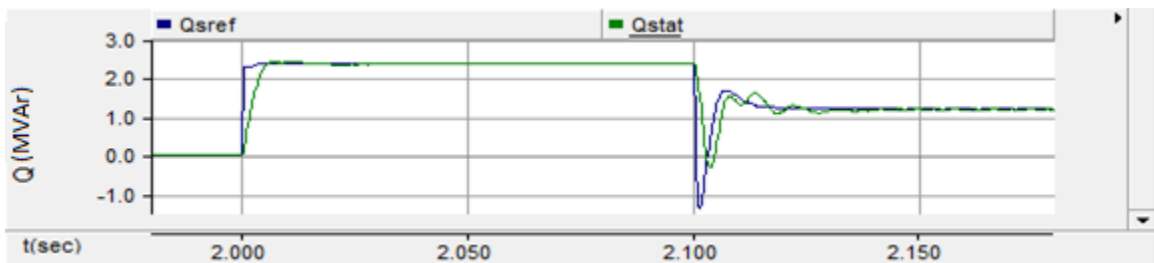
(d)

Figure 3.21 (a) STATCOM current, (b) capacitor voltage, (c) and (d) active and reactive power output for gross unbalanced load with $V_{dc} = 1.4$ kV

Figure 3.21 presents the parameters in same sequence as in Figure 3.18. With higher capacitor voltage, the active power in Figure 3.21 (c) does not change. But as can be seen

for Figure 3.21(b) that capacitor voltage in this case does not go under 1 kV. Therefore, less oscillations are seen in response of active power and reactive power after time $t = 2.1$ sec in Figures 3.21(c) and (d). No change in steady state active power input is seen with higher capacitor voltage since lossless capacitor is considered in this study. Nevertheless, it can be said that switching losses increases with unbalanced operation of STATCOM because active power input to STATCOM increases after $t = 2.1$ sec.

Figures 3.22(a) and (b) present the d- axis and q- axis parts of negative sequence component of STATCOM current. By comparing Figure 3.19 and Figure 3.22, it is obvious that much faster response is given in the latter case. In compensation of gross unbalanced load, no large overshoot is observed in Figure 3.22 after $t = 2.1$ sec. Settling time for this is also less than 2 cycle as has been reported for mild unbalance.
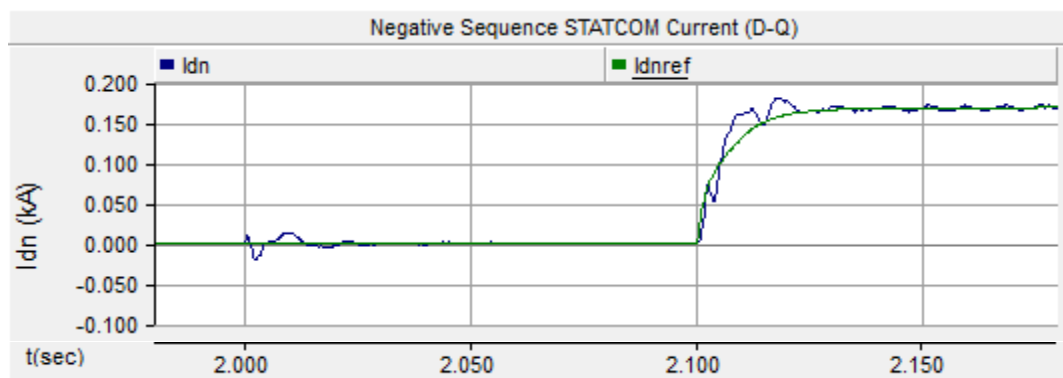
(a)
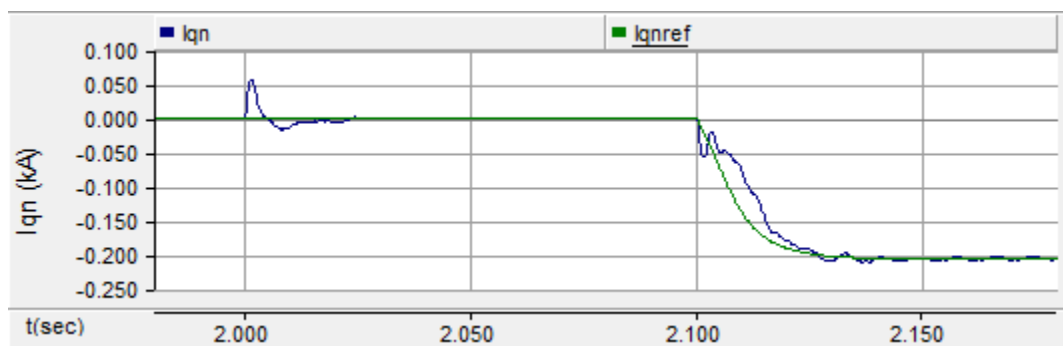
(b)

Figure 3.22 (a) d-axis and (b) q-axis parts of negative sequence component of STATCOM current for gross unbalanced load with $V_{dc} = 1.4$ kV

3.5　CASE STUDY 4

Two other aspects of STATCOM controller i) Voltage regulation and ii) Voltage balancing are discussed in this section. The network voltage imbalance generally occurs with untransposed lines. If the lines are not transposed, the line inductance will differ in the three phases. This results in unbalanced voltage even if a balanced load is connected to the system. Therefore, to evaluate voltage balancing feature of STATCOM control, a scenario of untransposed lines is created in the study.

3.5.1　Study System-4 Description

Figure 3.23 illustrates the Study System-4 for this study. This system is similar to Study Sytem-1 except that only balanced load is considered in the network. The asymmetry in the line is created by connecting additional impedance on one phase or between two phases of transmission line and cable. The STATCOM is connected at PCC to regulate the voltage of PCC and to make the voltage symmetric such that load sees a balanced grid. The STATCOM controller developed in Section 2.4.4 is employed for mitigation of voltage unbalance and voltage regulation. The STATCOM data is given in Appendix A.
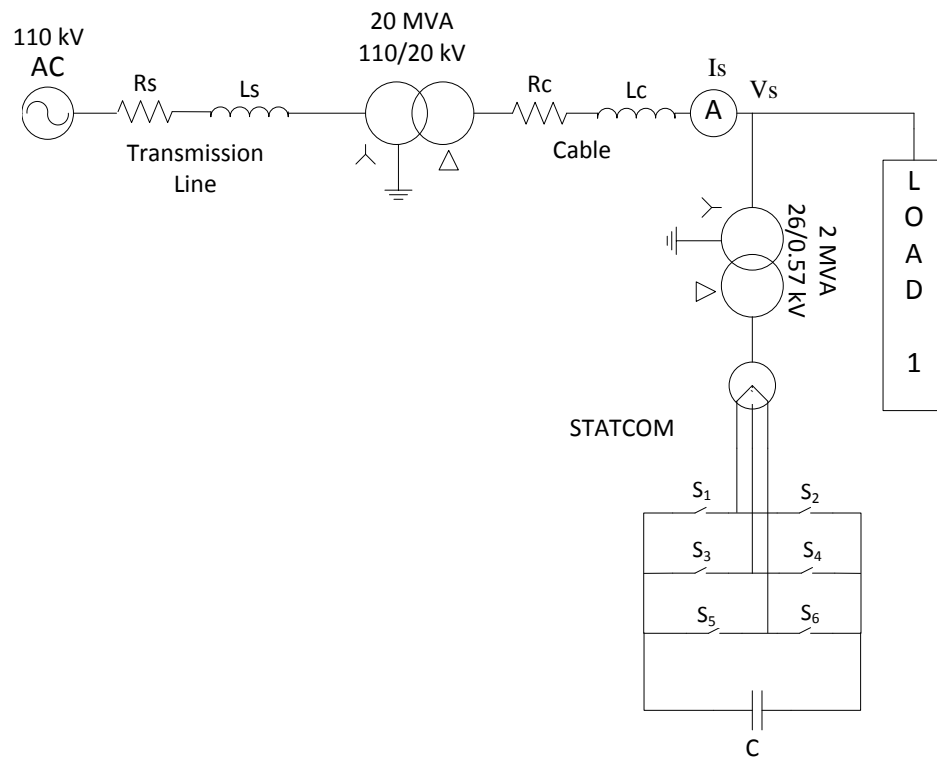
Figure 3.23 Schematic diagram for Study Sytem-4

3.5.2 Network Voltage Balancing and Voltage Regulation

Figures 3.24 (a), (b) and (c) represent the three phase voltages at PCC V_S, RMS voltage V_{RMS} at PCC and source current I_S respectively while STATCOM is not present. Before t = 3.1 sec, the system is balanced and V_{RMS} is 1 pu. At t = 3.1 sec, network unbalance occurs, hence three phase voltage in Figure 3.24(a) becomes asymmetric. Moreover, V$_{RMS}$ also reduces to 0.96 pu in steady state in Figure 3.24(b). The steady state oscillations in V_{RMS} are due to LC oscillations of network impedance which die out in 1-2 sec.

(a)

(b)

(c)
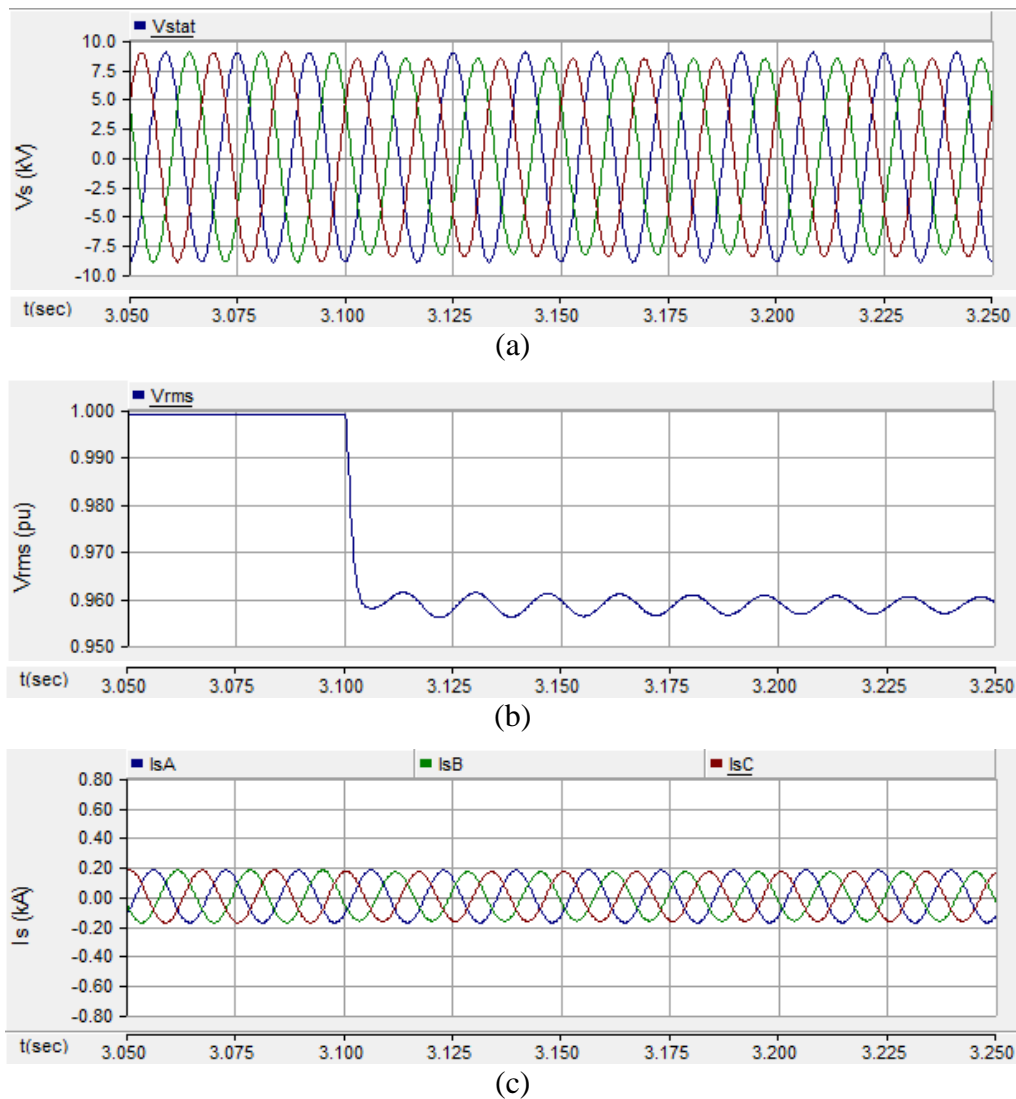
Figure 3.24 a) PCC Voltage, (b) RMS voltage and (c) source current with Study System-4 for voltage balancing and regulation without STATCOM

Figure 3.25 represents the *d*-axis and *q*-axis parts of negative sequence voltage at PCC. Steady state of negative sequence voltages can be seen in Figures 3.25(a) and (b) due to different impedance in the different phases of transmission lines. The steady state oscillations in V_{sdn} and V_{sqn} are network oscillations and are inconsequential to this study.

(a)

(b)
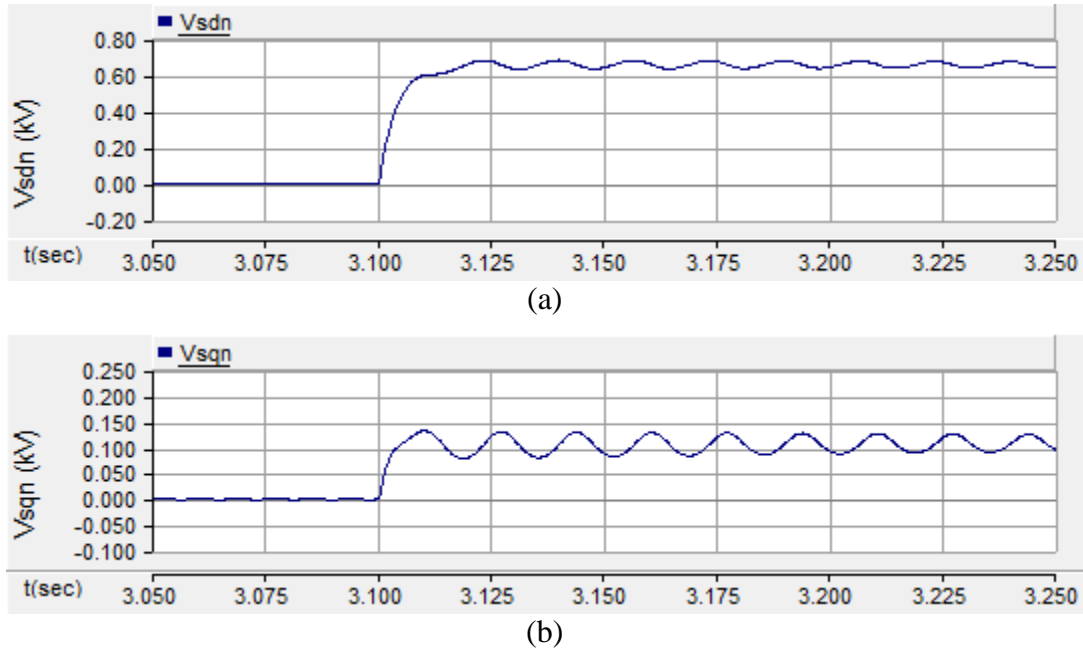
Figure 3.25 (a) *d*-axis and (b) *q*-axis parts of negative sequence component of PCC voltage for voltage balancing and regulation without STATCOM

Figure 3.26 presents the network voltage at PCC with STATCOM in operation. All controllers of STATCOM are active. The STATCOM regulates the voltage V_{RMS} to 0.99 pu in steady state. The system is balanced before $t = 3.1$ sec, and after the occurrence of network unbalance, all controllers of STATCOM operate instantly. Comparing Figure 3.24(a) and Figure 3.26(a) with STATCOM, the voltage at PCC are made symmetric even with different phase impedance in transmission line. Also STATCOM rises the PCC voltage from 0.96 pu in Figure 3.24(b) to 0.99 pu in Figure 3.26(b). The STATCOM compensates the negative sequence voltage by sending negative sequence currents back to the grid [15]. Therefore, even with a balanced load, source current is unbalanced in Figure 3.26(c) such that the voltage at the PCC becomes symmetric.

Figure 3.27 presents the controller performance for voltage balancing and voltage regulation. Figure 3.27(a) depicts the STATCOM current, Figures 3.27(b) and (c) outline

the *d*-axis and *q*-axis parts of negative sequence voltage at PCC and Figure 3.27(d) depicts the reactive power output for voltage regulation at PCC.
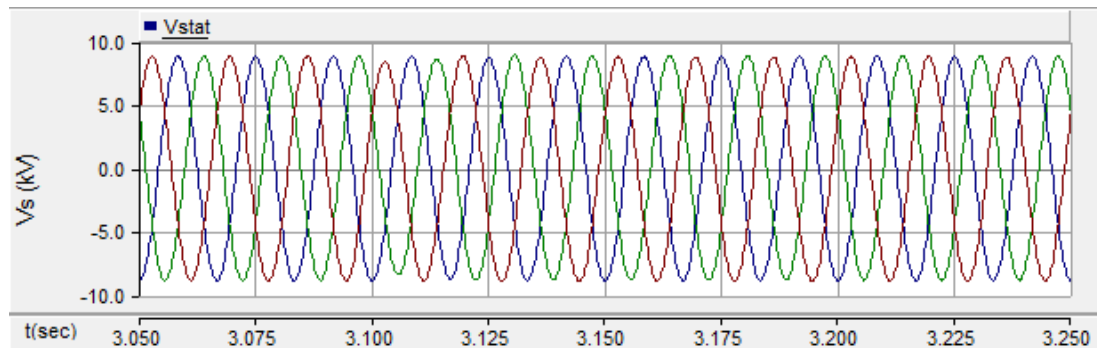
(a)
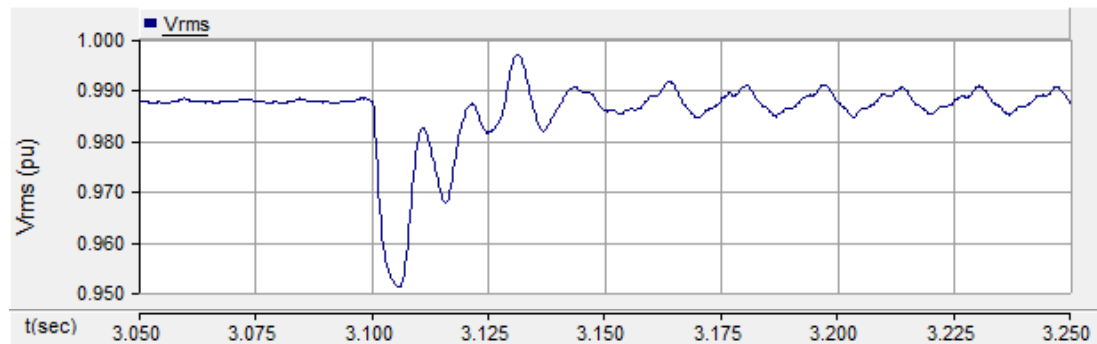
(b)
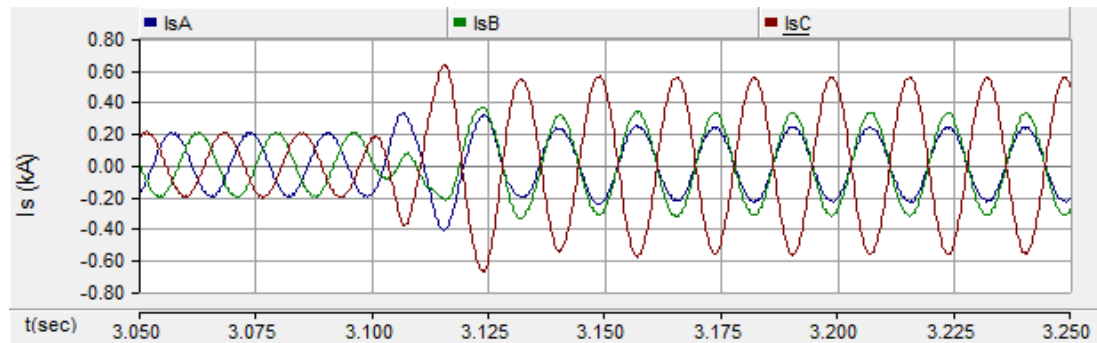
(c)

Figure 3.26 a) PCC Voltage, (b) RMS voltage and (c) source current with Study System-4 for voltage balancing and regulation with STATCOM

Initially, STATCOM regulates voltage to 0.99 pu in steady state. Therefore, there exists a small STATCOM current before $t = 3.1$ sec which absorbs 2 MVAr reactive power. At time $t = 3.1$ sec, voltage unbalance occurs. By comparing Figure 3.25 and Figures 3.27(b) and (c), it compensates the negative sequence voltage in 2 cycles. During this compensation STATCOM supplies unbalanced current to the grid in Figure 3.27(a) such that load sees

only positive sequence voltage at the PCC. Simultaneously, it supplies reactive power to the grid to regulate the voltage at PCC as shown in Figure 3.27(c).

(a)

(b)

(c)

(d)
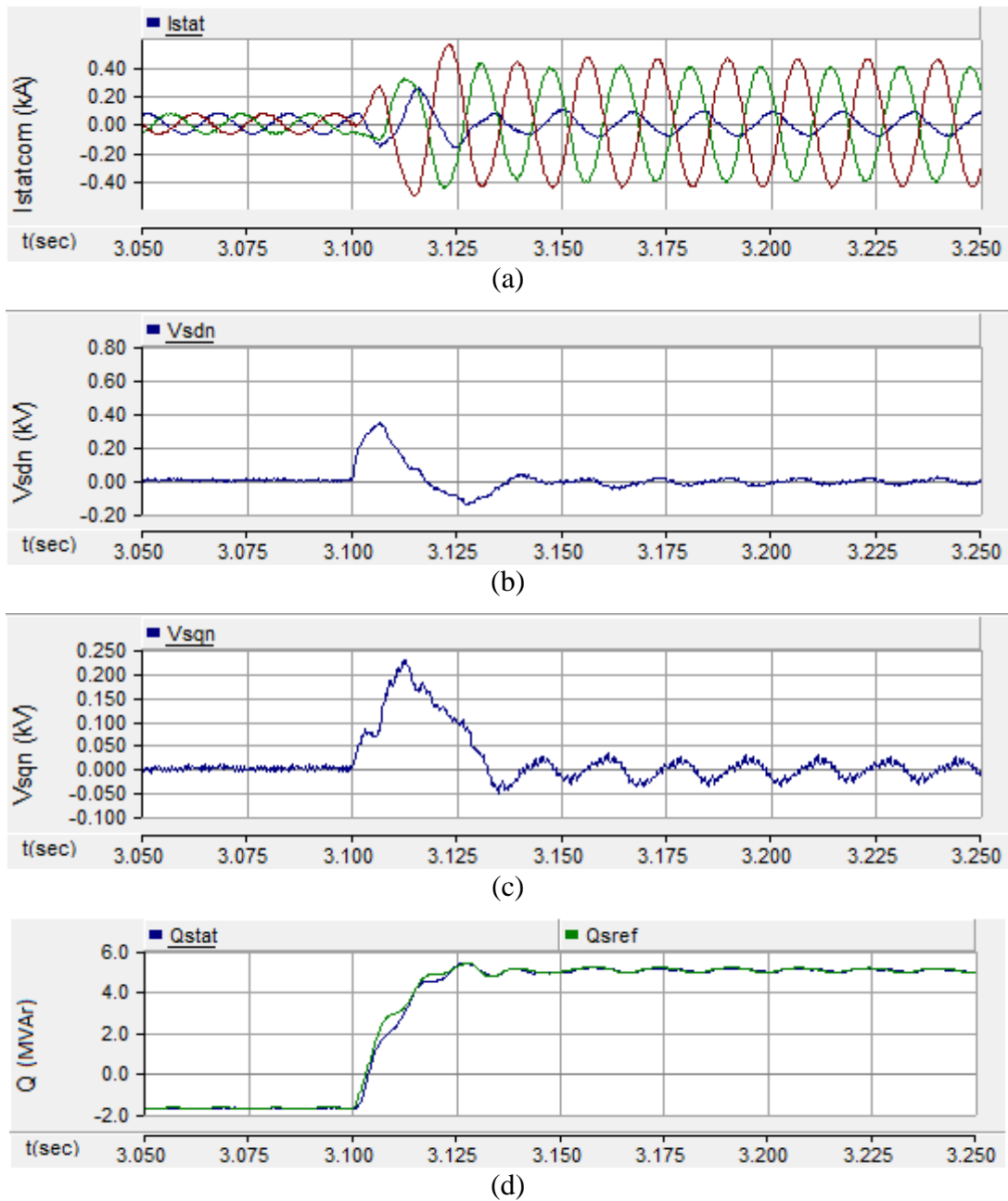
Figure 3.27 (a) STATCOM current (b) *d*-axis and (c) *q*-axis parts of negative sequence voltage at PCC and (d) reactive power output of STATCOM for voltage balancing and regulation with STATCOM

3.6 CONCLUSION

In this chapter, the performance of the designed STATCOM controller for load compensation, voltage balancing and voltage regulation is examined. Validation of controllers is successfully performed with the published results for a study system presented in [10].

Study system is modified to represent a North American feeder and to allow the simultaneous operation of positive and negative sequence controllers for unbalanced load connection. Subsequently, studies for steady state operation and transient case are performed with modified study system. It is observed that STATCOM is able to compensate reactive power in less than a cycle and negative sequence current in less than 2 cycles, instantly after occurrence of unbalance in the load. Harmonics in STATCOM current and PCC voltage are found under the limits specified in IEEE std 519 [34].

Successively, the controller performance is analyzed with gross unbalanced load which has only 2 operational branches of delta configured load. The settling time for this case is found to be 4 cycles, which significantly reduces to 2 cycles with a higher DC-link voltage. Hence, it is recommended that in case of higher imbalance, a large voltage rating DC-link capacitor may be utilized for appropriate controller response.

In the end, an untransposed line scenario is created by changing impedances between the lines to present controller performance to mitigate the voltage unbalance in the network and regulate the PCC voltage simultaneously. STATCOM is shown to effectively alleviate the asymmetry in voltage and regulate it in about 2 cycles.

Chapter 4

STATCOM CONTROL FOR LOAD COMPENSATION AND VOLTAGE REGULATION IN A REALISTIC DISTRIBUTION FEEDER

4.1 INTRODUCTION

In this chapter a realistic network from Ontario transmission utility, Hydro One, is considered for studying load compensation and voltage regulation by the comprehensive STATCOM controller developed in Chapter 2. Firstly, STATCOM is utilized in the utility feeder for load compensation which includes power factor correction and negative sequence load current compensation. Load compensation is performed during day time when different types of balanced and unbalanced loads are connected. In addition, STATCOM performance in compensating a grossly unbalanced load is investigated.

Next, the STATCOM is utilized for regulating bus voltage in a distribution feeder in order to increase the connectivity of wind farms. At night time, bus voltages in the line tend to increase due to reverse power flow caused by wind power generation. The overvoltage limit stipulated by Hydro One restricts more wind farms to be connected in the network. STATCOM is used to control bus voltage in the line to allow more wind farm penetration into this radial feeder.

Temporary over voltage (TOV) in the line, caused by asymmetric faults is another factor for limiting wind farm connectivity especially during light load conditions in the night. The performance of developed STATCOM controller mitigating the TOV is also presented in this chapter. System studies are conducted using electromagnetic transients simulation software PSCAD/EMTDC.

4.2 COMPENSATION OF UNBALANCED LOAD

The single line diagram of study system is given in Figure 4.1. A radial feeder is connected to the grid with a 40 MVA transformer at 'Bus 1'. The feeder has three segments, and supplies to a combination of balanced and unbalanced load at 'Bus 4'. Mechanical switch 'SW' is used to connect the unbalanced load to the network. STATCOM is connected at the 'Bus 4' for load compensation. Line data, load data and STATCOM data are given in Appendix B.
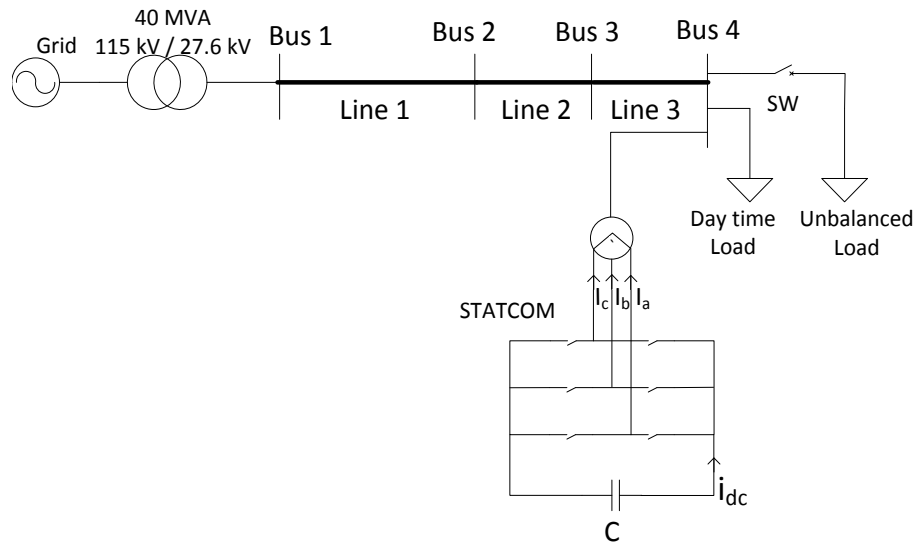
Figure 4.1 Single line representation of a realistic Hydro One feeder

4.2.1 System Performance without STATCOM

In Figure 4.1, firstly STATCOM is neglected and network response is presented in Figure 4.2. It illustrates (a) PCC voltage at 'Bus 4', (b) the RMS voltage V_{RMS} at same bus, (c) source current, (d) load current and (e) load power factor. Because of heavy day time load, V_{RMS} is initially less than 0.96 pu. Since unbalance is absent, source current and load current are symmetric before $t = 2.3$ sec. A power factor of 0.9 is seen in Figure 4.2(e).

The switch is turned ON at $t = 2.3$ sec to allow the unbalanced load into network. After inception of an unbalanced load at $t = 2.3$ sec, the voltage at the PCC bus goes low as observed in Figure 4.2(a). Additionaly, V_{RMS} goes to 0.9 pu which is below utility standard.
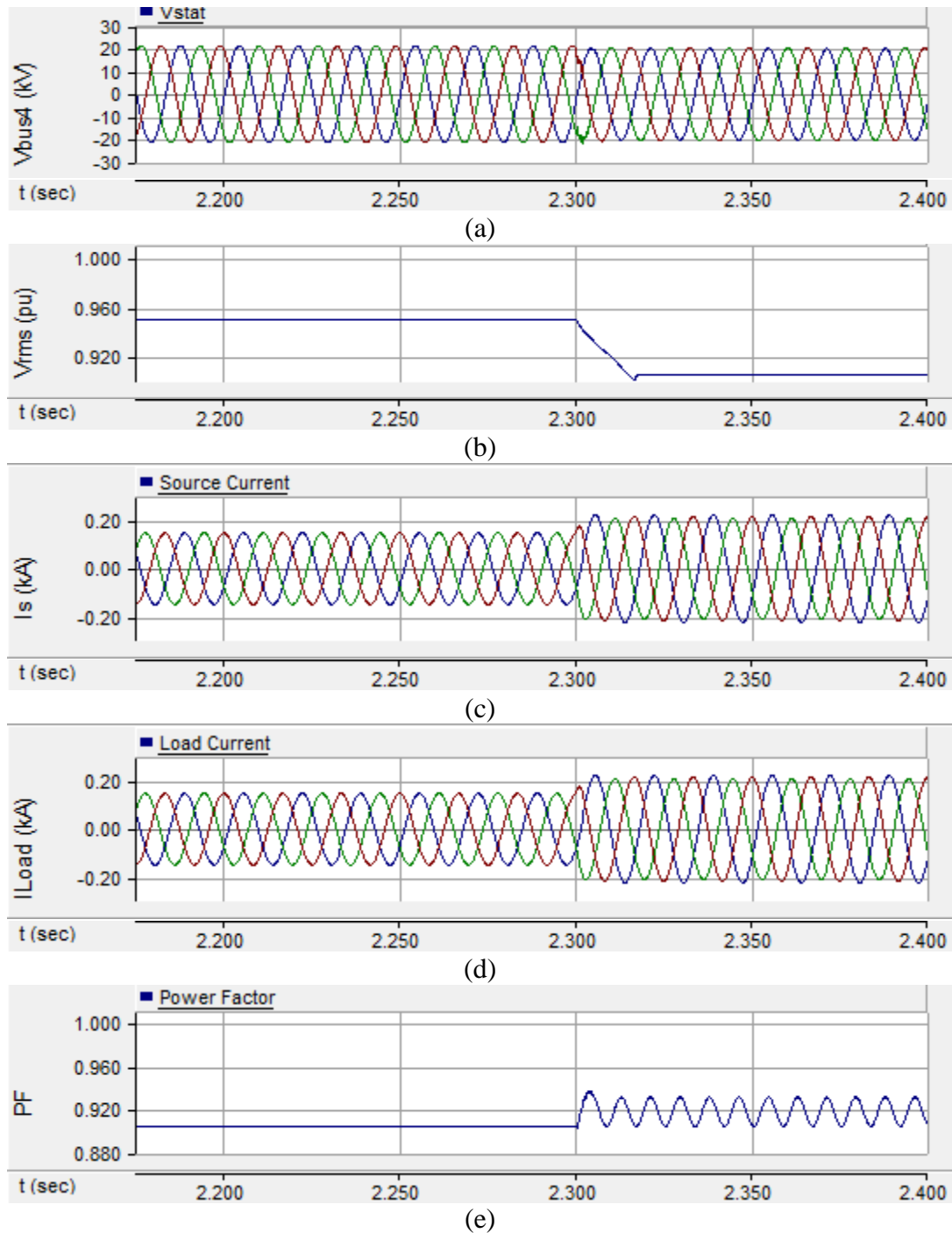
Figure 4.2 (a) PCC voltage, (b) RMS voltage, (c) source and (d) load current and (e) load power factor for load compensation in realistic feeder without STATCOM

The RMS is measured digitally with 64 samples per cycle that causes time delay of one cycle to calculate RMS voltage. Because of unbalanced load, the load current and source current become unbalanced as shown in Figure 4.2(c) and (d). Because of asymmetry in

the network, negative sequence active and reactive power flows into the system [8]. This causes the 2nd harmonic oscillations in the power factor calculation (Figure 4.2(e)).

4.2.2   System Performance with STATCOM

The rating of STATCOM is designed such that it is able to correct power factor to unity and also compensate the unbalance nature of load. Therefore, a 3 MVAr rating STATCOM is selected to compensate the load (4.82 MW, 2.2 MVAr).

Figure 4.3 depicts the ability of STATCOM to provide load compensation. The graphs are given in same sequence as in Figure 4.2 for comparison. At $t = 2.2$ sec, STATCOM with the developed comprehensive controllers is commanded to compensate the reactive power and thereby increases the power factor to unity as shown in Figure 4.3(e). RMS voltage in Figure 4.3(b) is also regulated to 1 pu because of reactive power support provided by STATCOM.

After switching-in unbalanced load at $t = 2.3$ sec, STATCOM instantly compensates the negative sequence component of load current. Due to an increase in load, a slight dip in three phase voltage as shown in Figure 4.3(a) can be seen after $t = 2.3$ sec. RMS voltage also lowers to 0.97 pu but is acceptable as per utility standard. Because of the unbalanced load, the load current is unbalanced but this does not affect the source current, as shown in Figures 4.3(c) and (d), respectively. Due to STATCOM operation grid sees only balanced component of load and the source current becomes symmetric. The power factor is controlled to unity and does not have 2nd harmonic oscillations due to symmetric source current as seen in Figures 4.3(e).

STATCOM controller performance for the above study is presented in Figure 4.4. Figure 4.4(a) depicts the current through device $I_{STATCOM}$, Figures 4.4(b) and (c) depict the dq reference frame parts of positive sequence currents (I_{dp} and I_{qp}) of STATCOM, respectively, and Figure 4.4(d) represents the DC-link capacitor voltage. Figures 4.4(e) and (f) illustrate the active and the reactive power flow out of STATCOM, respectively.

It is seen from Figure 4.4(a) that for load compensation, balanced current flows through STATCOM after $t = 2.2$ sec. As load unbalance occurs, STATCOM starts supplying negative sequence currents making STATCOM current asymmetric. I_{dp} signifies active power flow into STATCOM. To keep the capacitor voltage constant, a small amount of active power is required which is characterized by negative I_{dp} in Figure 4.4(b).
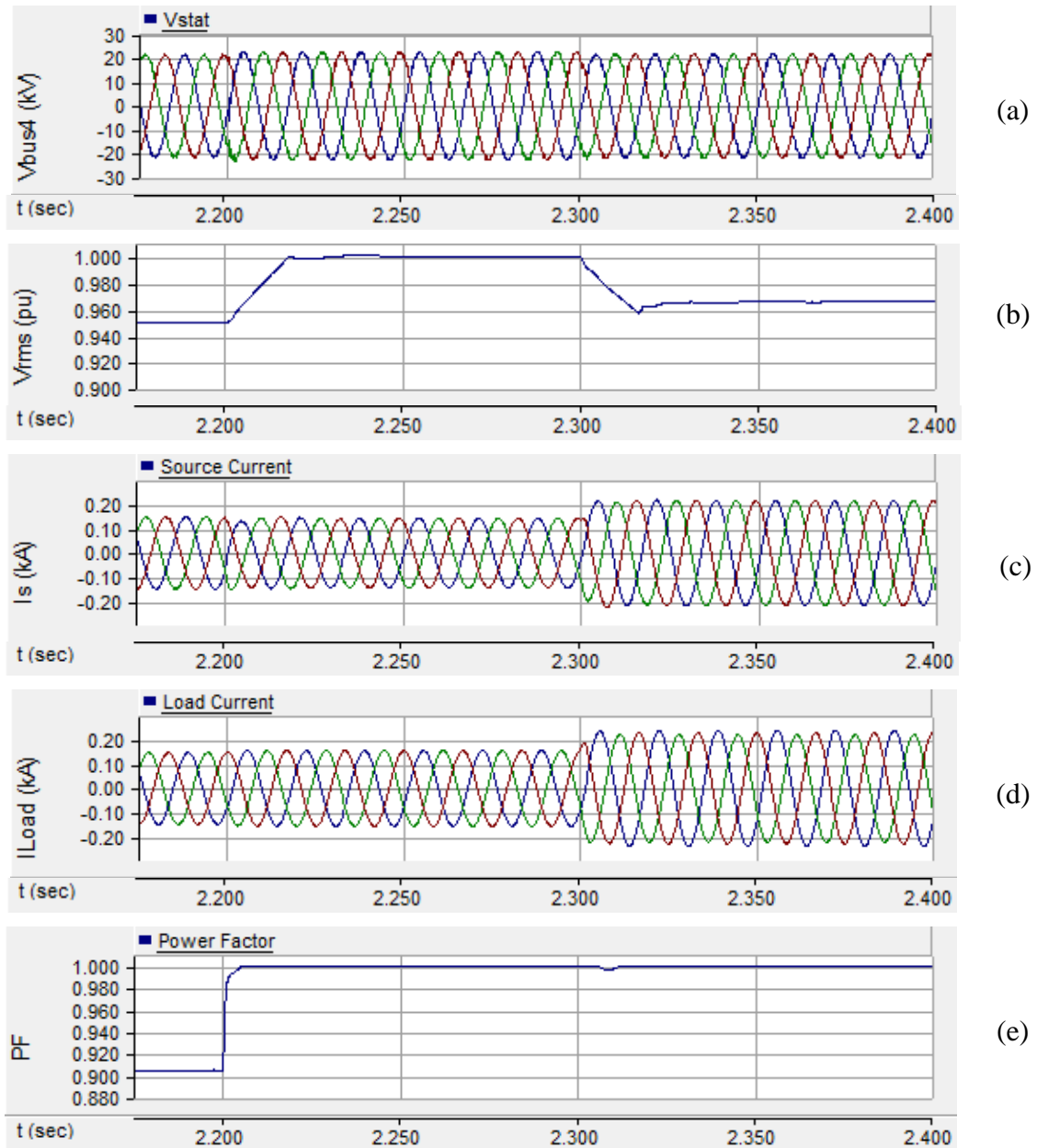
Figure 4.3 (a) PCC voltage, (b) RMS voltage, (c) source and (d) load current and (e) load power factor for load compensation in realistic feeder with STATCOM
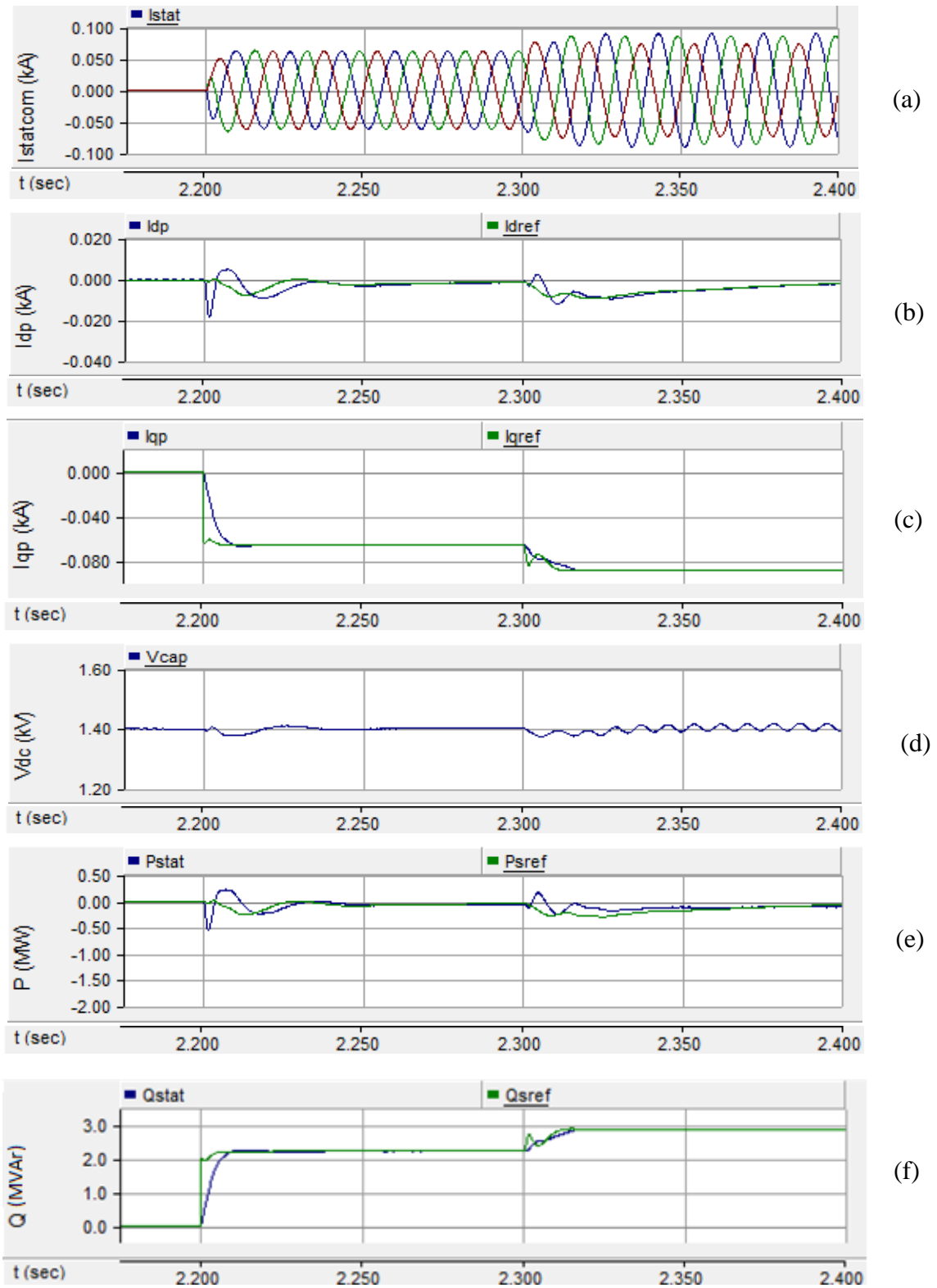
Figure 4.4 (a) STATCOM current (b) and (c) positive sequence component of current in *dq* frame, (d) DC-link voltage, (e) and (f) STATCOM active and reactive power output for load compensation in realistic feeder

I_{qp} characterizes the reactive power support from STATCOM in Figure 4.4(c). After t = 2.2 sec, it follows its reference value in less than a cycle and thus STATCOM corrects power factor in a cycle. Because of unbalanced load, I_{qp} attains more negative value to compensate additional load reactive power. After t = 2.3 sec, DC-link voltage is subjected to 2nd harmonic oscillations due to negative sequence current flows through STATCOM [10]. So, a large DC-link voltage (1.4 kV) is taken for appropriate response of controller [32]. After t = 2.2 sec, in less than a cycle STATCOM supplies 2.1 MVAr power to load as shown in Figure 4.4(f), such that source is not loaded with the reactive power and grid sees only unity power factor load. After t = 2.3 sec, STATCOM supplies additional reactive power due to connection of unbalanced load and reaches its rated power 3 MVAr as explained in section 4.2.1.
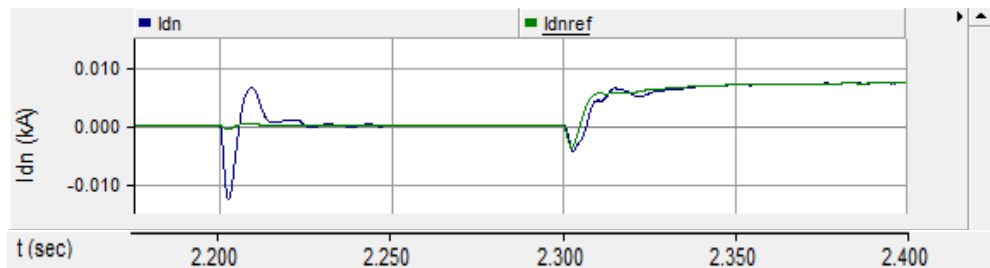
(a)
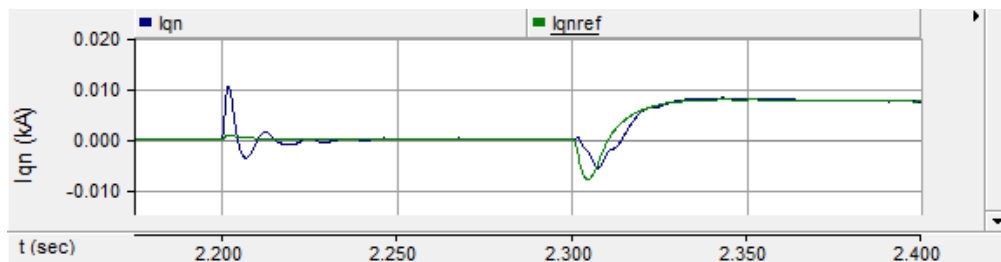
(b)

Figure 4.5 (a) d-axis and (b) q-axis parameters of negative sequence component of STATCOM current for load compensation in realistic feeder

Figure 4.5 represents the negative sequence component of STATCOM current in dq reference frame. It is observed that at t = 2.2 sec transients in I_{dp} and I_{qp} occur but die out as no unbalance exists in load. At t = 2.3 sec, STATCOM is subjected to unbalanced load. STATCOM therefore, tracks the negative sequence reference currents in two cycles as it evident from Figure 4.5. At t = 2.3 sec, undershoot can be seen because of the all pass filter which introduce a phase shift of 180° to high frequency components as shown in Figure

2.13. To reduce the magnitude of undershoot, a low pass filter is used to smoothen the reference currents (I_{dnref} and I_{qnref}) [15], [64].

4.3 COMPENSATION OF GROSSLY UNBALANCED LOAD

Figure 4.6 depicts the system for studying the compensation of gross unbalanced load. The feeder is similar as in Figure 4.1 except that a balanced three phase load is considered instead of a combination of balanced and unbalanced loads. The Δ connected load has a mechanical switch 'Sw' in one branch to allow the creation of gross unbalance. When switch 'Sw' is operated; only two branches of load are connected to network. The load data is given in Appendix B.
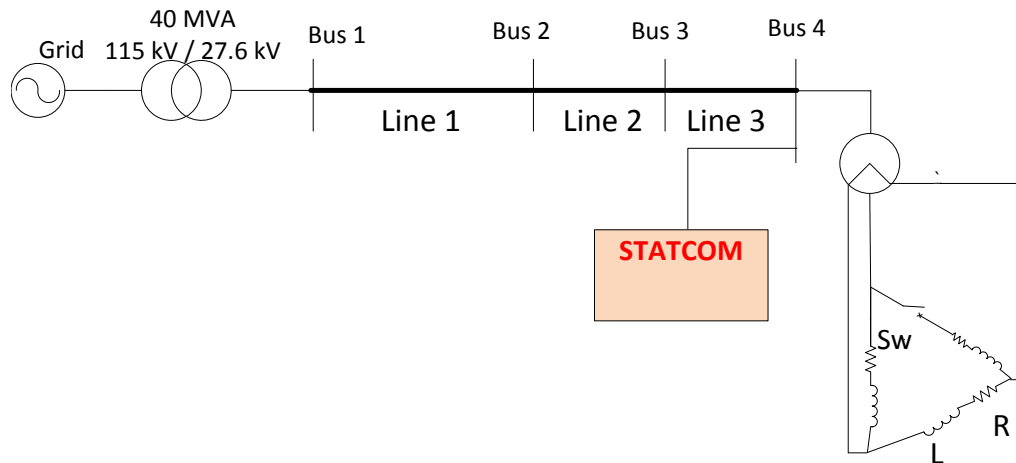
Figure 4.6 Single line representation of modified feeder for grossly unbalanced load

Figure 4.7 demonstrates various system variables when STATCOM is floating and not exchanging power with grid. Figure 4.7 depicts (a) PCC voltage at 'Bus 4', (b) the RMS voltage V_{RMS} , (c) source current I_S , (d) load current and (e) load power factor. Before $t =$ 2.3 sec, there is no unbalance in the network therefore PCC voltage, source current and load current are balanced. The power factor is observed as 0.92.

At $t =$ 2.3 sec, switch 'Sw' is opened isolating one branch from the load. Because of a reduced load, a small rise in V_{RMS} is seen in Figure 4.7(b). Because of inception of gross unbalance in load, the load current and thus source current become asymmetric as shown

in Figures 4.7(c) and (d). Increased oscillations in power factor are observed in Figure 4.7(e) compared to power factor presented in Figure 4.2(e).
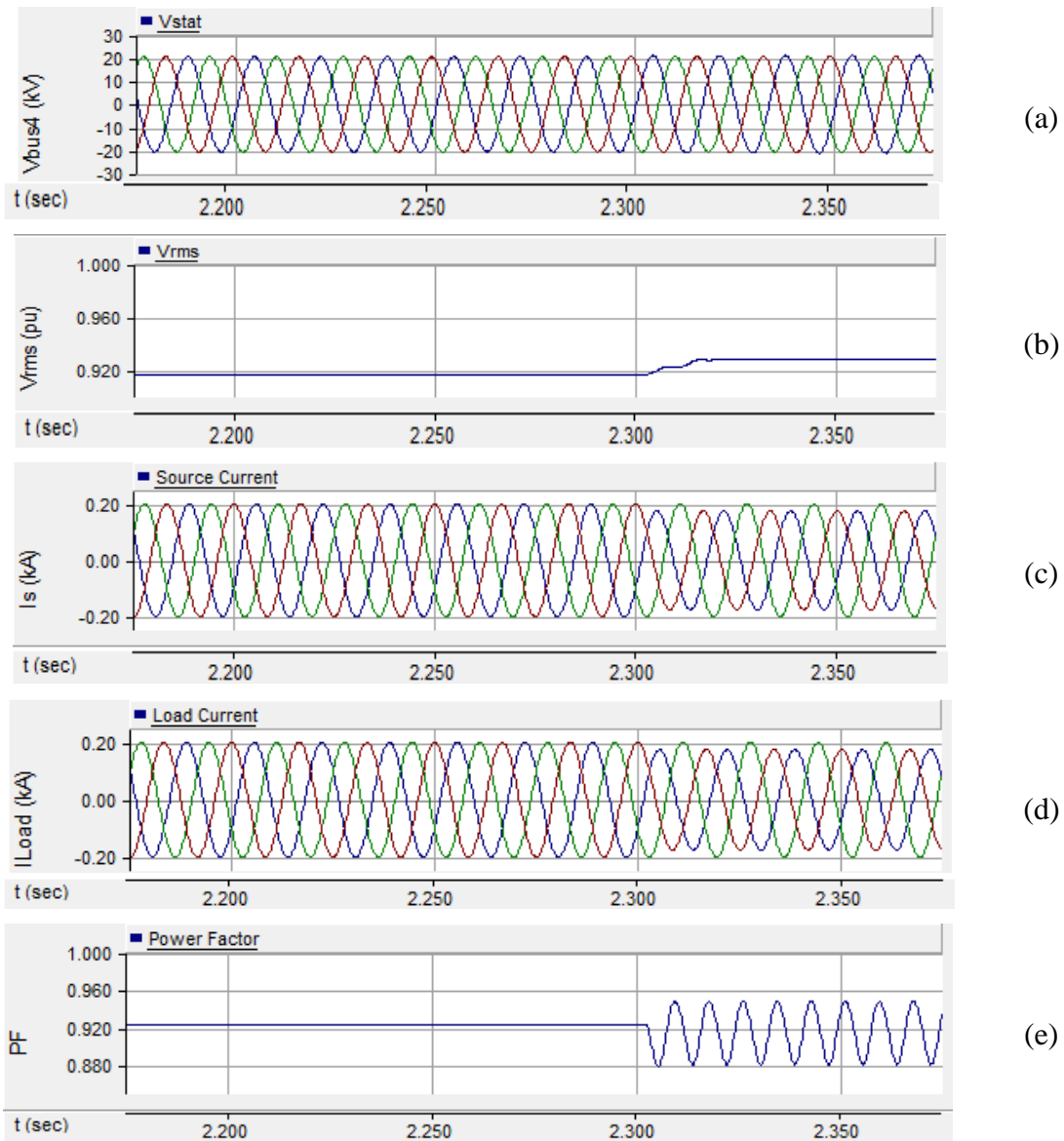
Figure 4.7 (a) PCC voltage, (b) RMS voltage, (c) source current and (d) load current and (e) load power factor with grossly unbalanced load in realistic feeder without STATCOM operation

Figure 4.8 represents the system variables with STATCOM in operation. The parameters are presented in the same sequence as in Figure 4.7 to compare the results. Without STATCOM, V_{RMS} at the PCC is 0.92 pu which is below the utility standard. At $t = 2.2$ sec, STATCOM starts compensating load reactive power and hence, in a cycle, the voltage rises

to 0.98 pu, which is within utility acceptable range as shown in Figure 4.8(b). Power factor also becomes unity after the STATCOM operation (Figure 4.8(e)).
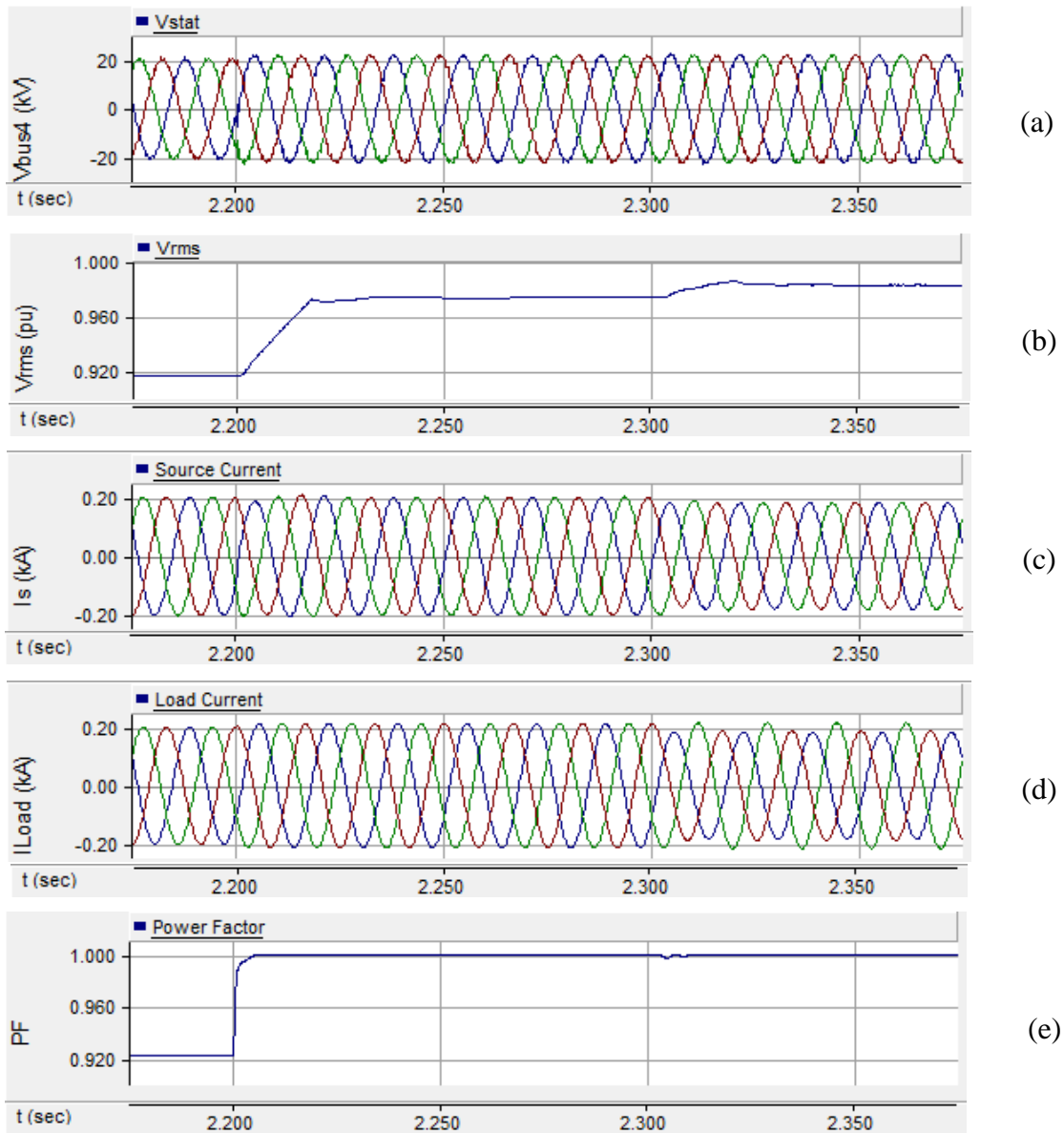
Figure 4.8 (a) PCC voltage, (b) RMS voltage, (c) source current and (d) load current and (e) load power factor with grossly unbalanced load in realistic feeder with STATCOM operation

After inception of gross unbalanced load at $t = 2.3$ sec, load current becomes asymmetric but it does not reflect on source current as STATCOM is compensating the unbalanced nature of load as presented in Figure 4.8(c) and (d). No oscillations in power factor are also observed with STATCOM in operation.
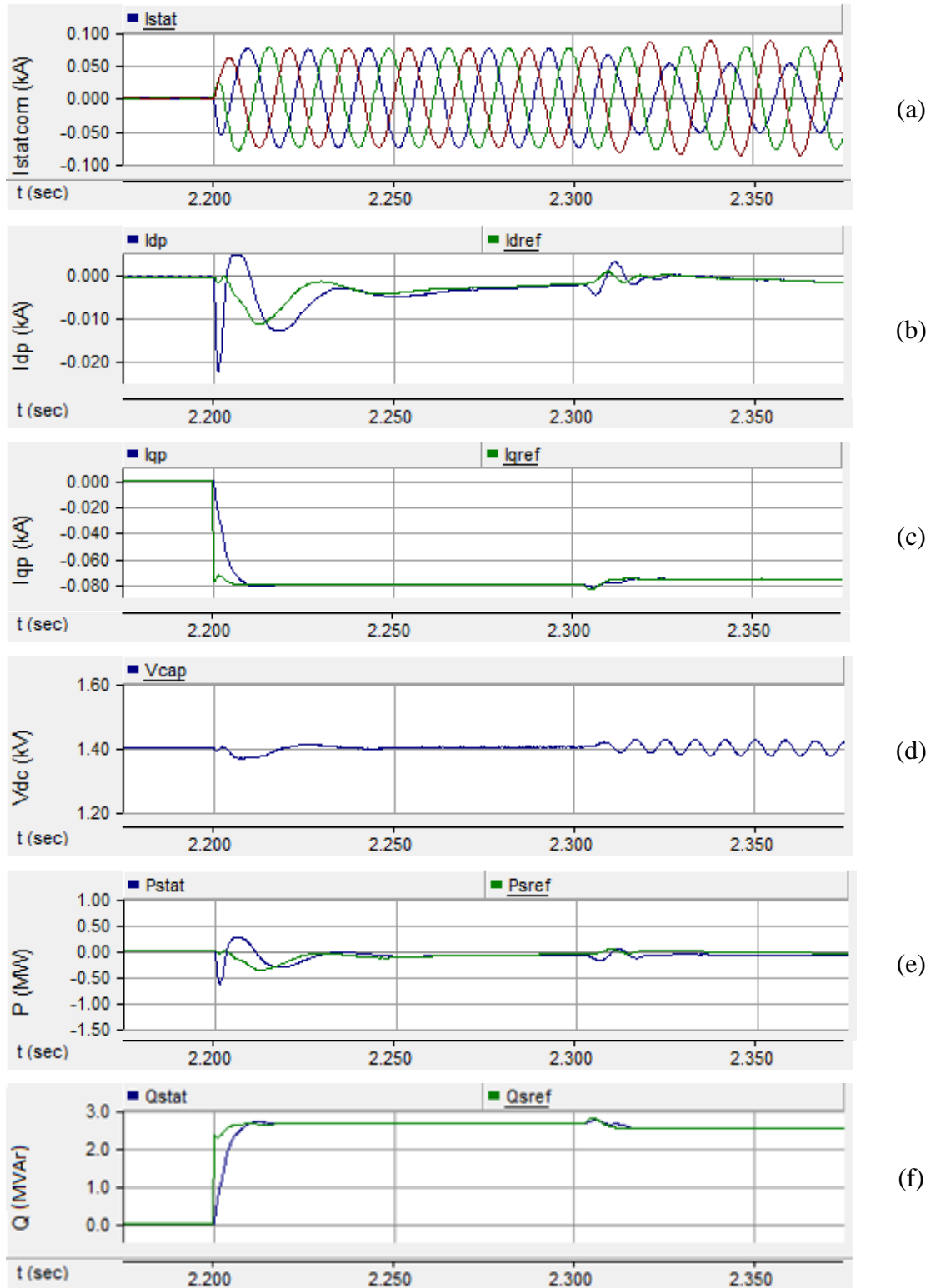
Figure 4.9 (a) STATCOM current (b) and (c) positive sequence component of current in *dq* frame, (d) DC-link voltage, (e) and (f) STATCOM active and reactive power output for grossly unbalanced load in realistic feeder

The performance of STATCOM controller is presented in Figure 4.9 and Figure 4.10. Figure 4.9(a) depicts the current through device $I_{STATCOM}$, Figures 4.9(b) and (c) depict the *dq* reference frame parts of positive sequence currents (I_{dp} and I_{qp}) of STATCOM respectively, and Figure 4.9(d) presents the DC-link capacitor voltage. Figures 4.9(e) and (f) illustrate the active and the reactive power flow out of STATCOM, respectively.

After t = 2.2 sec, three phase balanced STATCOM current can be seen in Figure 4.9(a). After activating reactive power compensation, in Figure 4.9(b) I_{dp} becomes slightly negative to supply active power loss due to switching. STATCOM tracks the I_{qp} reference command in less than a cycle in Figure 4.9(c). It is evident from Figure 4.9(f) that the settling time for reactive power compensation is 1 cycle.

(a)

(b)
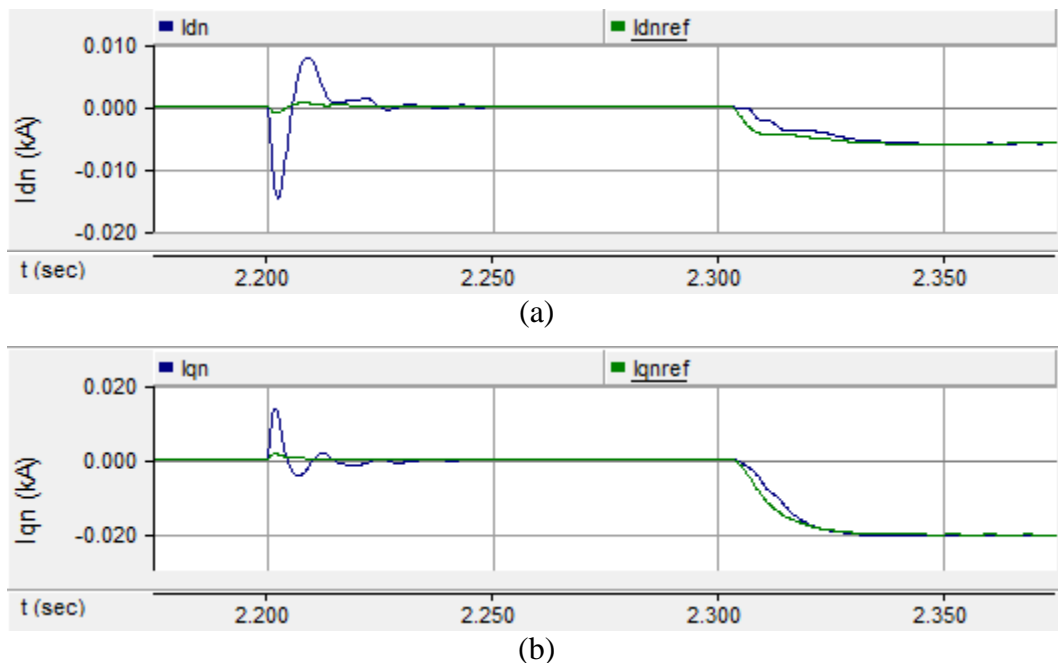
Figure 4.10 (a) *d*-axis and (b) *q*-axis parameters of negative sequence component of STATCOM current for grossly unbalanced load in realistic feeder

After t = 2.3 sec, $I_{STATCOM}$ becomes asymmetric due to compensation of negative sequence current. A slight increase in I_{qp} can be seen because load requires less reactive power (compared to Figure 4.9(f)) as only 2 branches are connected. The oscillations in capacitor voltage are stronger in this case compared to the mild unbalance case presented in Figure 4.4(d).

Figure 4.10(a) and (b) represent the *d*- axis and *q*- axis parts of negative sequence component of STATCOM current. Settling time for negative sequence controller is observed to be 2 cycles from Figure 4.10. Higher magnitude of negative sequence current is observed for gross unbalance than the mild unbalance case illustrated in Figure 4.5.

4.4 VOLTAGE REGULATION AT WIND FARM TERMINAL

The single line diagram of study system for voltage regulation is presented in Figure 4.11. A balanced night time load, which is typically lower than the day time load and constitutes a light load condition, is considered at 'Bus 4'. The wind farm is modelled by an aggregation of appropriate number of double cage induction generators each rated 2.3 MW. The remaining network is similar to Figure 4.1. Induction generator parameters and load parameters are provided in Appendix B and Appendix C, respectively.
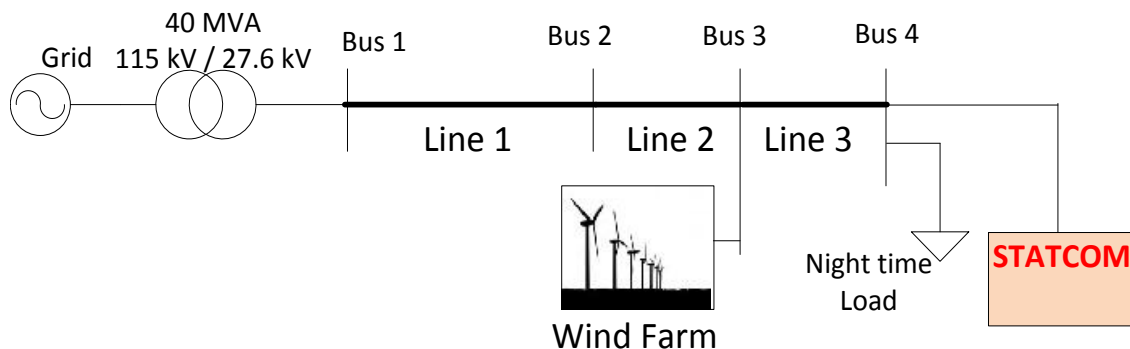
Figure 4.11 Single line representation of feeder network with wind farm and night time load

Wind farms typically generate power in the night. Since loads are lower at night, the excess power flows in reverse direction into the grid. This reverse power flow in the feeder, during night causes voltage rise at 'Bus 3'. In steady state, without STATCOM at load bus, the RMS voltages at the wind farm terminal are measured in PSCAD/EMTDC and are presented through Table 4.1 for different sizes of wind farm. According to Hydro-One technical interconnection requirement, steady state voltage at any point of distribution line should not exceed 1.06 pu [24]. It is clear from Table 4.1 that only 2 wind turbines can be added to the network resulting in feeding of 4.5 MW renewable energy into the grid. Hence,

a STATCOM is employed to regulate the voltage. Thereby enabling more wind turbines to be added onto the feeder. The voltage is regulated by STATCOM at 'Bus 3' because the voltage rise is maximum at the wind farm terminal. Voltage regulator explained in section 2.4.2 is utilized as STATCOM control.

Table 4.1 'Bus 3' voltage for different sizes of wind farm for night time loads

No. of wind turbines	Active power output (MW)	'Bus 3' RMS Voltage (pu)
1	2.27	1.041
2	4.54	1.055
3	6.8	1.066
4	9.08	1.074
5	11.34	1.093
6	13.61	1.102

Figure 4.12 shows the voltage at 'Bus 3' when 3 turbines are connected. Figure 4.12(a) depicts the RMS voltage V_{RMS} at 'Bus 3' and Figure 4.12(b) depicts the reactive power support by STATCOM. Before t = 12.2 sec, STATCOM is floating and at t = 12.2 sec, STATCOM starts regulating voltage at the bus.
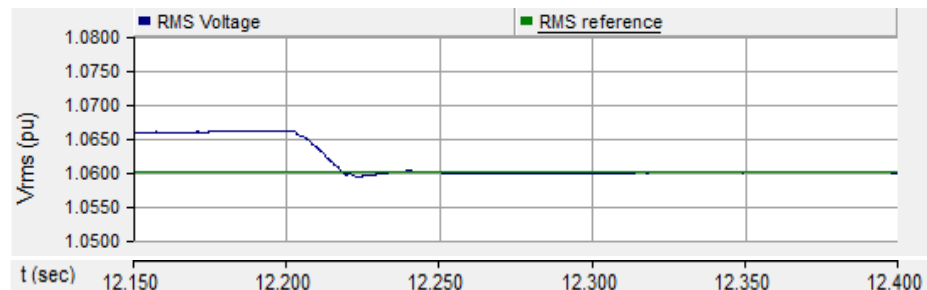
(a)
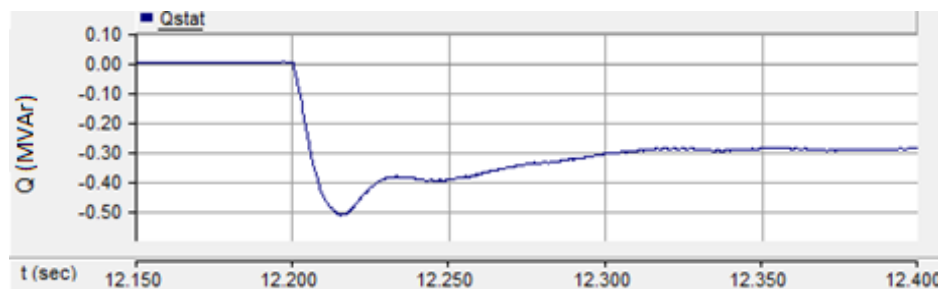
(b)

Figure 4.12 (a) Wind farm terminal voltage and (b) reactive power supplied by STATCOM when 3 turbines operational

Without voltage regulation, voltage at 'Bus 3' reaches 1.066 pu which is more than the specified utility limit. The STATCOM reduces the steady state voltage to 1.06 pu in one and half cycles as shown in Figure 4.12(a). In steady state, the STATCOM supplies **0.3 MVAr inductive** power as shown in Figure 4.12(b). An overshoot in reactive power is observed. This is attributed to generator load dynamics as induction generator has mechanical rotating mass causing large time constant in response.
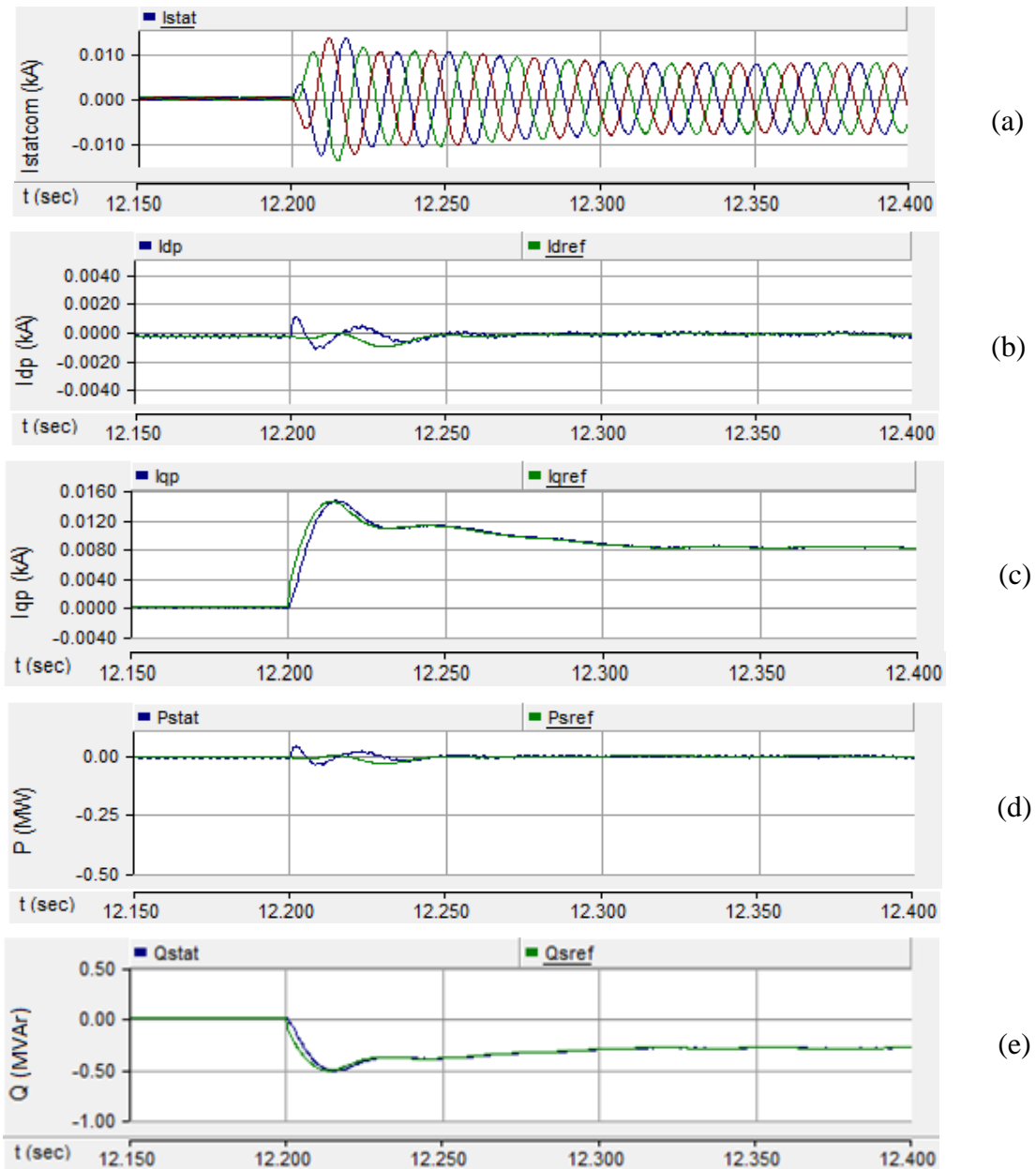
Figure 4.13 (a) STATCOM current (b) and (c) positive sequence *d*-axis and *q*-axis parts of current, (d) and (e) STATCOM active and reactive power output for voltage regulation in realistic feeder

The performance of STATCOM controller is presented in Figure 4.13 and Figure 4.14. Figure 4.13(a) depicts the current through device $I_{STATCOM}$, Figures 4.13(b) and (c) depict the dq reference frame parts of positive sequence currents (I_{dp} and I_{qp}) of STATCOM respectively. Figures 4.13(e) and (f) represent the active and the reactive power flow out of STATCOM, respectively.

After initialization of voltage regulator, three phase balanced current flows through STATCOM. Current magnitude varies for a few cycles but stabilizes later as observed in Figure 4.13(a). This is because current follows the reference reactive power for regulating voltage. A very small amount of real power is consumed by STATCOM towards its losses as shown in Figure 4.13(d). Therefore, I_{dp} is also very small. Fast response of I_{qp} enables STATCOM to follows its reference reactive power fast as shown in Figures 4.13(c) and (e). Figures 4.14(a) and (b) present the d- axis and q- axis parts of negative sequence component of STATCOM current. No steady state negative sequence current flows through STATCOM in Figure 4.14 as no unbalance is present. A little transient appears at $t = 12.2$ sec, but dies out fast.
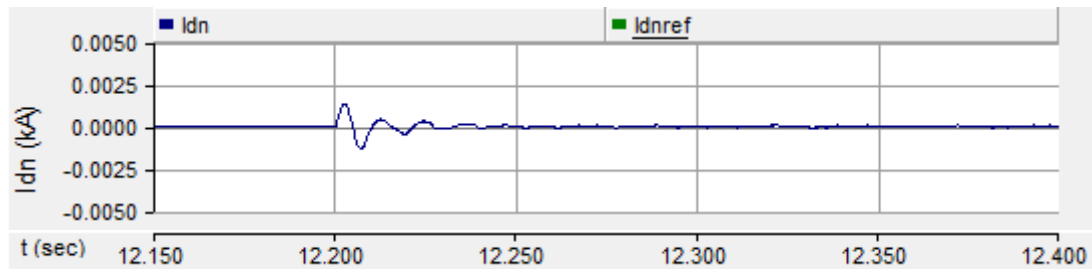
(a)
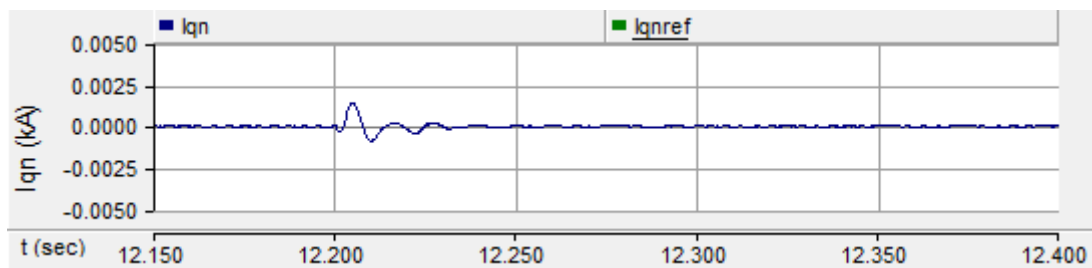
(b)

Figure 4.14 (a) d-axis and (b) q-axis parts of negative sequence component of STATCOM current for voltage regulation in realistic feeder

The capability enhancement of feeder to accommodate more wind generators is illustrated in Figure 4.15 and Figure 4.16. Figure 4.15 and Figure 4.16 present (a) the RMS voltage

at 'Bus 3' and (b) STATCOM reactive power support for 4 wind turbines (9.08 MW) and 5 turbines (11.34 MW), respectively.

The STATCOM successfully lowers the RMS voltage to the utility acceptable value of 1.06 pu in Figure 4.15(a). A low frequency oscillation in V_{RMS} can be seen after $t = 12.25$ sec. These oscillations relate to power oscillation in induction generator. Induction machines have rotating mass and the time constant of mechanical components is larger than that of electrical components. Therefore, these oscillations are of larger time period and decay in typically 1-2 second. If more turbines are added in wind farm, higher will be the moment of inertia and lower will be the frequency of power oscillations in generators. This can be clarified by comparing Figure 4.12(a), Figure 4.15(a) and Figure 4.16(a).
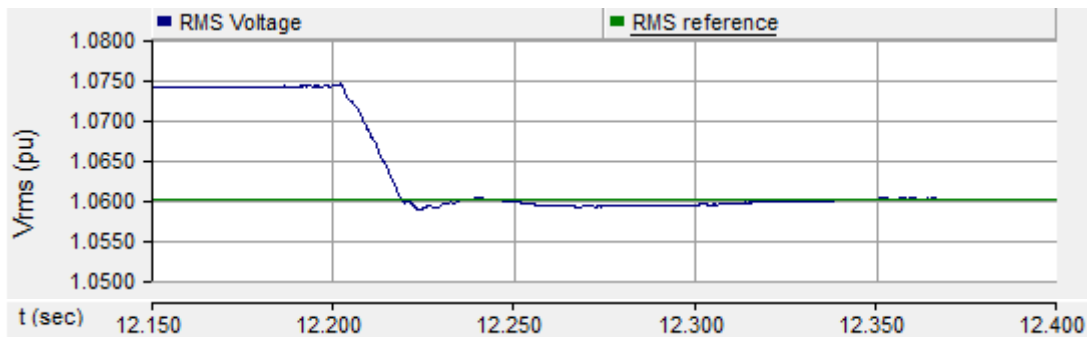
(a)
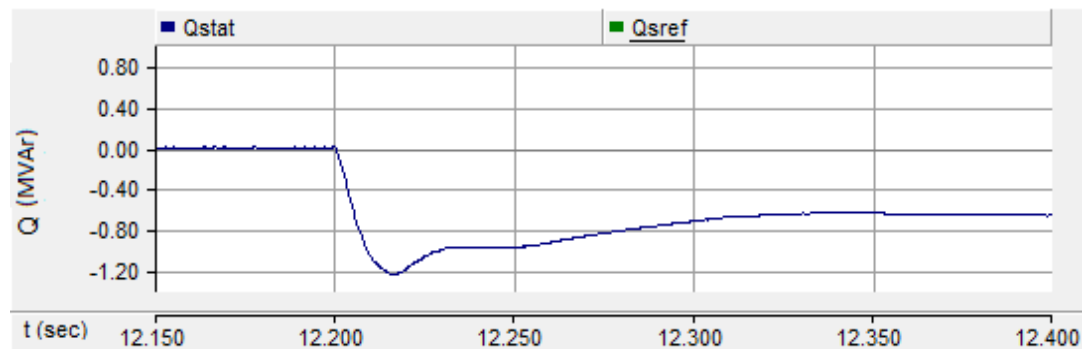
(b)

Figure 4.15 (a) Wind farm terminal voltage and (b) reactive power supplied by STATCOM when 4 turbines operational

For **four turbines**, STATCOM supplies **0.6 inductive MVAr** in steady state and **1.5 inductive MVAr** for **five turbines** (Figure 4.16). Therefore, with 3 MVAr STATCOM, more than five wind turbines can be integrated into network. The overshoot in the reference

value limits its ability to connect beyond five turbines as it reaches its rated capacity during transients.

(a)

(b)
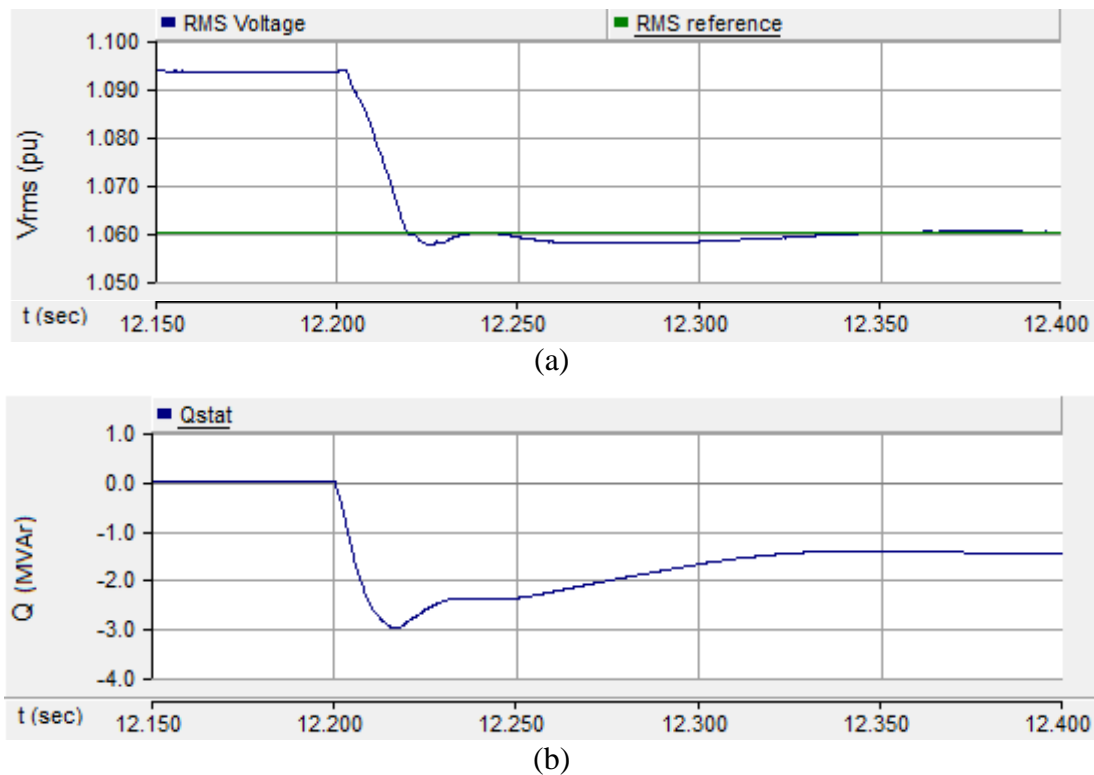
Figure 4.16 (a) Wind farm terminal voltage and (b) reactive power supplied by STATCOM when 5 turbines operational

4.5 TEMPORARY OVERVOLTAGE (TOV) STUDIES

Electrical networks are susceptible to faults. Due to asymmetrical fault in the line, a temporary overvoltage may occur on the unfaulted phases of the line. A single line to ground (SLG) bolted fault is created at 'Bus 3' in Figure 4.11. The fault is introduced at t = 13 sec for 4.5 cycles. Due to this fault, voltage at one phase goes to zero and voltage at other two phases goes high. Because of fault incidence, the power output of wind farm also reduces.

According to Hydro One technical interconnection report (TIR), in any fault situation voltage at the phases must not exceed 130% of rated value [24]. Figure 4.17 presents the phase voltages with single wind turbine. During SLG fault, voltage at one phase goes to

zero (Figure 4.17(a)). However, in the other phases the voltage does not exceed the limit as shown in Figure 4.17(b). Hence, one wind turbine can be installed without getting STATCOM support.

(a)

(b)
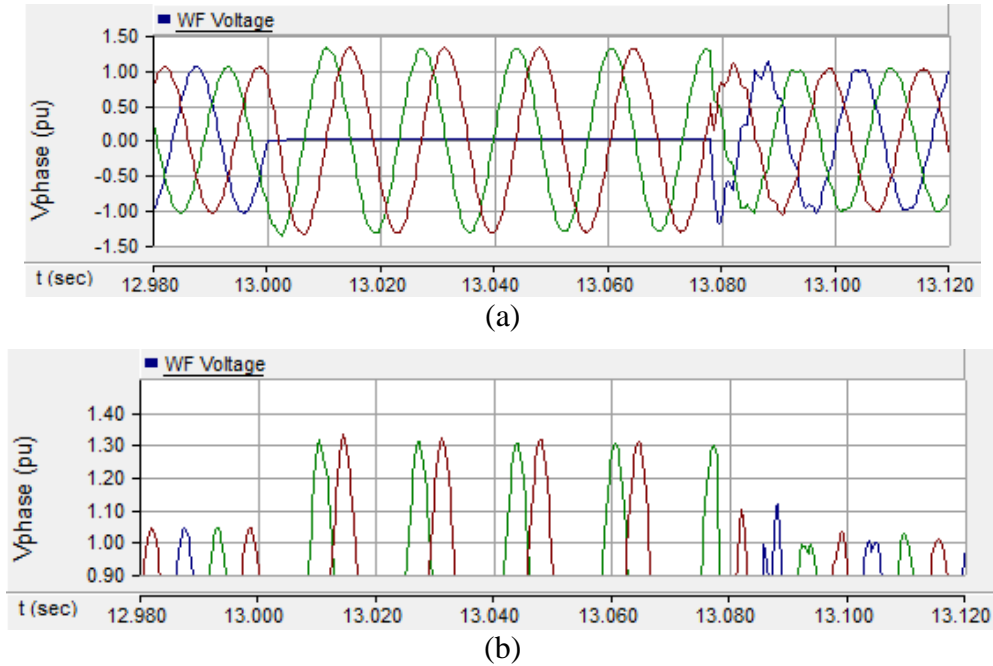
Figure 4.17 (a) Three phase voltage at the wind farm terminal (b) a magnified voltage plot without STATCOM when one wind turbine is operational

(a)

(b)
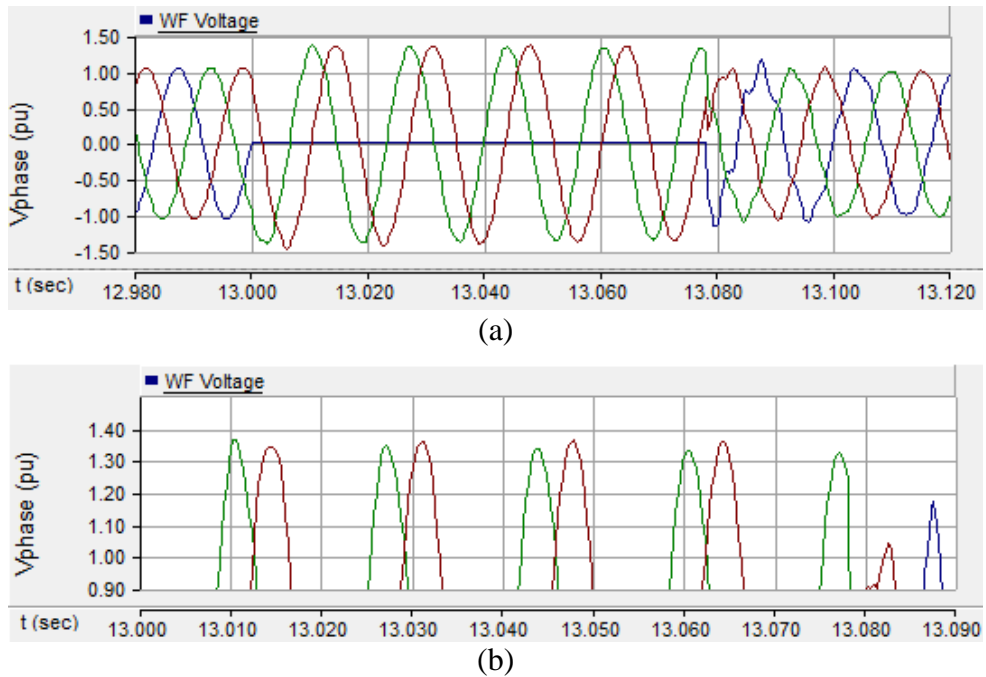
Figure 4.18 a) Three phase voltage at the wind farm terminal b) a magnified voltage plot without STATCOM when two wind turbines are operational

Figure 4.18 depicts the three phase voltages at wind farm terminal when two turbines are connected in the network. It is evident from the Figure 4.18b that TOV at the wind farm bus goes up to 1.38 pu. This violates the technical requirements of Hydro One. Therefore, STATCOM should operate in inductive mode to lower down the TOV.

Figure 4.19 presents the wind farm voltage with STATCOM. It supplies inductive reactive power to successfully lower the TOV to 1.3 pu as shown in Figure 4.19(b).
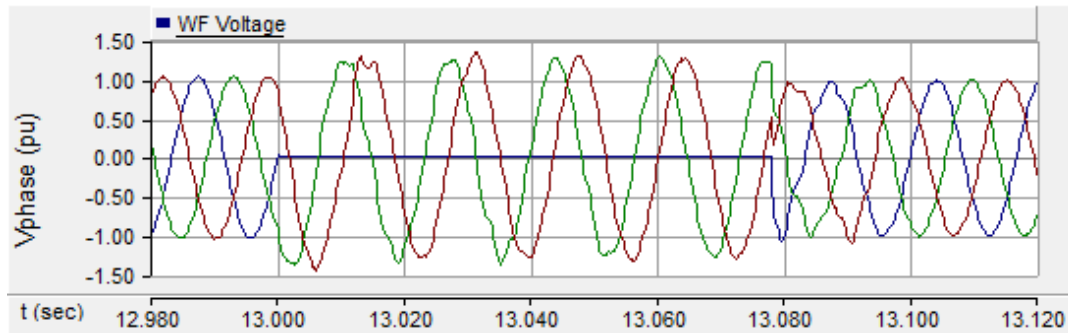
(a)
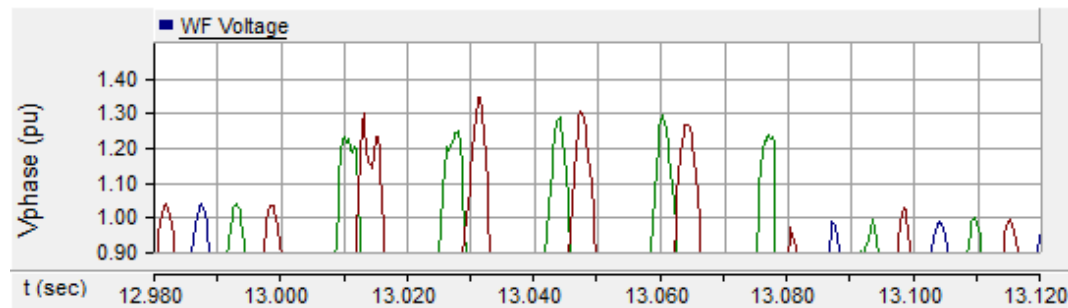
(b)

Figure 4.19 a) Three phase voltage at the wind farm terminal b) a magnified voltage plot with STATCOM when 2 wind turbines are operational

Figure 4.20(a) presents STATCOM current '$I_{STATCOM}$', (b) and (c) denote the dq reference frame parts of positive sequence currents (I_{dp} and I_{qp}) of STATCOM, respectively, (e) and (f) illustrate the active and the reactive power flow out of STATCOM, correspondingly. After fault inception, controller becomes active as TOV surpasses 1.3 pu. $I_{STATCOM}$ flows in response as shown in Figure 4.20(a). During fault, oscillations in STATCOM active power flow (representing losses) can be seen that settle down later (Figures 4.20(b) and (d). Since the compensator is working in inductive mode, the reactive power is negative in Figure 4.20(e). After fault gets cleared, the reactive power also attains zero value and the STATCOM starts floating in the network.
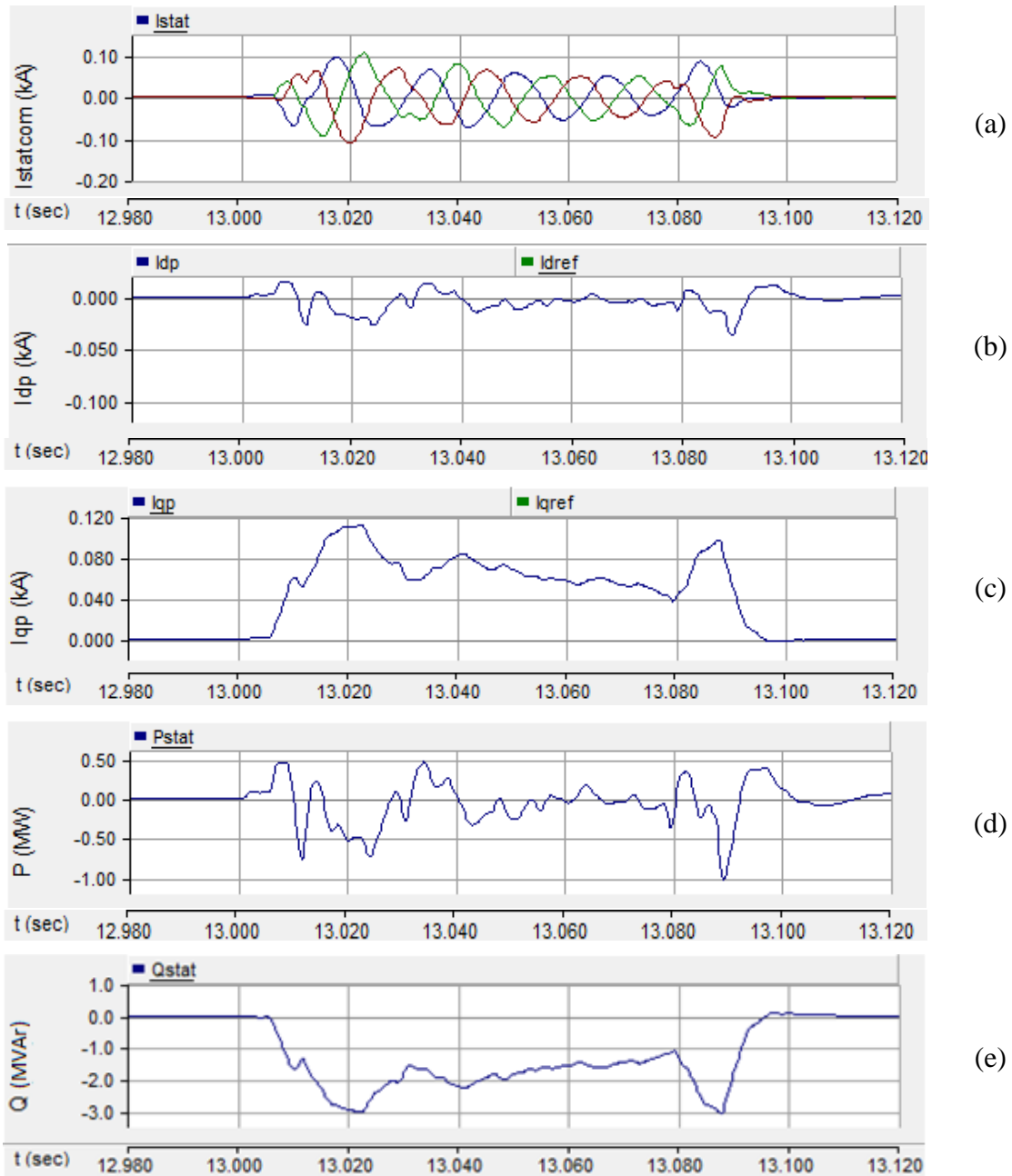
Figure 4.20 (a) STATCOM current (b) and (c) positive sequence component of current in *dq* frame, (d) and (e) STATCOM active and reactive power output for TOV regulation when 2 wind turbines are operational

Figures 4.21(a) and (b) present the *d*- axis and *q*- axis parts of negative sequence component of STATCOM current. As fault occurs, transients appear in the negative sequence current output at *t* = 13.0 sec, whereas as the fault clears, the negative sequence currents again become zero.
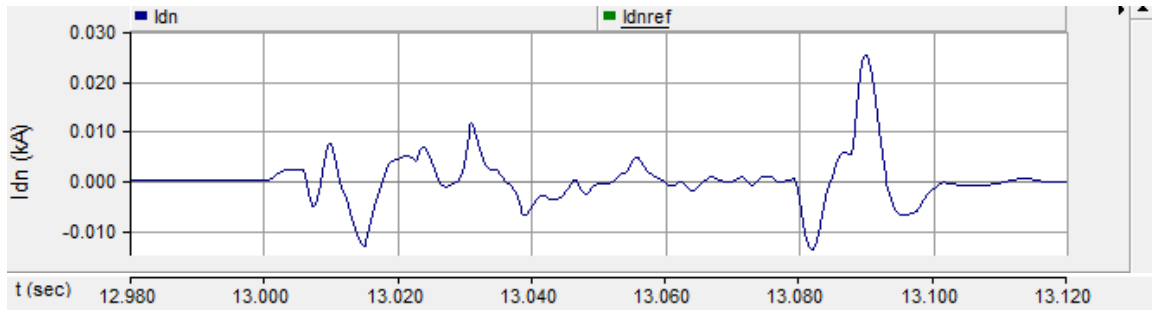
(a)
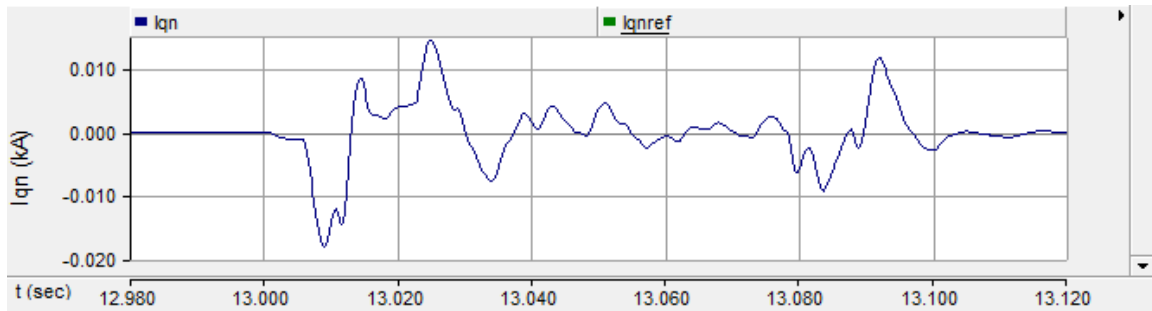
(b)

Figure 4.21 (a) *d*-axis and (b) *q*-axis parts of negative sequence component of
STATCOM current for TOV regulation when 2 wind turbines are operational
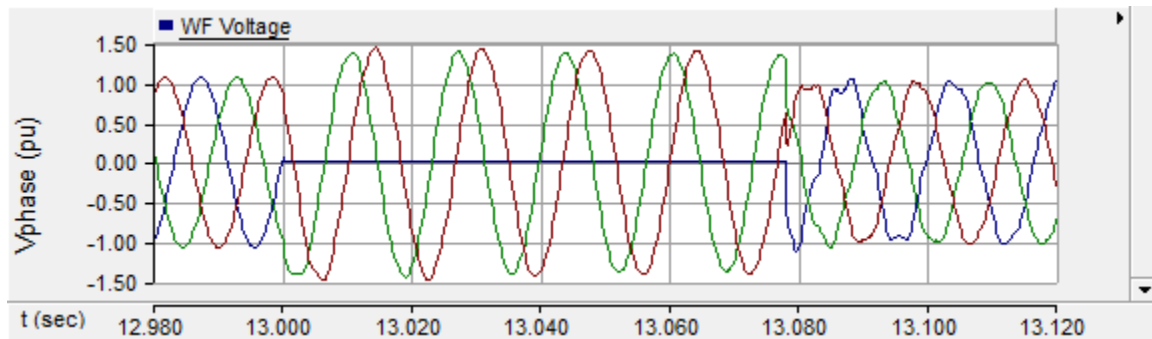
(a)
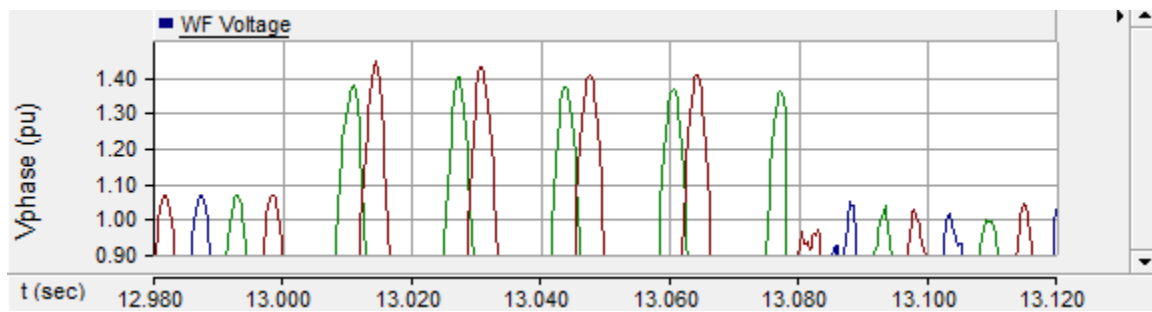
(b)

Figure 4.22 (a) Three phase voltage at the wind farm terminal (b) a magnified voltage
plot without STATCOM when three wind turbines are operational

Studies with 3 wind turbines (6.8 MW) are presented in Figure 4.22 and Figure 4.23. Without STATCOM, the TOV reaches 1.42 pu at wind farm bus during fault as shown in Figure 4.22(b). Figure 4.23 presents the STATCOM performance to reduce the voltage. It is evident from Figure 4.23(c) that the STATCOM supplies its rated inductive power to bring down the TOV to 1.3 pu, therefore, with 3 MVAr rated STATCOM only three wind turbines of total rating of 6.8 MW can be connected such that it does not violate the stipulated transient voltage limit of Hydro One. A bigger size of STATCOM will be required to provide additional amount of inductive power in case more wind turbines need to be connected to the network.

(a)

(b)

(c)
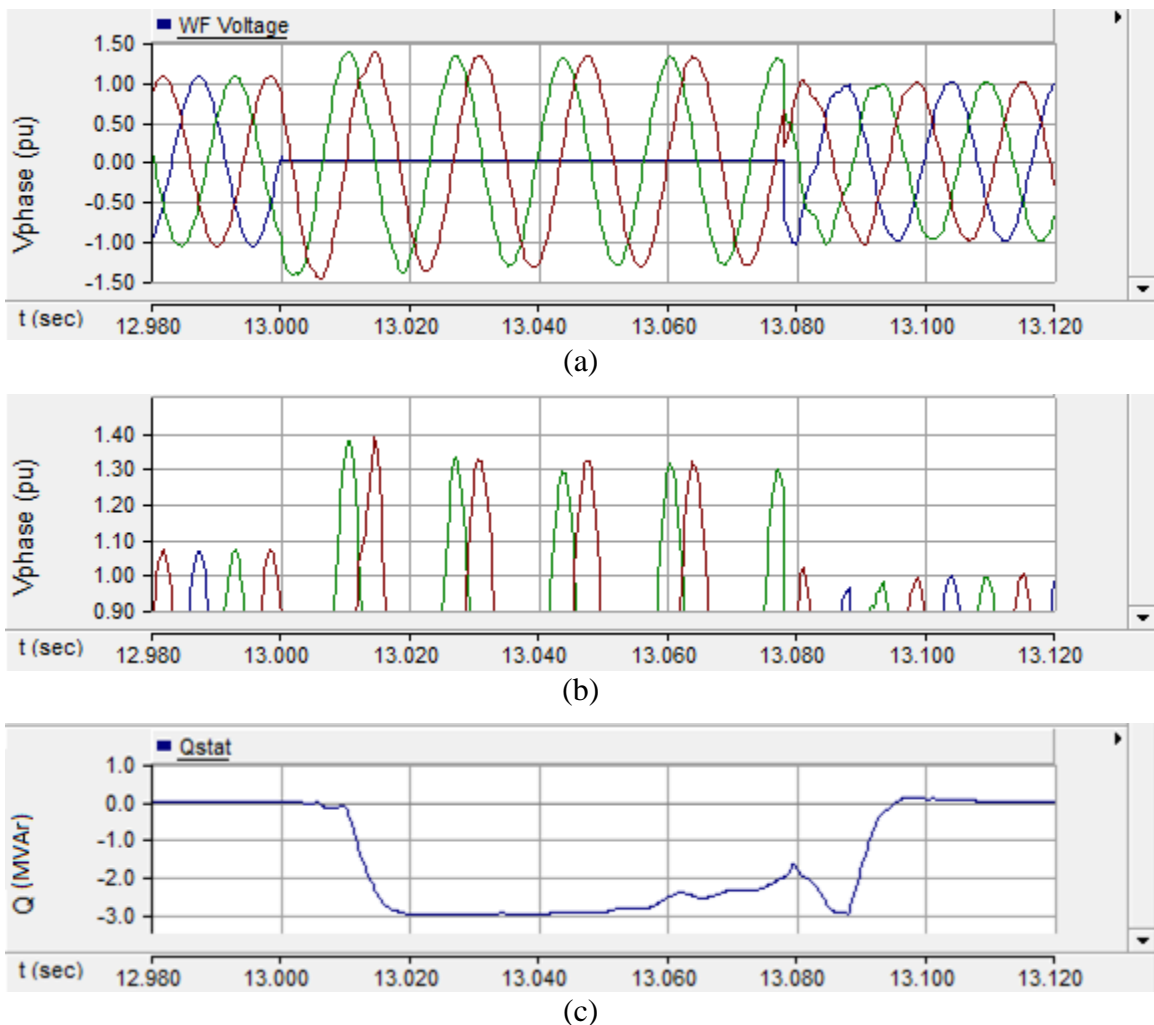
Figure 4.23 (a) Three phase voltage at the wind farm terminal (b) a magnified voltage plot with STATCOM (c) reactive power support of STATCOM when three wind turbines are operational

4.6 CONCLUSION

A realistic distribution feeder model of Hydro One, a transmission utility of Ontario, is considered to assess the performance of STATCOM for load compensation and voltage regulation. The STATCOM size is determined based on requirement for load compensation. The 3 MVAr STATCOM is successfully shown to correct load power factor to unity and to compensate the negative sequence current of load. Further, a case of grossly unbalanced load is also studied. The STATCOM provides power factor correction in 1 cycle and compensates the load imbalance in 2 cycles.

The problem of overvoltage with augmentation of more wind farms is also resolved with the same STATCOM control. Without STATCOM the feeder is able to accommodate only 2 wind turbines; but with STATCOM, five wind turbines can be successfully accommodated in the network without violating the stipulated steady state overvoltage limit of 1.06 pu.

The temporary overvoltages in case of an asymmetric fault at the wind farm terminal are also analyzed. It is found that with the given STATCOM, three wind turbines can be connected in feeder to keep TOV within the limit of 130% during SLG fault. Without STATCOM, only one wind turbine can be connected without violating the specified TOV limit of Hydro One.

It is therefore, demonstrated that the developed comprehensive STATCOM controller can successfully provide load compensation for both mildly and grossly unbalanced loads. Further the 3 MVAr STATCOM can increase the number of wind turbines to be connected in the feeder from one (2.3 MW) to three (6.9 MW), which is quite substantial.

Chapter 5

MITIGATION OF SUBSYNCHRONOUS RESONANCE IN WIND FARMS WITH STATCOM

5.1 INTRODUCTION

This chapter presents the performance of the developed comprehensive STATCOM controller in damping subsynchronous oscillations in induction generator based wind farms. It is shown [54] that IG based wind farms connected to series compensated lines are prone to SSR. Frequency scanning analysis is first presented for detecting the potential of subsynchronous resonance (SSR) in self-excited induction generator based wind farms. Two types of induction generator: single-cage and double-cage based wind farms are considered. The wind farms are connected to modified IEEE First SSR Benchmark [57] and IEEE Second Benchmark systems [58]. Detailed positive sequence model of the study systems are developed in MATLAB software. Frequency scanning analysis is carried out by calculating effective impedance, looking from the rotor circuit of the induction generator. The frequency scanning results are validated with eigenvalue analysis published in [26], [27], [54].

Once the conditions for SSR occurrence are determined by frequency scanning, the STATCOM is utilized for mitigating the SSR. The effectiveness of the STATCOM controller developed in Chapter 2 is examined with symmetrical and unsymmetrical faults. The simulations are conducted in PSCAD/EMTDC software.

5.2 STUDY SYSTEMS

The study systems for frequency scanning for the study of SSR and its mitigation with STATCOM are presented here. Study systems are taken from [26], [54].

5.2.1   Study system 1

The basic diagram of Study System 1 for frequency scanning studies is shown in Figure 5.1. It is constituted of wind farm, an interconnecting transformer L_t to step up the voltage and send power through transmission line to the grid.
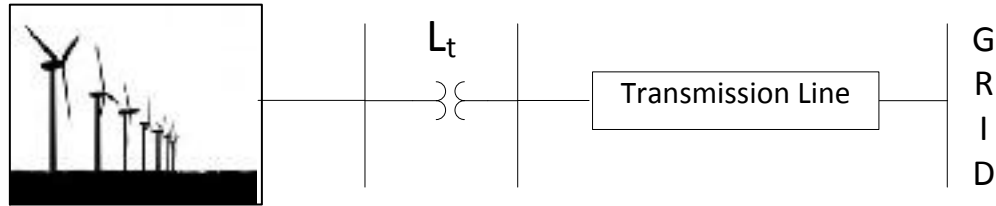
Figure 5.1 Study System 1 for frequency scanning

5.2.2   Study system 2 with STATCOM

Figure 5.2 presents the Study System 2 with STATCOM. For SSR mitigation a STATCOM is connected at the terminal of wind farm. Other components are the same as explained in section 5.2.1
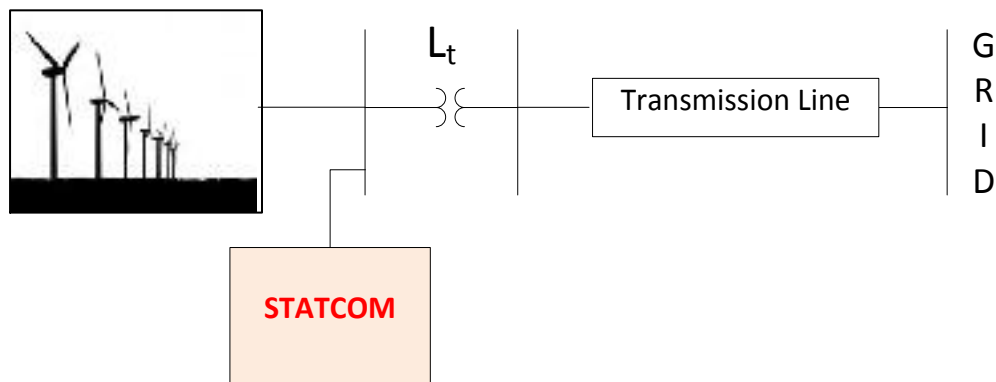
Figure 5.2 Study System 2 with STATCOM

5.3   SYSTEM MODELLING

5.3.1   Wind Turbine Generator

Subsynchronous resonance phenomenon in wind farm is due to induction generator effect [26]. Therefore, only electrical parameters of wind farm are modelled. The torsional system is omitted in the modelling. Two types of induction generators are considered i) single cage

and ii) double cage. All induction generators are connected in parallel and the wind farm is treated as an aggregated single induction generator having equivalent parameters.

5.3.1.1   *Single cage induction generator*

Figure 5.3 shows the positive sequence model of the single-cage induction generator based wind farm. In single-cage induction generator, the rotor circuit of the generator is equipped with only one winding which is represented by a series R-L (R_r -X_r). The effective rotor resistance is determined by the operating slip '*s*' of the induction generator. C_g represents the fixed capacitance connected at wind farm terminal to provide reactive power to wind farm. The generator parameters are given in Appendix C.
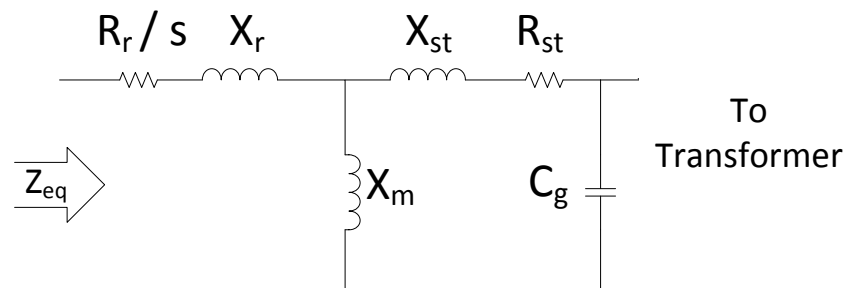
Figure 5.3 Positive sequence model of single cage induction generator

5.3.1.2   *Double cage induction generator*

Induction generators are commonly modeled as a simple squirrel cage induction machine as shown above. However, most of the induction generators have a double squirrel cage rotor. In comparison to single-cage machines, these generators are widely used in the wind farms where slip varies over a wide range. In the double cage rotor, there are two electrical circuits. One circuit is placed at the outer surface of the rotor which is very close to the stator winding. The other circuit is in the deeper part of the cage [27].

Figure 5.4 shows the positive sequence model of the double-cage induction generator based wind farm. Since two windings are present in the rotor circuit, a frequency dependent equivalent circuit is developed [66]. The generator parameters are given in Appendix C.
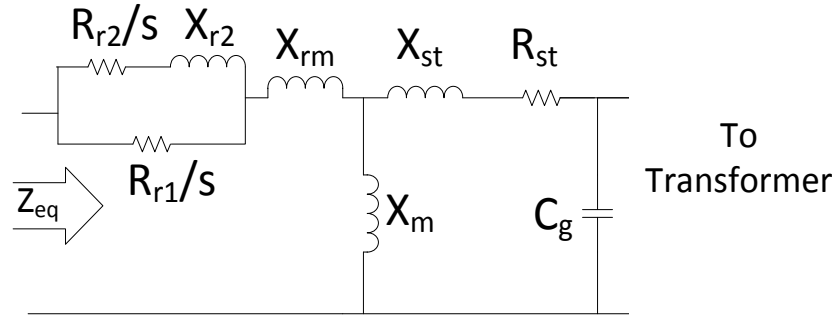
Figure 5.4 Positive sequence model of double cage induction generator

5.3.2　Transformer Modelling

The transformer is modeled as 'T' model as shown in Figure 5.5 [67]. The magnetizing current is taken as 1%. The modelling equations are provided in Appendix C.
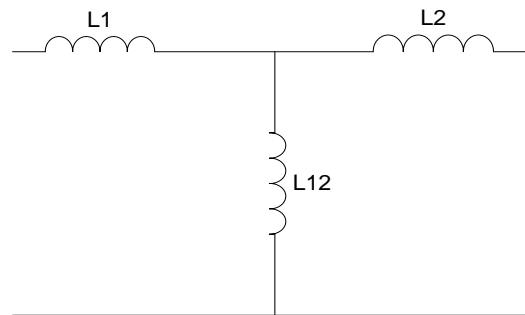
Figure 5.5 Equivalent 'T' model of transformer

5.3.3　Transmission Line Model

Figure 5.6 presets two study systems proposed in literature for the SSR study with synchronous generator (a) IEEE First SSR Benchmark Model (IEEE FBM) [57] and (b) IEEE Second SSR Benchmark Model (IEEE SBM) [58] respectively. In this chapter, the benchmark models are modified by replacing the synchronous generators with large aggregated induction generator based wind farms. All line parameters are provided in Appendix C.

(a)

(b)
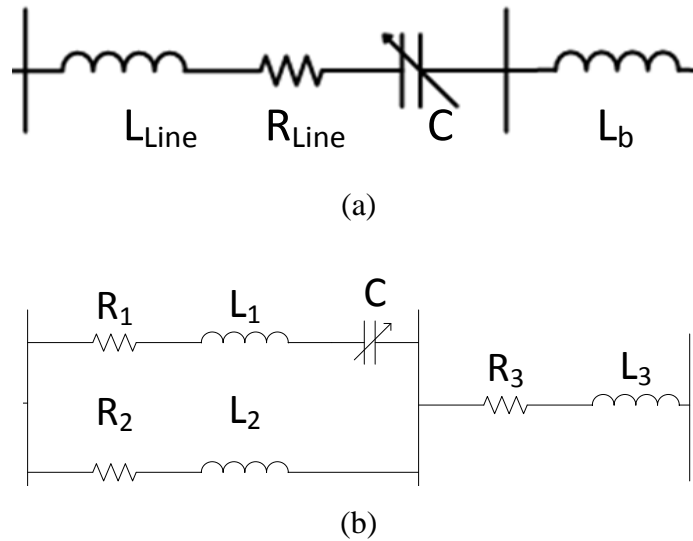
Figure 5.6 IEEE (a) First and (b) Second SSR Benchmark line models

5.3.4 STATCOM Modelling

STATCOM modelling is discussed in Chapter 2. For mitigation of SSR, STATCOM is connected to regulate the voltage at the PCC. The voltage regulator of STATCOM is modelled in section 2.4.2. A similar voltage regulator is employed in this study. The values of STATCOM components are given in Appendix D.

5.3.5 Complete System Model

The complete system models for frequency scanning studies are given in Figures 5.7(a) and (b) with IEEE First SSR Benchmark Model and Second SSR Benchmark Model, respectively. The wind farm size varies between 100 MW and 500 MW which is represented as an aggregated induction generator. The dynamic aggregation is carried out using weighted admittance method described in [54].
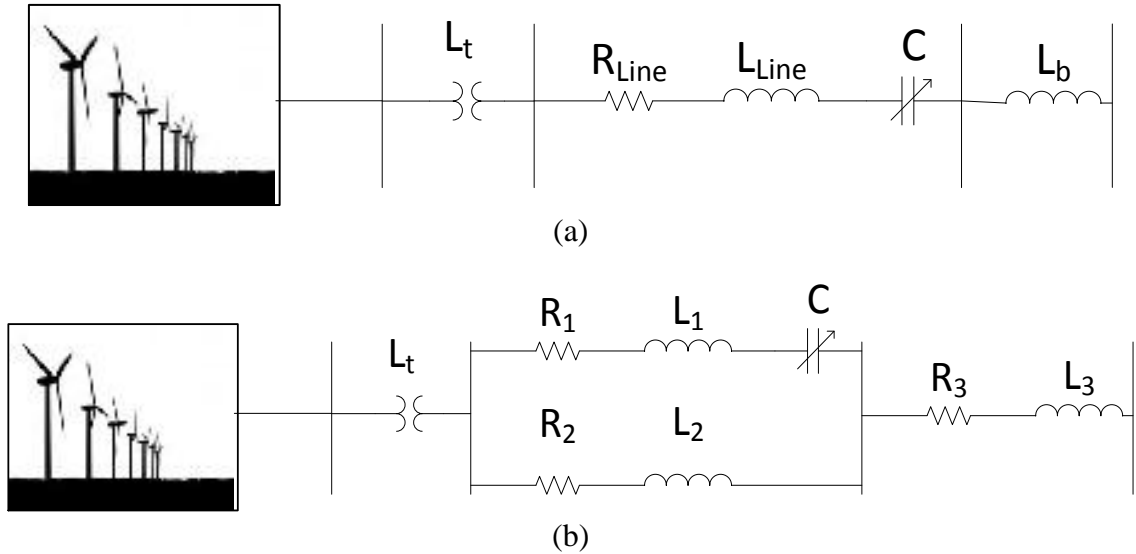
Figure 5.7 Study System 1 with IEEE (a) First SSR Benchmark and (b) Second SSR Benchmark line models

The complete diagram for STATCOM operation with Study System 2 is presented in Figure 5.8. The double cage induction generator given in section 5.3.1.2 is considered with IEEE First SSR Benchmark line model explained in section 5.3.3. Fault studies at two locations i) F_1 (close-in fault) and ii) F_2 (remote fault) are considered as illustrated in Figure 5.8. There is also a transformer (0.69 kV/ 34.5 kV) connected (not shown) between wind farm and STATCOM to raise the voltage at STATCOM bus. Fault parameters are given in Appendix D.
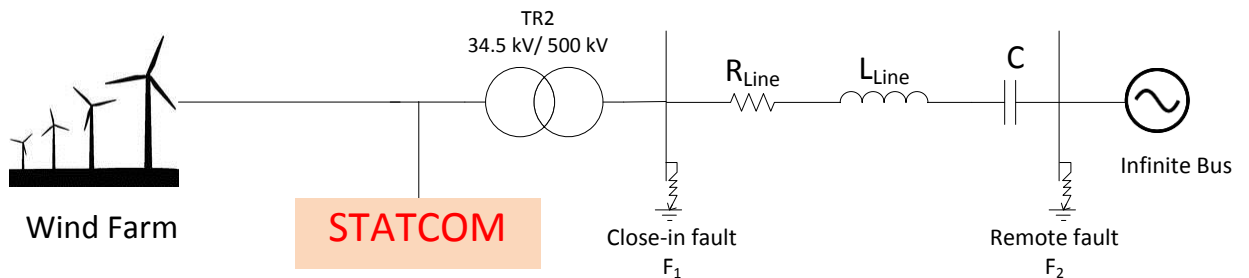
Figure 5.8 Study System 2 for fault analysis with STATCOM

5.3.6   Model Validation

Without STATCOM operation, the results for the Study System 2 are validated with results presented in [54], [65]. A 5 cycle fault consecutively at location F_1 and F_2 is considered with 100 MW wind farm at $t = 6.0$ sec in Figure 5.8 and results are presented in Figure 5.9 and in Figure 5.10, respectively.
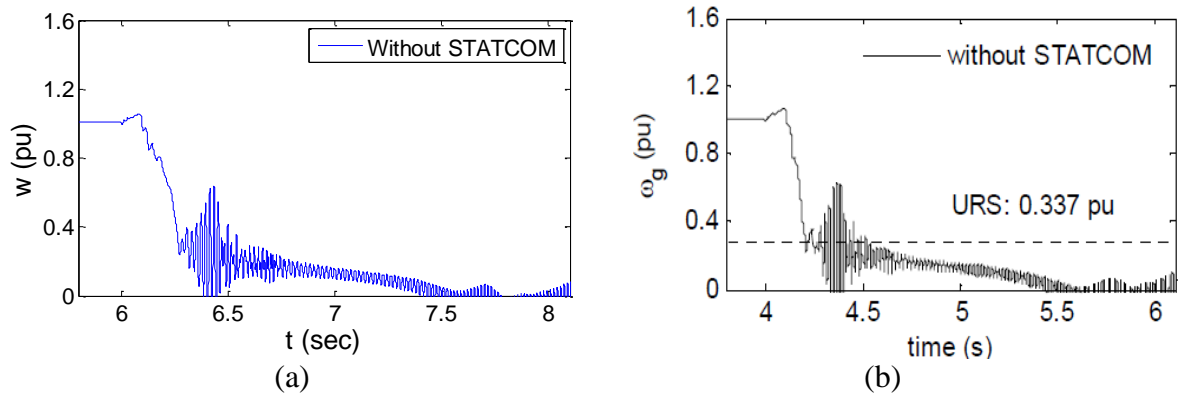
Figure 5.9 Speed of wind farm for close-in fault in (a) simulation and
(b) published paper [65]

In Figure 5.9(a), 50% series compensated line is considered that gives a stable operation and no SSR is seen. Nevertheless, at the occurrence of fault the speed of induction generator increases. When fault is cleared the speed reduces and machine is stalled. The same phenomenon is published in [65] and presented in Figure 5.9(b). This comparison successfully validates the study system.
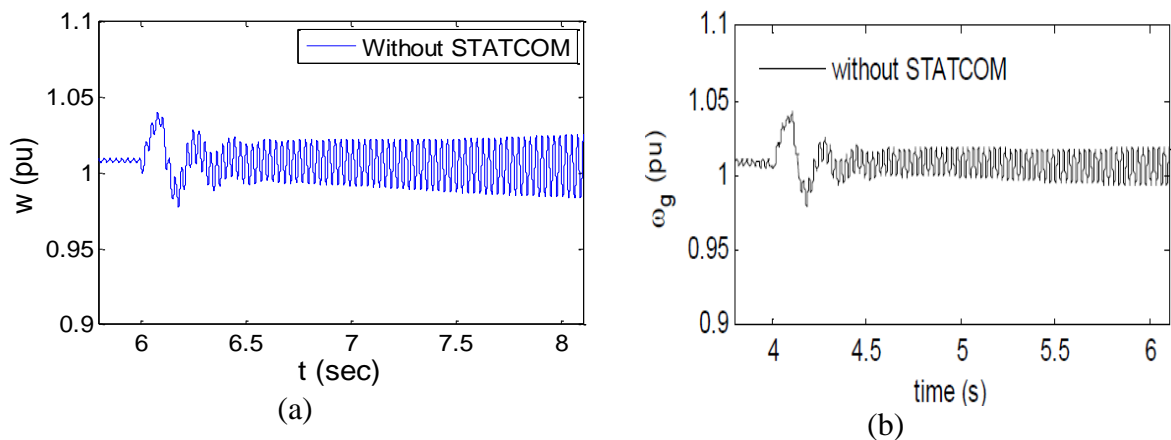
Figure 5.10 Speed of wind farm for remote fault in (a) simulation and
(b) published paper [54]

In Figure 5.10(a), 60% series compensated line is considered. After the fault, growing oscillations in speed are observed that lead to unstable operation of machine. This phenomenon illustrates SSR and matches well with the published result [54] presented in Figure 5.10(b).

5.4 ESTIMATION OF SSR WITH FREQUENCY SCANNING

5.4.1 Frequency Scanning Technique

Frequency scanning technique is a fundamental technique for preliminary analysis of subsynchronous resonance [46], [47]. In this technique, the equivalent impedance is computed by looking into the network from a point behind the rotor winding of a particular generator, as a function of the frequency. This impedance is known as SSR impedance. If a subsynchronous frequency exists at which SSR reactance becomes zero, or is close to zero, and the effective SSR resistance is negative, then SSR due to an induction generator effect occurs. The magnitude of the negative resistance is a measure of growth rate of electrical oscillations. These electrical oscillations do not cause undamped shaft oscillations but may be intolerable for the electrical system equipment [68]. The effective resistance $\left(R_{eff}\right)$ seen from the rotor plays a critical role in determining the SSR conditions in wind farms. For system described in Figure 5.7(a), it is calculated as [68]:

$$R_{eff} = \frac{R_r}{s} + R_{st} + R_{Line}$$

(5.1)

where, R_r and R_s are rotor and stator resistance of the single cage induction generator, respectively. R_{Line} is the line resistance including the transformer resistance and s is the slip of the induction generator.

The effective resistance comprises (i) transmission line resistance, (ii) stator winding resistance, and (iii) rotor winding resistance. The first two resistances are constant at all stator current frequencies. However, the equivalent rotor resistance is a function of electrical resonant frequency and it decreases with increase in the resonant frequency.

Further, the induction generators in wind farm always operate with negative slip which makes the rotor equivalent resistance negative. When the magnitude of effective negative resistance exceeds the sum of line resistance and stator resistance, it offers negative damping to the system. This may only happen for frequencies above the electrical resonant frequency (f_{er}).

To find the possible cases of SSR due to induction generator effect, zero crossing frequencies of the equivalent reactance and the effective resistance at or near these frequencies are monitored. The equivalent reactance is calculated as

$$X_{eq} = imag(Z_{eq}) = imag(Z_1 + Z_2 + Z_3) \tag{5.2}$$

where,

$$Z_1 = \left(\frac{R_r}{s} + jX_r\right)$$

$$Z_2 = (R_{st} + jX_s)||(jX_m)$$

$$Z_3 = \left(R_{Line} + j\omega(L + jL_t)\right)||\left(-j\frac{1}{\omega C_g}\right)$$

5.4.2   Frequency Scanning Study Results

A comprehensive frequency scanning analysis to detect the potential for SSR in induction generator based wind farms is carried out. Firstly, studies with single cage and double cage induction generators (explained in section 5.3.1) are carried out with IEEE FBM. Subsequently, studies with double cage induction generators are executed with IEEE SBM.

5.4.2.1 *Frequency scanning with modified IEEE First SSR Benchmark Model connected to single cage induction generator*

The effective resistances seen behind the rotor, defined by (5.1) for different wind farm sizes are depicted in Figure 5.11. In the Figure 5.11, effective resistances of the wind farms are presented with respect to subsynchronous frequency while the wind farm size is varied from 100 MW to 500 MW. By aggregating suitable number of 2 MW single-cage induction generators, the aggregated equivalent generator model is developed [25]. It is seen that as the frequency increases the effective resistance decreases and becomes negative at certain frequency. The zero crossing frequency increases, as the size of the wind farm increases. However, the effective resistance alone cannot predict any potential for SSR caused by induction generator effect. Therefore, effective resistance and reactance are to be monitored, simultaneously.

Figure 5.12 presents the equivalent reactances from (5.2) seen behind the rotor circuit of the aggregated wind turbine generator. Figure 5.12(a) shows the equivalent reactances of a 100 MW wind farm for four different series compensation levels (30%, 50%, 70% and 90%). It is found that when the reactance crosses zero the effective resistance remains positive. This is seen for all levels of series compensation considered. Therefore, no potential for SSR is anticipated when a 100 MW wind farm with single-cage induction generators is connected to a series compensated line. Figures 5.12(b) - (e) show the equivalent reactances for different series compensation levels for 200 MW to 500 MW wind farm, respectively. From Figure 5.12(b), in case of 200 MW, it is seen that the effective resistance becomes negative between 70% to 90% series compensation. If the effective reactance at a certain compensation level crosses zero with a negative resistance, the induction generator self-excitation may occur. This minimum compensation level is called critical compensation level for that wind farm size. Therefore, a 200 MW wind farm may experience SSR due to induction generator effect at a series compensation level between 70% and 90%.

Similar condition of SSR is anticipated at series compensation level of 80% for 300 MW wind farm in Figure 5.12(c). It is observed from Figure 5.11 that as size of wind farm increases, the frequency at zero crossing for effective resistance value shifts towards right.
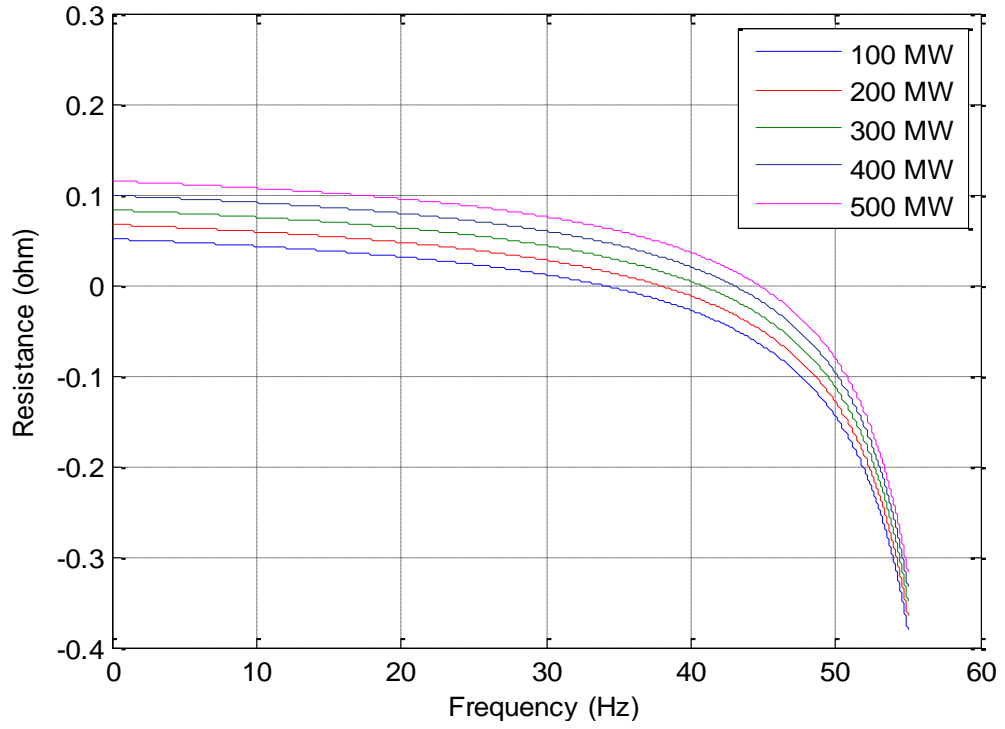
Figure 5.11 Effective resistances seen from the rotor for different sizes of single-cage induction generator based wind farms
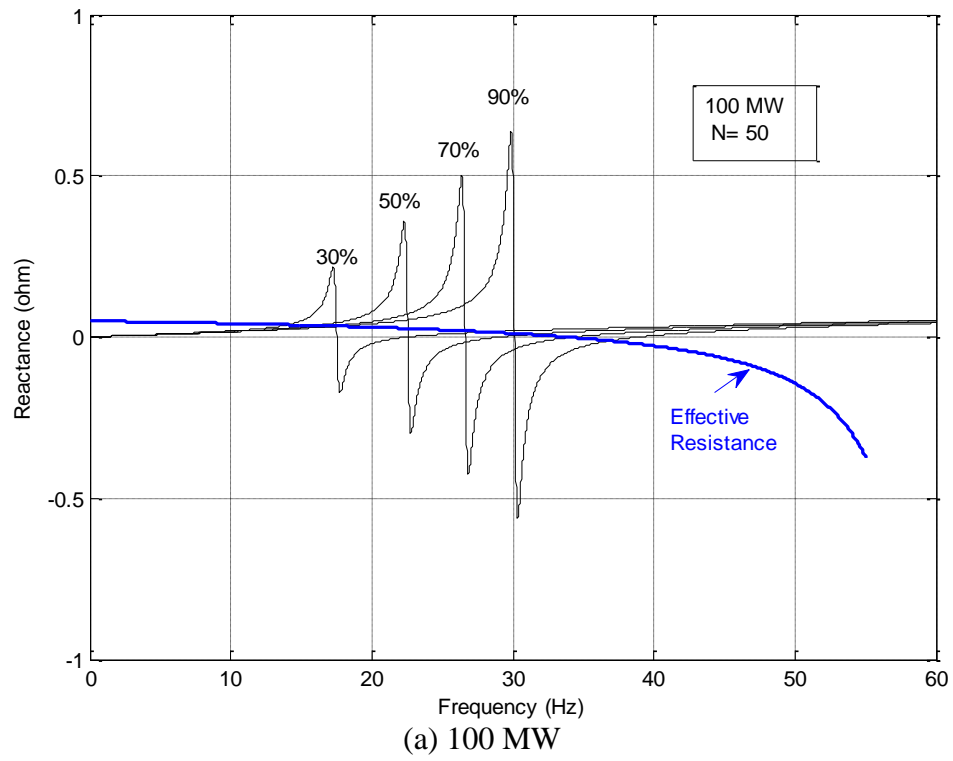
(a) 100 MW
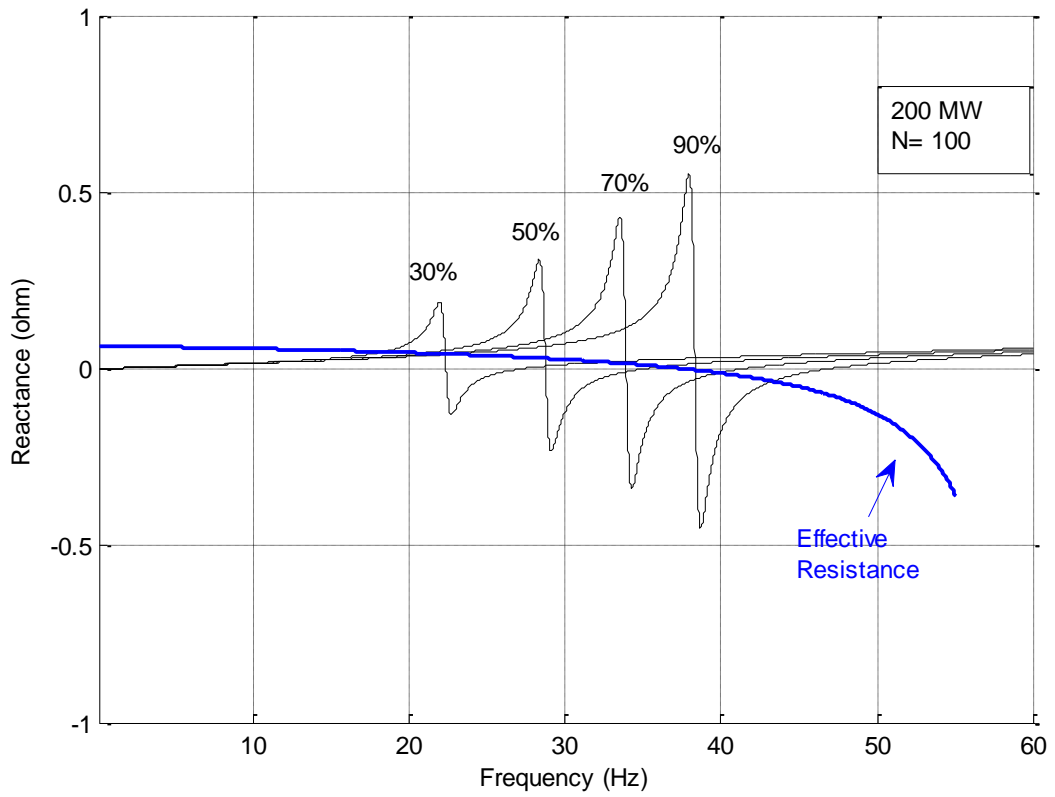
(b) 200 MW
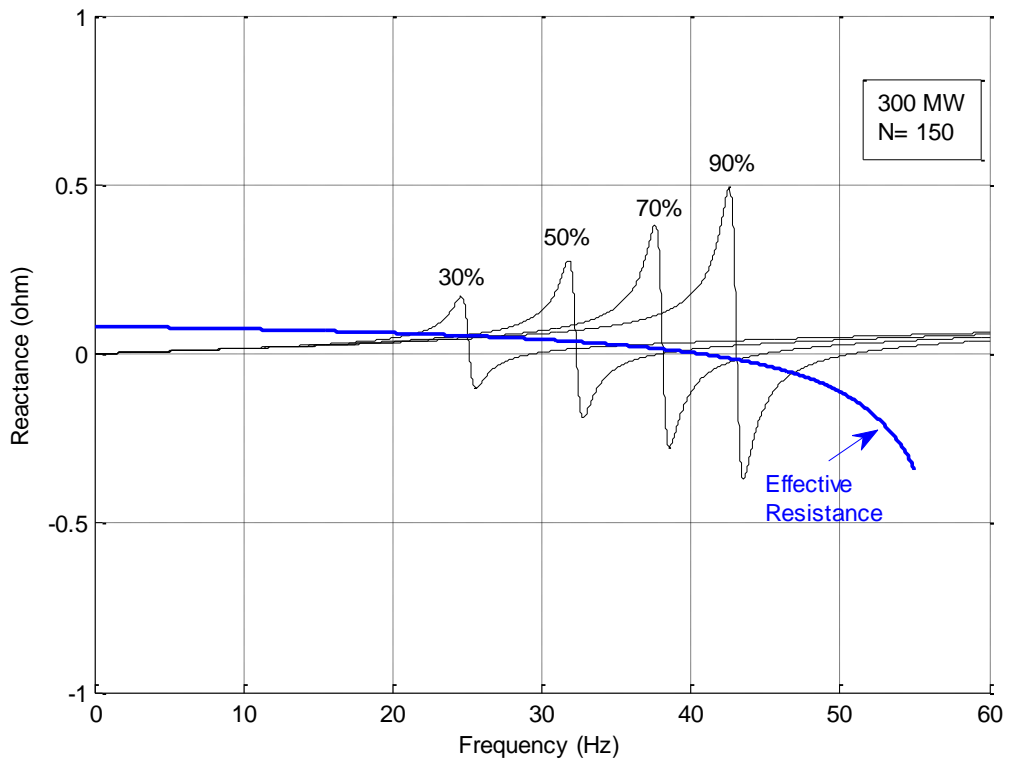
(b) 300 MW
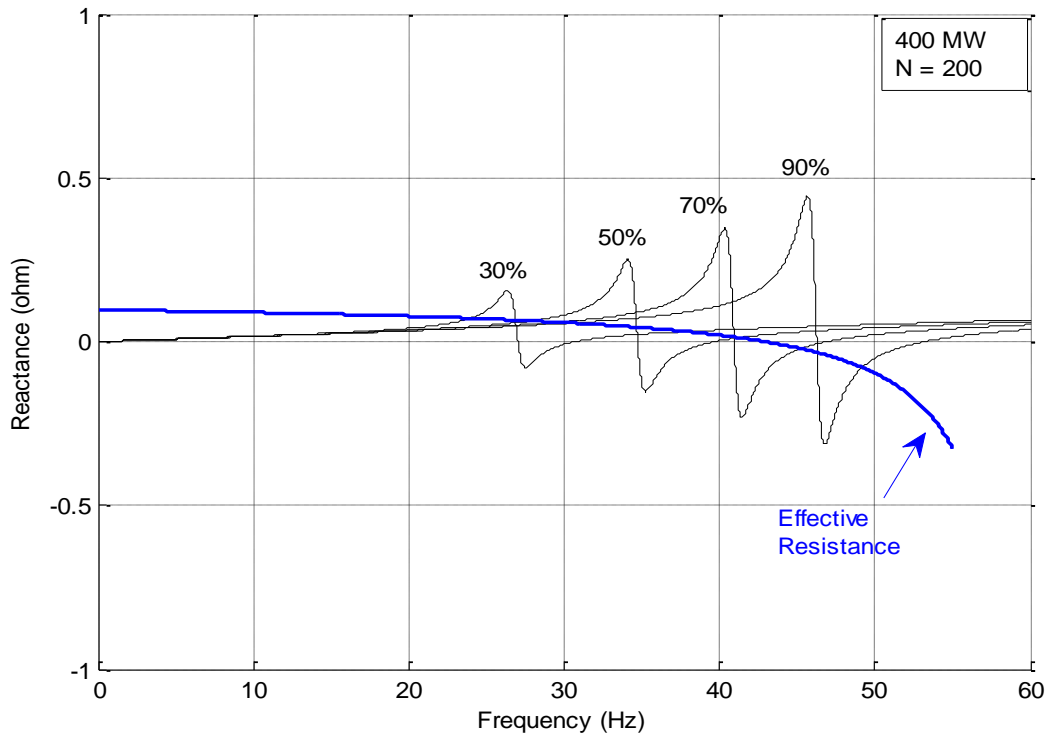
(b) 400 MW
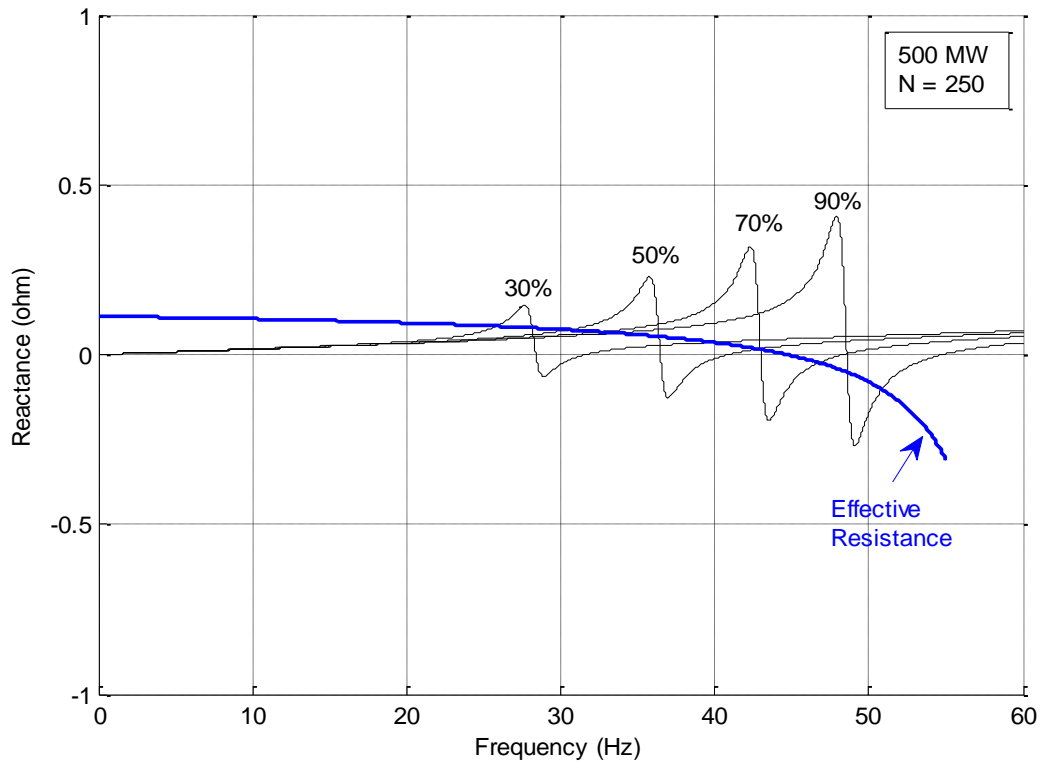
(e) 500 MW

Figure 5.12 Equivalent reactances seen from the rotor for different sizes of single-cage induction generator based wind farms connected to Study System 1

Also examining Figures 5.12(a) – (e), it is observed that frequency at zero crossing for reactance value also shifts towards right. But the shift is larger in Figures 5.12(a) – (e) compared to Figure 5.11. Therefore, smaller values of critical compensation (between 70% - 80%) are observed in case of 400 MW and 500 MW as depicted in Figures 5.12(d) and (e) in comparison to smaller wind farm sizes. The values of critical compensation levels are discussed later in section 5.4.3.

5.4.2.2 *Frequency scanning with modified IEEE First SSR Benchmark Model connected to double cage induction generator*

The frequency scanning is now performed with Study System 1 in Figure 5.7(a) considering a double-cage induction generator based wind farm. The wind farm size varies between 100 MW and 500 MW which is achieved by aggregating a suitable number of 2.3 MW double-cage induction generators.
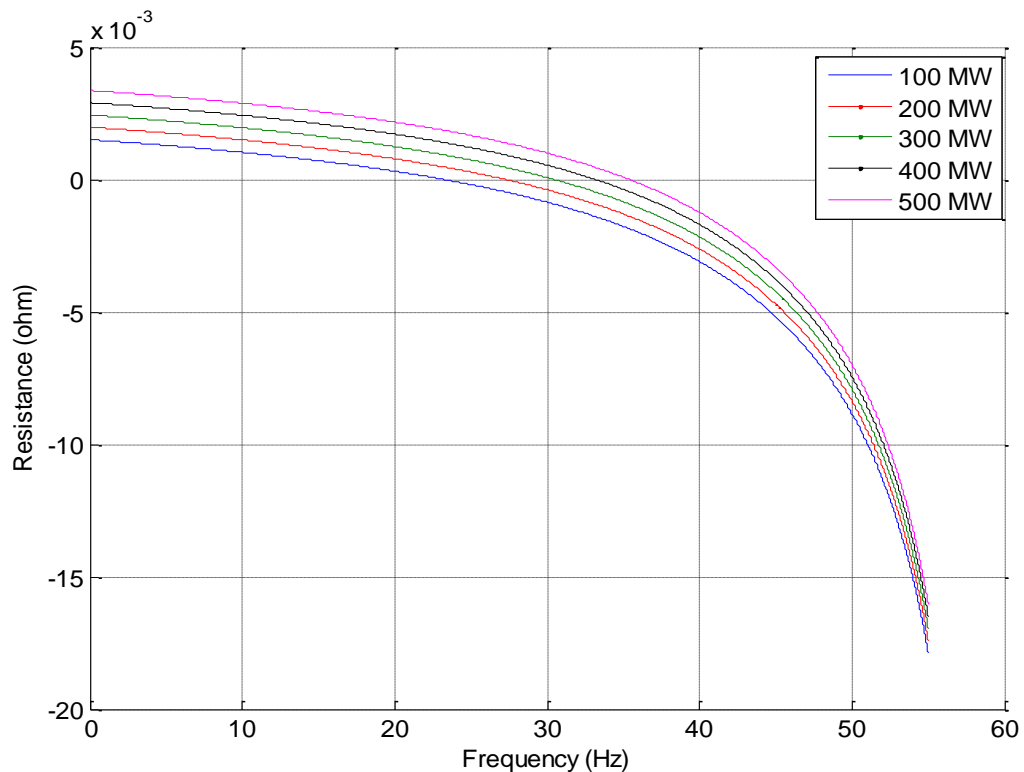
Figure 5.13 Effective resistances seen from the rotor for different sizes of double-cage induction generator based wind farms

(a) 100 MW

(b) 200 MW

(c) 300 MW

(d) 400 MW

(e) 500 MW
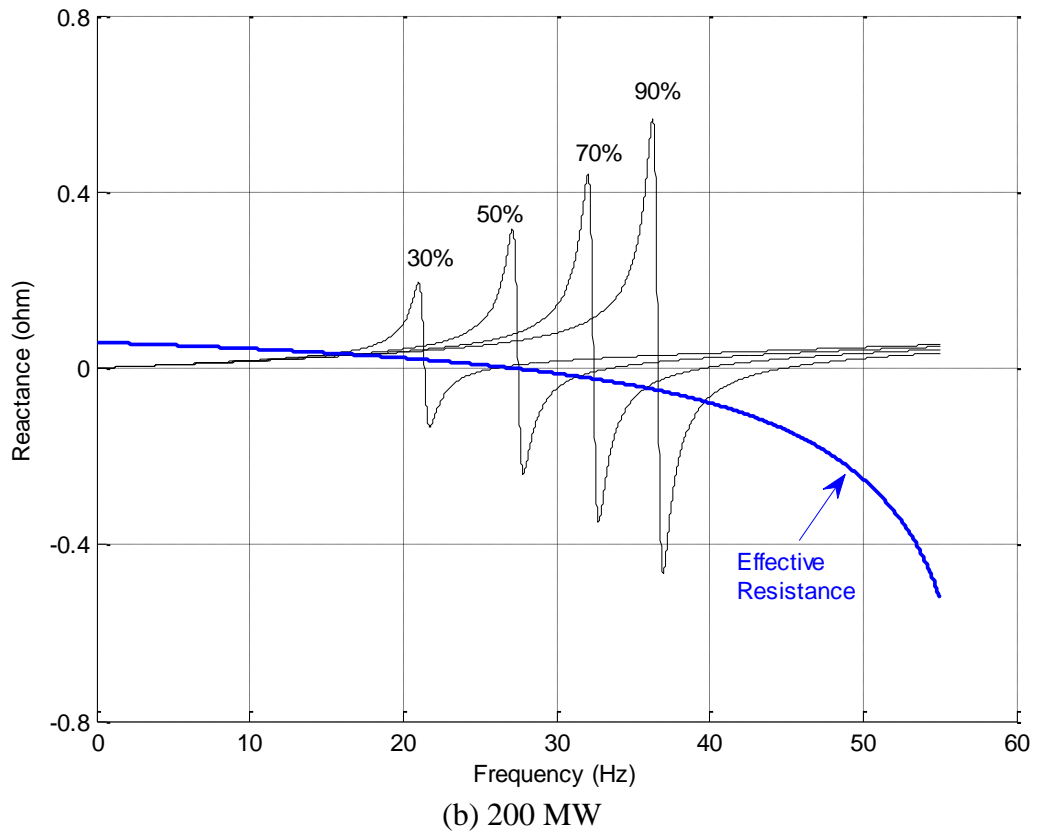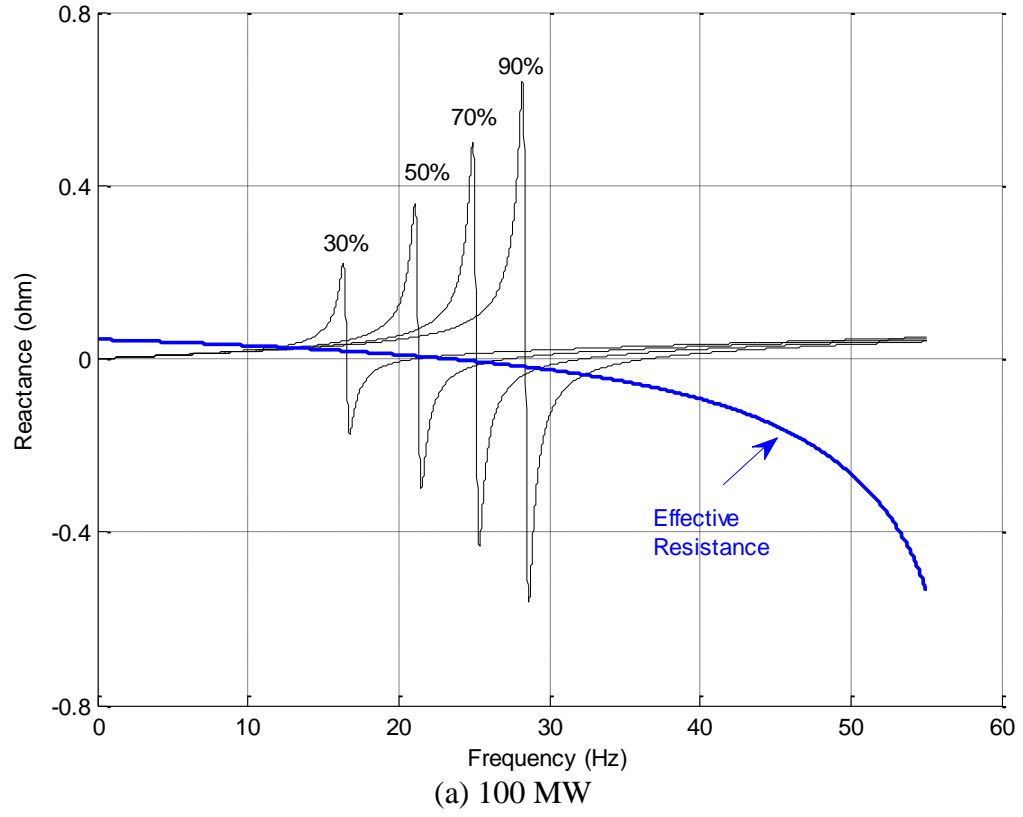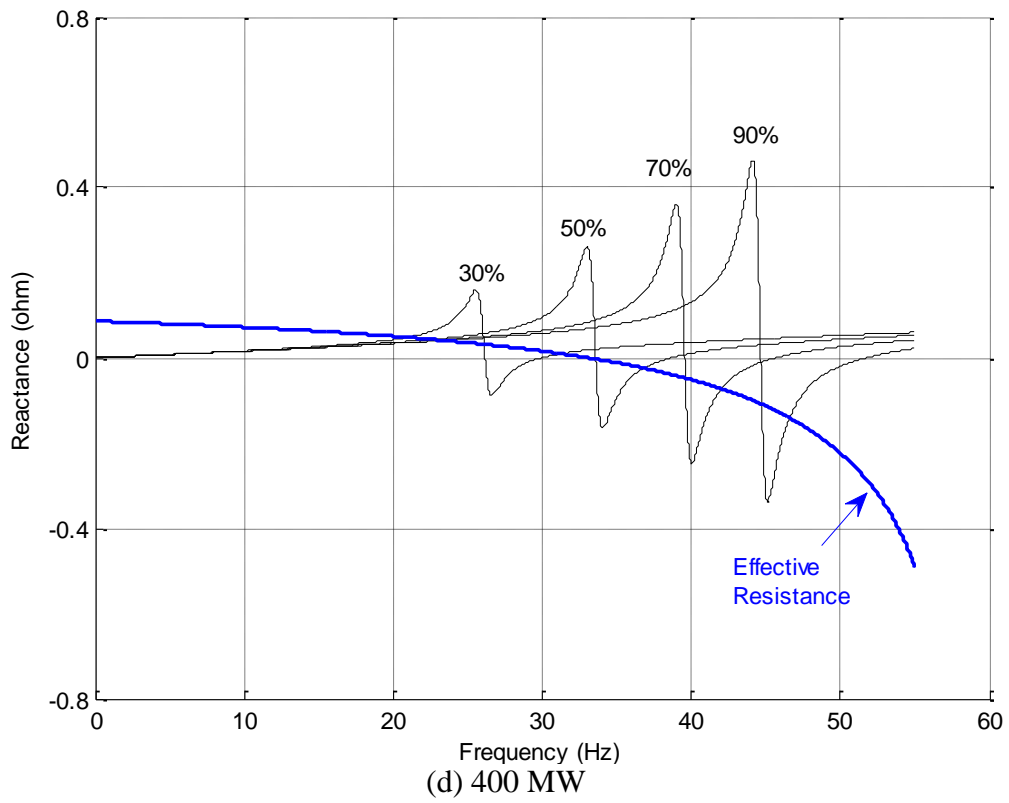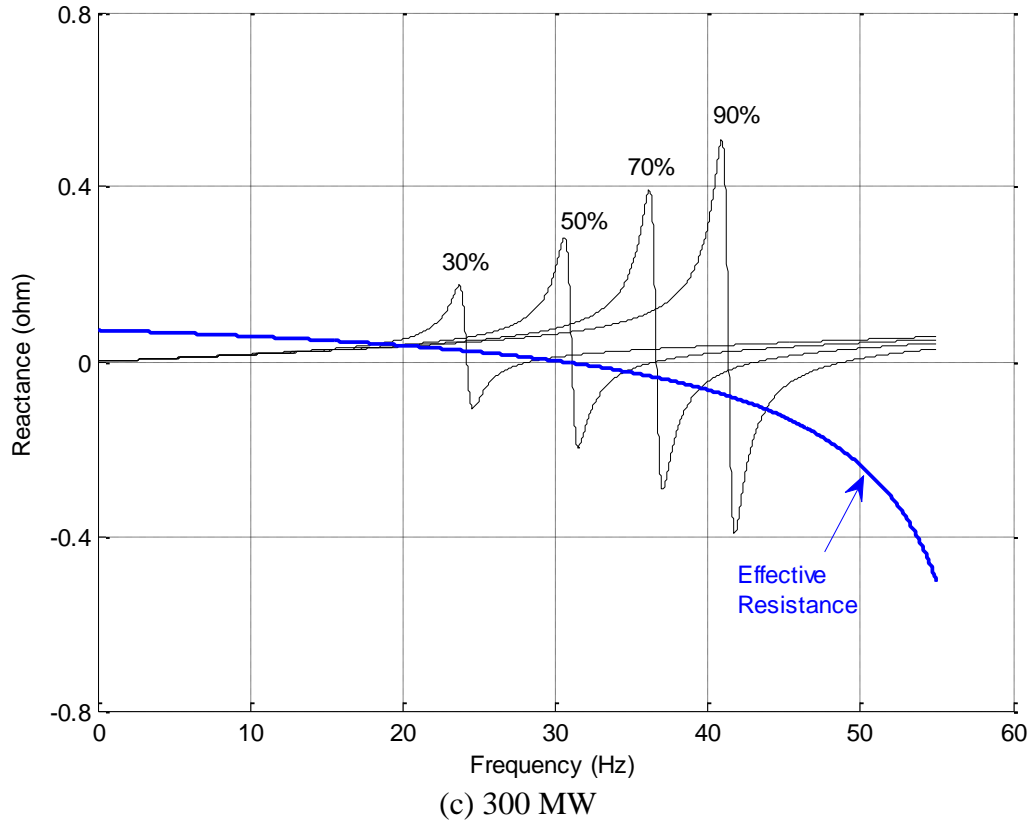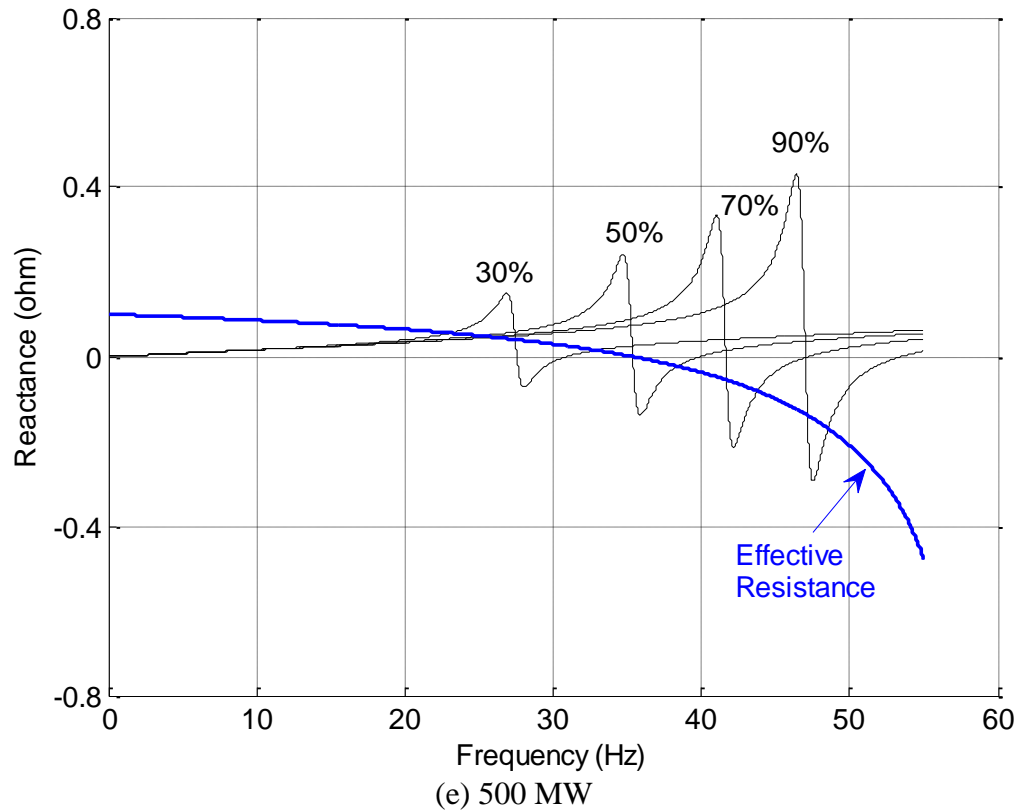
Figure 5.14 Equivalent reactances seen from the rotor for different sizes of double-cage induction generator based wind farms connected to Study System 1

Figure 5.13 shows the effective resistances from (5.1) measured behind the rotor of the equivalent induction generator model. The resistances decrease and cross the 'x' axis at certain crossover frequencies. In comparison to single-cage induction generators (Figure 5.11), in this case the zero crossing frequencies are lower.

Figure 5.14 shows the equivalent reactances obtained from the frequency scanning with different sizes of wind farm at various series compensation levels. In case of 100 MW wind farm, the effective resistance shown in Figure 5.14(a) becomes negative between 50% and 70% series compensation. Incidentally, if the effective reactance crosses zero, a potential for the induction generator self-excitation is expected. In this case, it may occur close to 60% series compensation. For a 300 MW wind farm with 50% series compensation, the effective resistance (Figure 5.14(c)) becomes negative at the zero crossing frequency of equivalent reactance. This clearly indicates the potential for induction generator effect SSR. The critical compensation may lie between 30% and 50% series compensation. Similarly, in case of 400 MW and 500 MW wind farm, with 50% series compensation the

negative resistance at zero crossing of equivalent reactance shows the prospective induction generator self-excitation as shown in Figure 5.14(d) and (e). Thus critical compensation level for these wind farms lies near 50%, which is a realistic compensation level utilized in transmission lines.

5.4.2.3 *Frequency scanning with modified IEEE Second Benchmark Model*

A similar frequency scanning study is carried out with modified IEEE Second SSR Benchmark Model and is presented in Figure 5.7(b). In this case the wind farm consists of double-cage induction generators because these are more vulnerable to SSR than single cage induction generator based wind farm, as shown in previous studies. Figure 5.15 shows the effective reactance and resistance for (a) 100 MW, (b) 300 MW and (c) 500 MW wind farms. The series compensation level is varied from 30% to 90%. As shown in Figure 5.15 the equivalent reactance never crosses zero and remains positive for all the series compensation levels considered, even though effective resistance becomes negative. Therefore, no potential for induction generator effect is anticipated in this case.

(a) 100 MW

(b) 300 MW
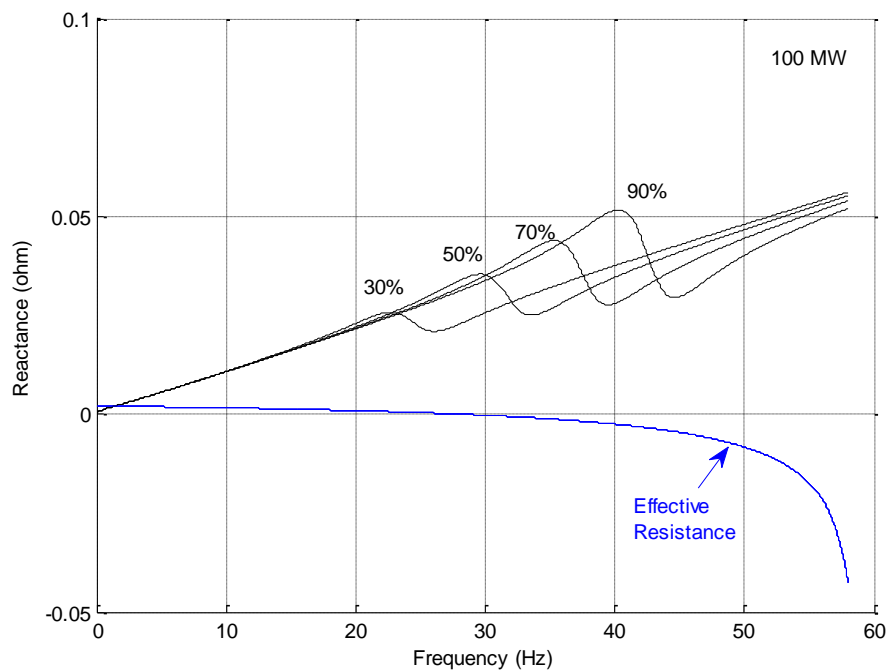
(c) 500 MW
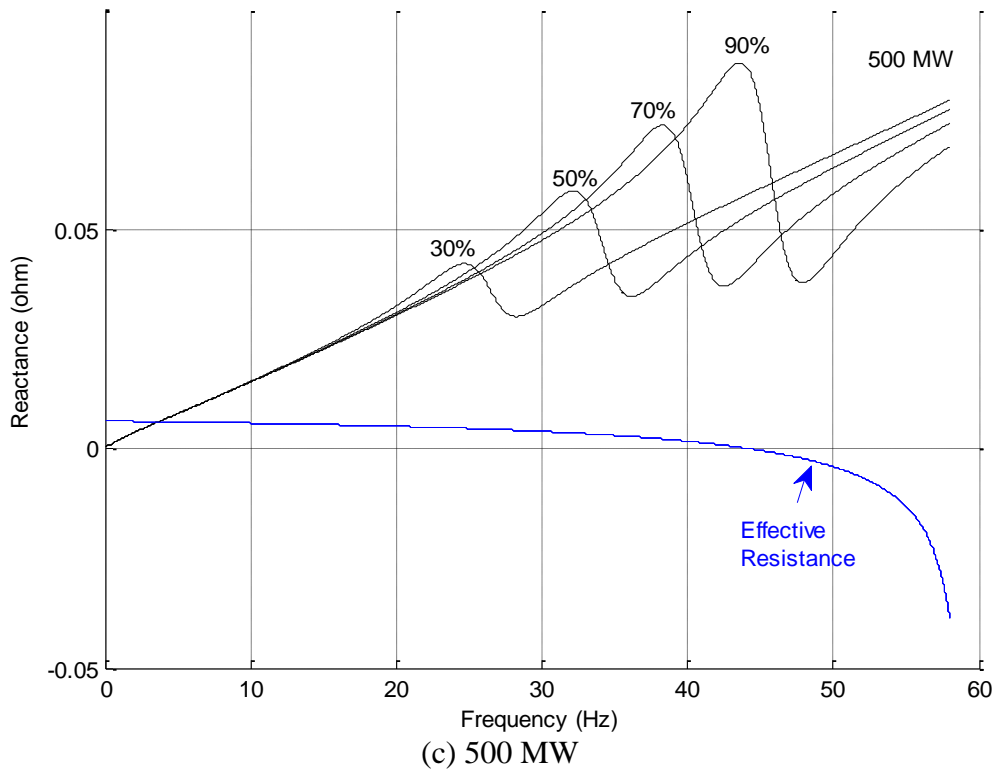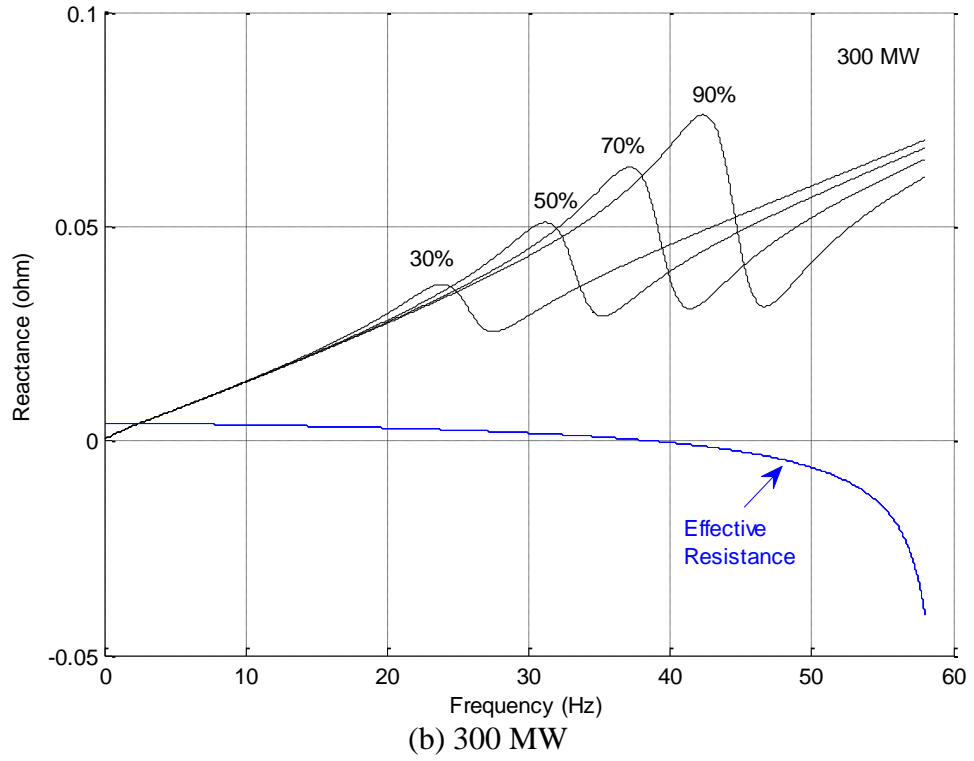
Figure 5.15 Equivalent reactances seen from the rotor for different sizes of double-cage induction generator based wind farms connected to Study System 1

5.4.3 Correlation between Frequency Scanning and Eigenvalue Analysis

In order to validate the frequency scanning study, the results obtained from frequency scanning studies are compared with the eigenvalue results reported in [26] and [54]. It is noted that the zero crossing frequency in Figure 5.12 and Figure 5.14 indicates the synchronous complementary frequency of the electrical resonant frequency. Eigen mode frequencies for 200 MW wind farm of both types connected to IEEE FBM are given in Table 5.1. It is observed that eigen frequencies coming from frequency scanning match well with the frequencies from eigenvalue analysis. Results for 200 MW single-cage IG based wind farms are plotted in Figure 5.16. The eigen mode frequencies are overlapping on one another. This validates the frequency scanning analysis. All other electrical eigen mode frequencies for different sizes of wind farms are provided in Appendix E.

Table 5.1 Electrical mode eigen frequency for single cage and double cage wind farm for different compensation levels

K (%)	200 MW Single cage wind farm		Potential for SSR	200 MW Double cage wind farm		Potential for SSR
	Frequency Scanning	Eigenvalue Calculation		Frequency Scanning	Eigenvalue Calculation	
10	47.0222	47.22	×	47.55	47.505	×
20	41.720	41.919	×	42.48	42.34	×
30	37.723	37.855	×	38.6	38.393	×
40	34.220	34.43	×	35.35	35.076	×
50	31.322	31.409	×	32.49	32.163	√
60	28.615	28.67	×	29.92	29.536	√
70	26.115	26.14	×	27.58	27.128	√
80	23.806	23.766	×	25.4	24.891	√
90	21.720	21.509	√	23.37	22.796	√

The critical series compensation levels estimated from frequency scanning studies are compared with the calculated levels from the eigenvalue analysis in Table 5.2 and Table 5.3. In [26], the critical series compensation levels for different single-cage induction generator based wind farms are given, whereas, in [54], critical compensation levels for double-cage induction generator based wind farms are reported.
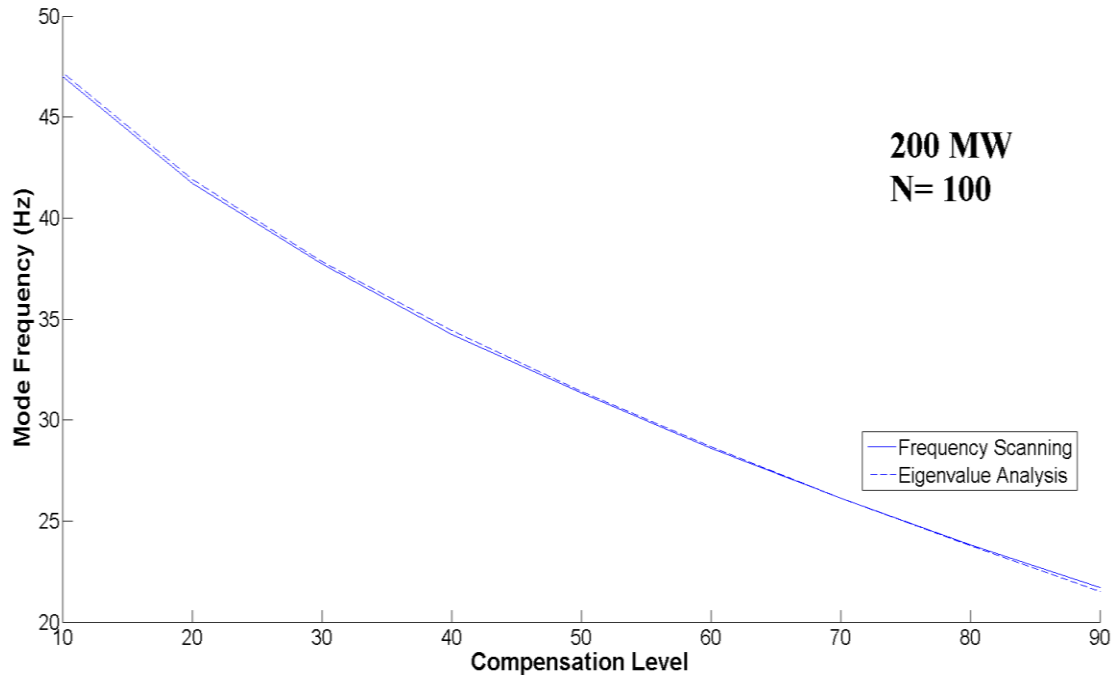
Figure 5.16 Comparison of the outcomes from eigenvalue analysis and frequency scanning analysis for 200 MW wind farm

Table 5.2 Critical series compensation level of single-cage induction generator based wind farms connected to IEEE First SSR Benchmark Model

Wind Farm size (MW)	Critical series compensation level	
	Frequency scanning	Eigenvalue analysis
100	x	x
200	87.6	88.7
300	80	82.95
400	77.3	81.15
500	76.00	80.60

Table 5.2 depicts the comparison of critical series compensation levels obtained from two different studies for single-cage induction generator based wind farm connected to IEEE First SSR Benchmark Model. Similarly, Table 5.3 shows the comparison for double-cage induction generator based wind farms connected to IEEE First SSR Benchmark Model. In the case of IEEE Second SSR Benchmark Model, both the studies show no potential for

SSR due to induction generator effect. In both tables, values of critical series compensation levels from frequency scanning are found to be close to values reported through eigenvalue analysis, thus validates the frequency scanning analysis.

Table 5.3 Critical series compensation level of double-cage induction generator based wind farms connected to IEEE First SSR Benchmark Model

Wind Farm size (MW)	Critical series compensation level	
	Frequency scanning	Eigenvalue analysis
100	59.90	56.00
200	49.27	48.25
300	48.10	48.60
400	48.85	50.5
500	50.2	52.6

5.5 SUBSYNCHRONOUS RESONANCE (SSR) ANALYSIS WITH STATCOM

Study System 2 from section 5.2.2 is considered for the SSR study with STATCOM. In Figure 5.8, a double cage induction machine based wind farm is connected with IEEE-FBM SSR model. The wind farm outputs power at 690 V that is increased to 34.5 kV for grid integration with a transformer (not shown). STATCOM is connected at 34.5 kV bus for voltage regulation. In this section, performance of STATCOM is examined for various changes in the network.

5.5.1 Impact of Series Compensation Level with Symmetrical Fault

The performance of STATCOM with 100 MW wind farm is examined for remote and close-in fault for three compensation levels of i) 40%, ii) 50% and iii) 60%. The fault impedance and STATCOM parameters are given in Appendix D.

5.5.1.1 *Remote fault at location F₂*

For remote fault studies a more severe symmetrical fault of 6 cycles is considered instead of 5 cycles [65]. The fault occurs at $t = 6.0$ sec at location F_2 in Figure 5.8. Two cases without STATCOM and with STATCOM are compared.

i) **40% compensation level**

(a) Generator speed

(b) Electromagnetic torque

(c) Shaft torque

(d) Generator terminal voltage
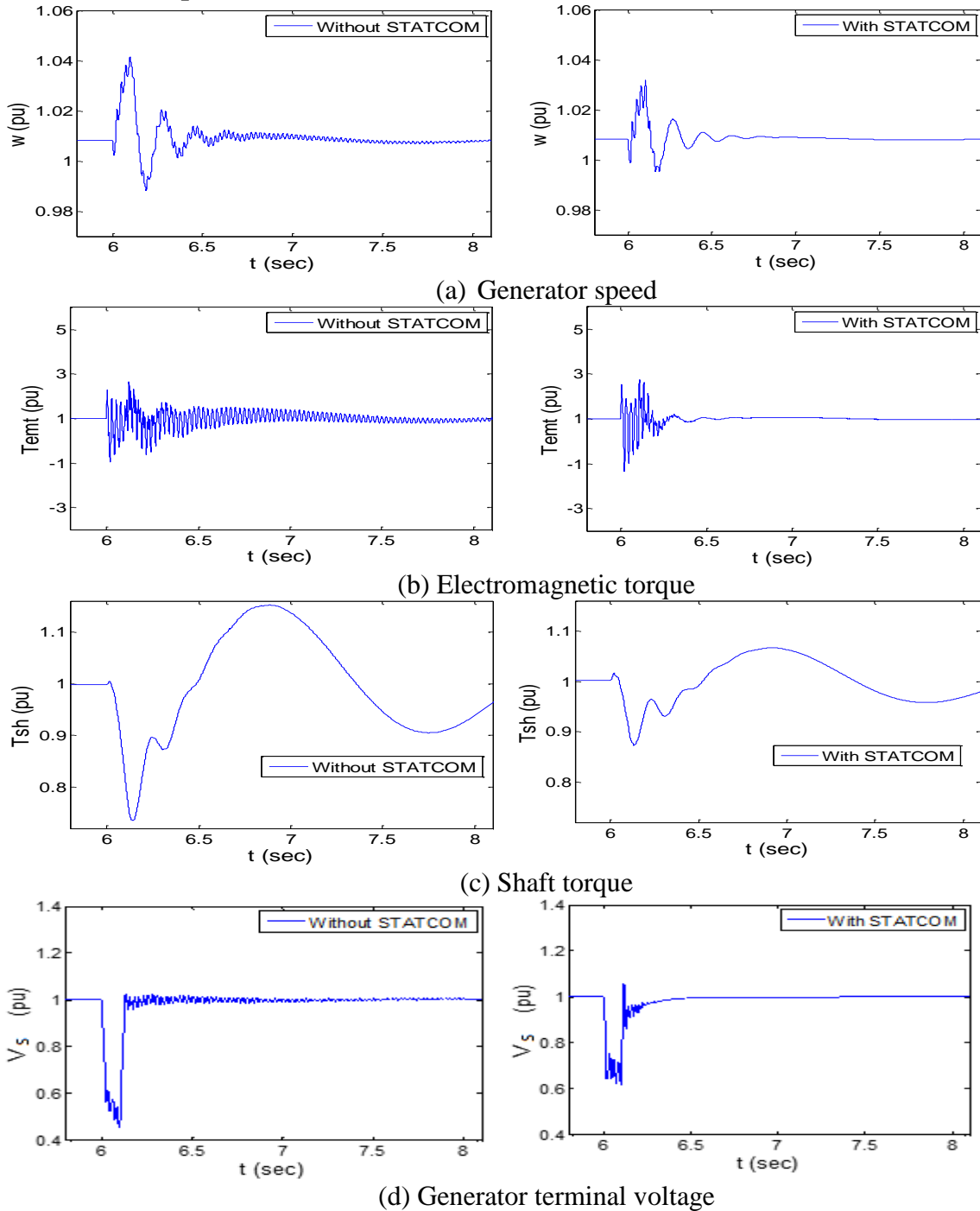
Figure 5.17 System parameters for 40% series compensated line with remote fault

Figure 5.17 presents the a) generator rotor speed w , (b) electromagnetic torque T_{emt} , (c) shaft torque T_{sh} and (d) the RMS voltage at generator terminal V_S . At the occurrence of fault, oscillations in generator speed are observed. With the STATCOM, the oscillations get reduced. The rotor oscillations of 5.5 Hz are seen in the speed.

The oscillations in electromagnetic torque and in shaft torque are also reduced significantly with STATCOM operation as illustrated in Figures 5.17(b) and (c). In Figure 5.17(d), the voltage at the wind farm terminal reduces to 0.5 pu during fault. The STATCOM manages to keep the voltage at the terminal above 0.6 pu. As fault clears, the STATCOM recovers the voltage to 1 pu with an overshoot in response.

ii)   50% compensation level

The response of system with 50% series compensation is presented in Figure 5.18. The parameters are presented in same sequence as in Figure 5.17. With higher series compensation, increased oscillations of subsynchronous frequency (38 Hz) can be seen in speed in Figure 5.18(a) as compared to Figure 5.17(a) after the fault clearance. With STATCOM, subsynchronous oscillations are absent in speed, however rotor oscillations (5.5 Hz) are still present in the speed.

In Figure 5.18(b), increased oscillations in electromagnetic torque persists in steady state as compared to response shown in Figure 5.17(b). This is due to higher series compensation level. However, it does not affect the shaft torque as shown in Figure 5.17(c) and Figure 5.18(c). The oscillation in electromagnetic torque are absent with STATCOM operation in Figure 5.18(b). The STATCOM also reduces the magnitude of shaft torque oscillations significantly. Figure 5.18(d) presents the improvement in generator terminal voltage oscillations during fault and in steady state.

(a) Generator speed

(b) Electromagnetic torque

(c) Shaft torque

(d) Generator terminal voltage
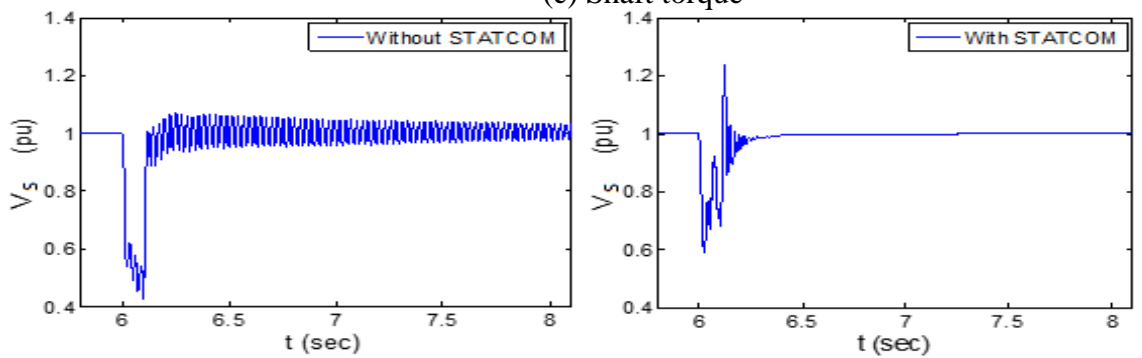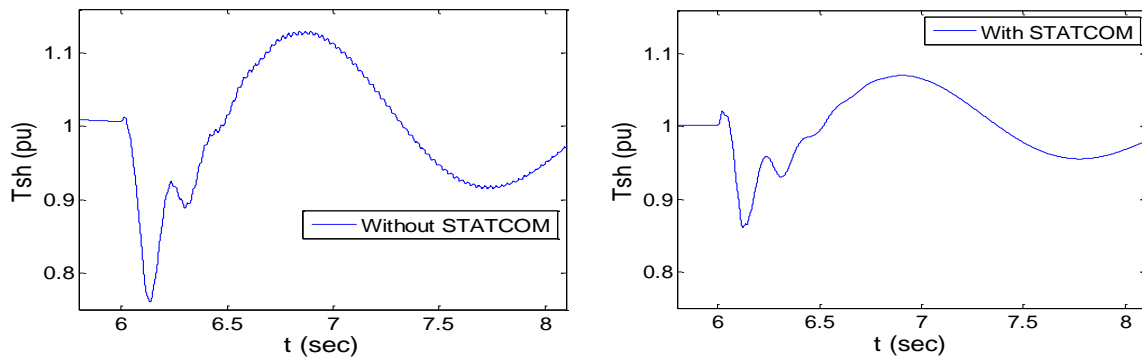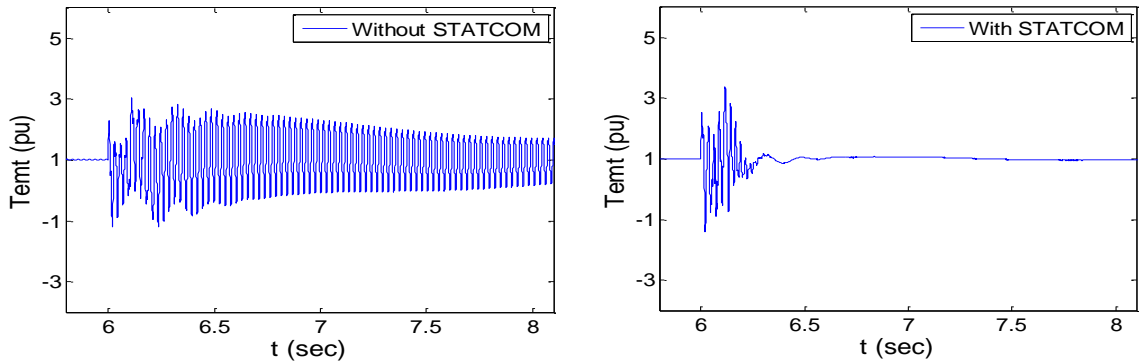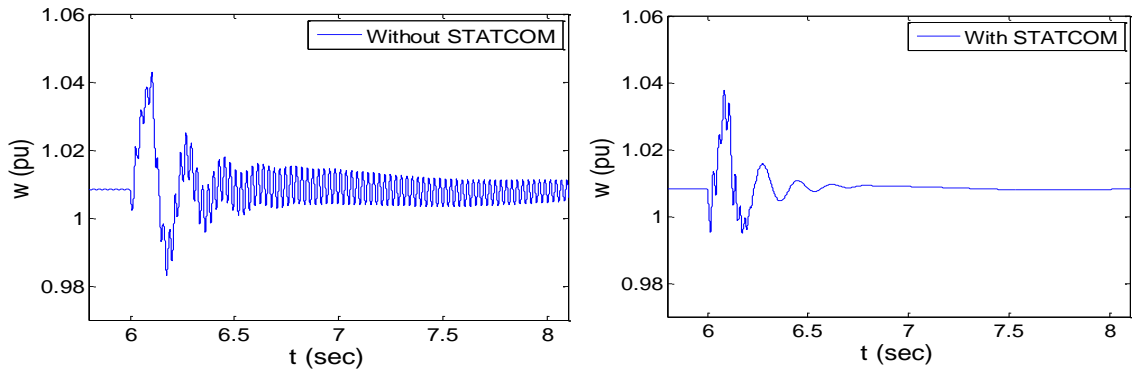
Figure 5.18 System parameters for 50% series compensated line with remote fault

iii) **60% compensation level**
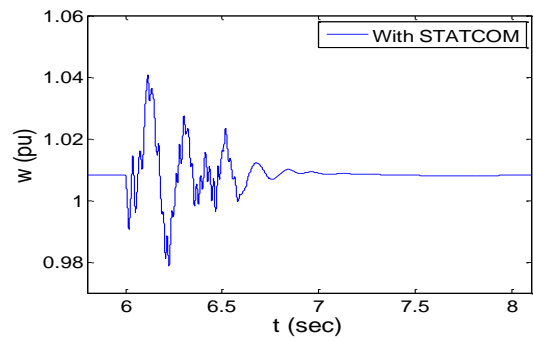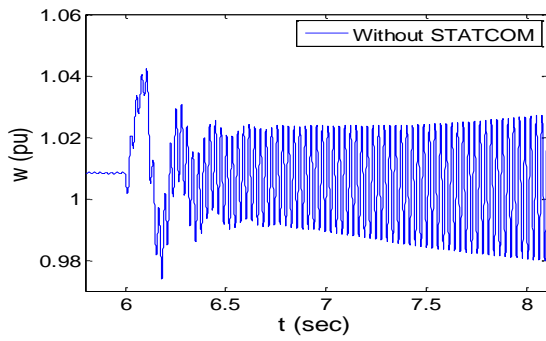
(a) Generator speed
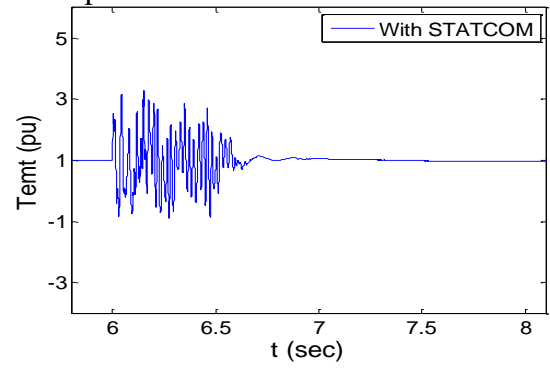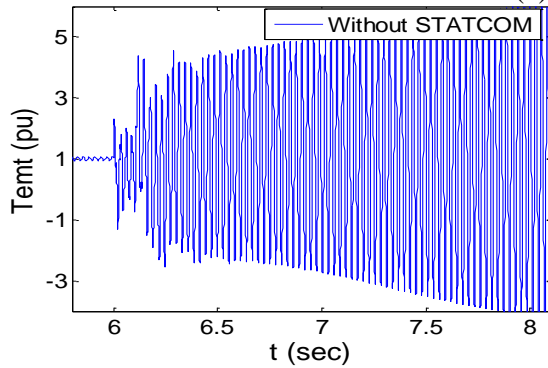
(b) Electromagnetic torque
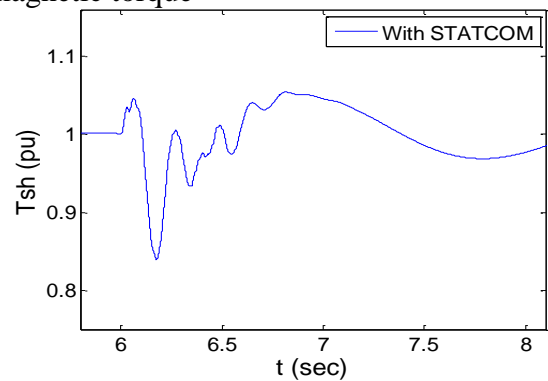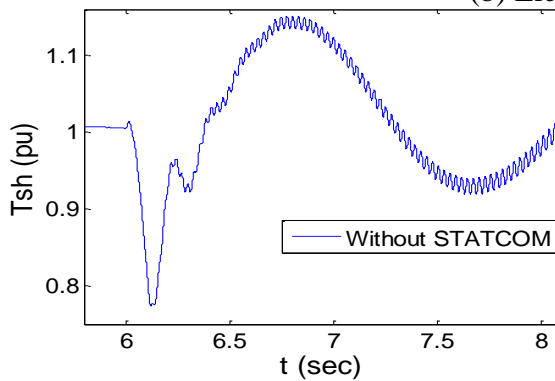
(c) Shaft torque
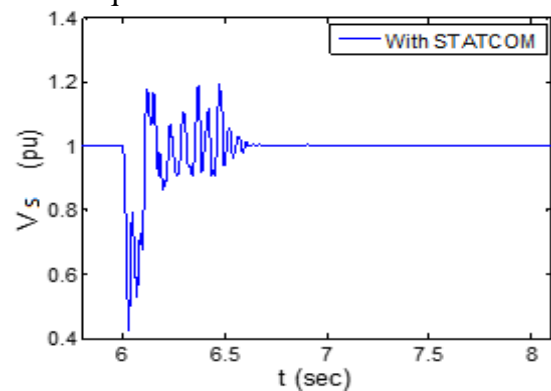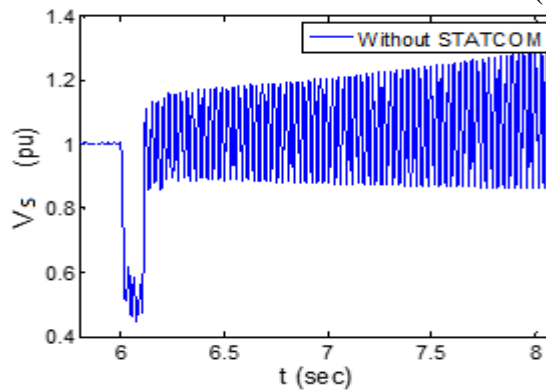
(d) Generator terminal voltage

Figure 5.19 System parameters for 60% series compensated line with remote fault

The series compensation level is increased to 60% in this case. The response of the system is presented in Figure 5.19. As given in Table 5.3 for 100 MW, this level is above the critical series compensation level. Therefore, growing sub-synchronous oscillations (SSO) in speed are present in Figure 5.19(a). With STATCOM, these oscillations die out and generator rotates with a stable speed in steady state. A similar phenomenon is seen in Figure 5.19(b) in the electromagnetic torque. The self-sustained oscillations are not present with STATCOM. The STATCOM hence successfully mitigates the SSR in wind farm during transient state. The shaft torque contains sub-synchronous oscillations due to higher compensation level in addition to oscillations due to fault in Figure 5.19(c). These SSOs are growing in steady state and may damage the shaft if not mitigated. With STATCOM, these oscillations diminish in steady state. In addition, lower frequency oscillations (0.57 Hz) in shaft torque are reduced significantly. In Figure 5.19(d), growing RMS voltage is observed in steady state after the fault due to SSR caused by induction generator effect. The STATCOM effectively regulates the voltage to 1 pu.

5.5.1.2   *Close-in fault at location F$_1$*

The same study (section 5.5.1.1) is carried out with close-in fault of 6 cycles to examine the performance of STATCOM to mitigate SSR. Fault occurs at $t = 6.0$ sec at location F$_1$ in Figure 5.8 and clears at $t = 6.1$ sec. Two cases without STATCOM and with STATCOM are compared.

i)   **40% compensation level**

Figure 5.20 presents the (a) generator speed and (b) shaft torque with 40% compensation level. The wind farm recovers its speed after close-in fault and no SSR is seen in Figure 5.20(a). Low magnitude oscillations in speed *w* occur after fault clearance and get diminished with STATCOM. In Figure 5.20(b), during close-in fault shaft torque goes as low as 0.4 pu compared to 0.7 pu with remote fault in Figure 5.17(c). Also as the fault gets cleared, shaft torque reaches 1.4 pu. This could be dangerous to the turbine shaft system. With STATCOM, the magnitude of these oscillations can be reduced as shown in Figure 5.20(b).

(a) Generator speed

(b) Shaft torque
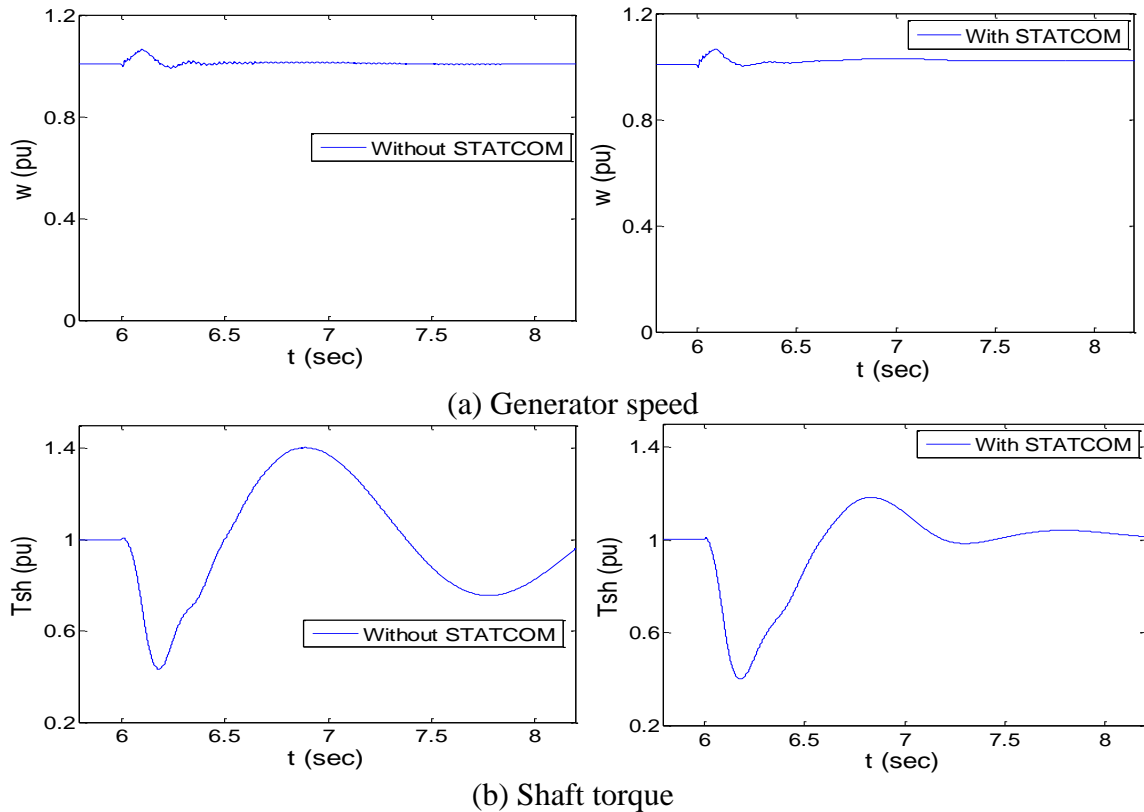
Figure 5.20 System parameters for 40% series compensated line with close-in fault

ii)   **50% compensation level**

System parameters with 50% series compensation level are illustrated in Figure 5.21 which presents (a) the generator rotor speed, (b) electromagnetic torque T_{emt} , (c) shaft torque T_{sh} and (d) generator terminal voltage. Compared to Figure 5.20(a), in this case as the fault clears, the speed goes down and finally stalls the machine as shown in Figure 5.21(a). With STATCOM wind generator continues to operate at a stable speed although with slight rotor mode oscillations.

Figure 5.21(b) depicts higher oscillations in electromagnetic torque compared to the remote fault case. The STATCOM reduces the intensity of the oscillations in T_{emt} and keeps its steady state value to 1 pu. More severe oscillations in shaft torque are observed in Figure 5.21(c) compared to Figure 5.20(b). It oscillates with an amplitude of 20 pu that is dangerous enough to break the shaft. With STATCOM, the severity of the oscillations is reduced, however T_{sh} still goes to 1.5 pu as fault gets cleared. In Figure 5.21(d), with the STATCOM the voltage profile at the generator bus gets much better.

(a) Generator speed

(b) Electromagnetic torque

(c) Shaft torque

(d) Generator terminal voltage
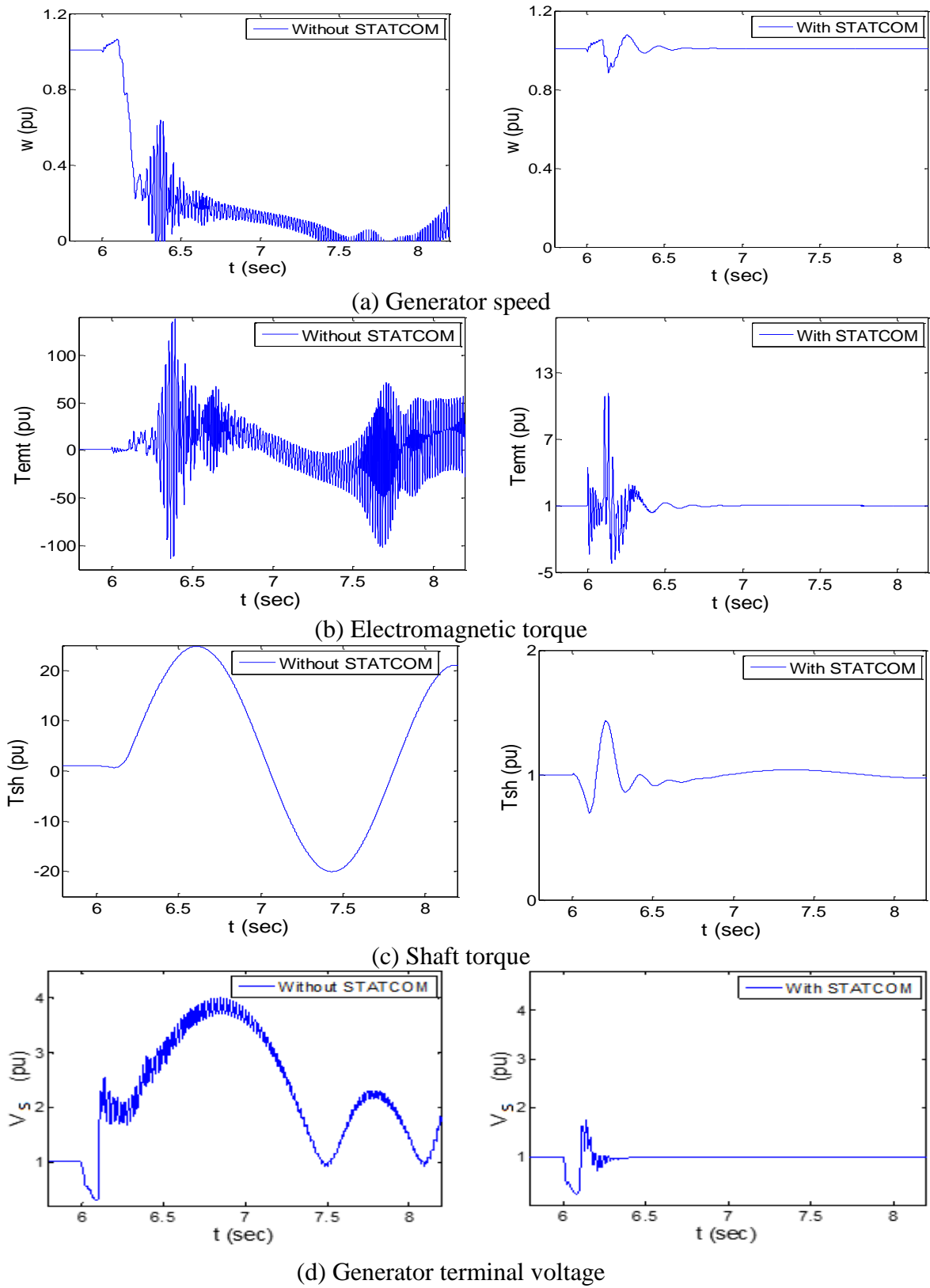
Figure 5.21 System parameters for 50% series compensated line with close-in fault

iii) 60% compensation level

With 60% compensation level, the system parameters with and without STATCOM are presented in Figure 5.22 in the same sequence as in Figure 5.21.

(a) Generator speed

(b) Electromagnetic torque

(c) Shaft torque

(d) Generator terminal voltage
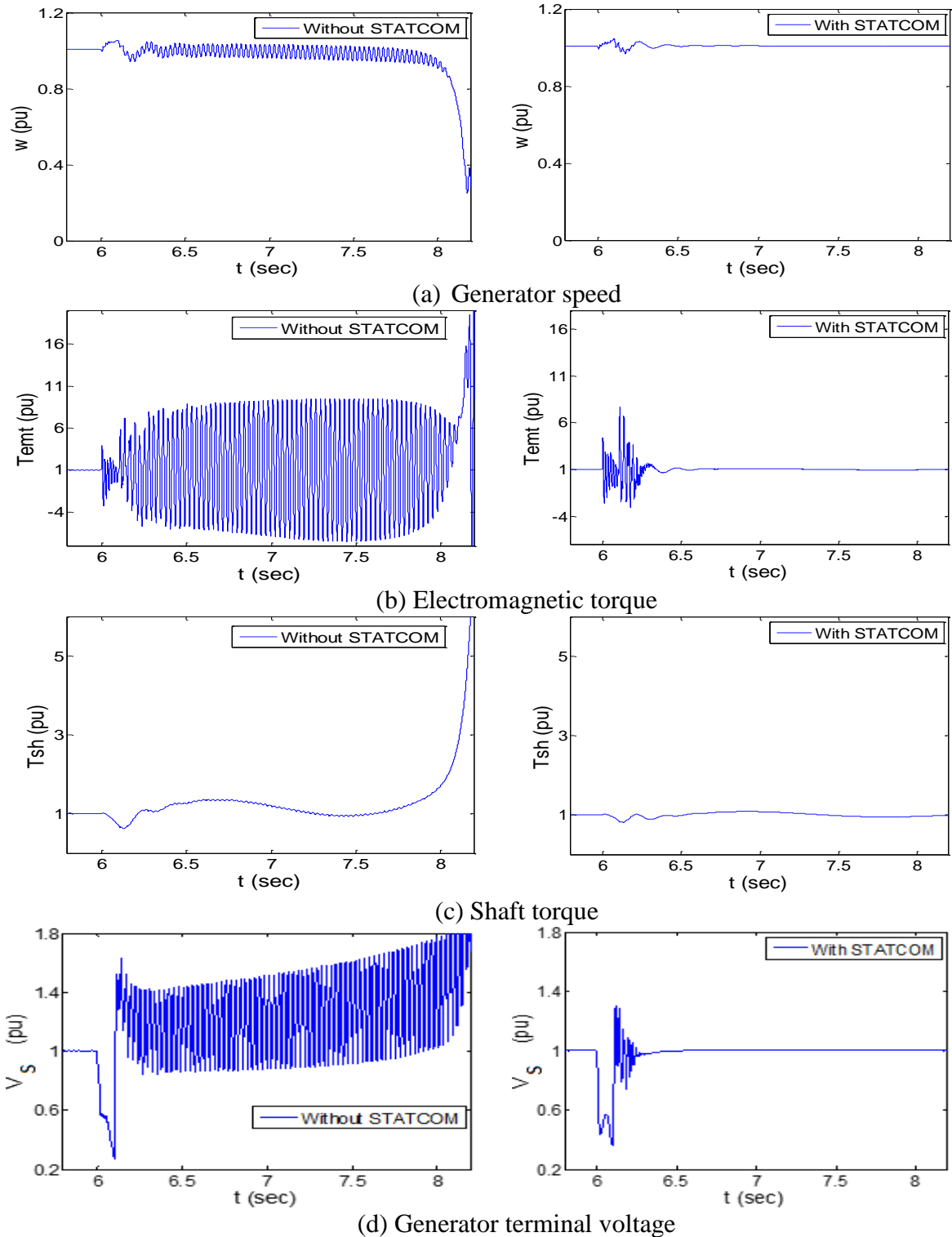
Figure 5.22 System parameters for 60% series compensated line with close-in fault

The generator speed in this case demonstrates subsynchronous oscillations initially. At $t =$ 8.0 sec, the speed starts declining and generator finally stalls as shown in Figure 5.22(a). With STATCOM, the speed remains 1 pu in steady state. The transient oscillations are small in this case compared to STATCOM operation presented in Figure 5.21(a) because in this case the machine does not stall instantly as the fault clears. Oscillations in torques in Figure 5.22(b) and (c) are lesser in magnitude compared to response presented in Figure 5.21. STATCOM limits the shaft torque to close to 1 pu after the fault and no serious damage to shaft is expected in this case. The voltage V_S at the terminal rises after fault gets cleared at $t = 6.2$ sec. The STATCOM is able to regulate the voltage to 1 pu. However, in transient state, the voltage reaches 1.3 pu and proper protection mechanism needs to be considered if utility does not allow such a high transient voltage.

5.5.2 Impact of Constant Step Change in Series Compensation Level

The series compensation level is increased by 10% at different series compensation levels and its effect on the speed of turbine is investigated. The Study System 2 given in Figure 5.8 is considered and no fault is considered in this study. Figure 5.23 presents the speed of generator for (a) 20%, (b) 30%, (c) 40% and (d) 50% compensated line. It is observed that as initial compensation level increases the oscillations in steady state grow stronger in response to 10% step change.

Self-sustained oscillations are seen in Figure 5.23(d). This is the case of SSR as compensation level exceeds the critical compensation as specified in Table 5.3. This case is then investigated with STATCOM and is presented in Figure 5.23(e). With STATCOM no SSR is observed when compensation level is changed from 50% to 60%. The oscillation of 5.5 Hz in speed is rotor mode oscillation [1].
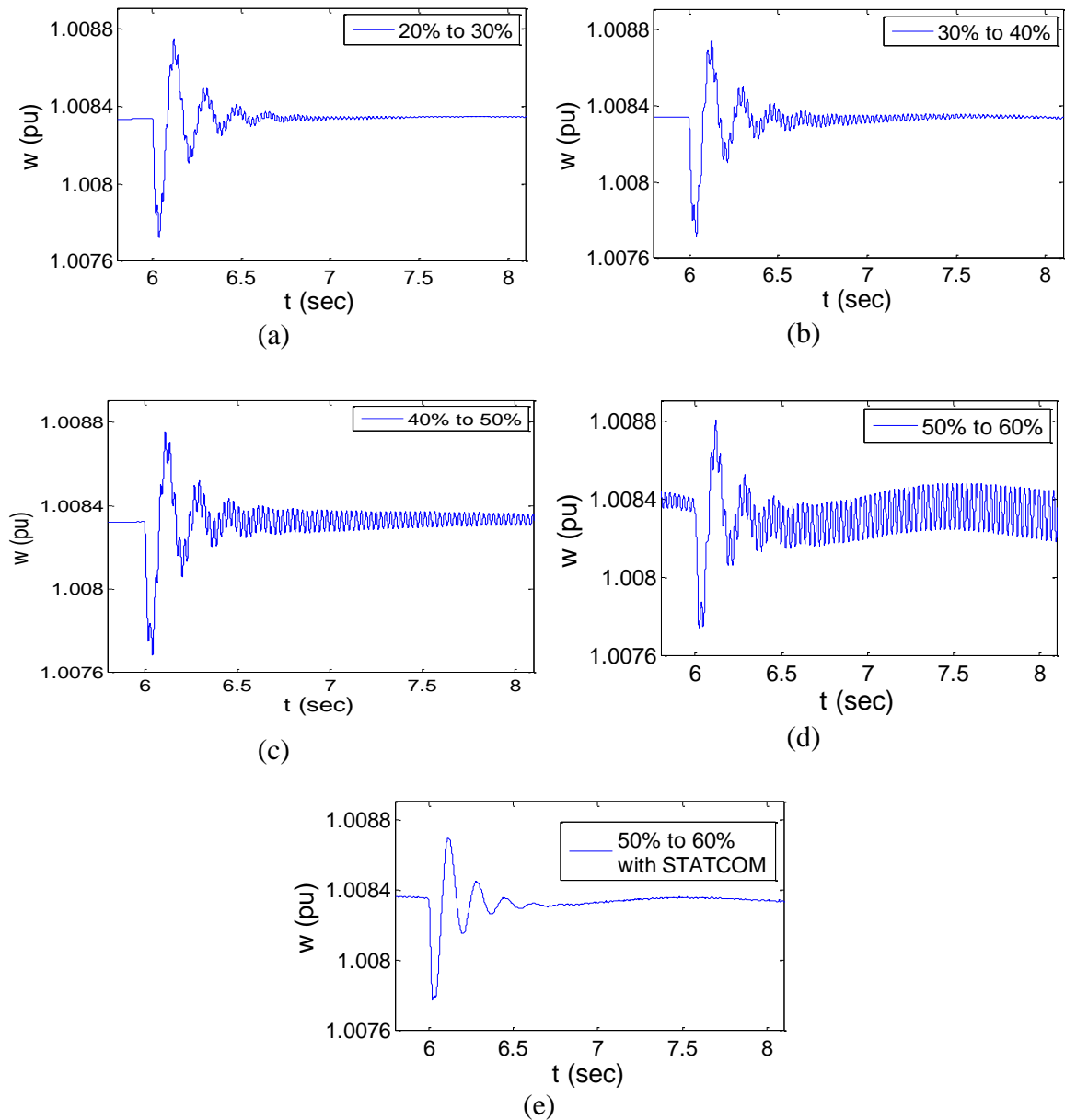
Figure 5.23 Speed of generator for different compensation level with a 10% step change
in series compensation

5.5.3 Impact of Variable Step Change in Series Compensation Level

The response of wind farm for increasing step change in compensation level is investigated in this section. The resulting compensation value is kept to be 55%, which is below the critical compensation limit. Figure 5.24 presents generator speed for (a) 20% , (b) 30% and

c) 40 % step increase in compensation. It is observed that as step size increases the magnitude of oscillations in steady state also increases. However, no SSR condition is reached in any case as compensation level is below 56% (Table 5.3).
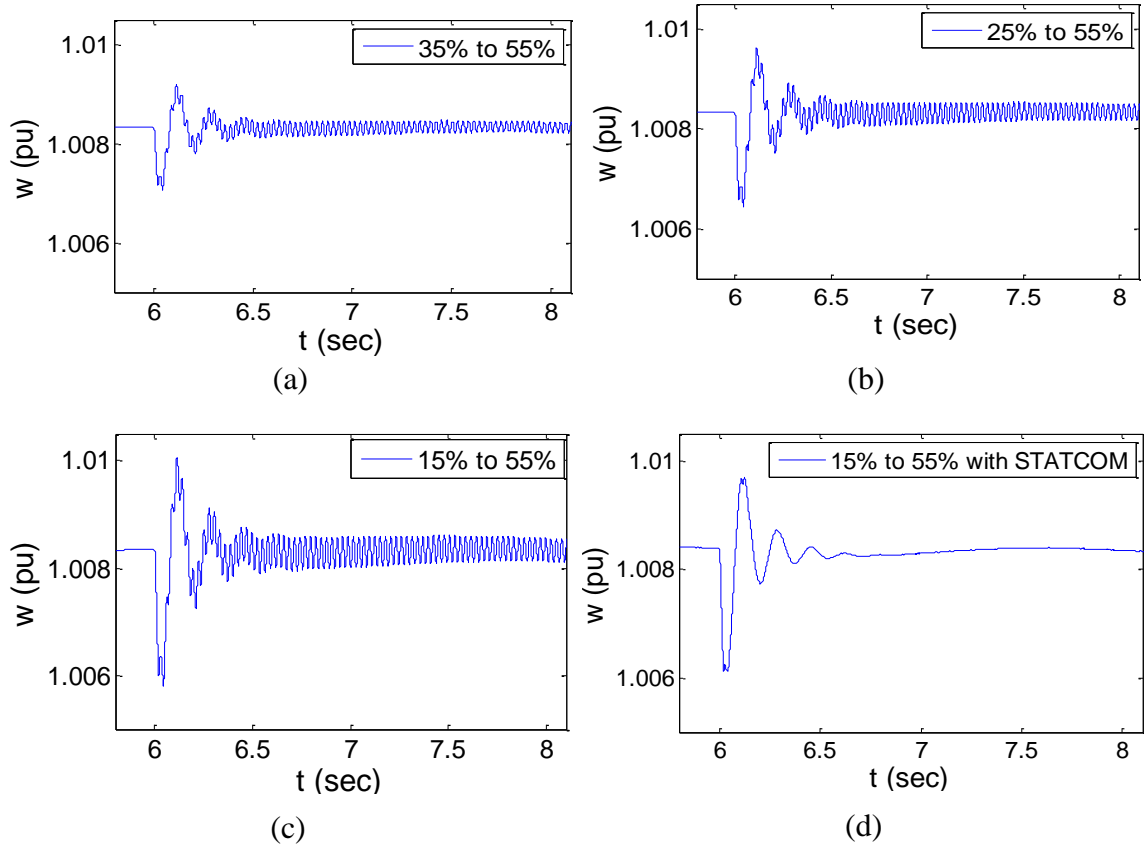
Figure 5.24 Speed of generator for different compensation level with a 10% step change in series compensation

The effect of STATCOM is investigated with 40% increase in compensation level (15% to 55%), because it has higher oscillations than other cases. The result is presented in Figure 5.24(d). The STATCOM successfully removes the subsynchronous frequency oscillations, although rotor oscillations can be seen in response.

5.5.4   Impact of Fault Duration

In this section, the impact of fault duration on wind farm and STATCOM operation is investigated. A 100 MW wind farm connected to 50% series compensated line is considered. Close-in fault occurs at $t = 6.0$ sec. Behavior of wind farm for different number

of cycles of fault duration is presented in Figure 5.25(a) - (d). With 4 cycles fault, oscillations in speed are seen to subside in steady state (Figure 5.25(a)). Whereas with 5 and 6 cycles fault, a decline in speed is observed after the fault gets cleared and finally machine stalls (Figure 5.25(b) and (c)). But with 7 cycles fault, the same behavior is not seen. Instead the generator speed increases initially but recovers to 1 pu after some damped oscillations. This phenomenon requires further investigation. The response with STATCOM for a 7 cycles fault is given in Figure 5.25(e). Subsynchronous frequency oscillations are found absent as STATCOM removes the SSO.

(a)

(b)

(c)

(d)

(e)
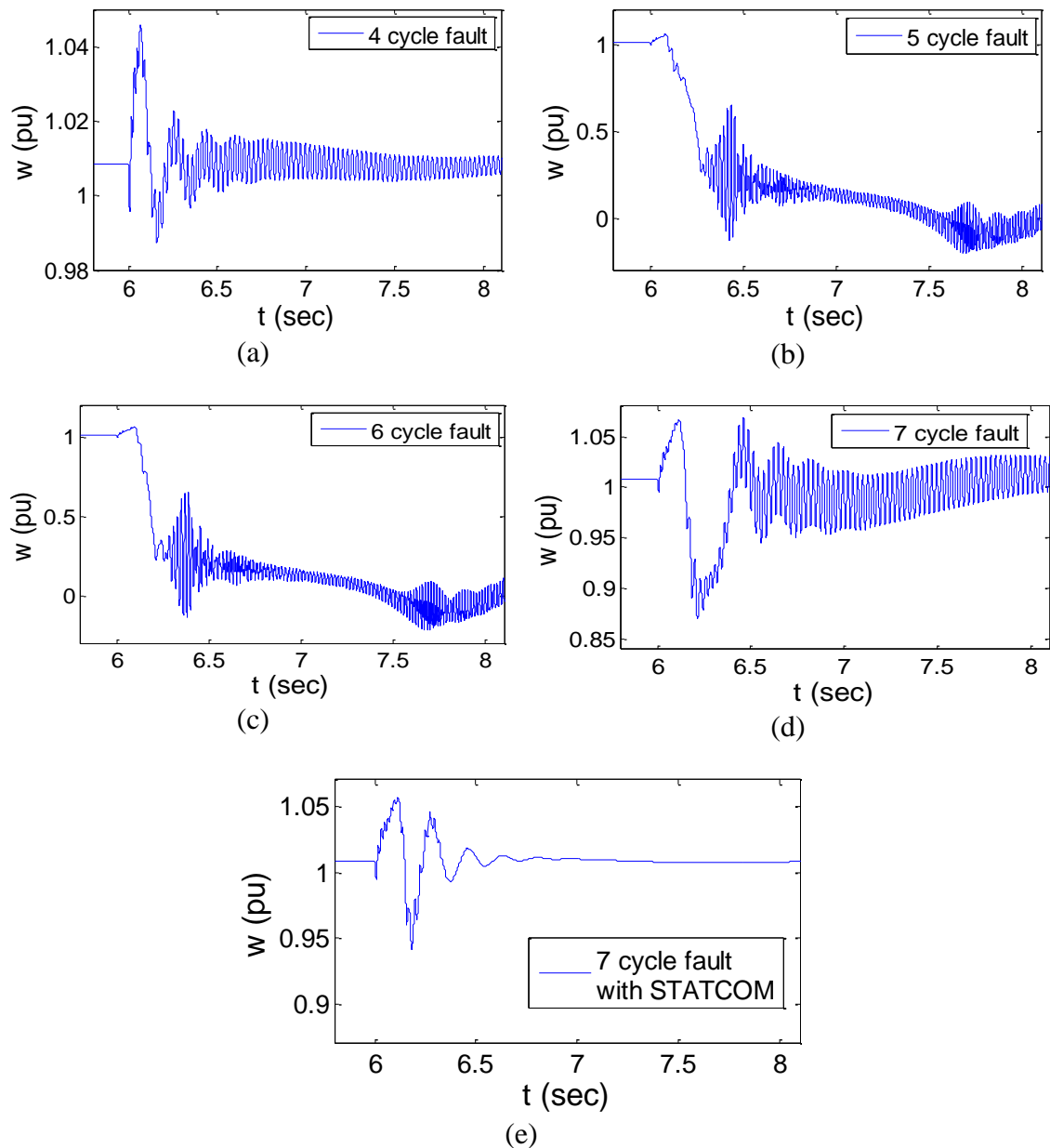
Figure 5.25 Speed of generator for different fault duration

5.5.5 Impact of Size of Wind Farm

The response of wind farm with and without STATCOM is analyzed for different sizes of wind farms in this section. Compensation level is taken as 50% in all cases. A remote fault of 6 cycles at location F_2 in Figure 5.8 is considered for three sizes of wind farms: i) 100 MW, ii) 200 MW and iii) 300 MW. Fault occurs at $t = 6$ sec and gets cleared at $t = 6.1$ sec.

i)   100 MW

Figure 5.26 is presented before in Section 5.5.1, however for ease of comparison it is again presented here. Figure 5.26 depicts (a) generator speed w and (b) generator terminal voltage V_S for 100 MW wind farm. Subsynchronous frequency component is observed in speed after fault. However, it does not create SSR. With STATCOM, these oscillations are found absent in the speed. Generator terminal voltage during fault goes to 0.4 pu as shown in Figure 5.26. With STATCOM, terminal voltage does not go below 0.6 pu and oscillations after fault also disappears.

(a) Generator speed

(b) Generator terminal voltage
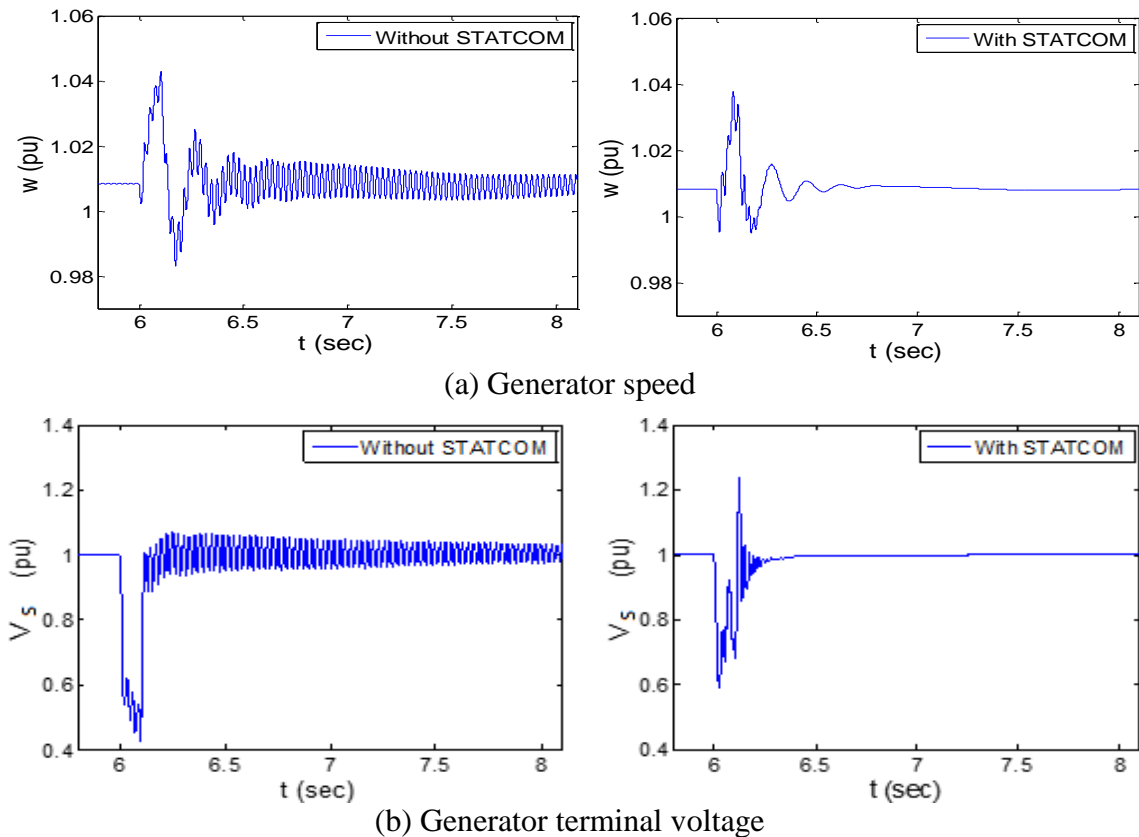
Figure 5.26 Generator speed and terminal voltage for 100 MW wind farm with and without STATCOM

ii)   200 MW

Figure 5.27(a) presents generator speed *w* and Figure 5.27(b) depicts generator terminal voltage V_S for 200 MW wind farm. Since 50% compensation is above critical compensation limit (Table 5.3), SSR is seen in the speed and voltage without STATCOM. SSR is mitigated with STATCOM. Also STATCOM successfully keeps voltage above 0.7 pu during fault as shown in Figure 5.27(b). Therefore, larger size of wind farms may operate without causing SSR in the network if STATCOM is installed at the wind farm terminals.

(a)

(b)
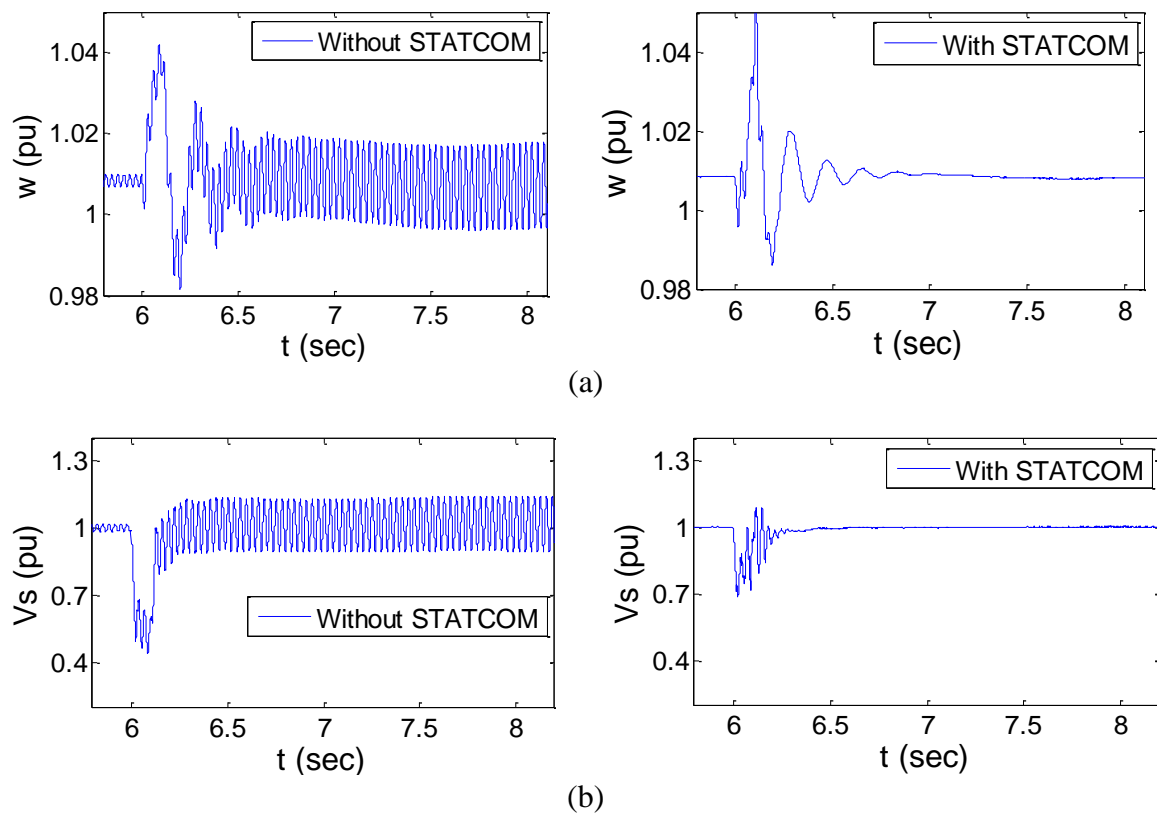
Figure 5.27 (a) Generator speed and (b) terminal voltage for 200 MW wind farm with and without STATCOM

iii)   300 MW

Figure 5.28 illustrates (a) generator speed and (b) generator terminal voltage for 300 MW wind farm. Comparing to Figure 5.27(a) and Figure 5.28(a), it is seen that the rotor mode oscillations are not affected by wind farm size. But, the sub-synchronous frequency (38

Hz) component grows as wind farm size increases. With 200 MW and 300 MW wind farm, this results in SSR in the network. STATCOM is shown to mitigate the SSR in speed in all cases (Figures 5.27 and Figures 5.28). Although, the voltage **Vs** in Figure 5.28(b) does not depict SSO, it reaches 1.3 pu after fault gets cleared and this may potentially become dangerous to the network. Therefore, with STATCOM even though SSR does not happen, proper protection mechanism are advised if large sized wind farms are connected radially with series compensated line.

(a)

(b)
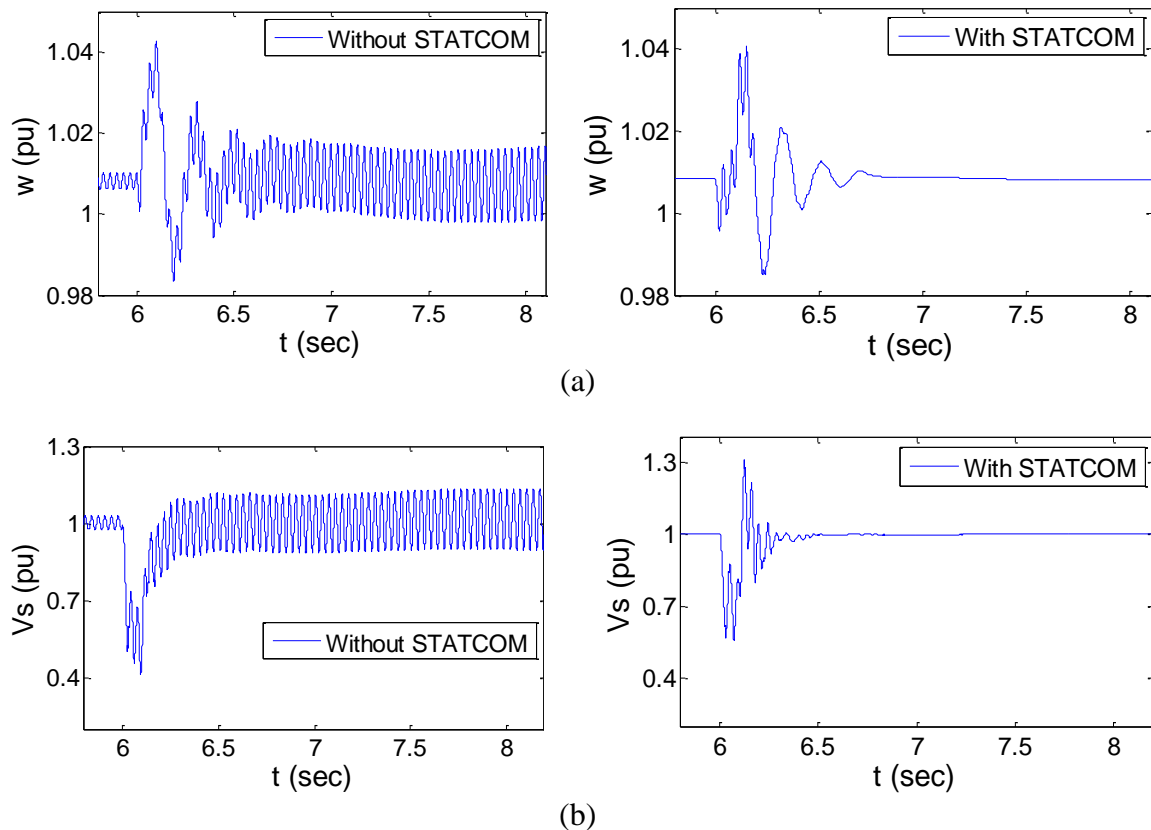
Figure 5.28 (a) Generator speed and (b) terminal voltage for 300 MW wind farm with and without STATCOM

5.5.6 Performance of STATCOM Controller with Unsymmetrical Fault

In case of symmetrical faults, only positive sequence controller works as there is no asymmetry in the network. Hence to assess the performance of negative sequence voltage regulator an asymmetric fault at location F_1 in Figure 5.8 is created for five cycles at $t =$

5.0 sec. A 100 MW wind farm connected with 50% series compensated line is considered. Figure 5.29 presents (a) generator speed and (b) the RMS voltage at the generator terminal when STATCOM is not present. Subsynchronous oscillations in speed can be seen, though these oscillations do not cause SSR and die out eventually. Voltage at the generator terminal goes up to 1.18 pu and in steady state oscillates up to 1.1 pu as shown in Figure 5.29(b).

(a)   (b)
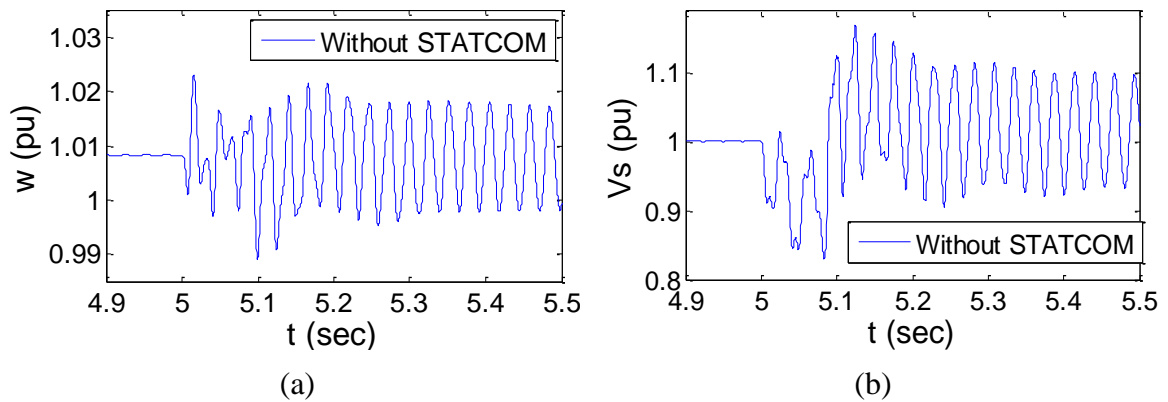
Figure 5.29 (a) Generator speed and (b) RMS voltage at terminal in case of asymmetric fault without STATCOM

The response of the network with STATCOM operation is presented in Figure 5.30. Only positive sequence controller is activated to regulate the RMS voltage **Vs** at the wind farm terminal. Figure 5.30 presents (a) turbine speed, (b) the RMS voltage at the generator, (c) and (d) *d*-axis and *q*-axis parts of negative sequence voltage at STATCOM terminal respectively and e) the reactive power output from STATCOM.

By comparing Figure 5.29(a) and Figure 5.30(a), STATCOM successfully mitigates the oscillations in speed. The voltage at the wind farm terminal also settles down to 1 pu in steady state. Lower oscillations are observed in Figure 5.30(b) during transient state compared to Figure 5.29(b). Negative sequence voltage is observed during the asymmetrical fault, which disappears after fault clearance. To support the voltage **Vs** during fault, STATCOM supplies about 80 MVAr reactive power as shown in Figure 5.30(e). Post fault oscillations are observed in reactive power to regulate the voltage at the wind farm terminal.
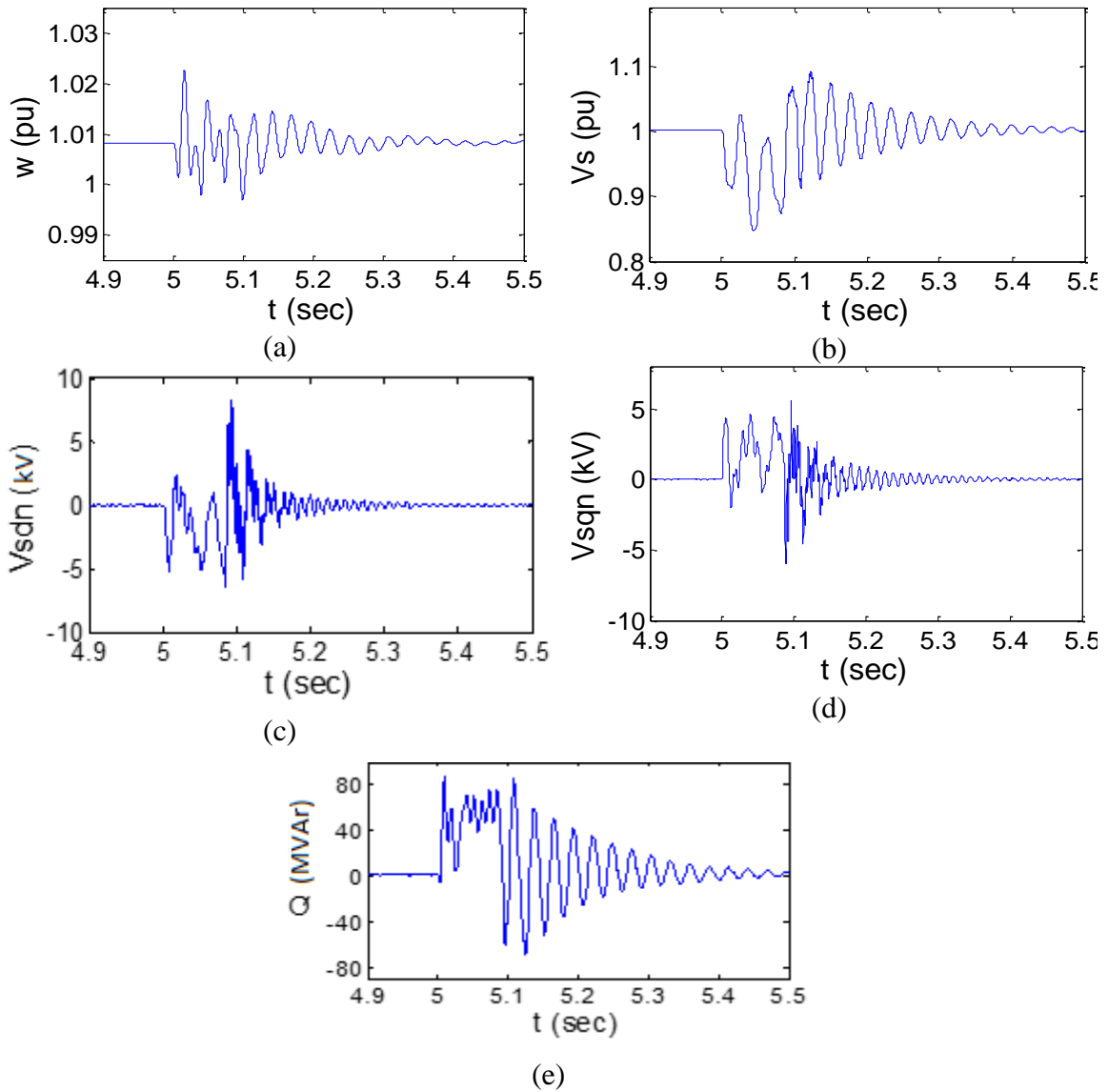
Figure 5.30 a) Generator speed and b) RMS voltage at terminal (c) *d*-axis and (d) *q*-axis parts of negative sequence voltage at STATCOM e) STATCOM reactive power output without negative sequence voltage controller in case of asymmetric fault

Figure 5.31 presents the network response with complete STATCOM controller which has both positive and negative sequence voltage regulator and is discussed in section 2.4.4. The response is presented in same sequence as in Figure 5.30 for sake of comparison. Speed and the RMS voltage in Figure 5.31 are observed as similar to Figure 5.30 during fault. Post fault oscillations are also unaffected as there is no asymmetry present and improvement is only contributed by positive sequence voltage regulator. Similar effect can be seen in reactive power output in Figure 5.31(e). Negative sequence voltages (V_{sdn} and V_{sqn}) reduces in Figure 5.31(c) and (d) compared to Figure 5.30 during fault ($t = 5.0$ sec

to 5.1 sec). Hence, because of negative sequence voltage controller, negative sequence voltage reduces appreciably.

(a)

(b)

(c)

(d)

(e)
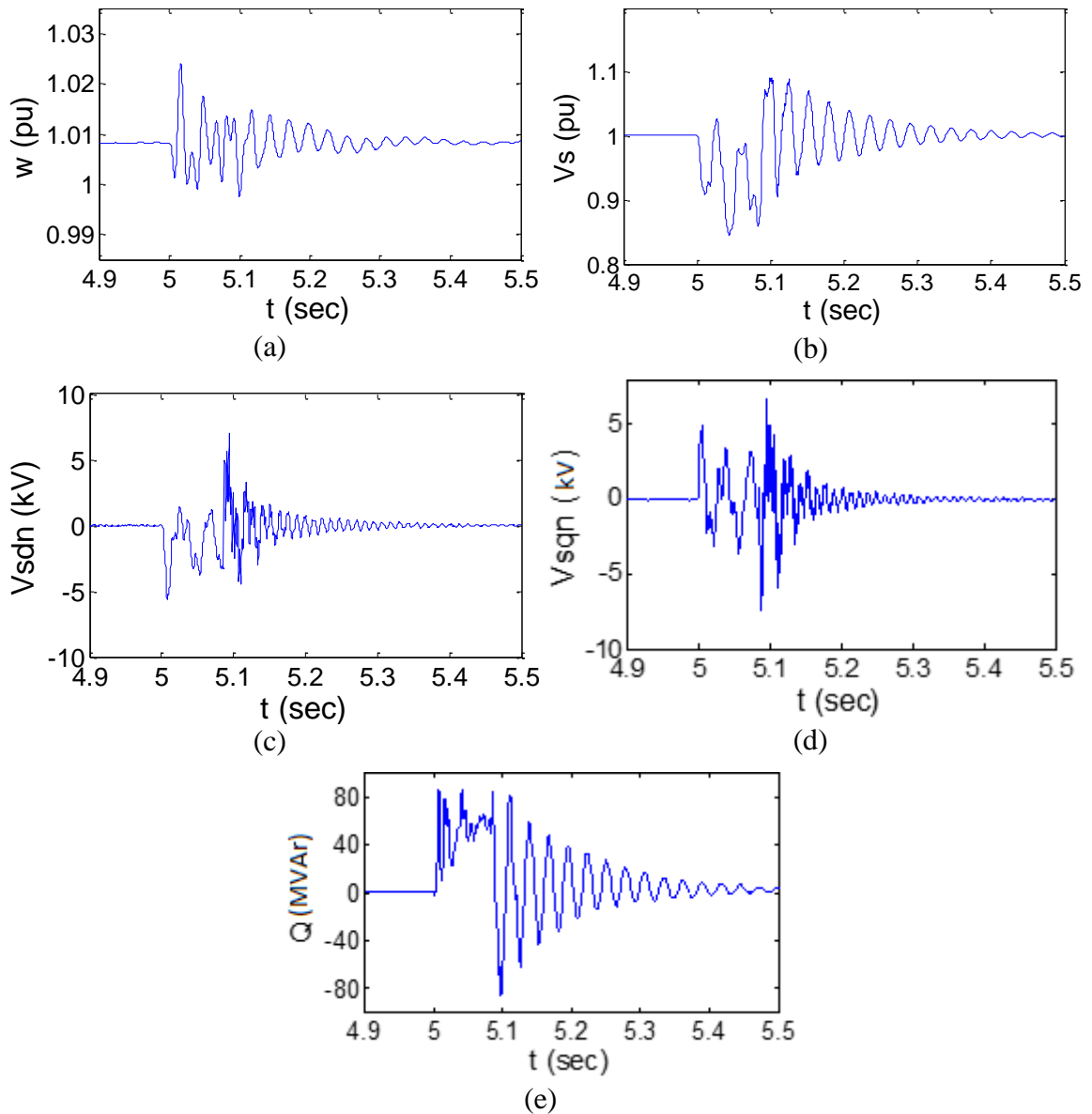
Figure 5.31 (a) Generator speed and (b) RMS voltage at terminal (c) *d*-axis and (d) *q*-axis parameters of negative sequence voltage at STATCOM e) STATCOM reactive power with positive and negative sequence controller in case of asymmetric fault

5.6   DISCUSSION

Not much improvement is seen in the negative sequence voltages (V_{sdn} and V_{sqn}) in section 5.5.6 with the complete STATCOM controller. This is because a less intense fault is simulated which already results in more than rated power output (60 MVAr) from STATCOM. To present a significant change in negative sequence voltage a more intense fault needs to be simulated that requires more power from STATCOM. Also during fault, rotor oscillations are present that may hinder the performance of controller. Therefore, a power system stabilizer also needs to be augmented at the wind farm terminal to regulate the rotor mode oscillations. A coordinated control of STATCOM with complete system should be achieved to get preferred network response for asymmetrical faults.

5.7   CONCLUSION

Sub-synchronous problem and its mitigation with the developed STATCOM controller in a series compensated transmission network is studied in this chapter. Frequency scanning technique to identify the SSR in self-excited induction generator based wind farms is explained and further validated with published results obtained with eigenvalue analysis. Both IEEE First SSR Benchmark Model and Second SSR Benchmark Model are considered and no SSR is found in wind farms connected to IEEE Second SSR Benchmark Model in steady state. With double cage IG based wind farm, SSR is found to occur at a realistic series compensation level of 50%. It is found that as wind farm size grows critical series compensation level reduces. Hence, bigger wind farms are more prone to SSR. The frequency scanning study is thus shown to be an effective screening tool for predicting SSR in series compensated wind farms.

The performance of STATCOM is also investigated with symmetrical and asymmetrical faults to alleviate the sub-synchronous oscillations in speed, electromagnetic torque, shaft torque and RMS voltage. It is found that the developed STATCOM controller successfully damps subsynchronous oscillations in case of remote faults of 6 cycles. In case of close-in faults a protection mechanism needs to be installed with STATCOM for higher

compensation level to protect system from transient overvoltage. Similar phenomenon is observed with large size of wind farms. An improvement in the negative sequence voltage is also observed with the developed STATCOM controller.

Chapter 6

CONCLUSIONS AND FUTURE WORK

6.1 CONCLUSIONS

This thesis presents the development of a comprehensive STATCOM controller for load compensation, voltage regulation and voltage balancing in electric power distribution and transmission networks. The behavior of this controller is first validated with published results. Subsequently, the performance of this STATCOM controller is examined in a realistic Hydro One distribution feeder for accomplishing the compensation of both mildly and grossly unbalanced loads, and balancing of network voltages. The STATCOM voltage control function is utilized for increasing the connectivity of wind plants in the same distribution feeder.

The thesis further presents a frequency scanning technique for simple and rapid identification of the potential of subsynchronous resonance in induction generator based wind farms connected to series compensated lines. This technique is validated by published eigenvalue analysis results. The voltage control performance of the developed comprehensive STATCOM controller is then demonstrated for different scenarios in the modified IEEE First SSR Benchmark transmission system for mitigating subsynchronous resonance in series compensated wind farms.

Major conclusions and contributions made in the thesis are outlined in this chapter. Suggestions are then provided for future research in the area of STATCOM controller design.

6.1.1 Comprehensive Controller Design

The thesis initially presents the modelling of STATCOM in rotating reference (dq) frame in Chapter 2. The comprehensive controller which includes positive sequence current

control and negative sequence current control, is developed for a Type I inverter described in Chapter 2. An all pass filter is utilized to isolate the positive and negative sequence components of the electrical variables in the STATCOM. The sequence components are then transformed into their respective rotating reference (*dq*) frames. This obviates the need for the conventionally used 2nd harmonic notch filter, resulting in a much faster settling time of the controller. Subsequently, the controller is modified to compensate phase shift and magnitude difference provided by the Y-Δ transformer which couples the STATCOM to the distribution network and also inhibits zero sequence current entering into inverter. A sinusoidal PWM technique is utilized to generate the firing pulses for IGBT switches in the STATCOM.

The controller action for each of the three functions of the comprehensive controller is illustrated using block diagrams. For load compensation, the negative sequence load current is used as a reference signal for negative sequence inner control loop. For voltage balancing, an integrator is employed to calculate negative sequence reference current. A PI controller is utilized to give reference reactive power command for voltage regulation. The concept of reduction of Temporary Overvoltage (TOV) is also described in Chapter 2.

6.1.2   Performance Assessment of the STATCOM Controller for Load Compensation, Voltage Balancing and Voltage Regulation

In Chapter 3, the comprehensive controller is tested for load compensation, voltage balancing and voltage regulation. A systematic trial and error method is adopted to obtain the controller parameters. The load compensation aspect of the controller is successfully validated with the results published for a typical European feeder in [10].

The simultaneous operation of positive and negative sequence controllers for unbalanced load connection is studied with a modified network. The proposed STATCOM is observed to have a settling time of half cycle for balanced load compensation and of about 2 cycles for unbalanced load compensation. The harmonics of the STATCOM voltage and current

with this controller are also demonstrated to be well within the limits specified in IEEE Standard 519.

Subsequently, the STATCOM controller performance is studied with a grossly unbalanced open-delta connected load. The settling time is found to be 4 cycles, which is significantly reduced to just 2 cycles with a higher DC-link voltage. Hence, a capacitor of higher voltage rating is recommended for appropriate controller response if greater unbalance is expected in the network. Voltage balancing and voltage regulation are also successfully illustrated with the developed STATCOM controller when connected to an untransposed distribution network. The settling time for this is also obtained to be 2 cycles, which is quite acceptable in industry.

6.1.3 Load Compensation and Voltage Regulation in a Realistic Distribution Feeder of Hydro One

The performance of comprehensive STATCOM controller is examined for load compensation and voltage regulation in a realistic feeder of Hydro One, in Chapter 4. A 3 MVar STATCOM is shown to effectively compensate the mildly and grossly unbalanced loads in the feeder. The controller provides power factor correction in 1 cycle and balances the load in 2 cycles. The STATCOM voltage controller is shown to successfully regulate the wind farm steady state terminal voltage to 1.06 pu during light load conditions in the nighttime. With such control, the number of wind turbines, each rated 2.3 MW, connected to feeder can be increased *two and half times* from 2 (4.6 MW) to 5 (11.5 MW) without violating the steady state overvoltage limit stipulated by Hydro One.

Subsequently, the Temporary Overvoltages (TOV) in the case of an asymmetric fault at the wind farm terminal are also analyzed. Without STATCOM only one wind turbine can be connected in order to not violate the 130% TOV limit specified by Hydro One. It is demonstrated that the 3 MVAr STATCOM can increase the number of wind turbines to be connected in the feeder *threefold* from one (2.3 MW) to three (6.9 MW), which is quite substantial.

6.1.4 Frequency Scanning Analysis for Detection of Subsynchronous Resonance (SSR), and Its Mitigation with STATCOM

The frequency scanning technique to rapidly detect subsynchronous resonance in Type I wind farms connected with series compensated line is presented in Chapter 5. The results of this frequency scanning analysis are validated with published results obtained with eigenvalue analysis [54]. Wind farms of size 100 MW to 500 MW, connected with IEEE First SSR Benchmark system and IEEE Second SSR Benchmark system are studied. No SSR is observed in wind farms connected with IEEE second SSR benchmark model in steady state. The double cage IG based wind farms are found to be prone to SSR even at a realistic compensation level of 50%. The critical series compensation level for the onset of SSR reduces with the size of the wind farms demonstrating that larger size wind farms are more susceptible to SSR. The frequency scanning technique is thus presented to be a simple, fast and effective tool for predicting SSR for preliminary analysis.

The STATCOM is shown to alleviate subsynchronous oscillations (SSO) in generator speed, electromagnetic torque, shaft torque and RMS voltage for 6-cycle symmetrical and asymmetrical faults. An improvement in the negative sequence voltage is demonstrated with the developed STATCOM controller. The developed controller thus successfully damps subsynchronous oscillations in the series compensated wind farms.

6.2 THESIS CONTRIBUTIONS

The following are the major contributions made in this thesis:

- A novel technique of extracting positive sequence and negative sequence components in rotating reference (dq) frame is utilized for STATCOM control which does not utilize a 2nd harmonic notch filter. Hence, the delay caused by the notch filter is avoided and the response time is improved to 2 cycles for load compensation and voltage balancing.

- A comprehensive fast-acting STATCOM controller is developed for load compensation, voltage balancing and voltage regulation. A specific control action for the same STATCOM can be initiated based on the system requirements. The performance of the controller is successfully demonstrated with a realistic distribution feeder of Hydro One and with wind farms connected to series compensated transmission lines as in IEEE First SSR Benchmark system.

- A frequency scanning technique is presented for the first time to detect the potential of SSR with Type I wind farms connected to series compensated lines. The results provided with this technique correlate very well with detailed eigenvalue analysis. Thus, it can be used for preliminary analysis of SSR potential in series compensated wind farms.

6.2.1   Publications from this Thesis

[1]   S. Gupta, A. Moharana and R.K. Varma, "Frequency scanning study of sub-synchronous resonance in power systems," *26th Annual IEEE Canadian Conference on Electrical and Computer Engineering (CCECE)*, pp.1-6, 5-8 May 2013.

[2]   S. Gupta and R.K. Varma, "Bibliography of HVDC Transmission 2012-13 IEEE Working Group Report" *2014 IEEE PES General Meeting,* 27-31 July 2014.

[3]   S. Gupta, R.K. Varma and G.N. Pillai, "Novel Composite Control of STATCOM for Voltage Balancing and Unbalanced Load Compensation", *2014 CIGRE Canada Conference* (Accepted for poster presentation)

[4]   S. Gupta and R.K. Varma, "Comprehensive STATCOM Control For Distribution and Transmission System Application" *(IEEE Transaction under preperation)*.

6.3 FUTURE WORK

The suggestions for future research work are mentioned below:

- The STATCOM controller parameters are selected by trial and error method in this thesis. Rigorous control design techniques may be utilized for determining optimal controllers to achieve an even better response of STATCOM.

- In this thesis, generators are considered as voltage sources without exciter and automatic voltage regulator. It is possible that other FACTS devices and generator excitation systems are electrically close to the STATCOM bus. Hence, a coordinated control of the STATCOM with other controls present nearby may be studied before their implementation.

- In the studies with series compensated wind farms, an aggregated model of wind farm is considered assuming all turbines are spinning at the same speed. In large wind farms, turbines are located in a wide geographical area, and typically have different speeds. The efficacy of the frequency scanning technique in this scenario may be investigated in future.

References

[1]   R. M. Mathur and R.K. Varma, "Thyristor based FACTS controllers for Electrical transmission systems" IEEE press 2002.

[2]   Q. Song and W. Liu "Control of a cascade STATCOM with star configuration under unbalanced conditions" *IEEE Trans. Power Elec., vol. 24, no. 1*, Jan. 2009.

[3]   G. Gueth, P. Enstedt, A. Rey and R. W. Menzies, "Individual phase control of a static compensator for load compensation and voltage balancing and regulation", *IEEE Transactions on Power Systems,* vol. 2, no. 4, pp. 898-905. 1987.

[4]   Xiong, Liansong; Zhuo, Fang; Zhu, Minghua, "Study on the compound cascaded STATCOM and compensating for 3-phase unbalanced loads," Applied Power Electronics Conference and Exposition (APEC), 2013 Twenty-Eighth Annual IEEE ,, pp.3209-3215, 17-21 March 2013.

[5]   M.G. Kashani, S. Babaei, S. Bhattacharya, "SVC and STATCOM application in Electric Arc Furnace efficiency improvement," *in Proc. 4th IEEE International Symposium on Power Electronics for Distributed Generation Systems (PEDG),* pp. 1-7, 8-11 July 2013.

[6]   http://www.abb.ca/

[7]   Benslimane, A.; Bouchnaif, J.; Azizi, M.; Grari, K., "Study of a STATCOM used for unbalanced current compensation caused by a high speed railway (HSR) sub-station," *in Proc. 2013 International Renewable and Sustainable Energy Conference (IRSEC),* pp.441-446, 7-9 March 2013.

[8]   A.G. Exposito, A.J. Conejo and C. Canizares, "Electric Energy systems Analysis and operation" CRC Press 2009.

[9]   http://edn.com/electronics-news/4363595/New-power--regulations-bring-power-factor--correction-to--lower-power-supplies

[10]   B. Blazıc and I. Papıc, "Improved D-StatCom control for operation with unbalanced currents and voltages," *IEEE Trans. Power Del.,* vol. 21, no. 1, pp. 225–233, Jan. 2006.

[11]   L.W. White, S. Battacharya,"Electric arc furnace compensation using LaGrange minimization," *in Proc. 2013 IEEE Energy Conversion Congress and Exposition (ECCE),* pp.2253-2256, 15-19 Sept. 2013.

[12]   E.T.B. Gross and S.W.Nelson, "Electromagnetic unbalance of untransposed transmission lines" *IEEE Trans. 1953*, vol. 7 , pp. 1323-1332

[13]   http://www.ece.mtu.edu/faculty/ljbohman/peec/globe/

[14]   M. M. Adibi, D. P. Milanicz and T.L. Volkmann, "Asymmetry Issues in Power System Restoration*" IEEE Transaction on Power Systems*, vol. 14, no. 3, August 1999.

[15]   C. Hochgraf and R. H. Lasseter, "Statcom controls for operation with unbalanced voltages," *IEEE Trans. Power Del.,* vol. 13, no. 2, pp. *538*– 544, Apr. 1998.

[16]   D. Patel, "Integration of Wind Turbine Generators in Distribution Networks", M.E.Sc. Dissertation, Dept. of ECE, University of Western Ontario, Canada, 2008.

[17]   N. G. Hingorani and L. Gyugyi, "Understanding FACTS: Concepts and Technology of Flexible AC transmission system" IEEE press 2000.

[18]   Singh, B.; Murthy, S.S.; Gupta, S., "A Stand-Alone Generating System Using Self-Excited Induction Generators in the Extraction of Petroleum Products," i*n Proc. IEEE Transactions on Industry Applications*, vol. 46, no. 1, pp.94-101, Jan.-Feb. 2010.

[19]   B. Singh, S.S. Murthy, R.S.R. Chilipi, "STATCOM-Based Controller for a Three-Phase SEIG Feeding Single-Phase Loads," *IEEE Transactions on Energy Conversion*, vol. 29, no. 2, pp. 320-331, June 2014.

[20]   http://www.energy.siemens.com/us/en/power-transmission/hvdc/hvdc-plus/modular-multilevel-converter.htm

[21]   P.S. Sensarma, K. R. Padiyar, V. Ramanarayanan, "Analysis and performance evaluation of a distribution STATCOM for compensating voltage fluctuations," *IEEE Transactions on Power Delivery*, vol. 16, no. 2, pp. 259-264, Apr 2001.

[22]   D. Patel, R.K. Varma, R. Seethapathy, M. Dang, "Impact of wind turbine generators on network resonance and harmonic distortion," in *Proc. 23rd Canadian Conference on Electrical and Computer Engineering (CCECE),* pp. 1-6, 2-5 May 2010.

[23] R.K. Varma, R. Seethapathy, O. Ben-Shlomo, "Increasing wind farm connectivity in a utility distribution system," in Proc. *2012 IEEE Power Electronics and Machines in Wind Applications (PEMWA)*, pp.1-6, 16-18 July 2012.

[24] http://www.hydroone.com/Generators/Documents/Distribution/Distributed%20Generation%20Technical%20Interconnection%20Requirements.pdf

[25] R. K. Varma, S. Auddy and Y. Semsedini, "Mitigation of Subsynchronous Resonance in a Series-Compensated Wind Farm Using FACTS Controllers," *IEEE Transaction on Power Delivery,* vol. 23, no. 3, pp. 1645-1654, Jul. 2008.

[26] A. Moharana and Rajiv K. Varma, "Subsynchronous Resonance in Single Cage SEIG based Wind Farm Connected to Series Compensated Line," *IET Generation, Transmission & Distribution,* vol. 5, no. 12, pp. 1221-1232, Dec. 2011.

[27] S. Gupta, A. Moharana, R.K. Varma, "Frequency scanning study of sub-synchronous resonance in power systems," in *Proc. IEEE Canadian Conference on Electrical and Computer Engineering (CCECE),* pp. 1-6, 5-8 May 2013.

[28] P. Pourbeik, R.J. Koessller, D.L. Dickmander and W. Wong, "Integration of Large Wind Farms into Utility Grids (Part 2 – Performance Issues)", in *Proc. 2003 IEEE PES General Meeting*, pp. 1520-1525.

[29] Electric Reliability Council of Texas, [Online]. Available, http://www.ercot.com/

[30] http://en.wikipedia.org/wiki/Synchronous_condenser

[31] Shih-Feng Chou; Bo-Siang Wang; Sheng-Wan Chen; Chia-Tse Lee; Po-Tai Cheng; Akagi, H.; Barbosa, P., "Average power balancing control of a STATCOM based on the cascaded H-bridge PWM converter with star configuration," *in Proc.* 2013 IEEE *Energy Conversion Congress and Exposition (ECCE)*, pp.970-977, 15-19 Sept. 2013.

[32] A. Yazdani and R. Irvani, "Voltage sourced converters in power system Modeling, control, and application" IEEE WILEY press 2010.

[33] Bingjie Zhao; Xiaojie Wu; Xiao Fu; Peng Dai, "A Novel 12-Pulse 3-Level Inverter for STATCOM Using Selective Harmonic Elimination Modulation," *in Proc. 2010 Asia-Pacific Power and Energy Engineering Conference (APPEEC)*, pp.1-5, 28-31 March 2010

[34] IEEE Recommended Practice and Requirements for Harmonic Control in Electric Power Systems," IEEE P519/D6ba, September 2013, pp.1-26.

[35] K. Li, J. Liu, Z. Wang, and B. Wei, "Strategies and operating point optimization of STATCOM control for voltage unbalance mitigation in three-phase three-wire systems," *IEEE Trans. Power Del., vol. 22, no.* 1, pp. 413–422, Jan. 2007.

[36] Hannan, M.A.; Mohamed, A.; Hussain, A., "Modeling and power quality analysis of STATCOM using phasor dynamics," *in Proc. IEEE International Conference on Sustainable Energy Technologies*, pp.1013,1018, 24-27 Nov. 2008.

[37] P. Kundur, *Power System Stability and Control*, McGraw-Hill, 1994.

[38] C. Schauder and H. Mehta, "Vector Analysis and Control of Advanced Static Var Compensator,", IEE Proc C. vol. 140, no. 4, pp 299-306, July 1993.

[39] J.M. Guerrero, Poh Chiang Loh; Tzung-Lin Lee; M. Chandorkar, "Advanced Control Architectures for Intelligent Microgrids—Part II: Power Quality, Energy Storage, and AC/DC Microgrids," *IEEE Transactions on Industrial Electronics*, vol. 60, no. 4, pp. 1263-1270, April 2013.

[40] G. Escobar, A. M. Stankovic´, and P. Mattavelli, "An adaptive controller in stationary reference frame for D-StatCom unbalanced operation," *IEEE Trans. Ind. Electron.,* vol. 51, no. 2, pp. 401–409, Apr. 2004.

[41] A.E. Leon, J.M. Mauricio, J.A. Solsona and A.G. Exposito, "Software sensor based STATCOM control under unbalanced conditins", *IEEE Trans. Power Del., vol. 24, no. 3*, July 2009.

[42] S.M. Fazeli, H.W. Ping, N.B. Abd Rahim, B. T. Ooi, "Individual-phase decoupled P-Q control of three-phase voltage source converter," *IET Generation, Transmission & Distribution*, vol. 7, no. 11, pp. 1219-1228, November 2013

[43] Guiping Yi; Renjie Hu, "The impact of grid negative sequence voltage to STATCOM and control," in *Proc. of International Conference on Electrical Machines and Systems (ICEMS)*, pp.1549-1553, 26-29 Oct. 2013.

[44] Babaei, S.; Bhattacharya, S., "Oscillatory angle control scheme for PWM static synchronous compensators under unbalanced conditions and system faults," *in Proc. IEEE Energy Conversion Congress and Exposition (ECCE)*, pp.1970-1977, 15-19 Sept. 2013.

[45]   Su Chen, G. Joos, Luis T. Moran, "Dynamic performance of PWM STATCOMs operating under unbalance and fault conditions in distribution systems", in *Proc. IEEE Power Engineering Society Winter Meeting 2001*, Vol. 2, pp. 950 - 955.

[46]   P. M. Anderson and R. G. Farmer, *Series Compensation of Power Systems*, California: PBLSH Publication, 1996

[47]   P. M. Anderson, B. L. Agrawal and J. E. Van Ness, *Subsynchronous Resonance in Power Systems,* New York: EEE Publication, 1990.

[48]   T. Ackerman, *Wind power in power systems*, New York: Wiley, 2005

[49]   E. Hau, Wind *Turbines: Fundamentals, Technologies, Application, Economics*, 2nd ed., Germany: Springer, 2006.

[50]   O. Anaya-Lara, N. Jenkins, J. Ekanayake, P. Cartwright and M. Guges, *Wind Energy Generation: Modeling and Contro*l, USA: Wiley, 2009.

[51]   http://www.thewindpower.net/, accessed Jan. 2013.

[52]   http://www.horizonwind.com, accessed Jan. 2013.

[53]   http://www.res-group.com, accessed Jan. 2013.

[54]   A. K. Moharana, Subsynchronous Resonance in Wind Farms, Ph.D. dissertation, Dept. of ECE, University of Western Ontario, Canada, 2012.

[55]   R. Nath and C. Grande-Moran "Study of Sub-Synchronous Control Interaction due to the interconnection of wind farms to a series compensated transmission system," *in Proc. IEEE PES Transmission and Distribution Conference and Exposition*, pp.1-6, 2012.

[56]   M.S. El-Moursi, B. Bak-Jensen, M.H. Abdel-Rahman, "Novel STATCOM Controller for Mitigating SSR and Damping Power System Oscillations in a Series Compensated Wind Park," *IEEE Transaction on Power Electronics*, vol. 25, no. 2, pp. 429-441, Feb. 2010.

[57]   "First Benchmark Model for Computer Simulation of Subsynchronous Resonance", by IEEE Sub-synchronous Resonance Task Force of the Dynamic System Performance Working Group, Power System Engineering Committee; IEEE Trans on PAS Sept/Oct, 1977.

[58]   "Second Benchmark Model for Computer Simulation of Subsynchronous Resonance", by IEEE Sub- synchronous Resonance Task Force of the Dynamic

System Performance Working Group, Power System Engineering Committee; IEEE Trans on PAS May 1985.

[59] Bin Wu, Y. Lang, N. Zargari and S. Kouro, "Power conversion and control of wind energy systems" IEEE Press 2011.

[60] P.C. Krause, O. Wasynczuk and S.D. Sudhoff, "Analysis of electric machinery and drive systems" 2nd ed., United states: IEEE press and Wiley Interscience, 2002.

[61] K. R. Pediyar, "FACTS controllers in Power Transmission and Distribution" New Age International Publishers 2007.

[62] http://linuxgazette.net/118/misc/sreejith/pwm.png

[63] J.D. Glover , M.S. Sarma and T.J. Overbye, "Power system Analysis and Design" 4th edition Thompson 2008.

[64] K. G. Masoud, M. R. Iravani, "A method for synchronization of power electronic converters in polluted and variable-frequency environments," *IEEE Trans. on Power Systems*, vol. 19, no.3, pp. 1263-1270, August 2004.

[65] A. Moharana, R.K. Varma, R. Seethapathy, "SSR Alleviation by STATCOM in Induction-Generator-Based Wind Farm Connected to Series Compensated Line," *IEEE Transactions on Sustainable Energy*, vol. 5, no. 3, pp. 947-957, July 2014.

[66] J. Pedra, F.Corcoles,LI. Monjo, S. Bogarra and A. Rolan, "On Fixed Speed WT Generator Modeling for Rotor Speed Stability Studies" *IEEE Transaction on Power systems*, vol. 27, no. 1, Feb 2012.

[67] K. R. Padiyar, "Power System Dynamics, Stability and Control" (BS publication, 2008)

[68] B.L. Agrawal, and R.G. Farmer, "Use of frequency scaning technique for subsynchronous resonance analysis", *IEEE Transaction on Power Apparatus and Systems*, vol. PAS-98, no. 2, pp. 341-349, March 1979.

Appendix A

Study System-1 Data

Operating frequency = 50 Hz

Table A.1 Study system-1 parameters [10]

Component	Parameters	Value
Stiff Voltage Source	S_{SC}''	2258 MVA
	U_N	110 kV
	R/X	0.1
TR1 110/20 kV	S_N	20 MVA
	U_{SC}	10.79%
	R/X	0.1
Transmission Line	Z_T	$4.13 + j3.56\ \Omega$
Cable connection	Z_C	$0.13 + j0.1\ \Omega$
Load 1	Z_{L1}	$90 + j14.1\ \Omega$
Load 2	Z_{L2} (phase A)	$190 + j11\ \Omega$
	Z_{L2} (phase B)	$110 + j31.4\ \Omega$
	Z_{L2} (phase C)	$530 + j18.8\ \Omega$

Table A.2 Values of STATCOM components [10]

Component	Value
L_S	0.191 H
R_S	$6\ \Omega$
C	39.788 mF
R_p	$8\ \Omega$
V_{dcref}	1.155 kV

Table A.3 STATCOM controller parameters

Controller	Gain	Time constant
DC-link voltage	$K_{pdc} = 6$	$T_{idc} = 0.003$
Active power	$K_{pd\_p} = 200$	$T_{id\_p} = 0.0001$
Reactive power	$K_{pq\_p} = 8.0$	$T_{iq\_p} = 0.0002$
d-axis negative sequence current	$K_{pd\_n} = 200$	$T_{id\_n} = 0.00005$
q-axis negative sequence current	$K_{pq\_n} = 1200$	$T_{iq\_n} = 1*e\ \text{-}05$

Table A.4 STATCOM base values [10]

Parameter	Value
Base power	2 MVA
Base voltage	0.46 kV
Base current	2.89 kA

Study System-2 Data

Operating frequency = 60 Hz

Load 1 : 90 + j*16.93 Ω

Load 2 : 190 + j*13.2 Ω , 110 + j*37.7 Ω and 530 + j*22.55 Ω

Table A.5 STATCOM controller parameters

Controller	Gain	Time constant
DC-link voltage	$K_{pdc} = 6.5$	$T_{idc} = 0.0035$
Active power	$K_{pd\_p} = 200$	$T_{id\_p} = 0.0001$
Reactive power	$K_{pq\_p} = 800$	$T_{iq\_p} = 0.00027$
d-axis negative sequence current	$K_{pd\_n} = 400$	$T_{id\_n} = 8*e\ -06$
q-axis negative sequence current	$K_{pq\_n} = 400$	$T_{iq\_n} = 2*e\ -05$

Study system-3 data:

Load 1 : 90 + j*16.93 Ω

Study system-4 data:

Table A.6 STATCOM controller parameters

Controller	Gain	Time constant
DC-link voltage	$K_{pdc} = 6.5$	$T_{idc} = 0.0035$
Active power	$K_{pd\_p} = 200$	$T_{id\_p} = 0.0001$
Reactive power	$K_{pq\_p} = 450$	$T_{iq\_p} = 0.00015$
d-axis negative sequence current	$K_{pd\_n} = 40$	$T_{id\_n} = 0.004$
q-axis negative sequence current	$K_{pq\_n} = 120$	$T_{iq\_n} = 0.001$

Appendix B

Hydro One Feeder's line data:

Positive sequence resistance: 0.1691 Ω/km

Positive sequence reactance: 0.4182 Ω/km

Zero sequence resistance: 0.4441 Ω/km

Zero sequence reactance: 1.1899 Ω/km

Positive sequence susceptance: 3.954 uS/km

Zero sequence susceptance: 0 uS/km

Length of lines:

Line 1 = 35 km, Line 2 = 5 km and Line 3 = 5 km

Day time load:

4.82 MW and 2.197 MVAr

Unbalanced load:

Z_{L2} (phase A)	880 + j188.5 Ω
Z_{L2} (phase B)	700 + j339.3 Ω
Z_{L2} (phase C)	720 + j188.5 Ω

Gross unbalanced load:

1000 + j263.9 Ω

Night time load:

1.6 MW and 0.73 MVAr

STATCOM data for Realistic Feeder:

Component	Value
L_S	0.05 mH
C	40 mF
V_{dcref}	1.4 kV

Appendix C

A. **Single-cage induction generator parameters [25], [26]**

Generator rated voltage (V_S)   =   690 V

Base power (S_{base})   = 892.4 MVA

Stator winding resistance (R_{st}) =   2.1765 pu

Rotor winding resistance (R_r)   =   2.4485 pu

Magnetizing leakage reactance (X_m) = 1762.9 pu

Rated Power (P_g)   =   2 MW

Stator winding leakage reactance (X_{st})   = 41.3 pu

Rotor winding leakage reactance (X_r)   = 44.4 pu

B. **IEEE First SSR Benchmark Model [57]**

AC transmission line data:

Base power (S_{base})   = 892.4 MVA

Line resistance (R_{line}) = 0.02 pu

Line reactance (X_2)   = 0.50 pu

Base voltage (V_{base})   = 500 kV

Transformer reactance (X_1) = 0.14 pu

Load reactance (X_3) = 0.06 pu

C. **Doublecage Induction Generator parameters [54]**

Generator rated voltage (V_S) =   690 V

Base power (S_{base}) = 892.4 MVA

$R_{r1} = 4.65$ pu

$R_{r2} = 7.4579$ pu

$L_{r2} = 82.111$ pu

$X_{rm} = 27.9$ pu

$X_m = 1508.3$ pu

$R_s = 1.9629$ pu

$X_s = 51.1$ pu

$C_g = 6.5$ mF

D. IEEE Second SSR Benchmark Model [58]

AC transmission line data:

Base power (S_{base})   = 100 MVA

Base voltage (V_{base})   = 500 kV

Compensated line resistance (R_1) = 0.0074 pu

Compensated line reactance (X_1) = 0.0800 pu

Un-compensated line resistance (R_2) = 0.0067 pu

Un-compensated line reactance (X_2) = 0.0739 pu

Load Resistance (R_3) = 0.0014 pu

Load reactance (X_3) = 0.03 pu

Transformer reactance = 0.12 pu (600 MVA)

E. Transformer Modelling

Primary side magnetizing current =Im_1

Secondary side magnetizing current= Im_2

Leakage Reactance (pu) = X_1

Primary Winding Voltage (RMS)   = V_1

Secondary Winding Voltage (RMS) = V_2

Transformer MVA rating = T_{mva}

k = Im_1/Im_2

$$Z_{base} = V_1^2/T_{mva}$$

$$a = \frac{V_1}{V_2}$$

$$L_1 = \left\{\frac{Z_{base}}{2 \times \omega_s}\right\} \times \left(\frac{X_1 - (k-1)}{Im_1}\right)$$

$$L_2 = \left\{\frac{Z_{base}}{2 \times \omega_s}\right\} \times \left(\frac{X_1 + (k-1)}{Im_1}\right)$$

$$L_{12} = \left\{\frac{Z_{base}}{Im_1 \times \omega_s}\right\} - L_1$$

Appendix D

STATCOM Data for SSR Mitigation:

Component	Value
Coupling Transformer	100 MVA 34.5/11 kV
L_S	4.9 mH
C	100 mF
V_{dcref}	25 kV
Switching frequency	6840 Hz

Fault Impedance: 4.83 kΩ || 34.5 mH

Appendix E

1. Subsynchronous Resonance analysis with Single-cage induction generator connected with IEEE First SSR Benchmark Model

Table E.1 Electrical mode eigen-frequency for different sizes of wind farm based on single cage induction generator

K (%)	100 MW		Potential for SSR
	Frequency Scanning	Eigenvalue Calculation	
10	49.825	49.723	×
20	45.732	45.454	×
30	42.516	42.184	×
40	39.825	39.43	×
50	37.420	37.004	×
60	35.318	34.811	×
70	33.423	32.793	×
80	31.624	30.912	×
90	29.920	29.142	×

K (%)	200 MW		Potential for SSR
	Frequency Scanning	Eigenvalue Calculation	
10	47.0222	47.22	×
20	41.720	41.919	×
30	37.723	37.855	×
40	34.220	34.43	×
50	31.322	31.409	×
60	28.615	28.67	×
70	26.115	26.14	×
80	23.806	23.766	×
90	21.720	21.509	√

K (%)	300 MW		Potential for SSR
	Frequency Scanning	Eigenvalue Calculation	
10	45.366	45.872	×
20	39.427	40.013	×
30	34.873	35.52	×
40	31.051	31.729	×
50	27.691	28.381	×
60	24.666	25.338	×
70	21.895	22.512	×
80	19.331	19.836	×
90	16.943	17.244	√

K (%)	400 MW		Potential for SSR
	Frequency Scanning	Eigenvalue Calculation	
10	44.220	45.017	×
20	37.866	38.803	×
30	32.994	34.037	×
40	28.885	30.013	×
50	25.287	26.455	×
60	22.038	23.212	×
70	19.076	20.187	×
80	16.322	17.291	×
90	13.748	14.405	√

K (%)	500 MW		Potential for SSR
	Frequency Scanning	Eigenvalue Calculation	
10	43.376	44.423	×
20	36.736	37.964	×
30	31.624	33.008	×
40	27.325	28.822	×
50	23.551	25.116	×
60	20.143	21.733	×
70	17.023	18.563	×
80	14.139	15.492	×
90	11.447	12.308	√

2. Subsynchronous Resonance analysis with double-cage induction generator connected with IEEE First SSR Benchmark Model

Table E.2 Electrical Mode eigen-frequency for different sizes of wind farm based on double cage induction generator

K (%)	100 MW		Potential for SSR
	Frequency Scanning	Eigenvalue Calculation	
10	50.40	50.012	×
20	46.46	45.879	×
30	43.45	42.719	×
40	40.92	40.064	×
50	38.70	37.732	×
60	36.70	35.63	√
70	34.86	33.703	√
80	33.16	31.914	√
90	31.57	30.239	√

K (%)	200 MW		Potential for SSR
	Frequency Scanning	Eigenvalue Calculation	
10	47.55	47.505	×
20	42.48	42.34	×
30	38.6	38.393	×
40	35.35	35.076	×
50	32.49	32.163	√
60	29.92	29.536	√
70	27.58	27.128	√
80	25.4	24.891	√
90	23.37	22.796	√

K (%)	300 MW		Potential for SSR
	Frequency Scanning	Eigenvalue Calculation	
10	45.89	46.107	×
20	40.17	40.365	×
30	35.8	35.974	×
40	32.13	32.283	×
50	28.91	29.039	√
60	26.02	26.112	√
70	23.37	23.422	√
80	20.92	20.919	√
90	18.64	18.565	√

K (%)	400 MW		Potential for SSR
	Frequency Scanning	Eigenvalue Calculation	
10	44.71	45.234	×
20	38.56	39.13	×
30	33.84	34.461	×
40	29.89	30.534	×
50	26.42	27.079	×
60	23.3	23.956	√
70	20.44	21.082	√
80	17.8	18.396	√
90	15.34	15.855	√

K (%)	500 MW		Potential for SSR
	Frequency Scanning	Eigenvalue Calculation	
10	43.85	44.611	×
20	37.4	38.249	×
30	32.44	33.379	×
40	28.28	29.281	×
50	24.63	25.673	×
60	21.35	22.407	√
70	18.35	19.393	√
80	15.57	16.562	√
90	12.98	13.864	√

Curriculum Vitae

Name: Shubham Gupta

Post-secondary Education and Degrees:

Indian Institute of Technology Roorkee
Roorkee, Uttarakhand, India
2009-2013 B.Tech.

The University of Western Ontario
London, Ontario, Canada
2013-2014 M.E.Sc.

Related Work Experience

Teaching Assistant
Research Assistant
The University of Western Ontario
Winter 2014

Publications:

[1] S. Gupta, A. Moharana, R.K. Varma, "Frequency scanning study of sub-synchronous resonance in power systems," *26th Annual IEEE Canadian Conference on Electrical and Computer Engineering (CCECE)*, pp.1-6, 5-8 May 2013.

[2] S. Gupta and R.K. Varma, "Bibliography of HVDC Transmission 2012-13 IEEE Working Group Report" 2014 IEEE PES General Meeting.

[3] S. Gupta, R.K. Varma and G.N. Pillai, "Novel Composite Control of STATCOM for Voltage Balancing and Unbalanced Load Compensation", 2014 CIGRE Canada Conference (Accepted for poster presentation)